DSPACE

https://dspace.org/

Nickel potential of the Molopo Farms Complex in the area of Jwaneng- Makopong shear zone

Bartolomeu, Bruno

2023
https://hdl.handle.net/10539/35681

Downloaded from a DSpace repository. https://dspace.org/

UNIVERSITY OF THE
WITWATERSRAND,
JOHANNESBURG

Nickel potential of the Molopo Farms Complex in the area of Jwaneng-Makopong shear zone

Supervisors:
- Prof. Judith Kinnaird
- Dr. Marina Yudovskaya

Bruno Bartolomeu
brunobartolomeu96@gmail.com
Student number: 2507865

Abstract

The Molopo Farms Complex (MFC), located in southern Botswana, is likely to have had the same origin as the Bushveld Complex. It has been a subject of several economic studies which reported Ni-Cu-PGE mineralisation associated with a suite of well-layered ultramafic rocks. Following previous studies and self-gathered data, Kalahari Key Minerals Exploration Company (KKME) has proceeded with exploration in the Jwaneng-Makopong shear zone in the MFC, where a gravimetric and electromagnetic anomaly was detected, motivating the drilling of two boreholes, KKME – 1/6 and KKME – 1/14.

Whole rock and initial petrographic data in borehole KKME – 1/6 indicated several mineralised portions with an anomalous Ni enrichment. This prompted further studies to understand the characteristics and potential of the Ni mineralisation. Borehole KKME – 1/6 is characterised by variably alternating sequences of mostly heavily serpentinised orthopyroxenite and harzburgite. Nickel mineralisation is observed in both orthopyroxenite and harzburgite in relatively narrow zones comprised of interstitial sulphide blebs or disseminated sulphide grains. There is a predominance of Ni-rich sulphides, mainly pentlandite and heazlewoodite, as well as a Ni-Fe alloy, awaruite, and a Ni arsenide, orcelite, locally associated with a disseminated chromite-enriched layer.

XRF data showed the existence of high Ni enrichment (28174 ppm Ni) in sample IMK – 05149, as well as a general enrichment of ~2000 Ni ppm. With the help of the TIMA, it was possible to calculate the Ni deportment, where results indicate that the overwhelming majority of Ni is present in ore minerals, especially in the most enriched samples, however, a base Ni amount was calculated to belong to the silicates and oxides (non-recoverable) around ~1000 – 1500 ppm Ni. The TIMA results show that a minor Ni proportion occurs within the gangue minerals, but the anomalous enrichment is attributed to the ore assemblages where Ni is recoverable. The textural and compositional characteristics of the mineralisation, as well as its assemblages, are suggestive of complete replacement of the primary magmatic sulphides and late formation of the present minerals, indicating a secondary origin for this mineralisation. The main serpentinisation event is suggested to have been the main contributor of ore mineral formation which implies a strong relevance of the alteration events and processes for the formation of the mineralisation in this study, and, by extension, the studied area of the Jwaneng-Makopong shear zone of the MFC.

Declaration

I, Bruno Bartolomeu, declare that this research report is my own original work and that the appropriate measures have been taken to appropriately reference and acknowledge the work of other authors where relevant. This research report submitted in partial fulfilment of the requirements for the degree of Master of Science in Economic Geology at the School of Geosciences, University of the Witwatersrand.

28/12/2022

Acknowledgements

I would like to express my sincerest gratitude to my supervisors, Prof. Judith Kinnaird and Dr. Marina Yudovskaya, that provided me with this opportunity. Without their continued assistance and knowledge this thesis would not been possible, their guidance through the planning, field trips, research and writing helped immensely in producing this work.

Outside the university, I would like to express my thanks to the staff of Kalahari Key Minerals Exploration (KKME) who provided the object of study for my thesis. Without their cooperation and supply of the material this thesis wouldn't be possible. Special thanks to Dr Andrew Edward Moore for hosting me, Dr. Marina Yudovskaya and Mr. Jason Borret on our field trip to Botswana and allowing for a detailed study of the boreholes.

I would also like to thank the Faculty of Science of Lisbon University (FCUL), namely Prof. António Mateus and Dr. Pedro Rodrigues, for providing me with the opportunity to use their equipment and do microprobe analyses that were crucial for the thesis.

Besides my advisors, I would like to thank the rest of the staff at Wits School of Geoscience, namely, Prof. Paul Nex, Mr. Marlin Patchappa, Mr. Caiphas Majola, Ms. Reshmi Singh and Prof. Grant Cawthorn for their help in the many steps of practical, technical and administrative processes needed for the realisation of this thesis.

My sincere thanks to my friend and colleague, Mr. Jason Borrett, with whom I carried out major portions of the practical work for the thesis, as well as, for making living in a foreign country easier and introducing me to it.

Finally, I would like to thank my family: my parents and grandmother, who encouraged me and financially supported my decision on going abroad to pursue my dream of realising an MSc in economic geology, as well as, for their patience in the last few months in order to complete the thesis whilst back at home.

Contents

Abstract 1
Declaration 2
Acknowledgements 2
List of figures 4
List of tables 7
Chapter 1 Introduction 8
1.1. Preamble 8
1.2. Aim and objectives of the research 11
Chapter 2 Geological Setting 12
2.1. Overview 12
Chapter 3 Methodology 15
3.1. Field work and core logging 15
3.2. Petrography 15
3.3. X-ray fluorescence – XRF 16
3.4. Tescan Integrated Mineral Analyser – TIMA 16
3.5. Electron Microprobe 18
Chapter 4 Magmatic stratigraphy of borehole KKME 1-6 19
Chapter 5 Petrography 26
5.1. Ultramafic Rocks 26
5.1.1. Harzburgite 26
5.1.2. Pyroxenite 26
5.1.3. (Massive) Serpentinite 27
Chapter 6 Whole rock geochemistry 29
6.1. X-Ray Fluorescence Spectrometry 29
Chapter 7 Mineral Chemistry 34
7.1. Primary Phases 34
7.1.1. Pyroxenes 34
7.2. Secondary Phases 39
7.2.1. Serpentine-group minerals 39
7.2.2. Chlorites 45
7.2.3. Amphiboles: 48
7.2.4. Ni content in silicates 53
7.3. Ore Minerals 54
7.3.1. Pentlandite 54
7.3.2. Pyrrhotite 55

7.3.3. Mackinawite 56
7.3.4. Heazlewoodite 57
7.3.5. Chalcocite 58
7.3.6. Samaniite 58
7.3.7. Awaruite 58
7.3.8. Maucherite 59
7.3.9. Orcelite 59
7.3.10. Unknown/Unnamed Nickel Antimonide 60
7.3.11. Parkerite 60
7.3.12. Chromite 61
Chapter 8 TESCAN Integrated Mineral Analyser 66
8.1. Description of the TIMA approach and its limitations 66
8.2. TIMA maps 67
8.3. TIMA quantitative estimates of the mineral proportions 72
Chapter 9 Discussion 80
9.1. Mineral Associations 80
9.1.1. General features of the main rock-forming processes 80
9.1.2. Observations in hand samples and polished sections 81
9.2. Nickel deportment 82
9.3. Hydrothermal Ni in serpentines 85
Chapter 10 Conclusions and recommendations 87

List of figures

Figure 1: Map of the Bushveld Igneous Complex and contemporaneous igneous complexes of South Africa and Botswana, adapted from Mapeo et al. (2004). 8
Figure 2: Map of the location of target areas for exploration and respective location of boreholes on the MFC's exploration project. 10
Figure 3: Location of the Molopo Farms Complex in southern Botswana (a), geological map (b) and simplified stratigraphic column (c), adapted from Kaavera et al., (2020). In the rectangle is the Jwaneng-Makopong (JM) shear zone showing the approximate location of borehole KKME 1-6 (Figure 1). 13
Figure 4: Stratigraphic column of the ultramafic section of borehole KKME – 1/6, with mineralised portions marked green at depths: ~294-319m, 446.3-451m, 506-520.7m, ~531m, 547-561m and 589-598m. 20
Figure 5: Altered ultramafic rocks in borehole KKME 1-6, from ~226m to ~232m depth. Core diameter is 4.76 cm (NQ) 21

Figure 6: Serpentine and talc veining in ultramafic rocks in borehole KKME 1-6, from ~239m to ~244.5m depth. Core diameter is 4.76 cm (NQ). 22
Figure 7: Fractured core in a fault zone in borehole KKME 1-6, from ~296m to ~302m and ~308 to ~315 m depth where mineralised samples IMK – 05139 and IMK – 05149 used in microprobe and the TIMA are located. Core diameter is NQ. 23
Figure 8: Talc and serpentine veinings in serpentinite in borehole KKME 1-6, from ~440m to ~446.5m depth where samples IMK – 05156 used in microprobe and the TIMA is located. Core diameter is NQ. 23
Figure 9: Massive serpentinite in borehole KKME 1-6, from ~521m to ~527m depth. Core diameter is NQ. 24
Figure 10: Thin section images of the ultramafic rocks showing degrees of alteration: a) Cross Polarised Light image of orthopyroxenite, IMK – 05139; b) Plain Polarised Light view of orthopyroxenite, IMK – 05139; c) Cross Polarised Light image of massive serpentinite after harzburgite, 1/6 – 591; d) Plain Polarised Light view of massive serpentinite after harzburgite, 1/6 – 591. 28
Figure 11: MgO vs LOI (wt%) plot, after Deer et al., (1992), indicating the alteration of the studied samples. The filtering line delineates between retained and discarded samples, due to their alteration. Serpentine, chlorite and filtering lines from Deer et al., (1992). 29
Figure 12: XRF compositional data of orthopyroxenite (green), harzburgite (blue) and magnetite vein (orange): a) SiO_2 vs MgO (wt%); b) Fe_2O_3 vs MgO (wt%); c) CaO vs MgO (wt%), d) Zr ppm vs MgO wt%; e) Cr ppm vs MgO wt%; f) Ni ppm vs MgO wt%. 30
Figure 13: XRF compositional data for orthopyroxenite (green), harzburgite (blue) and magnetite vein (orange): a) Cr/V (wt%) ratio vs MgO wt% and b) Ni ppm vs LOI wt% 32
Figure 14: Pyroxene ternary (En-Wo-Fs) plot for pyroxene analyses for sample IMK - 05139... 35
Figure 15: Pyroxene ternary (En-Wo-Fs) plot for mineral compositions for sample IMK - 05149 36
Figure 16: Pyroxene ternary (En-Wo-Fs) plot for pyroxene analyses for sample IMK - 05153... 37
Figure 17: Binary plots for all pyroxene analyses: a) NiO wt% vs Mg#; b) NiO wt% vs MgO wt%; c) NiO wt% vs CaO wt%. 38
Figure 18: Serpentine FeO-SiO_2-MgO ternary plot for sample IMK - 05139. 39
Figure 19: Serpentine FeO-SiO_2-MgO ternary plot for sample IMK – 05149. Different compositional groups are circled in green, yellow and red, for Si-enriched Mg-depleted antigorite, Si-Fe-enriched antigorite and the most similar compositional group to antigorite, respectively. 40
Figure 20: Serpentine FeO-SiO_2-MgO ternary plot for sample IMK – 05153. Shows two groups variably enriched in MgO. 41
Figure 21: Serpentine FeO-SiO_2-MgO ternary plot for sample IMK – 05156. 42
Figure 22: Serpentine FeO-SiO_2-MgO ternary plot for the 4 samples. 43
Figure 23: Binary plots of serpentine for the 4 samples: a) NiO wt% vs MgO wt%; b) NiO wt% vs Mg#; c) SiO_2 vs MgO wt%. 44
Figure 24: Plot for IMK - 05149 chlorite classification after Deer et al., (1992), with silica atoms per formula unit Vs Fe-Mg molecular ratio. 45
Figure 25: Plot for IMK - 05153 chlorite classification after Deer et al., (1992), with silica atoms per formula unit Vs Fe-Mg molecular ratio. 46
Figure 26: Plot for IMK - 05156 chlorite classification after Deer et al., (1992), with silica atoms per formula unit Vs Fe-Mg molecular ratio. 47
Figure 27: Compositional plot comparing the NiO wt% on chlorite and serpentine analyses in studied samples. 47

Figure 28: Compositional plots for all chlorite analyses in studied samples a) NiO wt% Vs Mg#; b) Cr_2O_3 Vs Mg#. 48
Figure 29: Amphibole classification plot after Deer et al., (1992), for sample IMK – 05139, with silica atoms per formula unit (apfu) Vs Mg-Fe^{2+} molecular ratio. 49
Figure 30: Amphibole classification plot after Deer et al., (1992), for samples IMK – 05149 and IMK – 05153, with silica atoms per formula unit (apfu) Vs Mg-Fe^{2+} molecular ratio. 50
Figure 31: Alkalis hornblende amphibole classification plot with a silica per atom formula unit Vs the sum of Na and K in the A-site of the formula (after Hawthorne, et al., (2012). 51
Figure 32: Whisker diagram of the NiO wt% content in the different silicates per sample. 53
Figure 33: Ni-Fe (Ni wt% and Fe wt%) distribution in pentlandite from samples IMK – 05139 and IMK – 05149 55
Figure 34: Ni-Fe (Ni wt% and Fe wt%) distribution in pyrrhotite from samples IMK – 05139.... 56
Figure 35: Ni-Fe (Ni wt% and Fe wt%) distribution in pentlandite, pyrrhotite and mackinawite from samples IMK – 0539 and IMK – 05149. 57
Figure 36: Compositions of the spinel group minerals represented on the spinel prism. The apices are defined by Fe^{3+}, Cr^{3+} and Al^{3+}, after Deer et al., (1992). 61
Figure 37: Chromium variation in chromites from sample IMK – 05139, with Cr# Vs Mg#, where Cr# is the Cr-Al molecular ratio and Mg# is the Mg-Fe molecular ratio. 62
Figure 38: Chromium variation in chromites from sample IMK – 05149, with Cr# Vs Mg#, where Cr# is the Cr-Al molecular ratio and Mg# is the Mg-Fe molecular ratio. 63
Figure 39: Chromium variation in chromites from sample IMK – 05156, with Cr# Vs Mg#, where Cr# is the Cr-Al molecular ratio and Mg# is the Mg-Fe molecular ratio. 64
Figure 40: Comparison of Cr variation in chromites from samples IMK – 05156, IMK – 05149, IMK – 05139, Uitkomst intrusion (Yudovskaya, et al., 2015) and Lower Bushveld Zone (Hulbert & Gruenewaldt, 1985). Values as Cr# Vs Mg#, where Cr# is the Cr-Al molecular ratio and Mg# is the Mg-Fe molecular ratio. 65
Figure 41: TIMA map for coarse-grained orthopyroxenite, sample IMK – 05139. Pn-Po = pentlandite-pyrrhotite; Bt = biotite; Mhs = magnesiohastingsite; En = enstatite; Atg = antigorite; Act = actinolite; Tr = tremolite; Chr = chromite. 67
Figure 42: TIMA map for heavily altered orthopyroxenite, sample IMK – 05149. Pn = pentlandite; Hzl = heazlewoodite; Mhs = magnesiohastingsite; En = enstatite; Atg = antigorite; Act = actinolite; Bt = biotite; Chl = chlorite; Di = diopside. 69
Figure 43: TIMA map for altered orthopyroxenite, sample IMK – 05153. Within the red circle is an example of the graphical glitches that occur due to the similar compositions of the various phases in those patches. Hzl-Awr = heazlewoodite-awaruite Mhs = magnesiohastingsite; En = enstatite; Atg = antigorite; Act = actinolite; Tr = tremolite; Bt = biotite; Chl = chlorite; Ap = apatite. 70
Figure 44: TIMA map for serpentinised harzburgite with chromite zone, sample IMK – 05156. Atg = antigorite; Chr = chromite; Orc = orcelite. 71
Figure 45: Pie chart of the Ni deportment in minerals of sample IMK – 05149. 72
Figure 46: Pie chart of the Ni deportment in minerals of sample IMK – 05153. 73
Figure 47: Pie chart of the Ni deportment in minerals of sample IMK – 05156. 74
Figure 48: Pie chart of the Ni deportment in minerals of sample IMK – 05139 using the minimum average Ni values. 76
Figure 49: Pie chart of the Ni deportment in minerals of sample IMK – 05139 using the maximum average Ni values. 77
Figure 50: Proportion of recoverable Ni ppm per sample (black) and total Ni ppm in those samples. 79

Figure 51: Proportion of unrecoverable Ni ppm per sample and total Ni in those samples. 79
Figure 52: Proportion of recoverable Ni ppm per sample (black) and total Ni ppm in those samples. 84
Figure 53: Plot of log fO_2 Vs T showing the equilibrium in Fe and Ni-bearing serpentines at $PH_2O + PH_2$ = 2 kb, after Frost (1984). Heavy lines separate the reaction temperatures for XMg olivine = 0.80. The box indicates the approximate fO_2 conditions for the antigorite-olivine-brucite-magnetite assemblage, inferred by the presence of awaruite, after Frost (1984). Ant = antigorite, Bru = brucite, Fo = forsterite, Tc = talc, Ta = taenite, Mt = magnetite, Aw = awaruite, Km = kamacite, IM = iron-magnetite, MQ = magnetite-quartz and F = fayalite. 86

List of tables

Table 1: Mineral groupings, their Ni deportment and proportions (wt%) in sample IMK – 05149. 73
Table 2: Mineral groupings, their Ni deportment and proportions (wt%) in sample IMK – 05153. 74
Table 3: Mineral groupings, their Ni deportment and proportions (wt%) in sample IMK – 05156. 75
Table 4: All minerals with >~0.1 wt% Ni, their average minimum Ni values and their average maximum Ni values for sample IMK – 05139..... 76
Table 5: Mineral groupings, their Ni deportment and proportions (wt%) in sample IMK – 05139, using the minimum average Ni values. 77
Table 6: Mineral groupings, their Ni deportment and proportions (wt%) in sample IMK – 05139, using the maximum average Ni values. 77
Table 7: Comparison of XRF whole rock data and TIMA Ni deportment with the calculation of unrecoverable and recoverable Ni in the samples. 78
Table 8: Comparison of XRF whole rock data and TIMA Ni deportment with the calculation of unrecoverable and recoverable Ni in the samples. 84

Chapter 1

Introduction

1.1. Preamble

The Molopo Farms Complex, measures around 13000 km^2 and is comprised of an ultramafic sequence with an overlying mafic sequence that occurs in south-eastern Botswana, and adjacent areas of South Africa (Figure 1). The Molopo Farms Complex was first described in the 1960s, after serpentinised ultramafic rocks were initially found in water wells near the Keng Pan area (Kaavera, et al., 2020) and geophysical anomalies, such as gravimetric and magnetic, discovered in a regional aeromagnetic survey (1962). The Complex, later became a subject of interest and further studied and surveyed by the British Geological Survey, BGS, and the Government of Botswana in a collaboration (1980-1984) Prendergast (2012); Gould et al., (1987). This survey by the BGS and the Government of Botswana included the drilling of many boreholes, such as MF38, and resulted in a report by Gould and his co-workers (1987) that elaborated on many of the characteristics of the Molopo Farms Complex, including its similarities with the Bushveld Complex, which in turn garnered attention for its potential for mineralisation (Reichhardt, 1994). Included in borehole MF38 was a grade of ~1.1 ppm Pt + Pd near the base of ultramafic cumulates (Kaavera, et al., 2020). Through the 1980s and 1990s, follow up work by Gold Fields Botswana (Pty) Ltd. and Molopo Australia was done, then later by Tau Mining and Impala Platinum in 2005 and 2008 respectively. A major geophysical project, Central Kalahari Project, funded by the Botswana government was a comprehensive study of the Molopo Farms Complex structure (Prendergast, 2012).

Figure 1: Map of the Bushveld Igneous Complex and contemporaneous igneous complexes of South Africa and Botswana, adapted from Mapeo et al. (2004).

The economic potential of a Bushveld Complex related intrusion is a major attractor for exploration companies, such was the case of many companies that worked on the Complex and revealed important information. However, the explorative endeavours on the Molopo Farms Complex haven't been met with the anticipated results and no significant economic resource has been found as of yet.

Kalahari Key Minerals (KKME) performed a re-interpretation of the previously available and newly obtained geophysical data and conducted the drilling of two boreholes, KKME 1-6 and KKME 1-14, with a third one planned as at the time of the writing of this thesis (Figure 2). The Boreholes KKME 1-6 and KKME 1-14 are located within the Jwaneng-Makopong shear zone, where a geophysical anomaly was previously established.

The previous exploration has been mainly focused on reef-style PGE mineralisation analogous to the renowned Bushveld Complex reefs, whereas the KKME exploration campaign targeted the Jwaneng-Makopong shear zone as a potential feeder for the ultramafic body and with related disseminated Ni mineralisation.

In 2020, whole rock assay results of mineralised intervals in the borehole KKME 1-6 have shown elevated Ni concentrations in serpentinised ultramafic rocks, as reported by the company (KKME press release of 2021). Understanding the Ni distribution in altered ultramafic rocks is of upmost importance as Ni present in primary silicates and sulphides can be remobilised, such that it would severely hamper the economic viability of the resources, challenging the continuation of the exploratory efforts and possible future mining endeavours. Furthermore, a detailed mineralogical analysis is crucial to determine the origin of the mineralisation. In addition, the typical Ni mineralisation in ultramafic rocks is commonly accompanied by variable amounts of Cu and platinum group elements (PGE), which could provide an increase in the value, as a potential by-product.

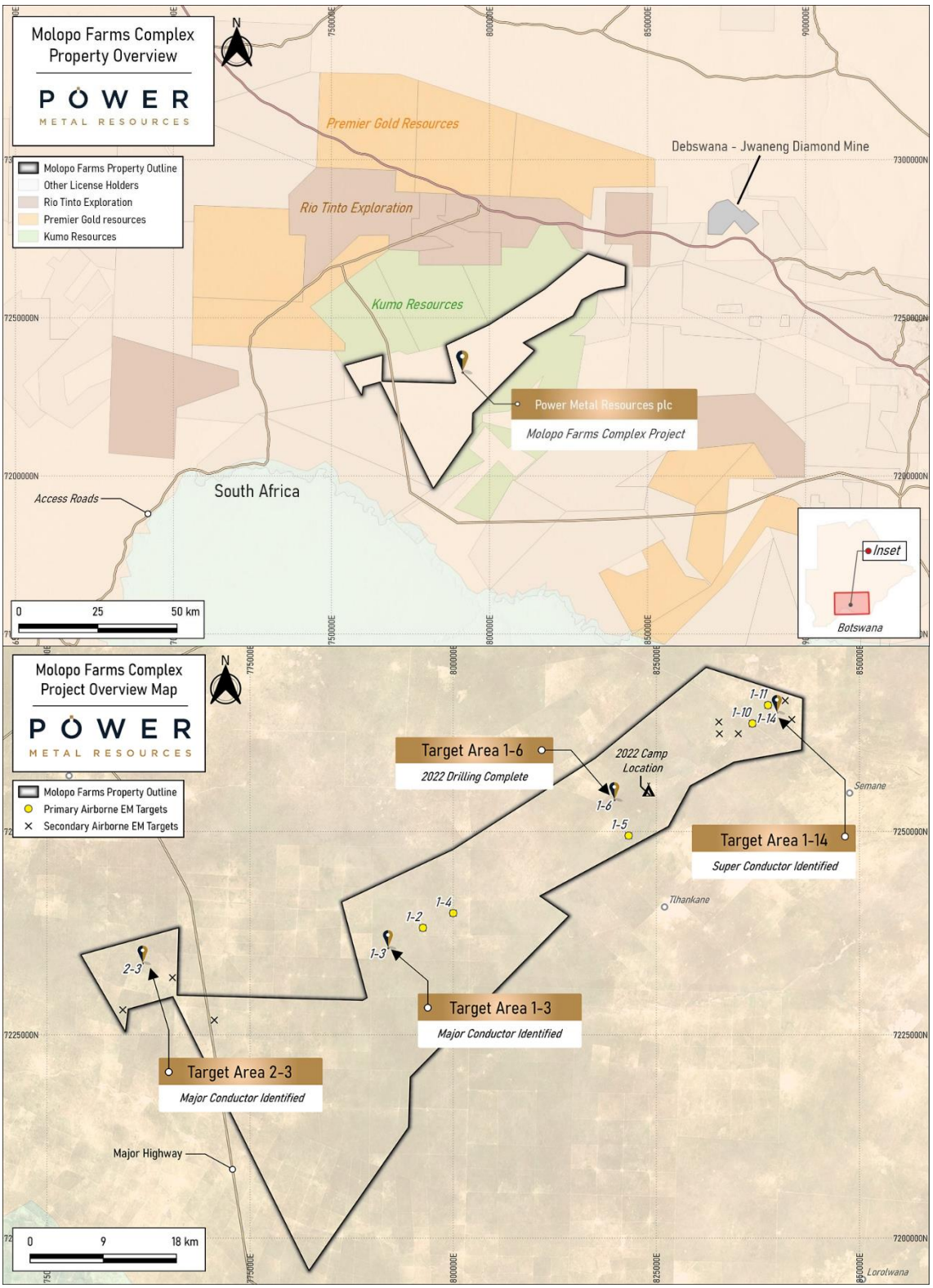

Figure 2: Map of the location of target areas for exploration and respective location of boreholes on the MFC's exploration project.

1.2. Aim and objectives of the research

In this study, the main aim is to characterise the economic potential of the study area, by an understanding of the origin of Ni mineralisation and the significance of the primary and secondary stages for the concentration of metals.

The objectives were to log borehole core to describe the stratigraphy of the studied area near the Jwaneng-Makopong shear zone through the newly drilled KKME 1-6 borehole that intersects the mafic-ultramafic sequences.

Another objective was to define the mineralogy of the intersected rock sequence, including primary and secondary mineral associations, and the main hosts of Ni in mineralised rocks using thin sections descriptions, and TIMA and microprobe analyses of minerals.

The final objective was to calculate the Ni mineral balance using the automated mineralogy technique, microprobe data on mineral compositions and whole-rock data

Chapter 2

Geological Setting

2.1. Overview

Data on the Molopo Farms Complex (MFC) from Gould, et al., (1987) and other authors (Reichhardt, 1994), especially gravimetric and borehole intersections, indicate an elliptical saucer-shaped mafic to ultramafic intrusion, with the longer axis in a NE-SW direction (Reichhardt, 1994). Although previously thought bigger, due to the interception of sills and dykes that were assumed to be part of the main body of the complex (Reichhardt, 1994), the area extension is now calculated to around 13000 km^2, with a thickness of around 3200 m (Prendergast, 2012) with only small variations (Reichhardt, 1994). The major structure has been interpreted as a lopilithic, sheeted intrusion (Beukes, et al., 2019). Due to the Jwaneng-Makopong, ENE-trending, and the Werda-Kgare, NE-trending, shear zones, the Molopo Farms Complex is divided into a northern and southern lobe of a post-deformational syncline (Prendergast, 2012). The former shear zones belong to the regional Kgomodikae-Thabazimbi-Murchison Lineament of which the Zoetfontein Fault is the western extension (Beukes, et al., 2019). The complex occurs mostly overlain by a thick, around 200 m, of mid-Proterozoic Waterberg Group and Phanerozoic Karoo Supergroup sequences, which lie unconformably over eroded portions of the intrusion and which in turn are covered by unconsolidated Kalahari Sands (Prendergast, 2012).

The Molopo Farms Complex is emplaced into the Kaapvaal craton of Archean age, since granitoids in the area have zircons with the same age as zircons of the Witwatersrand Basin, which in turn indicates the extent of the craton itself, believed to extend as far as Mabuasehube in Botswana, to the west of the Molopo Farms Complex (Mapeo, et al., 2004).

The Kaapvaal craton can be divided into an eastern Mesoarchean shield, dated over 3.1 Ga and gneiss-greenstone belts bordering to the north and west with ages of~3.1 and ~2.5 Ga (Mapeo, et al., 2004). This Mid-Archean shield is overlain by sedimentary basins that were deposited in an intra-cratonic environment with volcanic events (Mapeo, et al., 2004). These sedimentary basins include the Witwatersrand basin and the Transvaal basin which are aged 3.05 - 2.85 Ga and 2.6 – 2.1 Ga respectively (Mapeo, et al., 2004) (Figure 1). The Transvaal Supergroup, characterised by siliciclastic and carbonate sedimentary packages, is further split into two major lithostratigraphic units, the Chuniespoort Group and the Pretoria Group, which have been correlated to the sequences found in eastern Botswana, with the Taupone Dolomite Group and Segwagwa Group being correlatives of the Chuniespoort Group and the Pretoria Group (Mapeo, et al., 2004) (Figure 1).

As with the Bushveld Complex, the Molopo Farms Complex intruded the Transvaal Supergroup, and its correlated subdivisions mentioned previously. With the age of the Molopo Farms Complex of 2.054-2.056 Ga (Beukes, et al., 2019) and the Bushveld Complex age of 2.055-2.056 Ga (Scoates, et al., 2021), their emplacement seems to be contemporaneous, and, most likely, are from similar, or even the same, source and were formed through the same large-scale magmatic event (Prendergast, 2012). The Molopo Farms Complex is limited to the north by the Zoetfontein-Palala Shear zone of ~1.98 Ga and to the west by the Kheis orogenic belt, of 1.93 Ga (Beukes, et al., 2019) (Figure 1).

The characteristics of a typical layered intrusion, such as the Bushveld Complex to which the Molopo Farms Complex is most likely related to, are also similar in this intrusion. Layered ultramafic to mafic intrusions are characterised by ultramafic rocks alternating with mafic rocks. Typical ultramafic rocks are dominantly olivine or pyroxene-bearing, whereas typical mafic rocks are plagioclase dominant (Reichhardt (1994); Kaavera et al., (2020); Kaavera et al., (2018)).

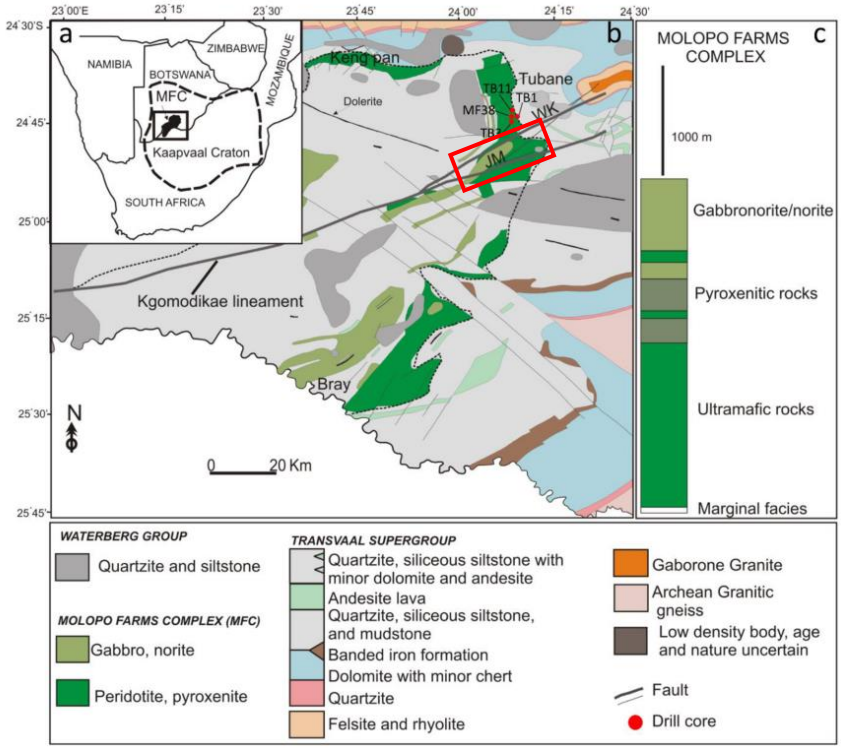

Figure 3: Location of the Molopo Farms Complex in southern Botswana (a), geological map (b) and simplified stratigraphic column (c), adapted from Kaavera et al., (2020). In the rectangle is the Jwaneng-Makopong (JM) shear zone showing the approximate location of borehole KKME 1-6 (Figure 2).

Kaavera et al. (2020) provided the descriptions of the MFC sequences intercepted by two boreholes in the Tubane section, TB1 and TB11, which were drilled in the area slightly north of the Werda Kgare Shear zone that occurs north of the Jwaneng-Makopong shear zone (Figure 3). Dolomitic siltstones belonging to the Transvaal Supergroup represent the country rock. They are characterised by fine-grained quartz within a carbonate matrix. Occasional disseminated pyrite occurs in most samples and rare banded biotite suggests possible low-grade metamorphism.

Marginal norite and feldspathic orthopyroxenite are the mafic units in borehole TB1 and TB11 described by Kaavera et al. (2020) and Kaavera et al. (2018). The marginal norite occurs above the country rock and below the feldspathic orthopyroxenite. It is comprised of leuco-norite and gabbronorite, with the former being more predominant, consisting of orthopyroxene, between 30 and 60 modal %, plagioclase, around 20 modal %, and, clinopyroxene, as an accessory phase with 5 modal % (Kaavera, et al., 2020). Mineralisation occurs up to 1 modal % sulphides (Kaavera, et al., 2020).

Feldspathic orthopyroxenite is dominated by 85 to 90 modal % orthopyroxene and with minor plagioclase (5 to 10 modal %) and rare clinopyroxene (Kaavera, et al., 2020).

Also described from boreholes TB1 and TB11, the ultramafic sequence consists mostly of harzburgite, interpreted as orthopyroxene and olivine cumulates (Kaavera, et al., 2020). Olivine accounts for 65 modal % and where extensive alteration occurs it is replaced with serpentine, talc and carbonates (Kaavera, et al., 2020). Fresh olivine is rare, appearing in a network of serpentine veins. A poikilitic texture is common, with olivine chadacrysts within orthopyroxene oikocrysts (Kaavera, et al., 2020). Orthopyroxene occurs as 30 modal %, locally replaced in the most altered portions of serpentinised samples, by amphiboles, carbonates and talc, however in a lesser degree compared to olivine (Kaavera, et al., 2020).

The magmatic origin of the Molopo Farms Complex is currently regarded as a part of the Bushveld Complex plume that rose up to the margin of the central portion of the thick Kaapvaal craton, most likely with the help of pre-existing, deep and extensive lithospheric fault zones, especially along the Murchison Lineament and Kgomodikae Lineament (Kaavera, et al., 2020). The boreholes were drilled into the Jwaneng Makopong shear zone which is a part of the main Kgomodikae Lineament (Figure 3). Kaavera and co-workers (2020) suggested that the feeder zones of the Molopo Farms Complex are spatially associated with the Jwaneng-Makopong and Werda Kgare shear zones, as suggested by the prominent magnetic anomalies. Petrographic data of the boreholes of the Tubane section indicates that the ultramafic rocks are likely to belong to the feeder zones due to the high Mg# in the orthopyroxenes implying a more primitive magma. This most likely would coincide with the Werda Kgare shear zones corroborated by the magnetic anomalies present (Kaavera, et al., 2020).

The nature of a shear zone implies a high degree of structural discontinuity, as is observed in the Tubane section. The possibility of different magma pulses can also explain the discontinuities (Kaavera, et al., 2020). Kaavera et al., (2020) suggested that the difference between mineralised and non-mineralised portions may depend on different magma pulses. Kaavera et al., (2020) also mentioned the variation in Ni concentrations, suggesting that Ni enriched harzburgites had been in contact with sulphide melt in the feeder conduit or staging-chamber before its emplacement.

Chapter 3

Methodology

3.1. Field work and core logging

A field trip to Botswana was undertaken in order to further increase the understanding of the stratigraphy of the boreholes. The cores were stored in the Molapawabojeng core yard of the Geological Survey of Botswana, south of Lobatse and in the farm area near the drilling location of the boreholes. Here, comprehensive logging work was done on both boreholes, focusing on description of the ultramafic rocks and attempting to find mineralisation in the reported areas and in new possible portions. This work included, besides description of the lithologies, occasional magnetic readings through a magnetic pen on magnetite/oxide-enriched ultramafic portions. Multiple samples were acquired in an attempt to have a representative collection of the sections, as well as, to increase the number of mineralised samples. Most samples selected during the field trip were later delivered to the University of the Witwatersrand, after being cut from the cores and being processed by Kalahari Key Minerals, in order to have a permission to cross the border. In total, after the sampling work performed on the field trip, 67 samples were in the collection at the University of the Witwatersrand. Out of the 67 sample, 44 were selected during the trip, while the remaining (22), except for one, were initially provided by Kalahari Key Minerals as representative of both KKME 1-6 and KKME 1-14 boreholes. At a later date, sample IMK – 05156, from borehole KKME 1-6, was added to the collection as Kalahari Key Minerals had identified relevant chromite mineralisation within.

3.2. Petrography

Petrographic work started with 22 samples from the boreholes KKME 1-6 and KKME 1-14 that were provided by Kalahari Key Minerals, these were delivered to the University of the Witwatersrand, where, firstly they were cut, and then, thin sections were made. From these initial samples, it was possible to gain an overview of the lithologies and mineralisation, although these samples did not represent the various lithologies found in both boreholes. The initial samples were concentrated in the mineralised portions and thus were used as exemplary samples for the mineralisation present on the boreholes which enabled detailed descriptions to be made.

The additional samples were described in hand sample and the representative thin sections were studied under an Olympus petrographic microscope at the School of Geosciences of the University of the Witwatersrand. Finally, a photographic record of the thin sections and a table of hand samples and thin sections descriptions were produced (Appendix I).

3.3. X-ray fluorescence – XRF

Of the 67 samples collected, 27 samples were selected for geochemical analysis. This selection was based on the objectives of the thesis and focussed on borehole KKME 1-6. The samples were picked in order to represent all known mineralised portions, as well as, most of the ultramafic rocks. For the samples, 17 came from borehole KKME 1-6 and 10 samples from borehole KKME 1-14. A total of 27 samples were then subjected to a milling process in the laboratories of the University of Witwatersrand where they were reduced to a fine-grained powder. This powder was then used in a PANalytical Axios XFR spectrometer at the Earth Lab of the University of Witwatersrand, where major and trace/minor element analyses were performed. The settings were as: Maximum current of 66 mA (for trace elements) and 125 mA; Maximum speed level at 4 kW; Maximum accelerator voltage at 60kV for trace elements and 32kV for major oxides. The major element results are measured as weight % while the trace elements are expressed as ppm values. The data is then recorded using the PW2450-SuperQ software. After receiving the preliminary results, a further selection of the most relevant samples for the objective of the thesis resulted in four samples being selected. These samples were chosen primarily on the basis of their elevated Ni and Cr content. In addition, the macroscopic and microscopic descriptions had shown that opaque minerals were more visible due to their apparent larger size and thus would be better for analyses by electron microprobe and Tescan Integrated Mineral Analyser (TIMA). The samples chosen were: IMK – 05139, IMK – 05149, IMK – 05153 and IMK – 05156.

X-ray fluorescence is a non-destructive analytical technique used to determine the elemental composition of material. Its process is based on the irradiation of a sample with high energy X-rays, which will induce a displacement of electrons if the energy of the beam is higher than the atom's binding energy. Afterwards, as the atom regains stability by filling the newly available spot in its orbitals with an electron of a higher energy orbital, it will release a fluorescent X-ray. The released X-ray's energy is equal to the specific difference in energy between two quantum states of the electron and will then be measured by the equipment. The peaks from the X-ray energy are varied and will create a spectrum as a single atom has several electron orbitals, thus, a graphical representation of X-ray intensity peaks is produced. Finally, the peak energies will allow the identification of the element/atom and the peak height/intensity is indicative of its concentration.

Since sample IMK – 05156 was received and processed separately, due to it being received at a later date, it had its own set of control standards. The whole rock X-ray fluorescence data, including the control standards, are shown in Appendix IV.

3.4. Tescan Integrated Mineral Analyser – TIMA

The thin sections of these four representative samples, IMK – 05139, IMK – 05149, IMK – 05153 and IMK – 05156, were used for Tescan Integrated Mineral Analyser (TIMA) and Electron Microprobe analysis.

The TIMA is able to use thin sections, and, through the program of the same name, is able to qualify the different mineral phases present on the samples, then, besides the graphical

information and overall classification of the various mineral phases present on each sample, it is also possible to extract statistical data.

The TIMA analyses were performed at the Earth Lab of the School of Geosciences. The thin sections were carbon coated, then put in the vacuum chamber of the device, and some parameters were selected for the analysis to be done by TIMA, including determination of the spacing of points for analysis, in order to acquire greater or lesser amounts of detail.

Currently, TIMA mineral identification by BSE and X-ray analysis has four different acquisition modes (HrsTka, et al., 2018), of which Dot mapping was used. This methodology uses a BSE grid that covers the entire sample with a specific resolution, based on the pixel spacing (HrsTka, et al., 2018). The spacing used was a 4 µm point grid where the energy-dispersive X-ray analysis were done at each point. The mapping was carried out at an accelerating voltage of 20 V, a beam current of 4 nA and a beam diameter of 1 micron. This method constitutes the best option between the higher resolution methods and the faster methods. The Dot mapping acquisition mode can provide three analysis types, the liberation analysis, as well as bright phase search and Section analysis. Furthermore, the mineral abundances are reported to the end user by volume with weight proportions calculated using specific gravity.

The TIMA software (HrsTka, et al., 2018), was used to process the results, here it was possible to access the data and further analyse it. Since every point that was analysed has an individual elemental signature, that shows a percentage value for each different element present in it, the program will correlate those values to the ones from mineral phases that are present in the TIMA database. This means that if the elemental signature of a point is very similar to a certain mineral phase, for example, pentlandite, it will classify the said point as a pentlandite.

Consequently, the thin section will appear colour coded based on what the program has classified the mineral phases as in the various points, giving the user a quick and graphical display of the different mineral phases present in the thin section. However, it is important to mention that these values are not as accurate as microprobe data due to using the Dot mapping method that has a smaller resolution comparatively to the electron microprobe.

Some portions of the thin sections might have not been classified by the program. This may be due to the values of those specific parts not being similar enough to the mineral phases present in the program's database. As such, the user will have to use an important function of the software and manually identify an unrecognised mineral phase. Thus, by adding new/variations of some mineral phases the program may now use the newly added phase by the user and review the thin sections, consequently altering some portions to the newly added phase. In extremely altered rocks this can become somewhat problematic, due to the high compositional variation that occurs in certain phases, like serpentine. There may be certain portions of the same overall mineral phase, that might be more or less altered, and, as such, have a higher or lower amount of the various elements that belong to the final alteration product or the protolith. In this work, many antigorite, actinolite and tremolite phases had to be added, due to their varying compositions relative to the 'standard' compositions that are present in the program database.

It is also important to mention that, in the case of trace/minor elements in certain silicate phases, as is the case of Ni, the elements will not be accurately analysed in those phases. If the user adds to a mineral phase Ni as a trace element, then the program assumes that the mineral phase has the value that the user added in all its portions. To overcome this, several

varieties with slightly varying Ni content of each secondary silicate (serpentine, amphibole or chlorite) were introduced into the database to give a higher statistical confidence and reliable representation of the Ni distribution.

The TIMA software is able to provide statistical data of the thin section, most importantly, the percentage of each mineral phase in the thin section and the amount of Ni in each mineral phase, either relative to its total weight percentage or to 100%. This means that it is possible to extract relevant Ni data, including the amount of Ni per mineral phase, and how much it accounts for in the overall amount of Ni present in the sample. This allows a statistical calculation as to how much of the Ni in the samples belongs to the silicate phases or to sulphide phases. However, this statistical data was only obtained for four samples which belong to borehole KKME 1-6 and, thus, are not representative of the whole borehole and much less the area of study. Nevertheless, this statistical data is a relevant starting point for the characterisation of the study object.

3.5. Electron Microprobe

The mineral compositions were determined on a JEOL SUPERPROBE electron probe, model JXA-8200 in dispersed wavelength mode (JEOL, 2006) in the Faculty of Sciences of the University of Lisbon, Portugal. Using the electron probe microanalyser, the samples were analysed with a 25 nA current, the electron beam accelerated to 15 kV and an ample beam of 5 µm. The analyses were calibrated using the internal material standards with an error reproduction lower than 2% and generally about 1%. The ZAF software correction provided by JEOL was used for matrix correction.

The four thin sections of the samples IMK – 05139, IMK – 05149, IMK – 05153 and IMK – 05156, were carbon coated in a vacuum chamber, where, a carbon filament was vaporised due to electric current flowing through it and the vaporised carbon particles fall and adhere to the thin sections in the vacuum chamber.

The thin sections were then put in the electron microprobe. Here, a four day-long work programme was undertaken in order to select the best possible array of data that is representative of the minerals in the samples and that are most important for the objective of the thesis. Consequently, there were 773 points for analysis selected, belonging mostly to minerals of the serpentine group, pyroxene group, and all mineralised portions, such as Ni-Fe sulphides, Ni-Fe alloys, chromite and Ni arsenides. The electron microscope analysis is dependent on the mineral group, therefore, all selected points for analysis were named and grouped in relation to the respective sample and mineral group so that the software analyses are done using the correct mineral parameters.

All data collected through electron microscope analyses is then processed in MS Excel, here the data is subject to a calculation of chemical formulas to discern between different types of mineral phases within a mineral group, leading to a more accurate description of which mineral phase it is and their elemental characteristics (Appendix V).

Chapter 4

Magmatic stratigraphy of borehole KKME 1-6

The focus of the petrographic work was on borehole KKME 1-6 because it has the best Ni mineralisation and thus all the geochemical data were gathered on this borehole.

The logged portions of boreholes KKME 1-6 and KKME 1-14 have considerable lithological differences. Borehole KKME 1-6 is comprised by an ultramafic sequence, while KKME 1-14 contains alternating sequences of ultramafic and metamorphosed sedimentary lithologies.

In borehole KKME 1-6, the studied ultramafic sequence is comprised of mostly thick layers of serpentinite, alternating with pyroxenite, dunite and harzburgite (Figure 4). An overall intense serpentinisation was observed, however, local relatively fresher portions of orthopyroxenite and olivine-bearing pyroxenite were also observed. The latter harzburgite generally contained fine- to medium-grained olivine but can occasionally display poikilitic textures due to large olivine oikocrysts.

Borehole KKME 1-6 was logged from a depth of 208 m to the end of the borehole at 597.7 m. The first 208 m correspond to Kalahari country rocks. All different lithologies occur with varied thicknesses, from small one-metre-long patches to near 100 m portions.

Besides matrix alteration, shown by the presence of wide spread serpentine alteration of the ultramafic rocks, a plethora of faults and fractures were also present. The fractures and faults displayed a variety of inclinations, from sub horizontal, angled and vertical, without a predominant inclination noted. Frequently, fault zones of larger dimensions, above 1 m, were characterised by a shattered core, common veining of calcite and/or quartz and intense alteration. Talc and asbestos-enriched veins were also present, which showed some association with the highly fractured fault zones. Veining was common throughout all the lithologies, with varying intensity, mostly as millimetric to centimetric veins of serpentinite, talc and asbestos, the latter sometimes occurring in a stockwork-like texture.

Magnetite-rich zones were also detected, either as small patches, up to 15 cm, in a magnetite-rich layer, or within the massive serpentinites, where a magnetic signal was detected through a magnetic pen.

The majority of the mineralisation found was as small, sporadic, sulphide specks, corresponding to less than 1% of the rock. However, some sulphide blebs, up to 5 cm, were visible in massive serpentinite after orthopyroxenite and additional localised sulphide blebs were also detected in other parts of the borehole.

Contacts between lithologies were mostly sharp, with the exception of some broken contacts, including the contacts between different ultramafic rocks and with the fracture zones. The degrees of alteration were gradual and, depending of the level of alteration, the transitions between massive serpentinite layers to highly altered ultramafic rocks were common as they intercalate where the protolith was more or less -fresh.

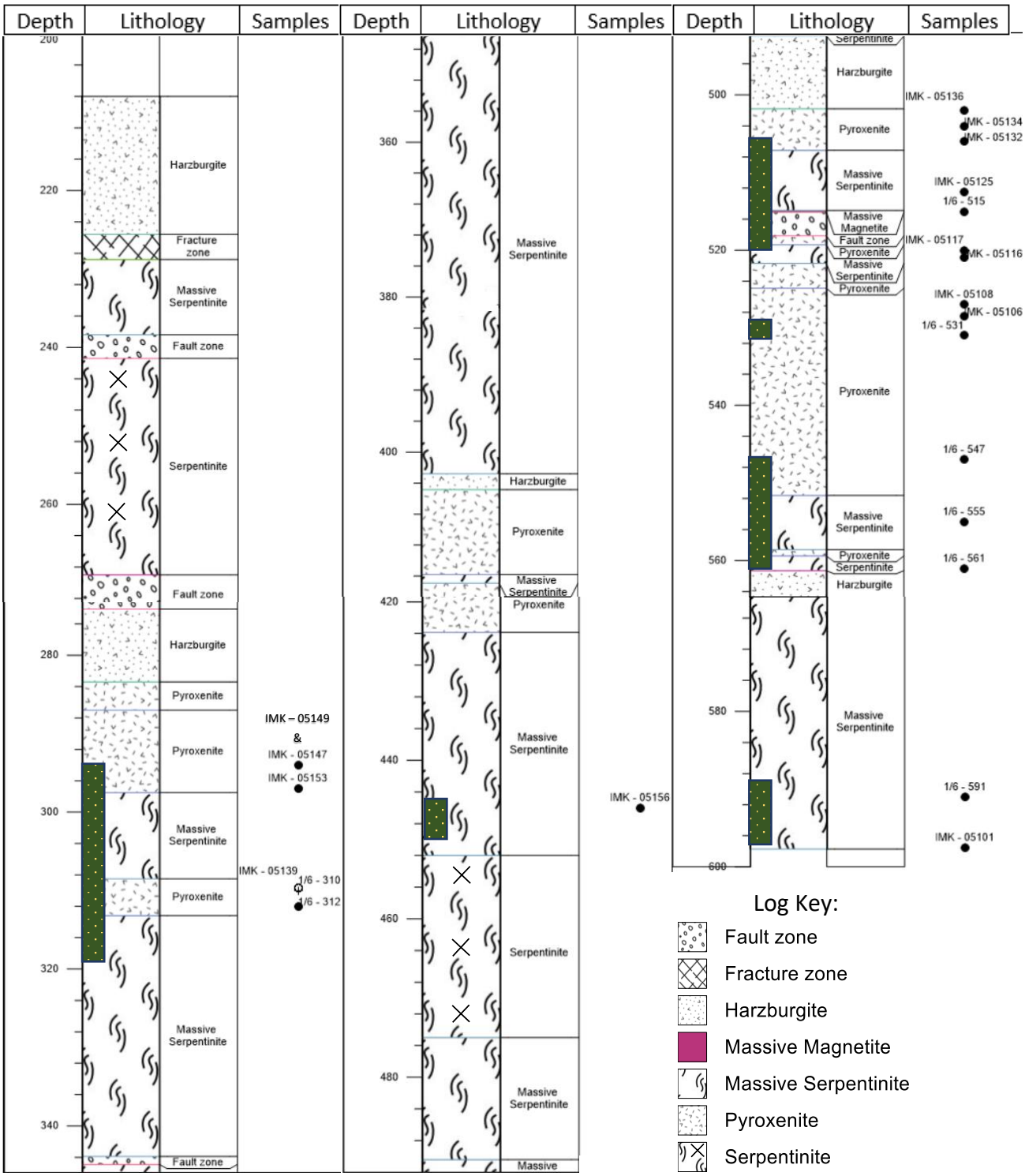

Figure 4: Stratigraphic column of the ultramafic section of borehole KKME – 1/6, with mineralised portions marked green at depths: ~294-319m, 446.3-451m, 506-520.7m, ~531m, 547-561m and 589-598m.

The ultramafic portion of borehole KKME – 1-6 begins at the depth of 208 m as a serpentinite after harzburgite, a highly altered, homogeneous portion characterised by local secondary sulphide disseminations that are confined in fracture veinlets (1-2 mm thick). As depth increases rocks become progressively more fractured and enriched in orthopyroxene oikocrysts, also, local magnetite veining (0.1-3 mm) at ~45º was observed. A sharp contact with serpentinised orthopyroxenite occurs at a 225.6 m depth with a ~3 m thick fault zone where the core is broken and altered into a clay-like material (Figure 5).

Figure 5: Altered ultramafic rocks in borehole KKME 1-6, from ~226m to ~232m depth. Core diameter is 4.76 cm (NQ)

Downwards, at a depth of 228.8 m, a further sharp contact with a ~10 m massive serpentinite after harzburgite occurs, where no relics were observed and an increase in core fracturing took place with increasing depth (Figure 5). Local magnetite veining is oriented generally subparallel and millimetric in thickness. At a 238.4 m depth a sharp contact with another ~3 m thick fault zone occurs with stockwork features filled with serpentine and talc veining (~30 modal % of the entire unit) parallel to perpendicular to the core axis.

At a depth of 241.4 m, a sharp contact with highly altered serpentinite after harzburgite with no relics occurs with an increase of fracturing towards another fault zone at a 269 m depth (Figure 6). Here, another sharp contact between the fault zone and underlying serpentinite occurs. The fault zone continues down to a 274.1 m depth and contains serpentine and talc veining (~30 modal %) at ~45º to core axis and with some stockwork textures.

Figure 6: Serpentine and talc veining in ultramafic rocks in borehole KKME 1-6, from ~239m to ~244.5m depth. Core diameter is 4.76 cm (NQ).

A new sharp contact occurs between the previous fault zone and harzburgite at a 274.1 m depth. Medium to coarse grained harzburgite with 20 modal % olivine is locally fractured and gradually changes into pyroxenitic lithology at a 283.4 m depth. From 283.4m to 287 m depth, medium to coarse grained olivine pyroxenite occurs with 5-12 modal % olivine and local serpentinite veining (0.3-1 mm thick) alternating with serpentinite zones. At a 287 m depth, the rock composition changes with a decrease in olivine to less than 1 modal %, indicating the transition to medium-grained pyroxenite, which is characterised by serpentine veining (45º-55º to core axis) and intercalates with massive serpentinite. Rounded sulphide blebs (<0.5 modal %) are associated with serpentine and other secondary silicates.

At a 297.5 m depth a new sharp contact occurs between overlying pyroxenite and massive serpentinite after harzburgite, which contains rare sulphide grains, common magnetite and talc veinlets (Figure 7). This massive serpentinite extends to a depth of 402.8 m but is intercepted by a 1 m thick fault zone between a 343.9 m and 344.9 m depth where the core is completely broken. At a 402.8 m depth massive serpentine changes to harzburgite with poikilitic texture of olivine chadacrysts to a 404.85 m depth, underlain by medium- to coarse-grained olivine pyroxenite. An increase in the degree of serpentinisation to massive serpentinite occurs downwards; additionally, veinlets of serpentinite and asbestos, up to 3 cm thick at 45º to core axis and magnetite veins, 1 mm to 1 cm thick at 45º to core axis, are abundant.

Figure 7: Fractured core in a fault zone in borehole KKME 1-6, from ~296m to ~302m and ~308 to ~315 m depth where mineralised samples IMK – 05139 and IMK – 05149 used in microprobe and the TIMA are located. Core diameter is NQ.

Massive serpentinite after harzburgite (and, possibly, dunite) starts at a 415.8 m depth. Harzburgite is characterised by asbestos veining (1 mm thick) and gradually changes to olivine pyroxenite, serpentinised to variable degrees, within an interval of 416.9 to 423.85 m depth.

Figure 8: Talc and serpentine veinings in serpentinite in borehole KKME 1-6, from ~440m to ~446.5m depth where samples IMK – 05156 used in microprobe and the TIMA is located. Core diameter is NQ.

This pyroxenite is followed downwards by massive serpentinite after pyroxenite until a 452 m depth, where thick magnetite veins occur (5-8 modal %), up to 4 cm thick and oriented at ~45º to core axis (Figure 8). An asbestos veinlet stockwork, sulphide mineralisation up to 2 modal %, disseminated sulphides along fractures and interstitial sulphide blebs up to 6-7 mm in size occur in this interval. Spots of green botryoidal mineral of secondary silicates or carbonates after sulphides were also observed. From a 452 m to 475 m depth massive serpentinites after harzburgite are characterised by brown to reddish relics of secondary magnetites after serpentinised olivine. Typical relic textures of cumulus olivine with interstitial chromite are also observed. Magnetite veinlets up to 3 mm thick and net-textured secondary magnetite and asbestos veining in stockwork-like texture are common. Then, from a 475 m to 490.4 m depth there is a similar massive serpentinite, however, it contains less veinlets compared to the upper portion. At a 490.4 to 492.4 m depth, a 2 m thick massive serpentinite with asbestos and talc veining up to 15 modal % and thin magnetite veinlets occur in the borehole section.

At a 492.4 m depth a sharp contact between overlying massive serpentinite and underlying harzburgite with poikilitic textures and completely serpentinised olivine chadacrysts occurs. A gradual increase in fracturing and brecciation cemented with talc and serpentinite veinlets toward the base of the layer is observed. At a 501.8 m depth harzburgite changes to orthopyroxenite, until a 507.15 m depth, Orthopyroxenite is locally enriched in olivine, with secondary silicate veinlets and fractures as well as an increasing degree of serpentinisation and magnetite segregations towards the base. From a 507.15m to 514.9m depth a massive serpentinite after pyroxenite occurs; serpentinite becomes more enriched in interstitial and veinlet magnetite toward the base. At a 514.9 m to 515.1 m depth serpentinite contains a 20 cm thick massive magnetite layer rimmed by phlogopite-rich zones. From 515.1m to 518.15m depth a large fault zone occurs as indicated by highly altered and broken core with talc and serpentine alteration/veining.

At a 518.15m depth, a sharp contact with a 1 m thick olivine-rich pyroxenite occurs. Pyroxenite gradually changes into olivine-free pyroxenite characterised by serpentine veining perpendicular to 45º to core axis. Then, massive serpentinite occurs in an interval of 519.3 to 521.7m depth, which changes back to an olivine-bearing variety and to olivine pyroxenite with serpentinite veining at a depth of 524.9m (Figure 9). In an interval between 524.9 to 551.6m depth pyroxenite does not contain olivine and is characterised by a fine- to medium-grained granular texture with regular serpentine veining at ~45º to core axis, magnetite alteration (reddish brown in colour) and sporadic elongated orthopyroxene needles up to 1.2 cm long that are slightly oriented parallel to the veining.

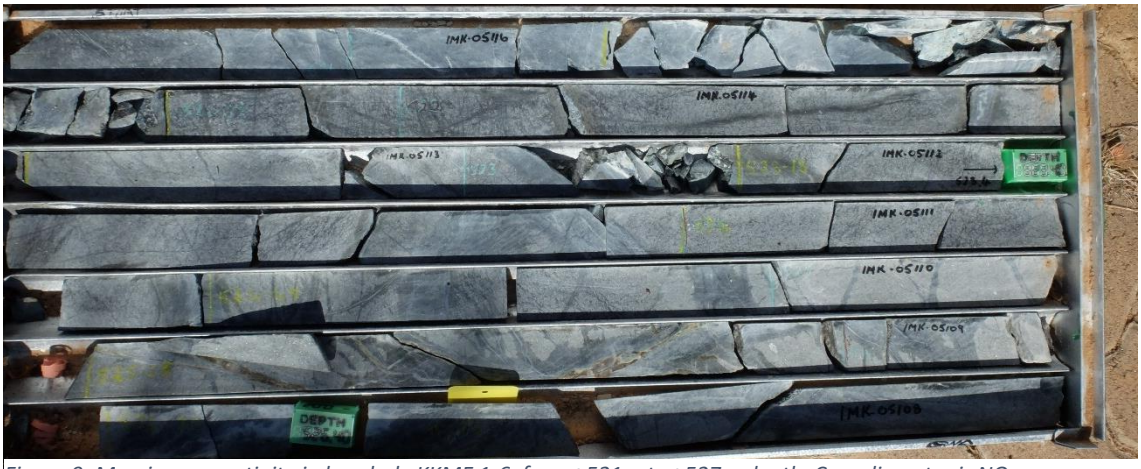

Figure 9: Massive serpentinite in borehole KKME 1-6, from ~521m to ~527m depth. Core diameter is NQ.

A narrow interval of olivine-bearing pyroxenite with possible interstitial plagioclase occurs at a ~531m depth. At a 536.2m depth a near vertical serpentine vein with sharp contacts and phlogopite-rich margins up to 5 cm thick occurs in the borehole section.

Downwards, a sharp contact at a 551.6m depth a massive serpentinite occurs after poikilitic harzburgite with relics and oikocrysts of orthopyroxene. Local veining of talc and/or magnetite continues down to a depth of 558.6 m. In an interval of 558.6 m to 559.4 m depth a pyroxenite layer contains ~15 modal % serpentine, changing into highly altered serpentinite downwards to a depth of 561.3m. Coarse grained poikilitic harzburgite with up to 2 cm orthopyroxene oikocrysts, 20 modal% serpentine and magnetite and sporadic sulphide blebs occurs in an interval of 561.3-565 m depth. Finally, the lowermost portion of the core, in an interval of 565m to 597.7m depth, exposes a broken contact with massive serpentinite after poikilitic harzburgite with extensive magnetite replacement and veining.

In summary, the studied section is characterised by the intercalation of highly variably serpentinised and altered harzburgite and orthopyroxenite. Visible sulphide mineralisation occurs in the depth intervals of 294-319, 446.3-451, 508-520.7 and 569-598 m. The thickness of the mineralised intervals varies from 2 to 25 m. The two thicker zones are confined to the intercalation of the pyroxenitic and harzburgitic lithologies whereas the narrower intervals of sulphide mineralisation occur within chromitiferous harzburgite nearing towards dunite.

Chapter 5

Petrography

The petrographic study was carried on 21 thin sections comprised of only ultramafic sequences from borehole KKME 1-6. This was due to the preliminary data gathered by KKM, which indicated a higher Ni anomaly and because this borehole was characterised by the most mineralised portions.

5.1. Ultramafic Rocks

5.1.1. Harzburgite

Harzburgite is as a dark-coloured, massive textured, phaneritic rock, characterised by euhedral to poikilitic and granoblastic orthopyroxene grains (0.5-2mm) of greyish brown tint that constitutes about 60 modal % of the rock, and a dark to green-coloured fine matrix, about 40 modal %, corresponding to olivine replacement by serpentine and tremolite-actinolite series amphiboles. Locally, the harzburgite has a poikilitic texture (poikilitic harzburgite) where relic, olivine chadacrysts can be observed in less altered samples. Olivine also occurs as interstitial grains between granoblastic orthopyroxene. Primary phlogopite (up to 5 mod %) occurs as interstitial platelets, which have been replaced by amphiboles and chlorite in altered rocks.

Secondary alteration is common (up to ~40-50 %) as most harzburgite portions are serpentinised to a variable degree. Serpentinisation is on average higher than in pyroxenite, in the form of fine-grained serpentine, talc and bastite aggregates. Additionally, late-stage cross-cutting veining of serpentine, talc, carbonate and chlorite with secondary magnetite and chromite are also present. The chromite proportion varies from 0.5-7 modal %. Chromite margins are variably replaced by magnetite and secondary silicates. Disseminated sulphides (<2 modal %) occur mostly within the olivine oikocrysts in localised zones. These sulphides are yellow to white-coloured intergrowths with other ore minerals and their diverse mineralogy is described in Chapter 7 . Harzburgites with a very high degree of alteration were logged as (massive) serpentinites.

5.1.2. Pyroxenite

Pyroxenite (Figure 10 a & b), is, generally, less altered compared to the rest of the ultramafic rocks. It is composed of medium sized pyroxene grains, 2 to 3 mm in size, of brown to light grey colour, which comprises about 60 modal % of the rock. Olivine is rare, with the exception of olivine-bearing pyroxenite, where 1 to 10 modal % olivine occurred, locally reaching 20 modal %. Pyroxenite is mostly altered to serpentine and secondary magnetite. A few samples characterised by a harrisitic texture are composed of elongated orthopyroxene crystals. Pyroxene is predominantly represented by orthopyroxene with none or very rare thin

clinopyroxene exsolutions. Primary phlogopite fills interstitial space between orthopyroxene grains. The proportions of the chromite in orthopyroxenite are lower than in harzburgite and the sizes of chromite grains are also smaller in pyroxene-dominant rocks.

Alteration is predominantly associated with olivine in olivine-bearing pyroxenite, with secondary alteration in the form of late-stage veining of serpentine, talc, carbonates, amphiboles of actinolite-tremolite series and magnetite. Orthopyroxene is replaced by bastite, amphiboles, chlorite and locally by fine-grained serpentine. Disseminated sulphide mineralisation in a serpentinised matrix is represented mostly by single grains 1-10 microns in size, but locally by intergrowths and complex blebs up to 5-10 mm in size.

5.1.3. (Massive) Serpentinite

Serpentinite, Figure 10 c) & d), is the most abundant lithology as it is the result of the serpentinisation of the original ultramafic protolith. Serpentinite occurs mostly as massive serpentinite characterised by a fine-grained texture and a composition of ~90 modal % serpentine-amphibole matrix with very rare local relics, up to 5 modal %, of pyroxenes and/or olivine, locally as relic oikocrysts. Serpentine is mostly fine-grained and can occur interstitially, in veining and as the major component of the matrix. The majority of amphiboles belong to the actinolite-tremolite series and correspond to a smaller portion of the matrix forming medium- to coarse-sized euhedral long prismatic crystals and radiating aggregates. Other alteration minerals include talc (<1 to 15 modal %), asbestos or fibrous chrysotile (<1 to 10 modal %), magnetite (locally up to ~90 modal %), phlogopite (<5 modal %) and local chlorite (up to 20 modal %). These alteration minerals are mostly associated with veining, thus, the proportion of these minerals is dependent on the presence of veining where it may account for up to ~90 modal %, but is more commonly between 5-20 modal %.

Asbestos and talc only occur in veins but magnetite can appear both interstitial and in veins where it may form massive lenses up to 20 cm thick as in the sample KKME 1-6 – 515. Chlorite alteration appears to be of a later stage and superimposed onto other alteration minerals. In the sample IMK - 05149 1-mm thick veinlets composed of fine-grained clinopyroxene with dusty magnetite disseminations cross-cut the serpentine-amphibole matrix. Sulphides can occur disseminated or in close association with veining, as very small grains (tens of microns in size), or larger blebs (4-5 mm in size) accounting for 1-2 up to 5 modal %. Locally, sulphides may replace altered chromite, as seen in the sample KKME 1/6 – 446 or occur inside serpentinised olivine chadacrysts. Sulphide aggregates have a light-yellow to white colour and are dominated by either pentlandite or pyrrhotite. The detailed description of the sulphide assemblages in serpentinite is given in Chapter 7 .

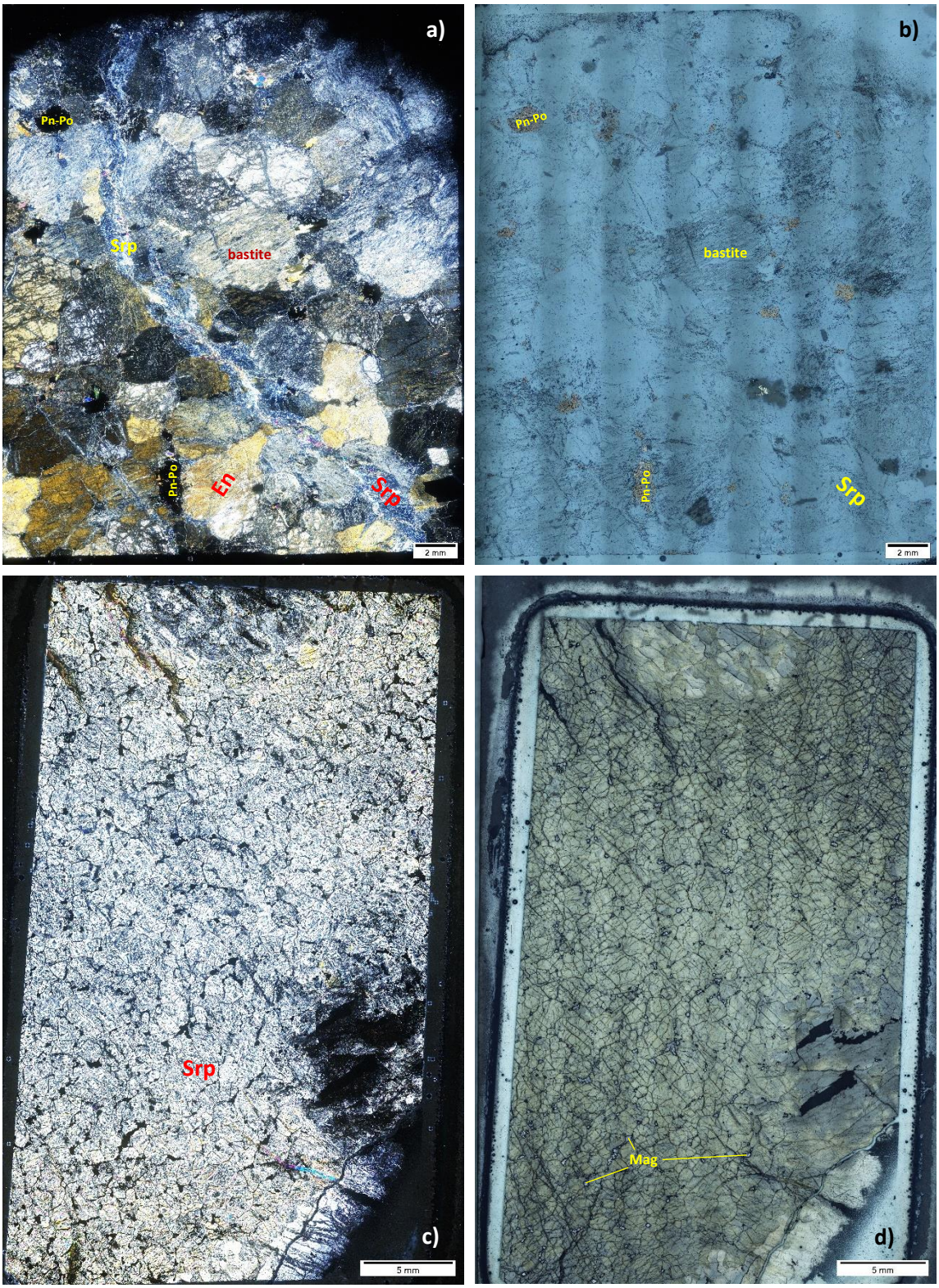

Figure 10: Thin section images of the ultramafic rocks showing degrees of alteration: a) Cross Polarised Light image of orthopyroxenite, IMK – 05139; b) Plain Polarised Light view of orthopyroxenite, IMK – 05139; c) Cross Polarised Light image of massive serpentinite after harzburgite, 1/6 – 591; d) Plain Polarised Light view of massive serpentinite after harzburgite, 1/6 – 591.

Chapter 6

Whole rock geochemistry

6.1. X-Ray Fluorescence Spectrometry

A total of 17 samples from the borehole KKME 1-6 were submitted for X-ray fluorescence analysis to determine the whole rock chemistry, including variations of the major and trace elements in the section and in the different lithologies.

One of the parameters obtained in these analyses, the abbreviation LOI - Loss of Ignition, represents the amount of volatiles present in rock, where a higher value of LOI denotes a more altered rock. The results are plotted in Figure 11, adapted from Deer et al., (1992), where the contents of MgO vs LOI (wt.%) are displayed and it's possible to verify the relative position of the samples with the filtering relative to the serpentine and chlorite composition lines. In Figure 11 the filtering line corresponds to the benchmark used to distinguish between altered and unaltered samples (Kaavera, et al., 2018); (Deer, et al., 1992).

The LOI values encountered are varied, and the variation depends on the rock type. In pyroxenites, LOI has a minimum value of 0.93 wt% and a maximum of 11.72 wt%, with a median of 5.48 wt%. These results show that some pyroxenite samples are highly altered occurring near the serpentine line and filtering line on Figure 11, while the others are relatively fresh. In contrast, harzburgite has a minimum LOI value of 4.80 wt%, a maximum of 13.28 wt% and a median of 11.32 wt%. This data supports the petrographic observations that confirms the generally higher level of alteration of harzburgites compared to that of pyroxenites.

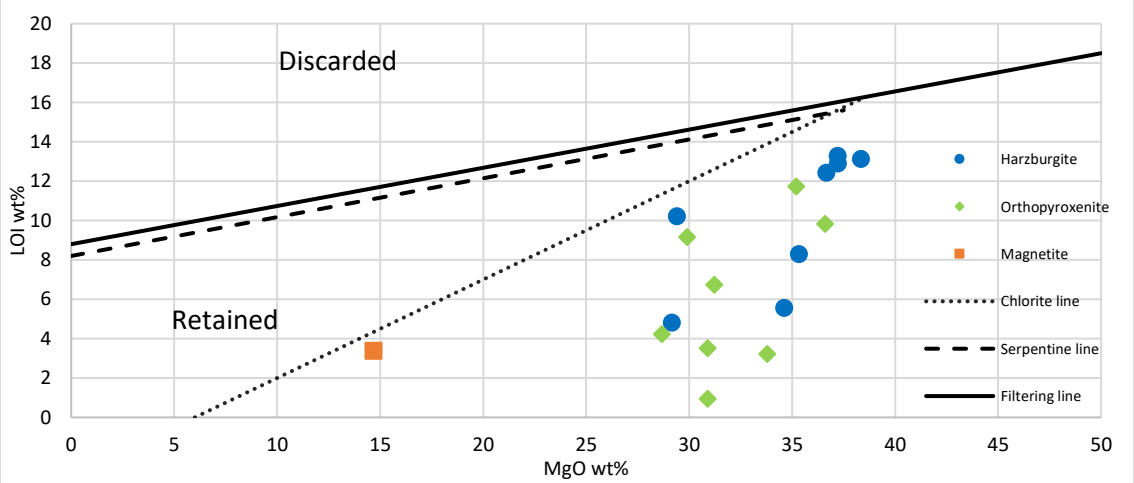

Figure 11: MgO vs LOI (wt%) plot, after Deer et al., (1992), indicating the alteration of the studied samples. The filtering line delineates between retained and discarded samples, due to their alteration. Serpentine, chlorite and filtering lines from Deer et al., (1992).

Keeping in mind the high level of alteration, all rocks were divided into harzburgite and pyroxenite based on their identification using relic textures observed during petrographic study, while none of these samples was characterised as dunite. The major rock types are harzburgite

and orthopyroxenite (Appendix IV and Appendix V) whereas massive magnetite is sampled from a single vein at the depth of 515m.

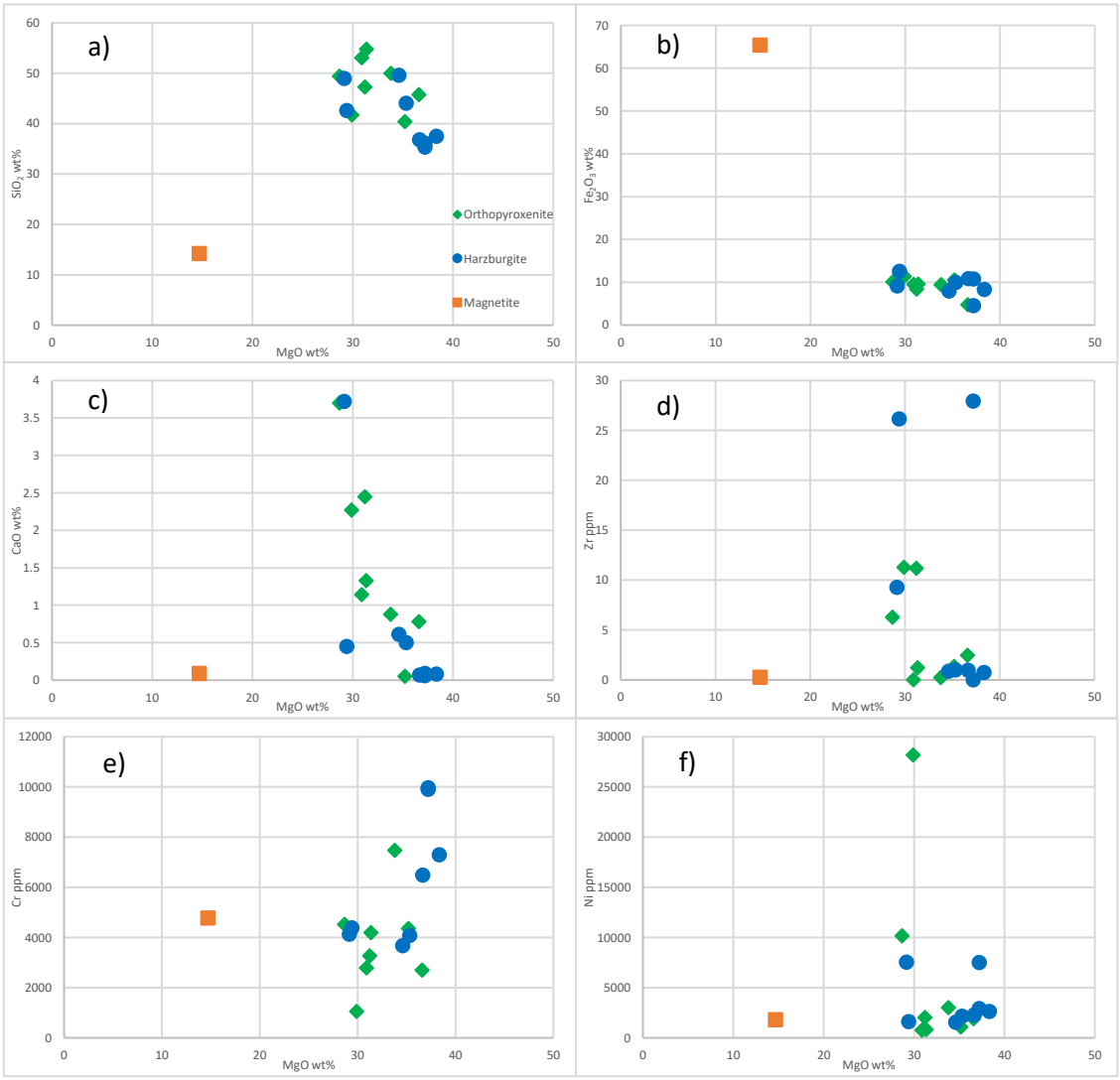

Figure 12: XRF compositional data of orthopyroxenite (green), harzburgite (blue) and magnetite vein (orange): a) SiO_2 vs MgO (wt%); b) Fe_2O_3 vs MgO (wt%); c) CaO vs MgO (wt%), d) Zr ppm vs MgO wt%; e) Cr ppm vs MgO wt%; f) Ni ppm vs MgO wt%.

The orthopyroxenite contains 40.38 to 53.02 wt% SiO_2, with a median of 48.31 wt% SiO_2, 28.68 to 36.6 wt% MgO, with a median of 31.29 wt% MgO, 4.76 to 11.33 wt% Fe_2O_3, with a median of 9.52 wt% Fe_2O_3 and 0.05 to 3.7 wt% CaO, with a median of 1.24 wt% CaO, as major oxides (Figure 12, Appendix IV).

The harzburgites contain 35.33 to 49.57 wt% SiO_2, with a median of 40.02 wt% SiO_2, 29.16 to 38.34 wt% MgO, with a median of 36.01 wt% MgO, 4.5 to 12.51 wt% Fe_2O_3, with a median of 9.54 wt% Fe_2O_3 and 0.06 to 3.72 wt% CaO, with a median of 0.27 wt% CaO, as major oxides (Figure 12, Appendix IV).

The magnetite vein, sample 1/6 – 515, contains, wt% 14.19 SiO_2, 14.69 MgO, 65.38 Fe_2O_3 and 0.09 CaO for the major oxides (Figure 12 a, b, c, Appendix IV).

The chromium content appears to be correlated with MgO content, as visible in Figure 12, where higher MgO values correspond to higher Cr, additionally, the same correlation is also visible with LOI as shown in Figure 12. The orthopyroxenite samples had a minimum of 1048 ppm Cr, a maximum of 7469 ppm Cr and a median of 3725 ppm Cr, whereas for the harzburgites, there is a minimum of 3675 ppm Cr, a maximum of 9970 ppm Cr and a median of 5428 ppm Cr (Appendix IV). Harzburgites have higher LOI, Cr and MgO values than pyroxenites (Figure 12 e), and Figure 11). The high LOI values present in the harzburgites are associated with the relative abundance of alteration/serpentinisation after olivine. It is possible to correlate Cr enrichment with the more altered samples, including sample IMK – 05156, where highest and anomalous value corresponds to the chromite-bearing horizon (Figure 12 e) and Figure 11).

The XRF trace element data shows that the chromite-bearing horizon of sample IMK – 05156 corresponds to 9899 Cr ppm and 2.44 Cr_2O_3 wt% according to the XRF major oxide data. In sample IMK – 05101, a serpentinised poikilitic harzburgite, the highest value is registered at 9970 ppm of Cr, although it has 1.66 Cr_2O_3 wt%. The median Cr value also denotes a general enrichment, at 4185 Cr ppm. The magnetite vein contained 4772 ppm Cr, higher than the orthopyroxenite median value but below the harzburgite median value (Appendix IV).

Besides Cr , XRF trace element analyses included other elements, such as V, Co, Cu, Zn, Zr and Sc. Vanadium values are similar in both pyroxenites and harzburgites where the median values were 54 and 73 ppm V respectively, additionally, the highest and lowest values belonged to pyroxenites (107 and 20 ppm V, respectively), (Appendix IV).

Cobalt (Appendix IV) displays some enrichment in certain samples, with a maximum value of 571 ppm Co in IMK – 05156, from a harzburgite that is also rich in Cr and with visible chromite segregations. For Co, there is a median value of 135 ppm Co and 87 ppm minimum for the pyroxenite samples denoting lower concentrations compared to the harzburgite samples with a maximum, a minimum and a median of 571, 65 and 115 ppm Co respectively. In the magnetite sample, a value of 177 ppm Co was detected, placing it above the median values of the orthopyroxenite and harzburgite.

Only three pyroxenite samples had values above the detection limit of 1 ppm for Cu, thus, Cu variations are extremely high, with a maximum of 1407 Cu ppm and a minimum below the detection limit in pyroxenites, whilst in harzburgite, Cu values are mostly below the detection limit except for the sample 1/6 – 310.6 (Appendix IV). Copper enrichment appears to correlate with Ni enrichment, since the three samples mentioned also have above average Ni values, and, the sample IMK – 05149 with the highest Ni concentration, has the highest Cu value. However, 1/6 - 446.9, chromitiferous harzburgite, with 7500 ppm Ni does not reveal elevated Cu values. The magnetite vein contains 60 ppm Cu (Appendix IV).

Zinc (Appendix IV) shows a narrow range of variations, with orthopyroxenite recording a highest value of 92 ppm Zn, versus a peak at 63 Zn ppm in harzburgites. Minimum Zn values are 48 ppm and 46 ppm in pyroxenites and harzburgites, whereas median values are 56 ppm Zn and 56 ppm Zn, both respectively. Thus, there is no evident distinction between both rock types in terms of their Zn content although, the highest and slightly anomalous maximum Zn value (92 ppm) occurs in the sample IMK – 05149 that has the highest Ni concentration.

Zirconium (Appendix IV) was detected in most samples, with a minimum value below the detection limit of 0.01 ppm Zr in olivine-rich harzburgite that is compositionally close to dunite in composition, with a maximum of 28 ppm Zr, and a median of 1 ppm Zr. In orthopyroxenite, the maximum value is 11 ppm Zr, the minimum is below the detection limit and the median is at 2 ppm Zr. These results show that the average Zr concentration is very low and near the detection limits whereas four samples of orthopyroxenite and harzburgite show the anomalous values relative to the average, furthermore, the orthopyroxenite median is slightly higher than in harzburgite.

Zirconium values may indicate the abundance of a trapped melt (Kaavera, et al., 2018), thus, the samples with the anomalous values may be correlated to a higher amount of trapped melt in these cumulates.

The ratio between copper and zircon, Cu/Zr, is also used to indicate the segregation of sulphide mineralisation (Kaavera, et al., 2018), thus, it was calculated for the samples that have the Cu contents above the detection limit. The calculated Cu/Zr has a minimum value of 70 and a maximum of 139. These values demonstrate the additional accumulation of chalcophile Cu relative to its expected concentrations due to solely magmatic differentiation and fractionation into residual liquids. However, the petrographic observations show that the studied sulphide assemblages are not primary magmatic so these deductions cannot be directly applied and require careful consideration.

The chromium-vanadium ratio, Cr/V, was calculated in order to better appreciate the degree of magmatic differentiation in the samples (Figure 13). A maximum value of 221 in IMK – 05101 serpentinised poikilitic harzburgite suggests that is likely to be the most chemically primitive rock, conversely, an altered olivine pyroxenite with a minimum Cr/V value of 26 may correspond to the most differentiated rock in the set. Both pyroxenites and harzburgites have similar median values and outliers of Cr/V (Figure 13).

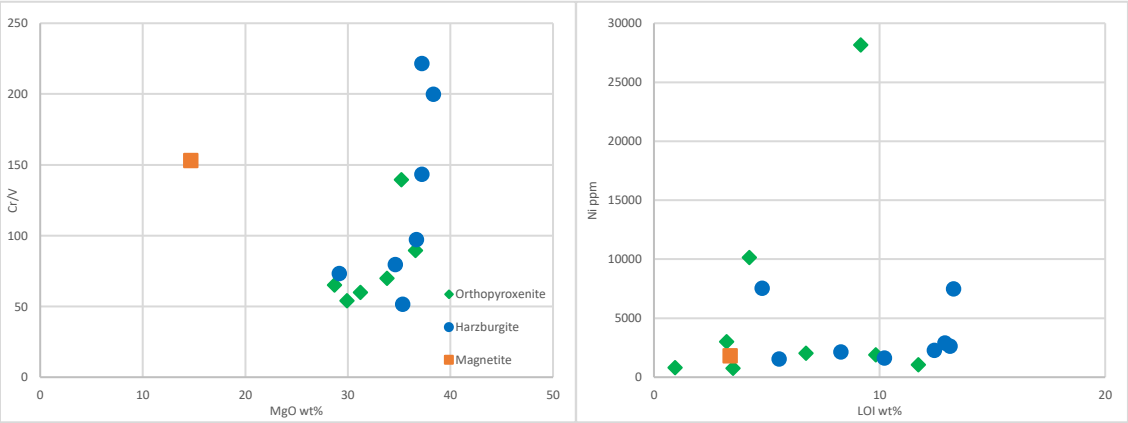

Figure 13: XRF compositional data for orthopyroxenite (green), harzburgite (blue) and magnetite vein (orange): a) Cr/V (wt%) ratio vs MgO wt% and b) Ni ppm vs LOI wt%

The most economically important element, Ni, appears generally enriched in all samples, although only four samples are enriched in Ni above the 0.5 wt% NiO. Pyroxenites show a maximum of 3.67 NiO wt% or 28175 ppm Ni in the sample IMK - 05149. Harzburgites display values between 0.2-1.4 wt% NiO with a median of 0.35 wt%, NiO which corresponds to 1617-7484 ppm Ni and a median of 2452 ppm Ni. A minimum Ni value in pyroxenite is 0.1 wt% NiO - (745 ppm Ni), which is the lowest of all samples, corresponding to altered olivine pyroxenite 1-6-531. Median Ni values for pyroxenites are 0.28 wt% NiO and 1962 ppm Ni. These values indicate higher median values in harzburgites, however, the most enriched samples with the Ni anomalous contents are pyroxenites. A weak correlation between the higher LOI values and Ni enrichment could be suggested from Figure 13, however, the most Ni enriched samples do not correspond to the highest LOI values. It is obvious from the observed distribution in the plot MgO vs Ni (Figure 12) that the Ni content of barren harzburgite should reflect a primary proportion of Ni-enriched olivine whereas the anomalous Ni values in olivine-poor pyroxenites are related to the presence of sulphide mineralisation. As olivine did not survive in serpentinised rocks, most of its Ni is redistributed between secondary silicates. A major aim of this research report is to assess the Ni distribution in minerals as it is shown in the following chapters.

Chapter 7

Mineral Chemistry

The mineral chemistry data was gathered on samples IMK – 05139, IMK – 05149, IMK – 05153 and IMK – 05156, through the use of a JEOL electron microprobe. These samples were chosen due to the mineralisation characterised through macroscopic and microscopic observations. Nickel and Cr values collected on the XRF analyses also played an important part on the sample selection.

7.1. Primary Phases

7.1.1. Pyroxenes

Pyroxenes show a relatively variable composition and classification, dependent on the sample. Five varieties of pyroxenes are present in Molopo Farms Complex rocks: orthopyroxene (enstatite), clinopyroxene (augite, diopside and hedenbergite) and pigeonite.

In coarse-grained orthopyroxenite, sample IMK – 05139, orthopyroxene is predominant, whilst 1 grain of diopside, 2 grains of interstitial augite and 2 grains of pigeonite were also analysed. In IMK – 05139 coarse pyroxenite, the molar Mg# of pyroxenes (calculated by the formula: Mg# = $\frac{100 \times Mg}{Mg + Fe2+}$, where Mg and Fe are in mol.%) varies between, approximately, 84.7 and 90.7, values which denote a Mg-rich composition of all these pyroxenes. Overall, IMK – 05139 pyroxenes are Fe poor, and the majority are Ca-poor as well, with a predominance of enstatite.

The predominant orthopyroxene in sample IMK – 05139 is characterised by an Mg# between 85.46 and 90.60, with a median of 90.14 denoting an Mg-rich character. The compositional ranges (Appendix V) are: 55.08 to 57.87 wt% SiO_2, with a median of 57.15 wt% SiO_2, 1.02 to 1.48 wt% Al_2O_3, with a median of 1.17 wt% Al_2O_3, 0.94 to 2.56 wt% CaO, with a median of 1.13 wt% CaO, 0.62 to 0.95 wt% Cr_2O_3, with a median of 0.75 wt% Cr_2O_3, from below the detection limit to 0.14 wt% TiO_2, with a median of 0.05 wt% TiO_2. The Ni values range from below the detection limit of 0.01 wt.% NiO up to 0.08 wt% NiO, with a median of 0.03 wt% NiO.

The two pigeonite grains in sample IMK – 05139 are characterised by an Mg# of 84.57 and 90.15, while the compositional ranges (Appendix V) are: 55.47 to 57.97 wt% SiO_2, 2.81 to 4.62 wt% CaO, 0.60 to 1.09 wt% Al_2O_3, 0.24 to 0.78 wt% Cr_2O_3, and from below the detection limit to 0.03 wt% TiO_2. The NiO values are from 0.02 to 0.04 wt% NiO.

The two augite grains in sample IMK – 05139 have an Mg# of 84.67 and 90.72 and contain: 57.62 to 57.97 wt% SiO_2, 12.44 to 14.27 wt% CaO, 0.09 to 0.10 wt% Al_2O_3, 0.07 to 0.09 wt% Cr_2O_3 with TiO_2 content below the detection limit (Appendix V). The NiO values are from 0.03 to 0.14 wt% NiO.

The single diopside grain has Mg# of 86.13 and is characterised by 55.32 wt% SiO_2, 25.27 wt% CaO, 0.04 wt% Cr_2O_3, 0.03 wt% TiO_2, with Al_2O_3 values below the detection limit (Appendix V). The NiO value was 0.13 wt% NiO.

In the pyroxene ternary (En-Wo-Fs) plot (Figure 14) the Mg-rich pyroxenes fall in the enstatite field, while the Ca-rich pyroxene is a diopside. The augite and pigeonite grains are in between these two fields, showing a variability of wollastonite and enstatite components but relatively stable and low ferrosilite proportions.

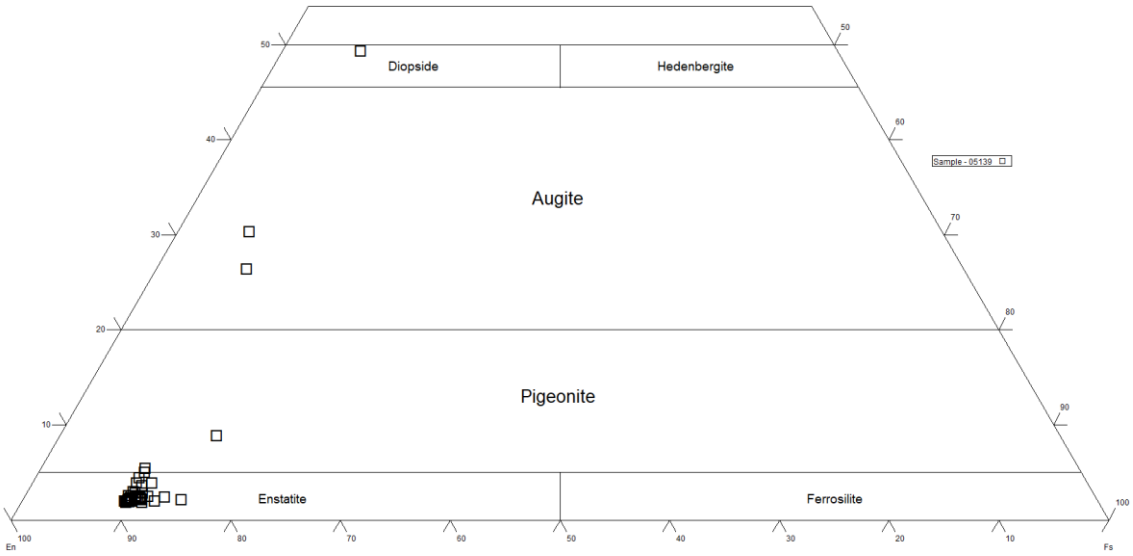

Figure 14: Pyroxene ternary (En-Wo-Fs) plot for pyroxene analyses for sample IMK - 05139

In serpentinised orthopyroxenite, sample IMK – 05149, three different pyroxene varieties are observed: augite, diopside and hedenbergite, indicating a predominance of clinopyroxenes with higher Ca contents compared to pyroxenes in samples IMK – 05139 IMK – 05153 (described later). Additionally, some analyses show an even higher Ca enrichment, slightly above the fields of diopside and hedenbergite. All these pyroxenes belong to the secondary silicate assemblage that form cross-cutting veinlets up to 2 mm thick whereas primary orthopyroxene did not survive and was replaced by amphiboles, chlorite, bastite and serpentine.

Diopside in sample IMK – 05149 is characterised by a variable Mg# between 51.93 to 87.20 with a median of 83.65, which indicates the coexistence of Mg-poor diopside with predominant Mg-rich clinopyroxene. The compositional ranges (Appendix V) are: ~51.18 to 55.06 wt% SiO_2, with a median of 54.64 wt% SiO_2, 22.63 to 24.77 wt% CaO, with a median of 23.90 wt% CaO, from below the detection limit to 0.43 wt% Al_2O_3, with a median of 0.02 wt% Al_2O_3, 0.017 to 0.13 wt% Cr_2O_3, with a median of 0.08 wt% Cr_2O_3, from below the detection limit to 0.02 wt% TiO_2, with a median of 0.01 wt% TiO_2. The Ni values are from below the detection limit to 0.05 wt% NiO, with a median of 0.02 wt% NiO.

Hedenbergite in sample IMK – 05149 is characterised by an Mg# value, between 27.14 to 50.14 with a median of 47.44, indicating the lower Mg proportion in this mineral relative to diopside. The compositional ranges of hedenbergite (Appendix V) are: 50.10 to 52.78 wt% SiO_2, with a median of 51.55 wt% SiO_2, 22.17 to 24.35 wt% CaO with a median of 23.79 wt% CaO, from below the detection limit to 0.01 wt% Al_2O_3 with a median below the detection limit of 0.01 wt% Al_2O_3, 0.01 to 0.10 wt% Cr_2O_3 with a median of 0,07 wt% Cr_2O_3, from below the detection limit to 0.03 wt% TiO_2 with a median below the detection limit of 0.01 wt% TiO_2. The Ni values are

from below the detection limit to 0.03 wt% NiO, with median below the detection limit of 0.01 wt% NiO.

Augite in sample IMK – 05149 also has variable Mg# from 43.38 to 87.70, denoting the coexistence of Mg-rich and Mg-poor augite. The compositional ranges (Appendix V) are: 52.04 to 55.91 wt% SiO_2, with a median of 54.98 wt% SiO_2, 18.37 to 22.51 wt% CaO, with a median of 21.36 wt% CaO, from below the detection limit to 0.11 wt% Al_2O_3, with a median of 0.05 wt% Al_2O_3, 0.003 to 0.10 wt% Cr_2O_3, with a median of 0.07 wt% Cr_2O_3, from below the detection limit to 0.06 wt% TiO_2, with a median of 0.02 wt% TiO_2. The Ni values are from below the detection limit to 0.08 wt% NiO, with a median of 0.03 wt% NiO.

In the pyroxene ternary (En-Wo-Fs) plot in Figure 15, it is possible to observe the Ca-rich character of IMK – 05149 diopside, augite and hedenbergite. The Mg-rich end-members are predominant over the Fe-rich variety (hedenbergite).

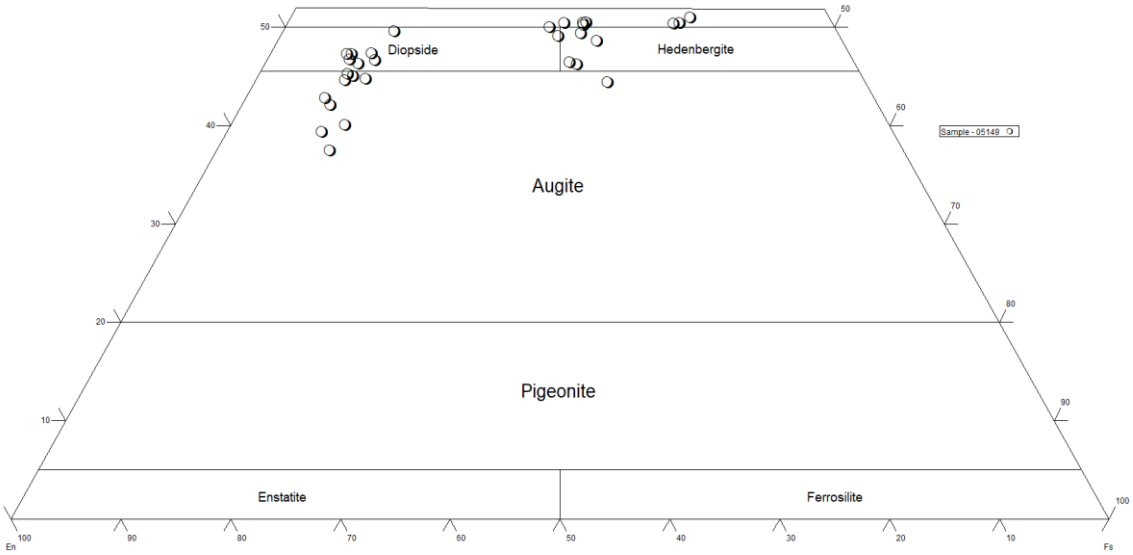

Figure 15: Pyroxene ternary (En-Wo-Fs) plot for mineral compositions for sample IMK - 05149

In highly serpentinised pyroxenite, sample IMK – 05153, orthopyroxene, as enstatite, is the predominant pyroxene, although two augite and one diopside analyses were also obtained.

Enstatite in sample IMK – 05153 is characterised by an Mg# between 85.77 and 89.22, with a median of 88.74. The compositional ranges (Appendix V) are: 55.89 to 57.31 wt% SiO_2, with a median of 56.83 wt% SiO_2, 0.327 to 1.18 wt% Al_2O_3, with a median of 1.08 wt% Al_2O_3, 0.15 to 1.71 wt% CaO, with a median of 0.85 wt% CaO, 0.15 to 0.59 wt% Cr_2O_3, with a median of 0.52 wt% Cr_2O_3, from below the detection limit to 0.15 wt% TiO_2, with a median of 0.05 wt% TiO_2. The Ni values are below the detection limit up to 0.17 wt% NiO, with a median of 0.05 wt% NiO.

The two augite grains showed an Mg# value of 73.65 and 74.35. The compositional ranges (Appendix V) are: 51.89 to 52.02 wt% SiO_2, 21.59 to 21.68 wt% CaO, 0.34 to 0.46 wt% Al_2O_3, 0.49 to 0.79 wt% Cr_2O_3 and TiO_2 content is below the detection limit. The Ni values are from 0.01 to 0.03 wt% NiO.

The grain of diopside with an Mg# of 58.56 has a composition: 52.17 wt% SiO_2, 23.20 wt% CaO, ~0.09 wt% Al_2O_3, 0.26 wt% Cr_2O_3, 0.01 wt% TiO_2 (Appendix V). The Ni value is below the detection limit.

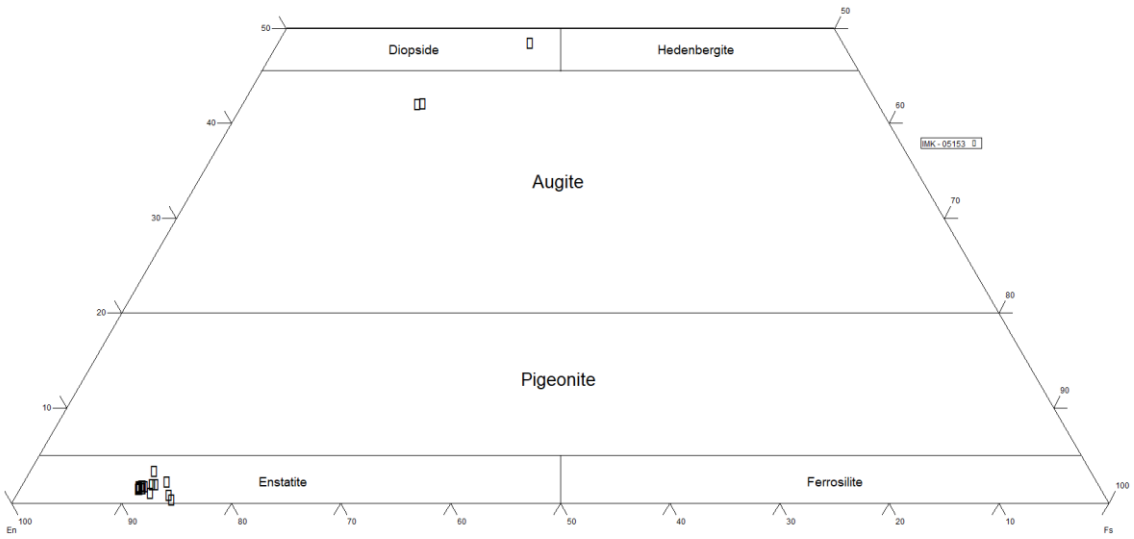

Figure 16: Pyroxene ternary (En-Wo-Fs) plot for pyroxene analyses for sample IMK - 05153

In serpentinised harzburgite sample IMK – 05156 all primary pyroxene and olivine are completely replaced by secondary serpentine, amphiboles, chlorite and magnetite.

In summary, orthopyroxenes are major primary minerals in the mineralised samples, with samples IMK – 05139 and IMK – 05153 being orthopyroxenite dominated by enstatite with homogeneous compositions. Heavily serpentinised olivine pyroxenite, IMK – 05149, bears 1-mm thick veinlets composed of three varieties of secondary clinopyroxene: Mg-rich diopside and Mg-poor hedenbergite, as well as Mg-rich and Mg-poor augite. The Ni content in pyroxenes is generally low, with the exception of enstatite, rare augite and some diopside grains in sample IMK-05139, that can be enriched in Ni up to 0.2 wt% NiO. The median values for enstatite are 0.05 and 0.03 wt% NiO in samples IMK – 05139 and IMK – 05153, respectively, for diopside 0.02 and below detection limit in samples IMK – 05149 and IMK – 05153, respectively, for hedenbergite 0.01 and for pigeonite 0.04 wt% NiO. The Ni content in pyroxenes, therefore, shows a general positive correlation with Mg# and MgO content (Figure 17 a & b) and negative correlation with CaO content (Figure 17 c). The widest variations of the Ni content are found in enstatite that is likely to be related to a variable alteration degree as is shown further in the chapter on Ni balance.

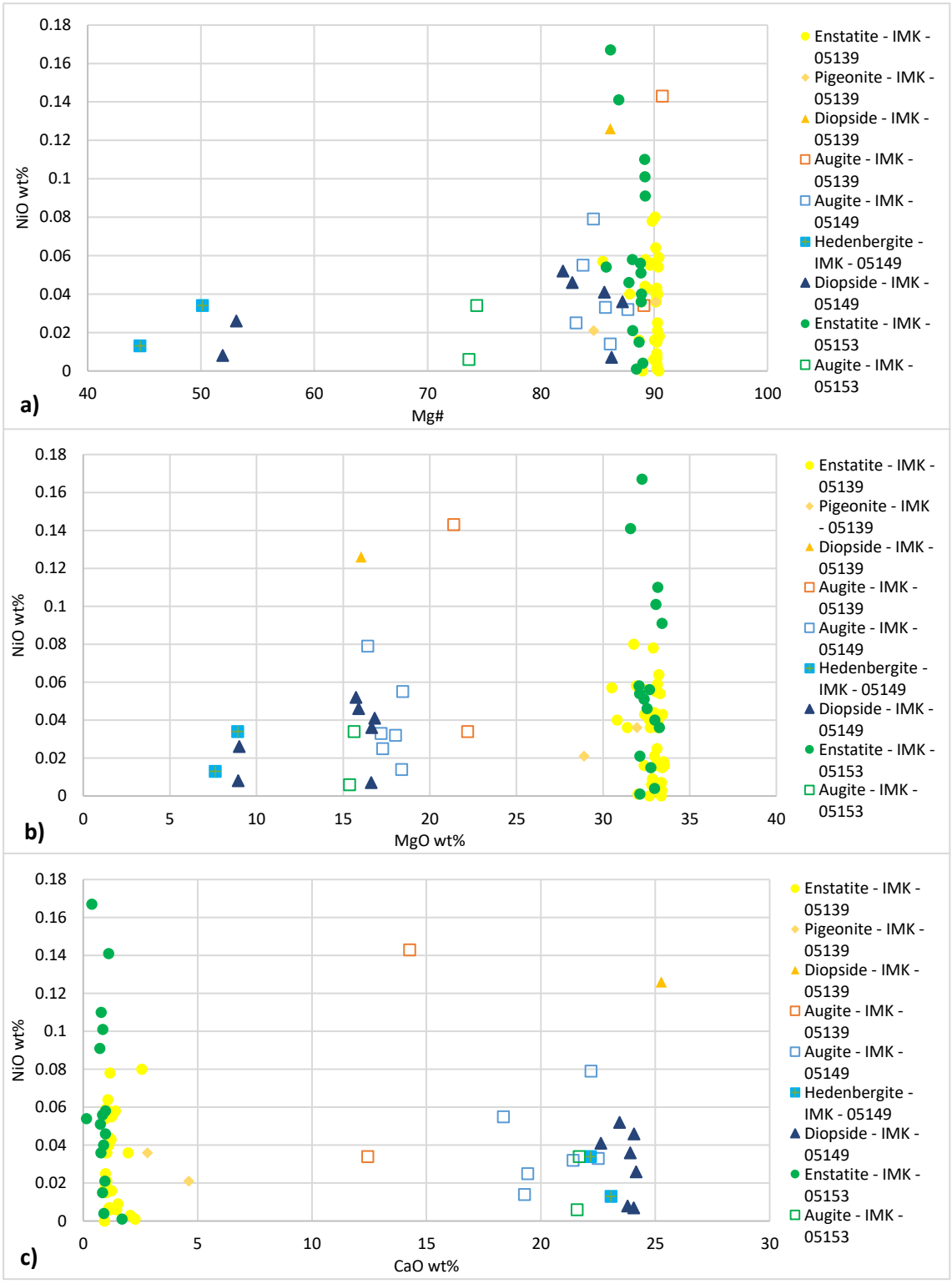

Figure 17: Binary plots for all pyroxene analyses: a) NiO wt% vs Mg#; b) NiO wt% vs MgO wt%; c) NiO wt% vs CaO wt%.

7.2. Secondary Phases

7.2.1. Serpentine-group minerals

Serpentine-group minerals are the most common minerals in all samples due to the extremely altered state of the lithologies. The possible Ni accumulation in these phyllosilicates and their high abundances in the samples increases the importance of the characterisation of this mineral phase.

In coarse-grained orthopyroxenite, sample IMK – 05139, serpentine has the lowest Mg# of 82.53, a maximum value of 94.34 and a median Mg# of 86.4. Additionally, the proportion between number of Fe atoms and Mg atoms in the normalised serpentine formula was also calculated as the molar ratio: XFe = $\frac{100 \times Fe2+}{Fe2+ + Mg}$. A maximum XFe of 17.5, a minimum of 5.7 and a median of 13. 6 were calculated, which denotes the variations within the serpentine-group minerals. Nickel content varies from below the detection limit to a maximum of 0.13 wt% NiO with a median of ~0.02 wt% NiO that indicates variable Ni enrichment within these serpentines. Serpentine-group minerals contain: 0.09 to 6.07 wt% CaO, 0.49 to 1.98 wt% Cr_2O_3, 0.02 to 0.42 wt% MnO and 0.76 to 3.15 wt% Al_2O_3 (Appendix V).

On the FeO-SiO_2-MgO compositional diagram, all the serpentine analyses in this sample belong to the antigorite variety. Compositional data in Figure 18 confirms that these points are confined to the antigorite field.

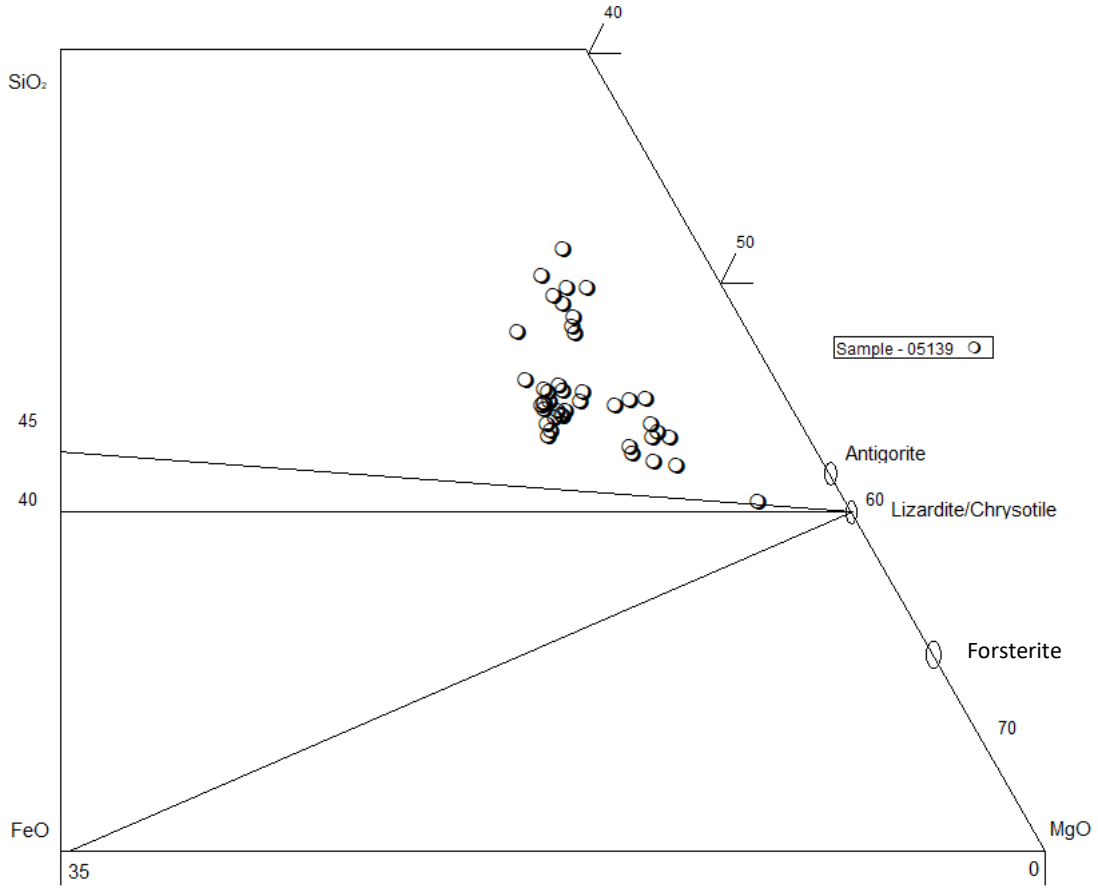

Figure 18: Serpentine FeO-SiO_2-MgO ternary plot for sample IMK - 05139.

In highly serpentinised olivine orthopyroxenite sample IMK – 05149, the Mg# of serpentine varies between ~79.8 and ~92.4 while a median for the Mg# is ~85.6. As for the XFe values, they vary between ~7.6 and ~20.2 with a median of ~16.4. These values show a higher variation compared to the previous sample, also, there was a slight increase in the average XFe and a slight decrease in the average #Mg, denoting local Mg deficiency and Fe enrichment. Nickel oxide values also show a higher variation, with minimum values below the detection limit but a maximum of 1.91 NiO wt%. A median value is as low as 0.08 wt.% NiO, thus, in this sample, serpentine is slightly more enriched in Ni compared to the sample IMK – 05139. The compositional ranges of the minor and trace elements are: from below detection limit to 3.65 wt% CaO, 0.02 to 0.90 wt% Cr_2O_3, from below detection limit to 0.48 wt% MnO, 0.14 to 5.08 wt% Al_2O_3 (Appendix V).

In the FeO-SiO_2-MgO compositional diagram, two distinct groups of serpentines are distinguished: a group of Mg-enriched Si-depleted compositions and a group of Mg-depleted Si-enriched compositions. There is no correlation between the NiO content and the contents of the major oxides (MgO, SiO_2 and Al_2O_3) in serpentine.

As observed in the Figure 19, the Mg-enriched compositions marked by a red circle are closer to the composition of lizardite-chrysotile. The compositions outlined by a yellow circle are clearly identifiable due to the high point density, higher SiO_2 and FeO values, and, lower MgO values that correspond to the composition of Fe enriched antigorite. Finally, a smaller group of compositions outlined by the green circle corresponds to Si-enriched Mg-depleted antigorite.

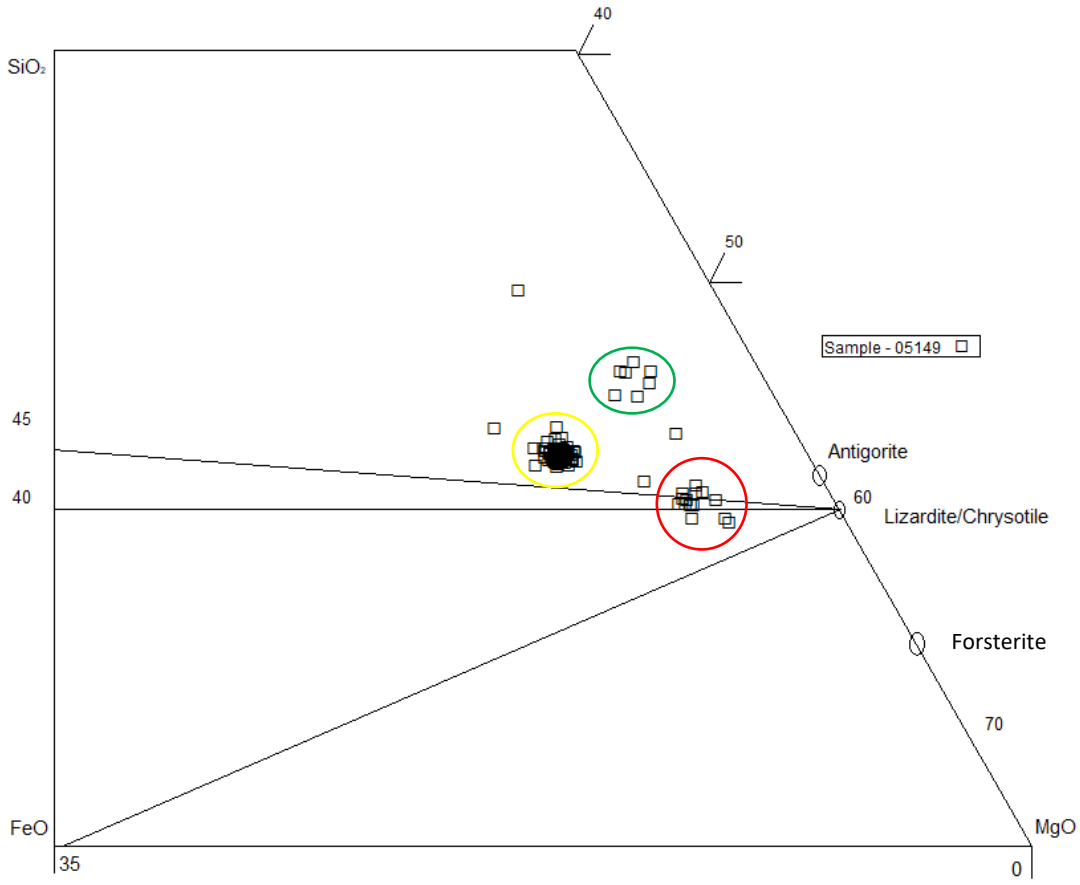

Figure 19: Serpentine FeO-SiO_2-MgO ternary plot for sample IMK – 05149. Different compositional groups are circled in green, yellow and red, for Si-enriched Mg-depleted antigorite, Si-Fe-enriched antigorite and the most similar compositional group to antigorite, respectively.

Serpentine from serpentinised orthopyroxenite, sample IMK – 05153, has an Mg# from ~81.2 to ~93.6 with a median of 86.22 and the XFe values ranging from ~6.4 to ~18.8 with a median of ~13.8 XFe. These results are similar to those in the sample IMK – 05139, with IMK – 05153 serpentines showing a slight to mild Mg deficiency and Fe enrichment relative to that sample. The NiO content varies between 0.08 and 0.58 wt% NiO, with a median of 0.21 wt% NiO. These values show a narrow variation where the maximum value is much lower than the previous samples, but the median value is higher. The ranges of the other minor and trace elements (Appendix V) are: 0.02 to 3.65 wt% CaO, 0.05 to 0.8 wt% Cr_2O_3, 0.09 to 0.92 wt% MnO, and 0.51 to 3.17 wt% Al_2O_3. Two groups of serpentines in this sample can be defined in the FeO-SiO_2-MgO compositional diagram. As shown in Figure 20, all analysed serpentine has the composition of antigorite, with two varieties being variably enriched in Mg.

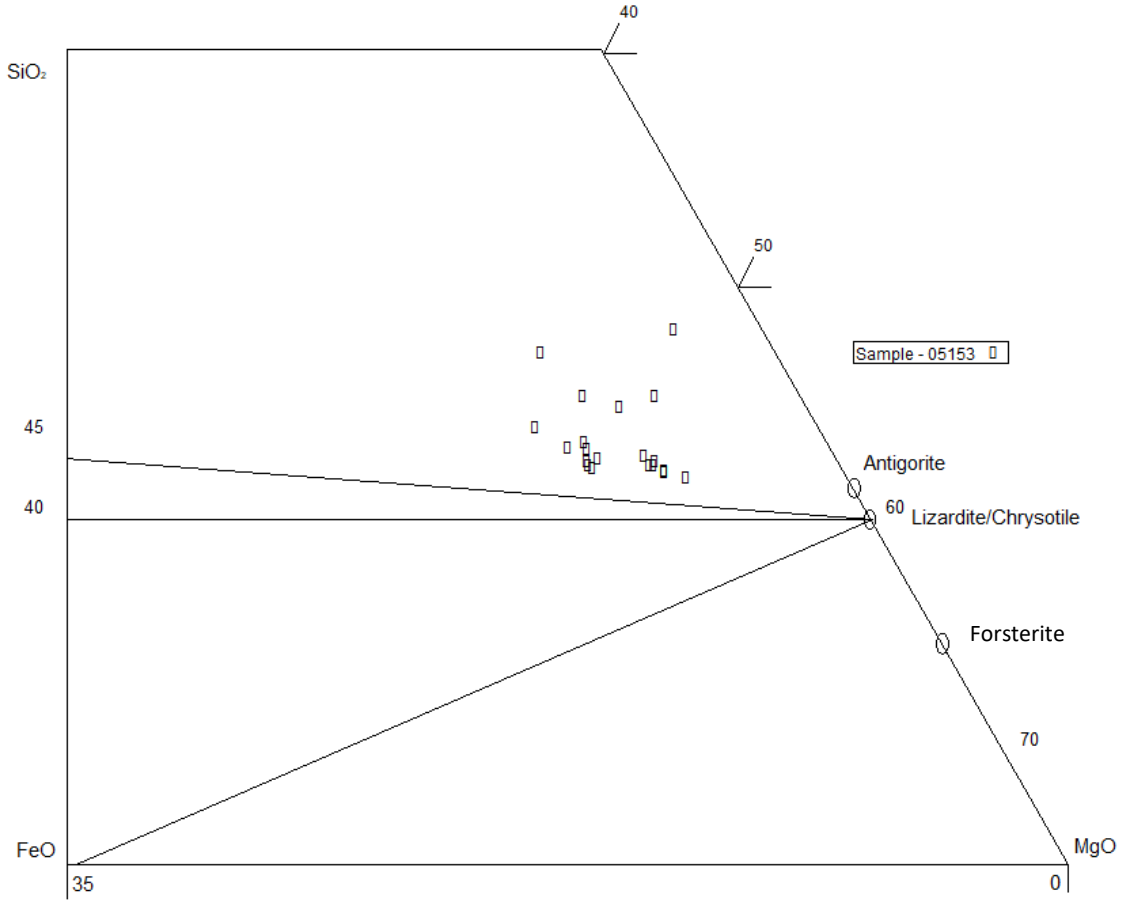

Figure 20: Serpentine FeO-SiO_2-MgO ternary plot for sample IMK – 05153. Shows two groups variably enriched in MgO.

In serpentinised chromitiferous harzburgite, sample IMK – 05156, serpentine has Mg# values between ~88.4 and ~98.2, with a median of ~96.7, whereas XFe values vary between ~1.76 and ~11.60 with a median of ~3.31 XFe. Therefore, the Mg# demonstrates a higher Mg enrichment and an Fe deficiency relative to the previous samples. Compositional ranges of the minor and trace elements (Appendix V) are: 0.002 to 0.04 wt% CaO, 0.12 to 3.27 wt% Cr_2O_3, 0.001 to 0.09 wt% MnO, 0.37 to 4.92 wt% Al_2O_3. The higher Cr values in this sample's serpentines are due to the presence of up to 7 modal % chromites. As shown in Figure 21, all analysed serpentine has the composition close to that of lizardite/chrysotile that is slightly enriched in MgO.

Nickel contents vary between 0.003 and 2.17 wt% NiO, with a median of 0.05, these results denote a high variability that may be associated with the proximity of some points to Ni-rich minerals in the sample although this was generally avoided during the analysis. The median values are much lower than the highest value, thus, on average, the serpentines are generally Ni-poor in the sample IMK – 05156.

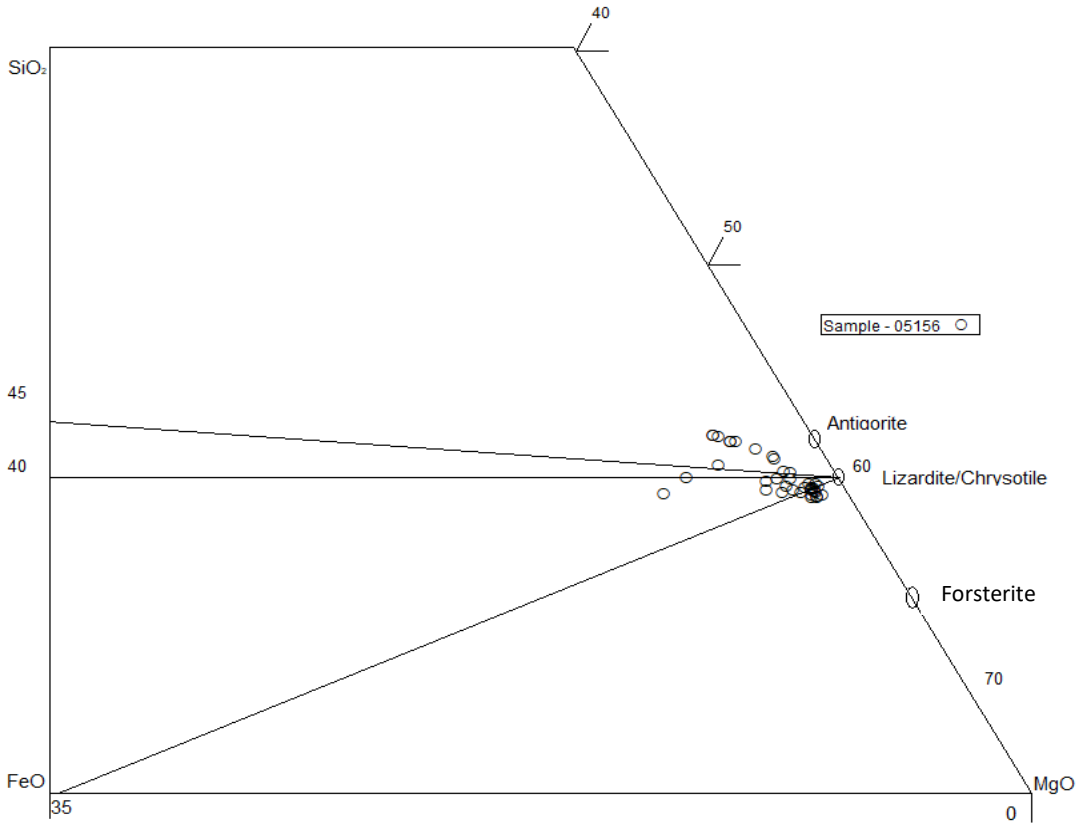

Figure 21: Serpentine FeO-SiO_2-MgO ternary plot for sample IMK – 05156.

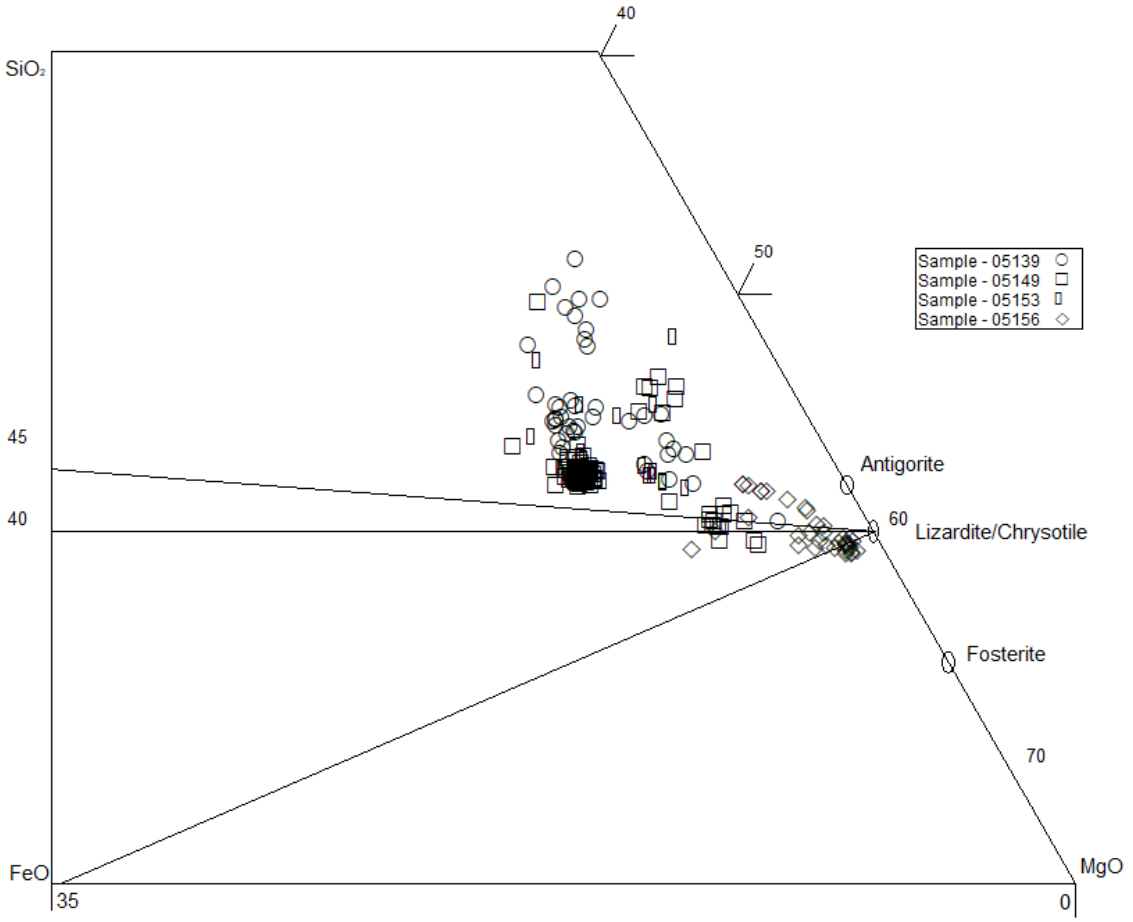

Figure 22: Serpentine FeO-SiO_2-MgO ternary plot for the 4 samples.

In all the samples, the NiO content in serpentine generally does not exceed 0.5 wt%, however, some serpentines in samples IMK – 05149 and IMK – 05156, can be enriched in Ni over 1 wt% NiO (Figure 23 a & b). The highest Mg# is observed in serpentine from serpentinised chromite-rich harzburgite IMK – 05156 that may reflect the presence of olivine as a precursor whereas the lowest Mg# is found in serpentinised and amphibolitised olivine orthopyroxenite IMK – 05149 with 12 modal % sulphides. Three different varieties of serpentine occur in the sample IMK – 05149 that may be related to replacement of olivine and orthopyroxene and Ni redistribution during the formation of the secondary clinopyroxene veinlets (Figure 19 and Figure 23 a & b).

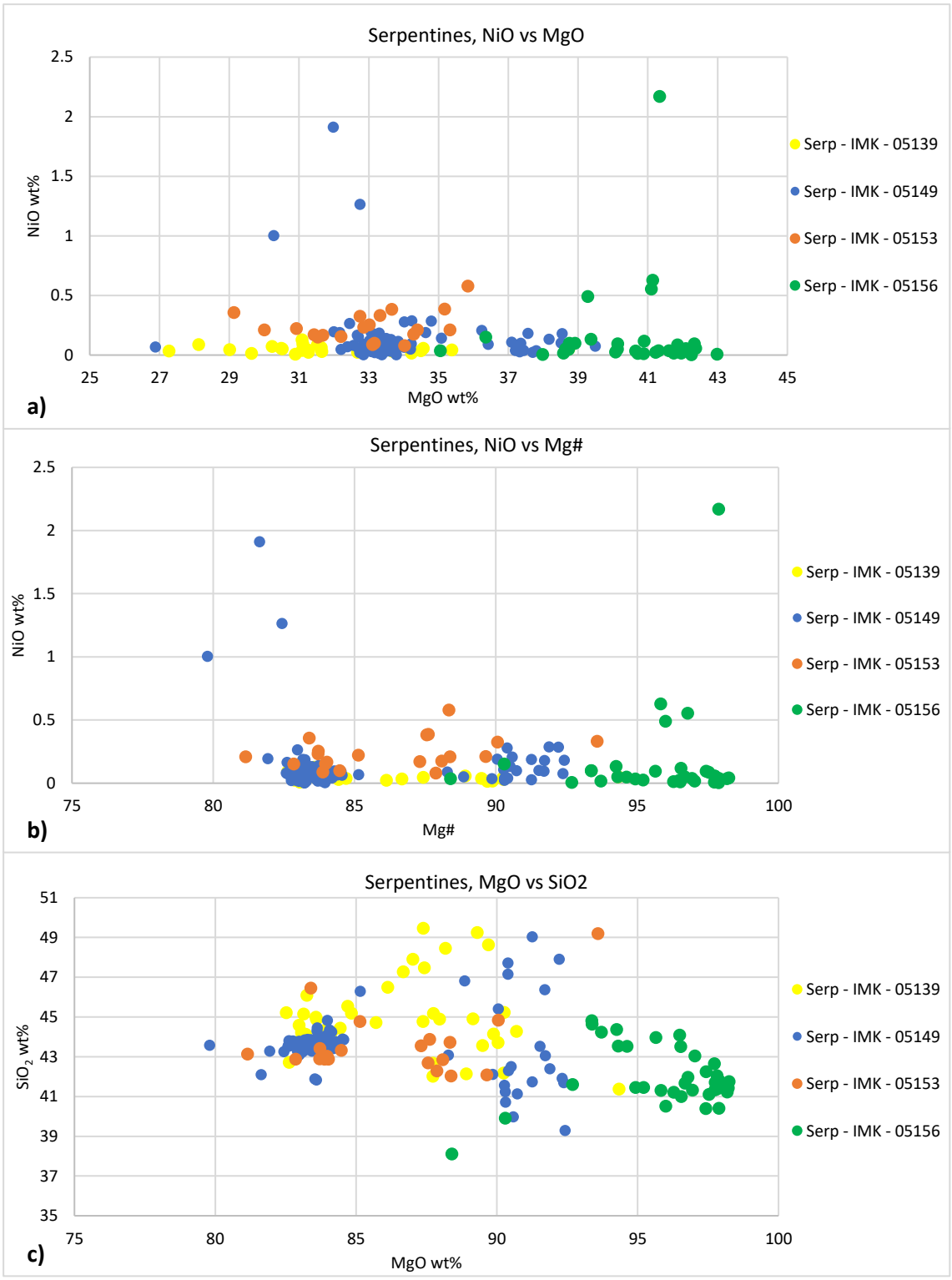

Figure 23: Binary plots of serpentine for the 4 samples: a) NiO wt% vs MgO wt%; b) NiO wt% vs Mg#; c) SiO_2 vs MgO wt%.

7.2.2. Chlorites

Another type of secondary alteration in the samples occurs in the form of chlorite. The chlorite-group minerals occur associated with serpentine alteration and in much smaller proportions compared to serpentines and secondary amphiboles. Chlorite composition shows a general increase in Al proportions relative to serpentine compositions, as it represents an aluminous silicate mineral. However, this chlorite-group does comprise different minerals, which differ in proportions of certain elements, such as Fe, Mg, Si, Al, Mn and others. To help identify a mineral, which the analyses belong to, a chlorite classification scheme based on Si (apfu) vs Fe/(Fe+Mg) after Deer et al., (1992) was used (Figure 24, Figure 25 and Figure 26). This plot helps to identify the minerals of the chlorite group and recognises possible transitional phases (mixes) between secondary alterations minerals, mostly between serpentine, talc and chlorite.

In sample IMK – 05149, a total of four analyses corresponds to the chlorite-group minerals. Silica values on these points varies between 32.47 and 40.45 wt% SiO_2, with a median of 34.29 wt% SiO_2. Chlorite contains from 32.83 to 34.24 wt% MgO with a median of 33.51 wt% MgO, from 5.32 to 15.12 wt% Al_2O_3 with a median of 12.72 wt% Al_2O_3, and from 4.34 to 6.87 wt% FeO, with a median of 5.99 wt% FeO (Appendix V). Among trace elements, chlorite contains 0.14 to 1.97 wt% Cr_2O_3 with a median of 0.34 wt% Cr_2O_3, as well some Zn at 0.07 to 0.13 wt% ZnO with a median of 0.12 wt% ZnO. These values denote the Al increase relative to the serpentine compositions, with some analyses being close to the compositions of serpentine that may represent a transitional mineral similar to septochlorite or chlorite-serpentine intergrowths. Nickel values detected are between 0.17 and 0.39 wt% NiO, while a median is 0.26 wt% NiO. Therefore, chlorite is enriched in Ni compared with other secondary minerals. The Fe-Mg molar ratio, calculated by the formula: $\frac{Fe}{Fe+Mg}$, and the Si value in apfu are shown in Figure 24. Chlorite compositions correspond to clinochlore transitional to penninite and talcochlorite.

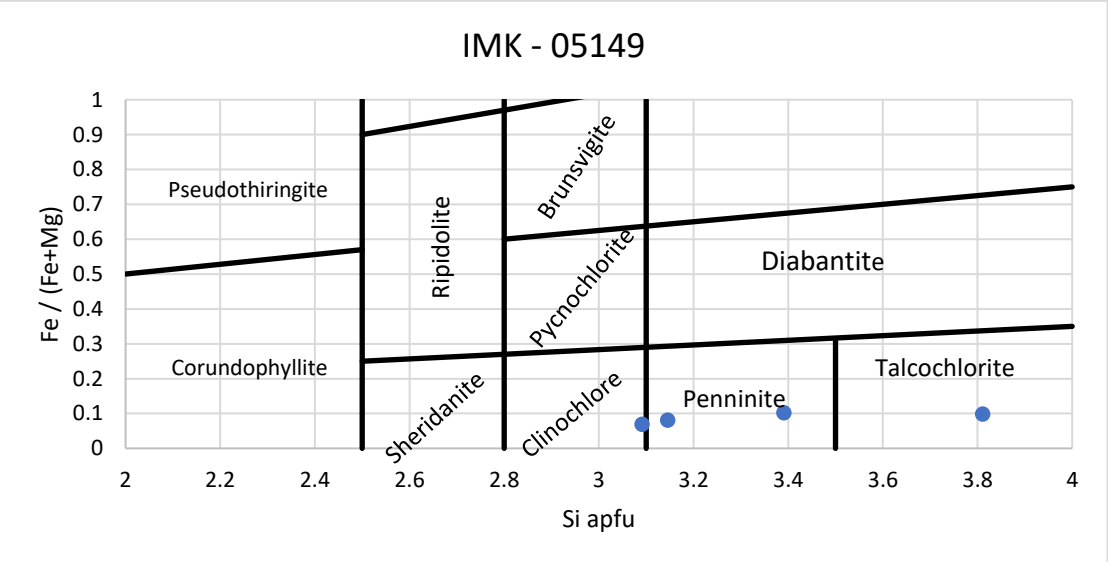

Figure 24: Plot for IMK - 05149 chlorite classification after Deer et al., (1992), with silica atoms per formula unit Vs Fe-Mg molecular ratio.

In the serpentinised pyroxenite sample IMK – 05153, a total of 12 analyses correspond to minerals of the chlorite group. Of these, 2 analyses showed increased K contents, which

indicate phlogopite as a precursor of secondary chlorite. This is consistent with relics of phlogopite identified in hand sample, under the microscope and in TIMA. Silica values in IMK – 05153 chlorites vary between 32.81 and 43.70 wt% SiO_2 with a median of 38.89 wt% SiO_2, Mg values between 25.50 and 34.10 wt% MgO with a median of 32.29 wt% MgO, Al from 6.81 to 15.43 wt% Al_2O_3 with a median of 9.71 wt% Al_2O_3, Fe from 4.25 to 8.16 wt% FeO with a median of 6.04 wt% FeO (Appendix V). Chlorite also contains from 0.06 to 1.47 wt% $Cr_2O_3$with a median of 0.72 wt% Cr_2O_3 as well as up to 7.23 wt% K_2O in chlorite after phlogopite, although the lowest value is 0.002 and a median is 0.49 wt% K_2O. Similar to the previous sample, these results denote an increase in Al and decrease in Si in chlorites with respect to minerals of the serpentine group. In this sample the Ni values occur at a minimum of 0.11 and a maximum of 0.72 with a median of 0.42 wt% NiO, showing the much higher Ni abundance and medians compared to those of serpentine in the same sample. Thus, similar to the previous sample, chlorites, that are replacing pyroxenes, amphiboles and phlogopite in the sample 05153, on average are more enriched in Ni compared to serpentine.

The plot Si (apfu) vs Fe/(Fe+Mg) shows that the majority of the analyses fall into the talcochlorite field (Figure 25).

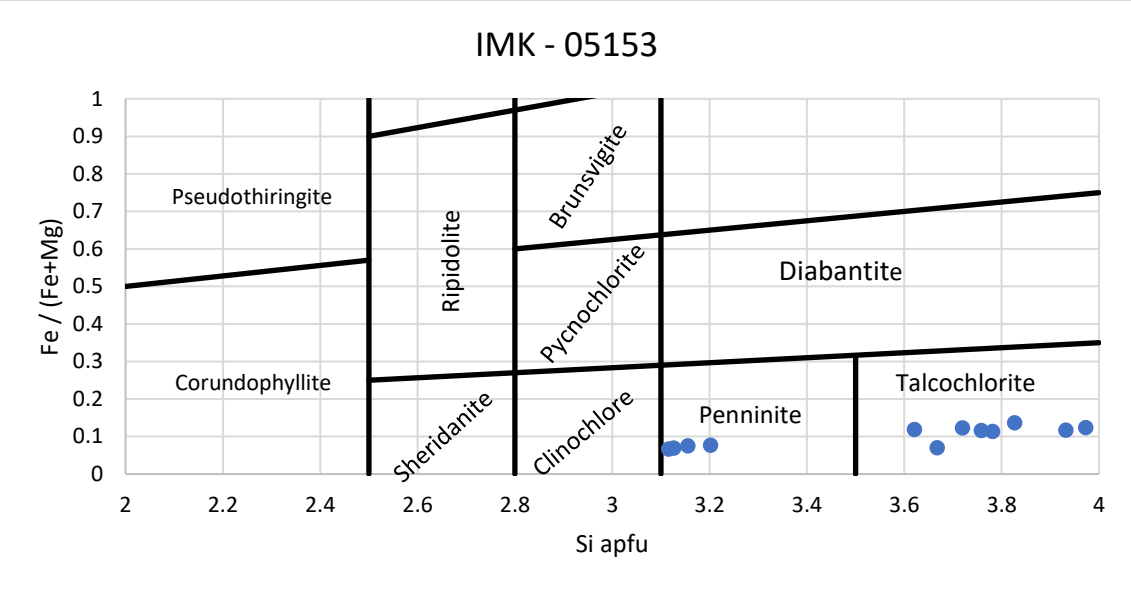

Figure 25: Plot for IMK - 05153 chlorite classification after Deer et al., (1992), with silica atoms per formula unit Vs Fe-Mg molecular ratio.

The composition of chlorite-group minerals from the serpentinised chromite-rich harzburgite sample IMK – 05156 is represented by 23 analyses. Silica values are between 33.58 and 38.09 wt% $SiO_2$with a median calculated to 34.89 wt% SiO_2, Mg values are from 34.28 to 37.06 wt% MgO with a median of 35.46 wt% MgO, Al varies from 5.94 to 12.11 wt% Al_2O_3 with a median of 10.87 wt% Al_2O_3, and Fe varies between 3.76 and 5.51 wt% FeO with a median of 4.54 wt% FeO (Appendix V). Chromium content has a minimum value of 0.66 and a maximum value of 1.39 wt% Cr_2O_3 and a median of 0.97 wt% Cr_2O_3. Nickel content in chlorite varies from 0.025 to 0.39 wt% NiO with a median of 0.25 wt% NiO, which are similar to the values in the other samples. The median Ni content in chlorite of this sample is higher than the Ni content in serpentine of the same sample. This is in agreement with the higher Ni enrichment of chlorites relatively to serpentines in the studied Molopo Farms Complex samples.

In the plot Si (apfu) vs Fe/(Fe+Mg) (Figure 26) the compositions of the IMK – 05156 chlorite mostly fall in the field of penninite, with only one point being in the talcochlorite field. As with the previous samples, the data suggests an occurrence of the transitional talc-serpentine-chlorite minerals.

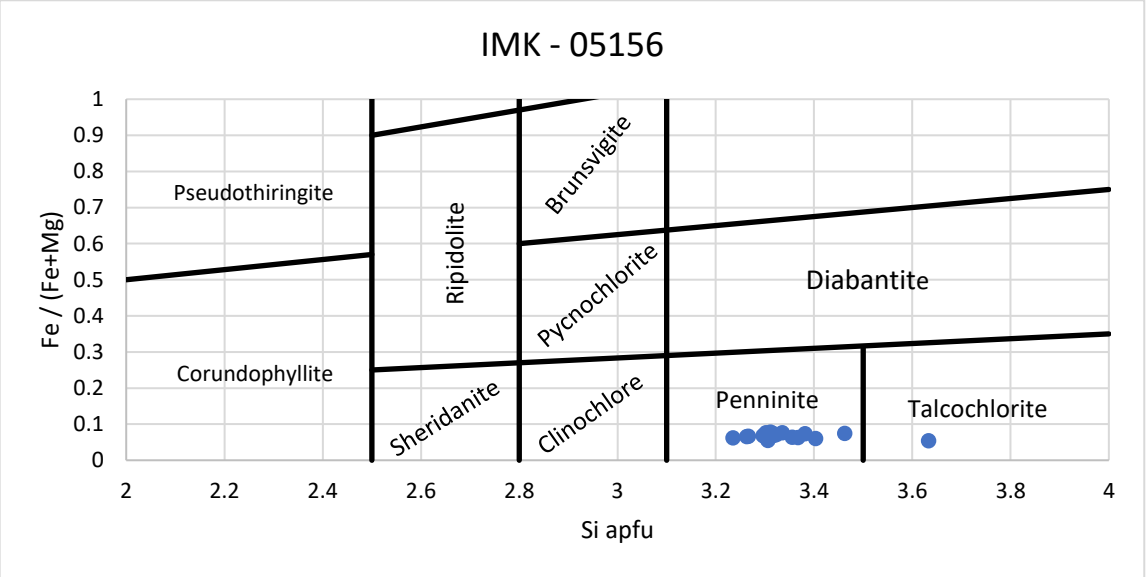

Figure 26: Plot for IMK - 05156 chlorite classification after Deer et al., (1992), with silica atoms per formula unit Vs Fe-Mg molecular ratio.

The overall chlorite-group mineral data show a consistent Mg# ranging from 86 to 95 corresponding to high-Mg chlorite varieties transitional towards serpentine and talc by composition. Silica values, however, varied from near 3 atoms per formula unit (apfu) up to 4 apfu, reflecting the presence of clinochlore, penninite and talcochlorite. The majority of the analyses belong to penninite or talc-chlorite, indicating the dominance of the higher Si values. Thus, these chlorites data suggest a transitional characteristic of this mineral phase, with the varied Si proportions denoting the general enrichment in this element towards the values representative of serpentines. The median Ni content in chlorite is notably higher than the Ni content in serpentine in all samples indicating significant Ni redistribution during formation of secondary hydrous silicates, Figure 27. Nickel shows a positive correlation with Mg# in the sample IMK – 05153 whereas Cr demonstrates a positive correlation with Mg# for the entire dataset (Figure 28).

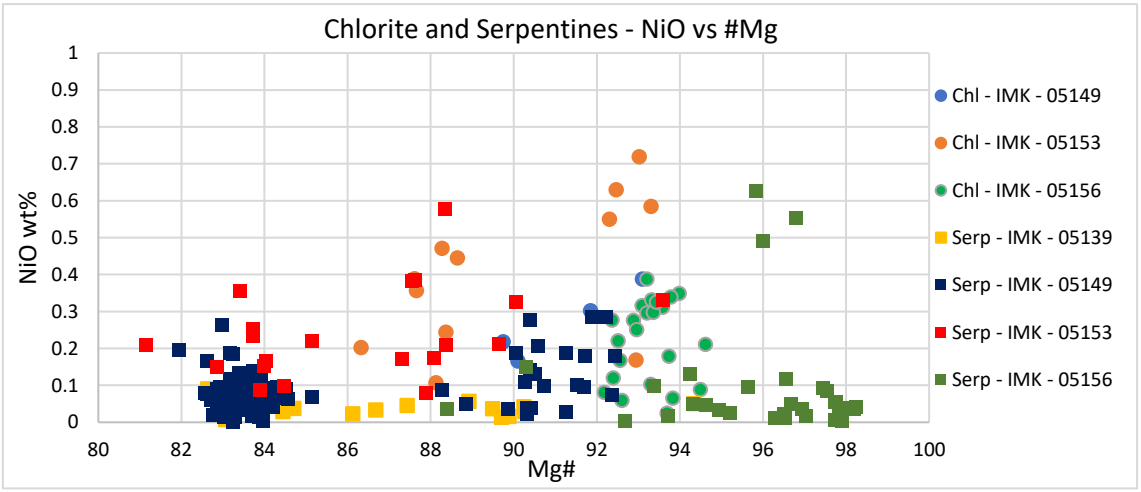

Figure 27: Compositional plot comparing the NiO wt% on chlorite and serpentine analyses in studied samples.

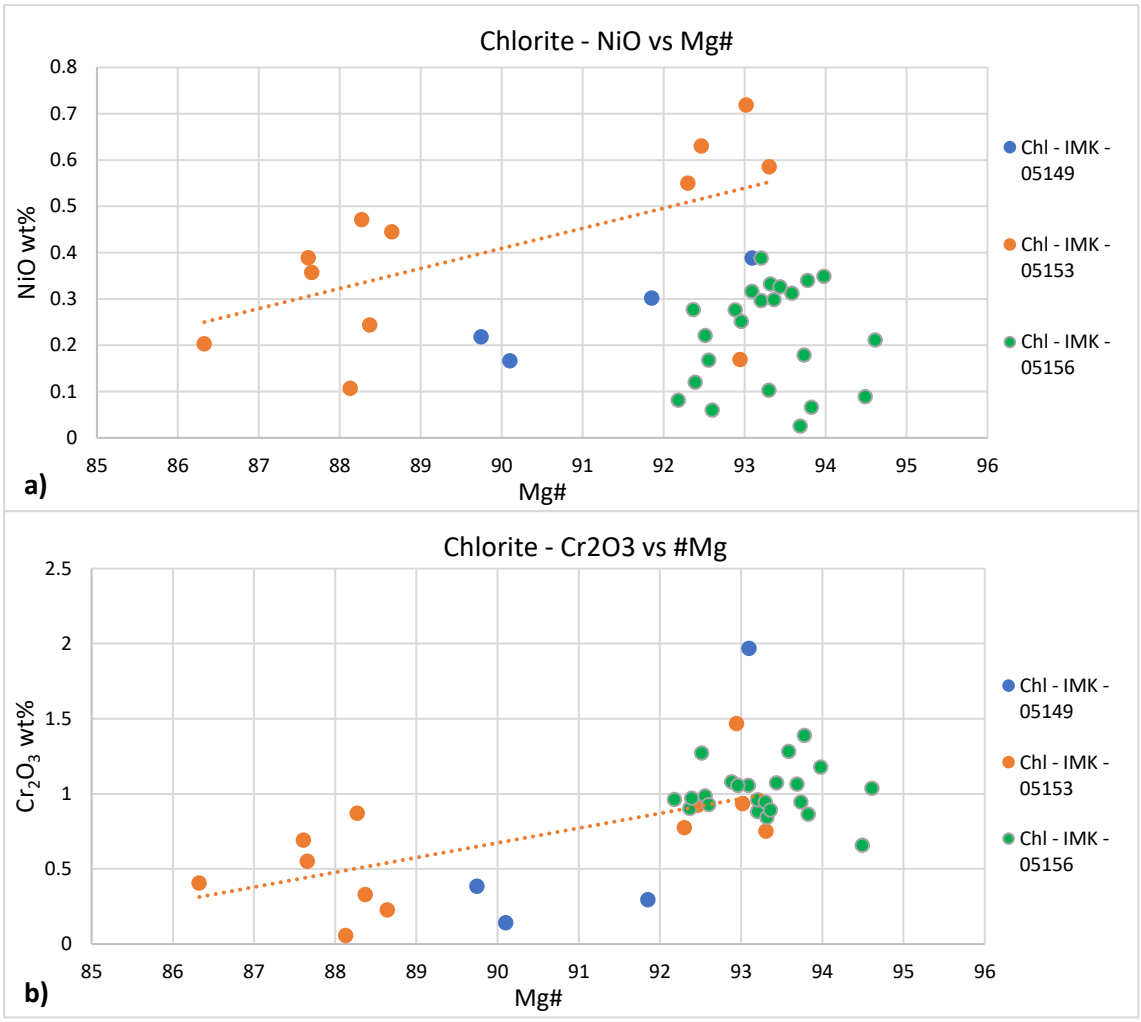

Figure 28: Compositional plots for all chlorite analyses in studied samples a) NiO wt% Vs Mg#; b) Cr_2O_3 Vs Mg#.

Due to the much lower proportions of the chlorite-group minerals (1-3 mod. %) compared with the proportion of major serpentine within the studied samples, the Ni accommodation in chlorite is not significant, nonetheless, the occurrence of chlorite veins and other chlorite segregations in rocks should be taken into account during evaluation of Ni balance.

7.2.3. Amphiboles:

Another group of secondary minerals present in these samples are amphiboles, which are secondary in origin based on the petrographic observations. These minerals are less common than serpentine-group minerals in the majority of the samples, although amphibole accounts for up to 27 modal % in the sample IMK – 05153 and up to 38 modal %, in the samples IMK – 05139. The latter value is higher than the abundance of serpentines, at 29 modal % as verified by the results of the Tescan-Integrated Mineral Analyser (TIMA) mapping (see the TIMA chapter of the thesis). Therefore, amphiboles may represent an important contributor to the total Ni mineral balance. The sample IMK – 05156 does not have any visible or detected secondary amphiboles as they are completely replaced by chlorite.

The amphibole supergroup minerals have a general formula, $AB_2C_5T_8O_{22}W_2$, where A = Na, K, Ca, Pb, Li; B = Na, Ca, Mn^{2+}, Fe^{2+}, Mg, Li; C = Mg, Fe^{2+}, Mn^{2+}, Al, Fe^{3+}, Mn^{3+}, Ti^{4+}, Li; T = Si, Al, Ti^{4+}, Be; W = (OH), F, Cl, O^{2-} (Hawthorne, et al., 2012).The recent classification is based on the A, B, and C groups of cations and the W group of anions, as these groups show the maximum compositional variability in the amphibole structure (Hawthorne, et al., 2012). Amphiboles with OH, F, Cl dominant at W are divided into eight subgroups according to their chemistry: magnesium-iron-manganese amphiboles, calcium amphiboles, sodium-calcium amphiboles, sodium amphiboles, lithium amphiboles, sodium-(magnesium-iron-manganese) amphiboles, lithium-(magnesium-iron-manganese) amphiboles and lithium-calcium amphiboles.

Microprobe data indicates that all analytical points in the samples studied correspond either to Ca-rich series of calcium amphiboles or to Mg-Fe series of amphiboles. This distinction is clearly seen in the plot of Si (apfu) vs $\frac{Mg}{Mg + Fe2+}$ (Figure 29 and Figure 30 after Deer et al., (1992)).

The actinolite-tremolite series are calcium amphiboles with a compositional gradient between Fe and magnesium. With the help of the molecular ratio, $\frac{Mg}{Mg + Fe2+}$, it is possible to distinguish between two members where values above 0.9 are indicative of tremolite, and, values between 0.5 – 0.9 indicate actinolite. The number of Si atoms in the chemical formula (apfu) of amphiboles can distinguish between an actinolite-tremolite and hornblendes (Figure 29, Figure 30). Hornblendes are also within the subgroup of the calcium amphiboles, but they have higher Al content and lower Si content compared with amphiboles of the actinolite-tremolite series.

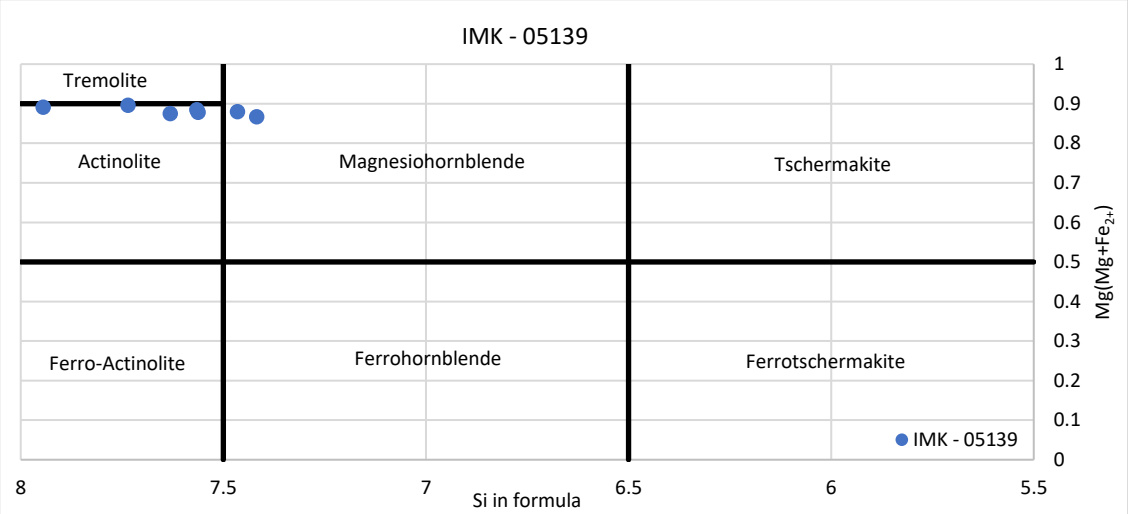

Figure 29: Amphibole classification plot after Deer et al., (1992), for sample IMK – 05139, with silica atoms per formula unit (apfu) Vs Mg-Fe^{2+} molecular ratio.

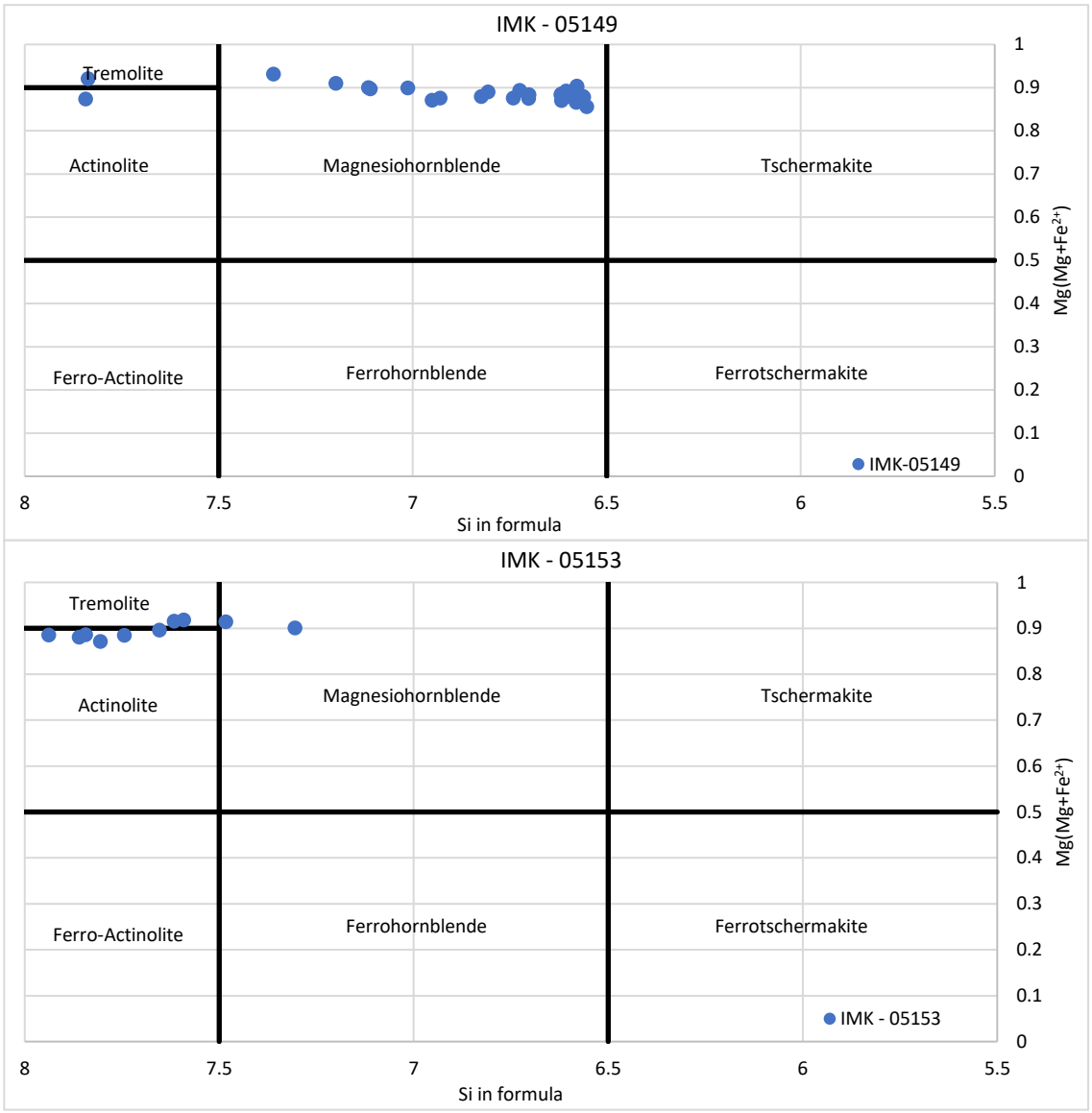

Figure 30: Amphibole classification plot after Deer et al., (1992), for samples IMK – 05149 and IMK – 05153, with silica atoms per formula unit (apfu) Vs Mg-Fe^{2+} molecular ratio.

7.2.3.1. Actinolite-Tremolite series

In the pyroxenite sample IMK – 05139, nine analysed compositions belong to calcic amphiboles (Figure 29). Of those, seven are of the actinolite-tremolite series and two are of hornblende. According to the Mg/(Mg+Fe) mol. ratio, five of the actinolite-tremolite compositions have a value below 0.9, thus being characterised as actinolite, as opposed to the other two points, which showed a value above 0.9 and are characterised as tremolite. The microprobe analyses on these minerals of the actinolite-tremolite series (Appendix V) show: from 52.47 to 58.70, with a median of 55.49 wt% SiO_2, from 21.03 to 25.34, with a median of 23.08 wt% MgO, from 4.20 to 6.28 with a median of 4.78 wt% FeO, from 0.021 to 0.71 with a median of 0.58 wt% Al_2O_3, from 0.07 to 0.23 with a median of 0.12 wt% MnO, and from 9.03 to 14.03 wt% CaO and a median of 12.28 wt% CaO. The Ni values are very low, ranging from below detection limit up to 0.07 wt% NiO with a median value of 0.02 wt% NiO.

Amphiboles in the sample IMK – 05149 are exclusively represented by calcium amphiboles in the analyses. In total, 34 samples corresponded to calcium amphiboles, out of which only two analyses correspond to minerals of the actinolite-tremolite series (Figure 30). According to the Mg/(Mg+Fe) ratio, a mineral with a value below 0.9 is actinolite and those with a value above 0.9 is tremolite. Both minerals (Appendix V) contain around ~56.28 wt% SiO_2, whereas the MgO values are between 21.78 and 22.35 wt% MgO, FeO values are from 3.45 to 5.62 wt% FeO, Al_2O_3 values are between 1.31 and 1.46 wt% Al_2O_3, and, finally, CaO values are from 10.89 to 12.26 wt% CaO. Nickel occurs in a relatively low concentration of 0.08 wt% NiO in actinolite, whilst tremolite contains up to 0.23 wt% NiO.

In the sample IMK – 05153, a total of thirteen points are characterised as calcium amphiboles. Out of the thirteen points, and according to the Mg/(Mg+-Fe) ratio, seven analyses are compositionally actinolites with a Mg/(Mg+Fe) value below 0.9, whereas four are tremolites with a value above 0.9. Two remaining analyses are of hornblendes, with a Si value below 7.5 apfu (Figure 30). Amphiboles of the actinolite-tremolite (Appendix V) contain: from 53.50 to 58.81 with a median of 55.73 wt% SiO_2, from 21.47 to 26.05 with a median of ~22.62 wt% MgO, from 3.40 to 6.35 with a median of 5.23 wt% FeO, from 0.23 to 4.66 wt% Al_2O_3 with a median of 0.78 wt%, and lastly, from 3.35 to 11.40 with a median of 9.28 wt% CaO. Nickel values vary between 0.04 and 0.41 wt% NiO.

The Ni values observed in the actinolite-tremolite series amphiboles are generally low, as indicated by the median values, additionally, there are slightly higher median values in tremolites, however, the maximum value belongs to an actinolite. Overall, sample IMK – 05149 and IMK – 05153 had the higher Ni concentrations in actinolite-tremolites, comparatively to sample IMK – 05139.

7.2.3.2. Hornblende

Hornblendes contain a higher proportion of Al and a lower proportion of Si, as shown in Figure 29 and Figure 30. Alkali enrichment is also visible in Figure 31 (after Hawthorne, et al., (2012).

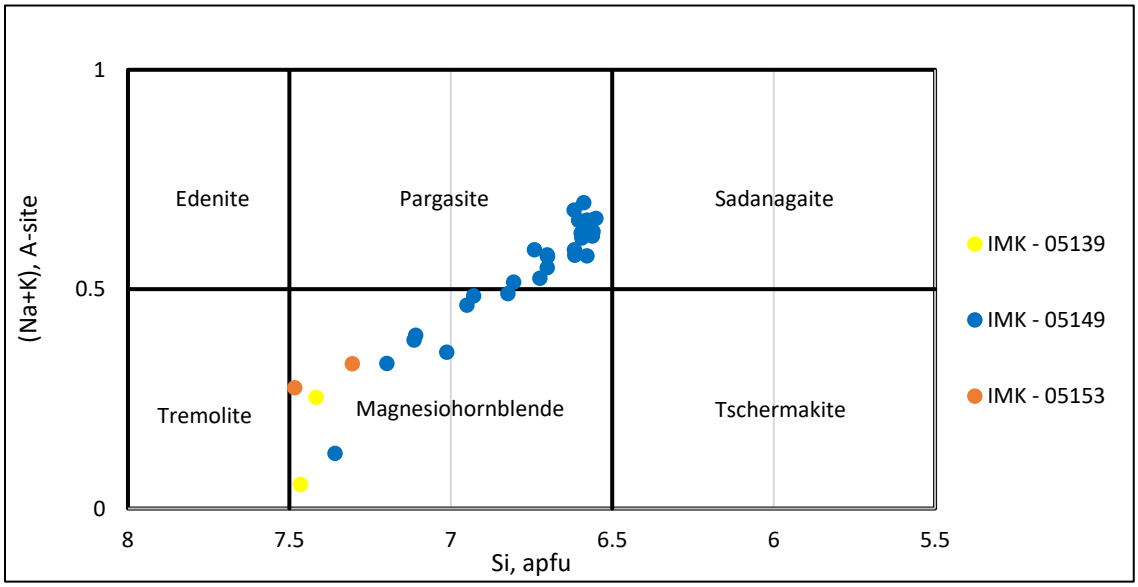

Figure 31: Alkalis hornblende amphibole classification plot with a silica per atom formula unit Vs the sum of Na and K in the A-site of the formula (after Hawthorne, et al., (2012).

The sample IMK – 05139 provided two analyses of calcic amphibole of the magnesiohornblende type (Figure 29). They are characterised by 52.26 - 52.43 wt% SiO_2, 19.65 - 23.81 wt% MgO, 5.41 - 5.82 wt% FeO, 1.75 - 5.25 wt% Al_2O_3 and 10.25 - 11.41 wt% CaO (Appendix V). MnO value was below detection limit and 0.07 wt% MnO, whereas Ni was observed at 0.03 and 0.11 wt% NiO. As for the alkalis, Na appears between 0.16 and 0.88 wt% Na_2O, and, K between 0.05 and 0.07 wt% K_2O. Both analyses correspond to low alkali enrichment (Figure 31).

In the sample IMK – 05149, thirty-two of the thirty-four calcium amphiboles analytical points correspond to a magnesiohornblende composition (Figure 30). The Si content varies between 44.80 and 52.93 wt% SiO_2 with a median value of 46.73 wt% SiO_2. Magnesiohornblende also contains (Appendix V) from 18.33 to 20.97 wt% MgO with a median of 18.88 wt% MgO, from 2.68 to 5.69 wt% FeO with a median of 4.41 wt% FeO, from 5.93 to 12.67 wt% Al_2O_3, with a median of 11.86 wt% Al_2O_3, from below the detection limit up to 0.081 with a median of 0.017 wt% MnO, and, lastly, from 10.6 to 12.67 wt% CaO. Nickel values are as low as 0.071 NiO wt% up to a maximum of 0.198 wt% NiO with a median value of 0.15 wt% NiO. The compositional ranges of the alkalis are from 0.46 to 2.45 wt% Na_2O, with a median of 2.07 wt% Na_2O, and, from 0.01 to 0.18 wt% K_2O, with a median of 0.11 wt% K_2O. Alkalis enrichment is more present in the amphiboles of sample IMK – 05149 where the majority (24) analyses contain a Na + K, apfu, value over 0.5, whilst only eight samples contained a value below 0.5 (Figure 31).

Only two of the analysed calcic amphiboles in the sample IMK – 05153 correspond to hornblendes (Figure 30). The IMK – 05153 magnesiohornblende (Appendix V) contains: 51.56 and 53.32 wt% SiO_2, 20.27 and 20.84 wt% MgO, 3.47 and 3.98 wt% FeO, 5.63 and 6.31 wt% Al_2O_3, and, 10.02 to 10.24 wt% CaO. Manganese occurs below detection limit in one sample and at 0.004 wt% MnO in another. The Ni contents are 0.398 and 0.62 wt% NiO, which indicate a slightly higher enrichment relative to the other amphiboles in all three samples. Alkalis appear between 0.98 and 1.15 wt% Na_2O, and between 0.05 and 0.08 wt% K_2O. In sample IMK – 05153 the hornblende is characterised by a low alkali enrichment Figure 31.

The data gathered on magnesiohornblende of these samples demonstrate the increased Al content relative to the other calcium amphiboles, including actinolite-tremolite, contrarily, the Si values are lower. The Ni values are relatively low although slightly more homogenous, with the highest values observed in sample IMK – 05153. Similarly, the number of actinolite-tremolite points were too low on samples IMK – 05139 and IMK – 05153 to be able to produce enough data to be of statistical significance. The alkalis appear enriched in most analysis of IMK – 05149, however, in IMK – 05139 and IMK – 05153 there is no evidence of alkalis enrichment, Figure 31.

7.2.3.3. Mg-Fe-Mn amphiboles

Some of the amphiboles have low Ca, Na and K concentration, whereas they are characterised by elevated Mg and Fe values.

In total, 6 analytical points correspond to amphiboles of the Mg-Fe-Mn series, 5 of which occur in the sample IMK – 05139. These amphiboles ere characterised by compositions that show from 49.13 to 56.32 with a median of 55.62 wt% SiO_2, from 23.80 to 31.99 with a median of 29.69 MgO, from 5.89 to 7.81 with a median of 6.52 wt% FeO, from 1.14 to 3.19 with a median of 1.36 wt% Al_2O_3, from 0.08 to 0.17 with a median of 0.09 wt% MnO, and from 1.12 and 6.62 with a median of 3.05 wt% CaO (Appendix V). The Ni concentration observed has a minimum value of 0.02 wt% NiO and a maximum value of 0.12 wt% NiO while a median is around 0.07 wt% NiO.

In the sample IMK – 05153, amphibole of the Mg-Fe-Mn series contains, 51.63 wt% SiO_2, 26.69 wt% MgO, 7.21 wt% FeO, 0.70 wt%Al_2O_3, 0.43 wt% MnO and 4.99 wt% CaO. Nickel occurs with a similar concentration to the other amphiboles (0.17 wt% NiO) (Appendix V).

These results show an increase of the Mg and Fe median values of the Mg-Fe-Mn amphiboles compared to the calcic amphiboles. As for the Ni, the values appear similar across the different amphiboles.

7.2.4. Ni content in silicates

Through the previous chapters, it is possible to observe that Ni occurs in different proportions within the various silicates present in our samples. In Figure 32 the NiO wt% values in the silicates are displayed on a whisker diagram.

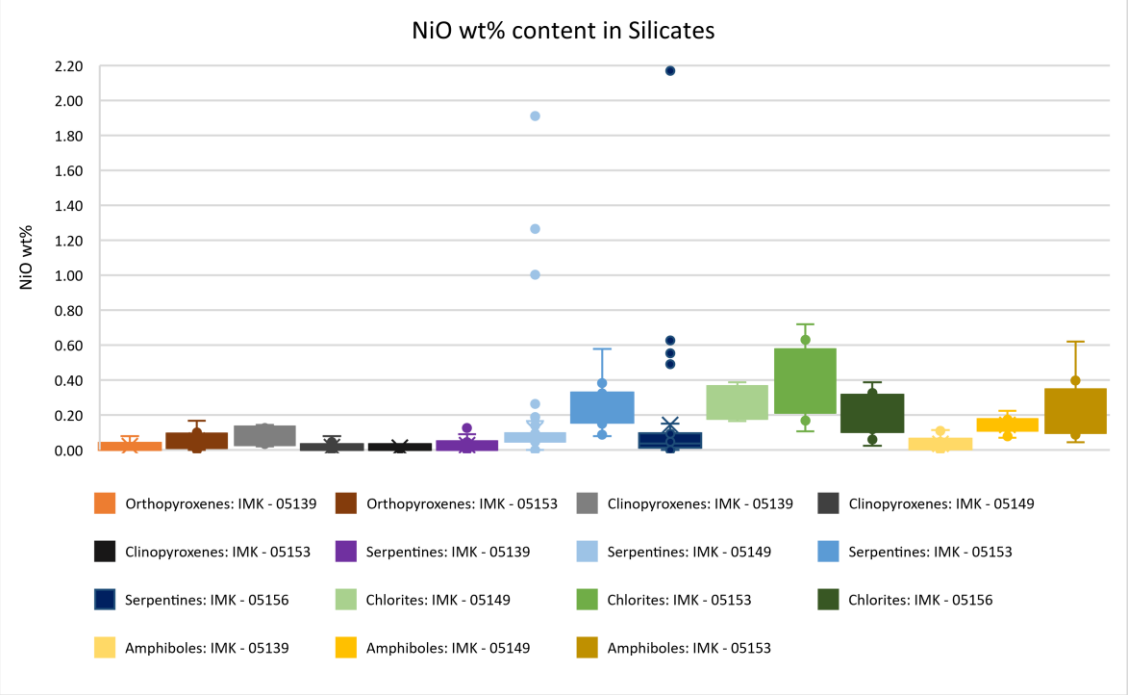

Figure 32: Whisker diagram of the NiO wt% content in the different silicates per sample.

The primary silicates have an average value of NiO wt% lower than the secondary silicates, indicating a relative enrichment of Ni in the secondary silicates. Within the secondary silicates, chlorites have higher average values, while serpentines have the highest values in the outliers.

These results indicate an enrichment of Ni in the secondary silicates with the serpentines having the highest values observed. The higher Ni content in the secondary silicates is due to the suggested genetic relation between the serpentinisation events and the origin of Ni-rich minerals (see Chapter 9). Serpentine is the most common secondary silicate and occurs closely associated with the mineralisation (see chapter 8.3), thus, the outliers are likely to originate in the proximity with Ni-rich minerals.

7.3. Ore Minerals

Four samples were selected for the investigation based on presence of visible sulphides. Samples were studied in detail using microprobe and automated mineralogy. Three main types of mineralisation are observed, the first group and most common are sulphides, followed by chromites and non-sulphide mineralisation of alloys and As-Sb-Bi and Pb minerals. With the exception of the chromite-rich assemblages, the ore mineral associations are predominantly composed of Ni-rich minerals.

7.3.1. Pentlandite

Pentlandite is one of the most common Ni-Fe sulphides worldwide, with a stochiometric (IMA) formula: $(Ni_xFe_y)_{\Sigma 9}S_8$, it has a compositional range of Fe and Ni, with possible Co, Cu, PGE and Au impurities. This mineral was found and analysed in the samples IMK – 05139 and IMK – 05149 (Figure 33).

In sample IMK – 05139, pentlandite is the most common ore mineral, corroborated by TIMA results, with fifty-one analyses of pentlandite performed by the microprobe. A varying amount Ni and Fe is present in pentlandite: from ~27.11 to ~30.71 wt% Ni with a median of 29.10 wt% Ni and from 34.78 to 36.63 wt% Fe with a median value of 35.83 wt% Fe. The molecular proportion of Ni versus Fe was calculated with following formula $XNi = \frac{Ni*100}{Ni+Fe}$. Results show a median *XNi* value of 44.83, with a maximum of 46.56 and minimum of 42.84. Pentlandite in IMK – 05139 pyroxenite has up to 0.93 wt% Co, a minimum value of 0.63 wt% Co and a median of 0.75 wt% Co (Appendix V). The sulphur values are from 33.11 to 34.18 wt% S with a median of 33.75 wt% S. These values denote no significant Ni enrichment in Molopo Farms Complex pentlandite, with the majority of the analyses within the standard compositional ranges of Fe-rich variety with the relatively low Co content.

In contrast to sample IMK – 05139, in sample IMK – 05149, orthopyroxenite, pentlandite is not the predominant ore mineral as the sulphide assemblages are dominated by heazlewoodite (see section 7.3.4).
The compositional ranges in IMK – 05149 pentlandite are slightly different with a Ni value varying between 32.14 and 36.86 wt% Ni resulting in a median of 36.18 wt% Ni. Pentlandite in the sample IMK – 05149 (Appendix V) contains: from 22.64 to 26.14 wt% Fe with a median of 25.25 wt% Fe. The proportion of Ni and iron, *XNi*, calculated the same way as previously, shows

a maximum of 60.60, a minimum of 57.77 and a median of 58.86. Finally, Co appears more enriched with a minimum value of 3.08 wt% Co, a maximum of 4.89 wt% Co and a median of 3.86 wt% Co.

These results show a Ni and Co enrichment compared to the sample IMK – 05139, along with a relative Fe deficiency, Figure 33. Sulphur values are relatively similar to those in IMK – 05139 pentlandite, whilst in sample IMK – 05149 they vary between 32.03 and 33.67 wt% S with a median of 33.45 wt% S. A couple of analytical points show elevated Cu values up to 0.87 wt% Cu, although median values are below detection limit.

The presence of heazlewoodite in sample IMK – 05149 and the higher Ni enrichment of coexisting pentlandite shows an overall Ni (and Co) enrichment of the sulphide assemblage in this sample.

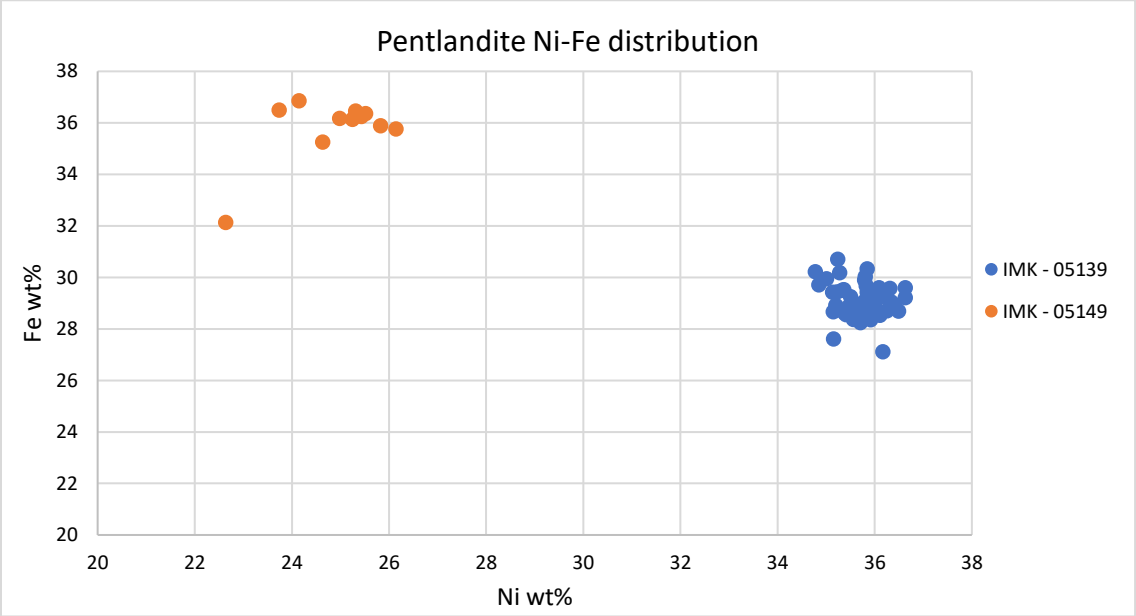

Figure 33: Ni-Fe (Ni wt% and Fe wt%) distribution in pentlandite from samples IMK – 05139 and IMK – 05149

7.3.2. Pyrrhotite

Pyrrhotite is a minor mineral phase only in the sample IMK – 05139, where it occurs in close association with pentlandite. It corresponds to a sulphide with the mineral formula (IMA) dependent on the polytype, but, generalised to: $Fe_{1-x}S$, where the common impurities are Ni, Cu and Co (Anthony, et al., 2001-2005). A total of fourteen points were classified as pyrrhotite, with a compositional range from 53.34 to 57.20 wt% Fe with a median of 56.07 wt% Fe, from 4.74 to 8.96 wt% Ni with a median of 5.45 wt% Ni, and from 35.35 to 36.87 wt% S with a median of 36.44 wt% S (Appendix V). In one sample 4.21 wt% Cu was detected; however, the median value is below detection limit. Minor amounts of cobalt were also detected, between 0.41 and 0.76 wt% Co, with a median of 0.60 wt% Co. These results denote an overall pyrrhotite enrichment in Ni, where the calculated XNi was from 8.12 to 14.38 and the median 8.74. The extremely high Ni in the IMK-05139 pyrrhotite suggests the progressive replacement by mackinawite, which coexist with pyrrhotite and is highly enriched in Ni compared to its pyrrhotite precursor.

The high Ni enrichment in this typically Ni poor sulphide implies significant Ni remobilization during serpentinization-related fluid circulation. This is consistent with the

presence of Fe-rich pentlandite in the association with Ni rich pyrrhotite and mackinawite in the sample IMK – 05139. It is possible that both Ni-rich pyrrhotite and mackinawite extracted Ni from primary pentlandite depleting it in Ni. Alternatively, and more probable, additional Ni could be contributed from decomposed olivine as indicated by increasing Ni enrichment with progressing degree of primary sulphide replacement by secondary Ni-rich sulphides, alloys and arsenides.

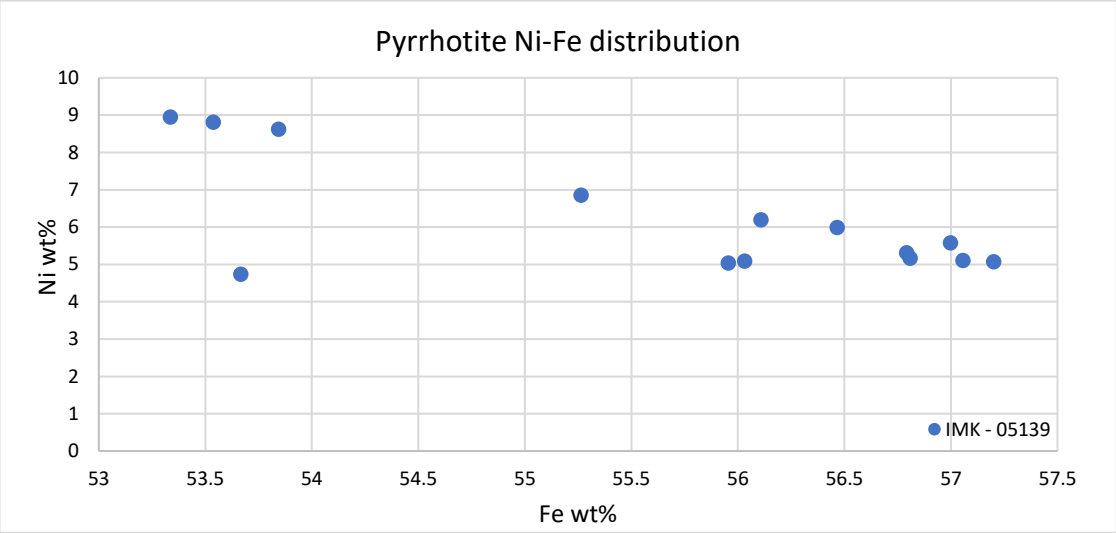

Figure 34: Ni-Fe (Ni wt% and Fe wt%) distribution in pyrrhotite from samples IMK – 05139

7.3.3. Mackinawite

This mineral phase is detected in pyroxenite, sample IMK – 05139, where three points were correlated to mackinawite. It corresponds to a Ni-Fe sulphide, similar to pentlandite, with a formula: $(Fe,Ni)_9S_8$, or, $(Fe,Ni)_{1+x}S$ $(x = 0\text{-}0.07)$ IMA formula, as it occurs with a lower Ni-Fe ratio, XNi, meaning, it is less rich in nickel compared to pentlandite (Anthony, et al., 2001-2005). Nickel values vary from 14.29 to 17.99 wt% Ni with a median of 15.77 wt% Ni. Mackinawite contains 44.93 up to 47.97 wt% Fe with a median of 47.37 wt% Fe and from 34.54 to 35.86 wt% S with a median of 36.65 wt% S (Appendix V). Cobalt is also detected, with a maximum of 0.96 and a minimum of 0.84 wt% Co with a median of 0.94 wt% Co. The Ni-Fe ratio, XNi, is between 22.98 and 28.59, with a median of 24.98 that denotes the lower Ni concentration relative to those in pentlandites, but the higher values compared to those in pyrrhotite.

Figure 35 displays the Ni-Fe compositional differences between the three Ni-Fe sulphides present in the samples, where it is possible to observe the gradual decrease in Ni proportion from the Ni-rich pentlandite to Ni-poor pentlandite to mackinawite and to pyrrhotite. The plot shows the notable higher Ni enrichment of pentlandite from the sample IMK – 05149 relative to pentlandite from the sample IMK – 05139.

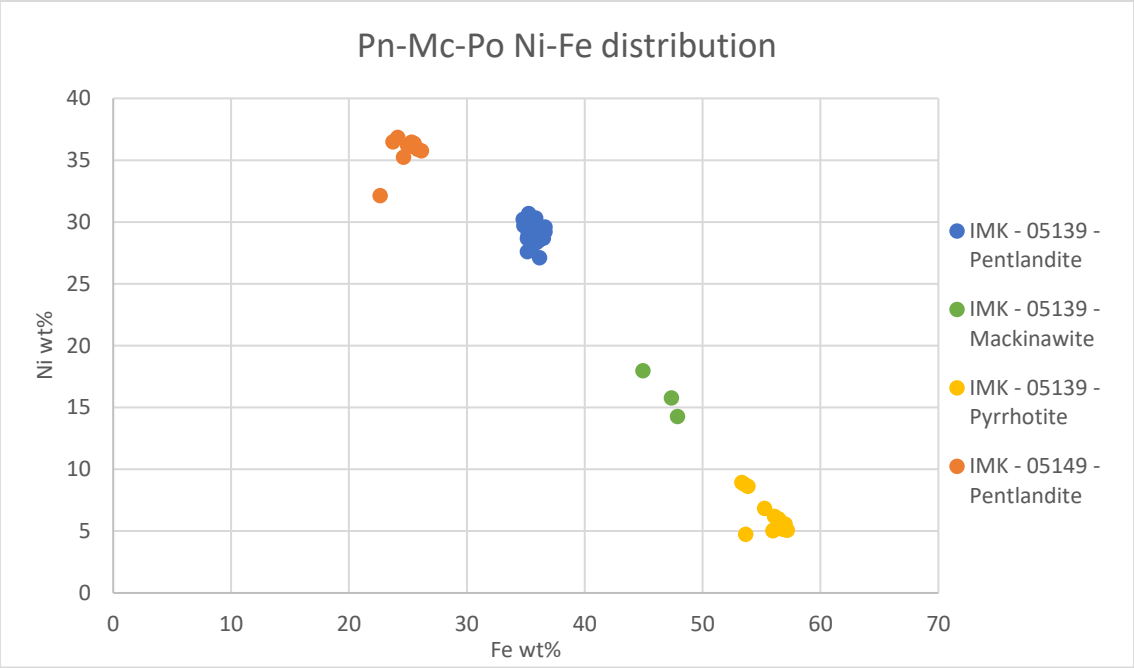

Figure 35: Ni-Fe (Ni wt% and Fe wt%) distribution in pentlandite, pyrrhotite and mackinawite from samples IMK – 0539 and IMK – 05149.

7.3.4. Heazlewoodite

Heazlewoodite is a Ni sulphide with the chemical formula (IMA) Ni_3S_2, and although it is a predominantly Ni mineral, it may contain some minor Fe impurities (Anthony, et al., 2001-2005). This mineral occurs in several mineralised samples and was analysed in the samples IMK – 05149, IMK – 05153 and IMK – 05156.

In the sample IMK – 01549, thirty-seven analytical points correspond to heazlewoodite as it is the predominant sulphide in the ore mineral assemblage. The results show a near pure heazlewoodite, with Ni values within 69.82 and 72.16 wt% Ni with a median of 70.96 wt% Ni, whilst Fe values reach a maximum of 0.894 compared to a minimum of 0.013 and a median of 0.181 wt% Fe (Appendix V). Although the Fe values are low, it still constitutes, on average, the highest value of the trace elements in heazlewoodite. Sulphur content has a maximum, a minimum and median value of 27.84, 27.25 and 27.49 wt% S, respectively.

In the sample IMK – 05153 heazlewoodite is also the most common sulphide and fifteen analyses correspond to this mineral. Nickel values vary between 69.53 and 73.53 wt% Ni, with a median of 72.40 wt% Ni. Iron values show a wider variation with a minimum value of 0.02 and a median of 0.33 wt% Fe, a maximum value of 4.12 wt% Fe and 2 more compositions with 1.12 and 1.11 wt% Fe (Appendix V). Sulphur shows a maximum value of 27.86 wt% S, a minimum value of 26.77 wt% S and a median of 27.58 wt% S. Overall, heazlewoodite in this sample shows a slight Fe enrichment and S deficiency that may be related to its co-existence in intergrowths with awaruite, a Ni-Fe alloy (Ni_3Fe), that occurs in this sample.

Only two analyses of sulphides in the sample IMK – 05156 correspond to heazlewoodite, which was not found in this sample during petrographic and TIMA studies. The total of the analyses was not complete. Nonetheless, the two analyses show Ni values from 69.84 to 70.06 wt% Ni, the Fe values from 0.16 to 0.18 wt% Fe, and S values from 27.13 to 26.42 wt% S

(Appendix V). These results show that the Ni values are similar to those from the other samples with heazlewoodite so tiny speckles of this mineral are present in the assemblage.

7.3.5. Chalcocite

Chalcocite is a Cu sulphide, with a formula (IMA) Cu_2S. The mineral contains near 80 wt% Cu (Anthony, et al., 2001-2005). Chalcocite was found in the sample IMK – 05149 under optical microscope and 5 microprobe analyses confirmed its composition. Copper values have a maximum of 77.80 and a minimum of 76.71, with a median of 77.16 wt% Cu, whereas S values stayed relatively constant between a maximum of 21.51 and a minimum of 21.20 wt% S (Appendix V). Overall, the composition is very homogeneous and denotes a slight Cu deficiency compared to the values of the handbook of mineralogy (Anthony, et al., 2001-2005). Furthermore, some Fe and Ni impurities were detected, with a median value at 0.56 wt% Ni and 0.53 wt% Fe, which may have contributed to the Cu deficiency. These chalcocite analyses represent the most Cu-rich mineral among those analysed, although minor chalcopyrite is present as interstitial filling and crosscutting veinlets among pentlandite in the samples IMK-05139. Tiny grains of associated bornite and covellite observed under the microscope in IMK – 05149 were not analysed.

7.3.6. Samaniite

One microprobe analysis in the sample IMK – 05139 corresponds to a rare Ni-Fe-Cu sulphide, samaniite with the formula (IMA) $Cu_2Fe_5Ni_2S_8$ (Anthony, et al., 2001-2005). The measured proportions do not perfectly fit the formula. The Ni, Fe, Cu and S values are 19.59 wt% Ni, 33.62 wt% Fe, 11.32 wt% Cu and 34.50 wt% S (Appendix V) which recalculated to the atoms per formula unit proportions of 2.58 Ni, 4.65 Fe, 1.38 Cu and 8.31 S. These results denote a Ni enrichment, an Fe-Cu deficiency, as well as a higher S proportion with respect to the IMA approved composition, so this may indicate a mix of minerals or an unknown mineral.

7.3.7. Awaruite

With the chemical formula (IMA) Ni_3Fe, awaruite is a Ni-Fe alloy that is common in the sulphide-dominant assemblages of the sample IMK – 05153. The known common impurities are Co, Cu, S, P and Si (Anthony, et al., 2001-2005). A total of 19 of the analyses in the sample IMK – 05153 correspond to awaruite. Its composition includes a maximum of 75.74, a minimum of 74.05 and median of 74.93 wt% Ni, and a minimum of 23.0, a maximum of 25.25 wt% Fe, with a median of 24.47 wt% Fe (Appendix V). Of the most common impurities, Cu demonstrates the highest values, with variations between 0.20 and 0.72 wt% Cu with a median value of 0.50 wt% Cu. Awaruite also contains 0.18, 0.75 and 0.36 wt% Co as a minimum, a maximum and a median value, respectively. Sulphur shows a wide variation from a minimum of 0.001 wt% S to a maximum of 1.69 wt% S, however, a median value of only 0.02 wt% S suggests that the maximum corresponded to an outlier and could be a result of contamination. These results show

relatively homogeneous awaruite compositions with the impurities constituting less than 1% of the total.

The molecular ratio between Ni and Fe, XNi, was calculated, and the results show near constant values between 74.76 and 76.71, with a median of 75.4, close to the stoichiometric ratio in the formula, Ni_3Fe, of 3 Ni atoms to 1 Fe atom, that is 75 % Ni to 25 % iron.

7.3.8. Maucherite

Maucherite is a Ni arsenide with the chemical formula (IMA): $Ni_{11}As_8$ and, according to the handbook of mineralogy (Anthony, et al., 2001-2005), with the composition of ~49-51 Ni wt% and ~46-48 As wt%. Maucherite is one of two Ni arsenides found in the samples along with orcelite described below. Common impurities include Co, Fe, Cu, Sb and S. In the sample IMK – 05139 maucherite is a very minor mineral that forms rounded grains up to 100 microns in size. Three analyses (Appendix V) yielded the following compositions: from 48.30 to 50.70 wt% Ni with a median of 50.28 wt% Ni, from 47.70 to 49.72 wt% As with a median of 48.88 wt% As. Fe is present up to a maximum of 1.87 wt% Fe, with a minimum of 1.14 wt% Fe and a median of 1.60 Fe wt%, Cu shows the second highest values among the impurities, with 0.221 to 1.03 wt% Cu and a median of 0.85 wt% Cu. In addition, maucherite contains 0.70 - 0.91 wt% Co with a median of 0.70 wt% Co, 0.67 wt% Sb (a median value) and 0.40 S wt% (a median value). The impurities account for the totals of around 3 to 5 wt% of the composition whereas Ni and arsenic values are within the approved range.

7.3.9. Orcelite

Orcelite is another Ni arsenide, with the formula (IMA): $Ni_{5-x}As_2$ $(x=\sim0.25)$, where Ni content varies slightly dependent on the impurities present as represented by x, which includes Fe, S, Si, Mg and water (H_2O). According to the handbook of mineralogy (Anthony, et al., 2001-2005), Ni content varies between 57 and ~65 wt% Ni and arsenic between 32.5 and 35.6 wt% As. The impurities may account for up to a total of ~10 wt%.

The sample IMK – 05153 (Appendix V) yielded 2 analyses that correspond to the expected composition of orcelite, as such, both these analyses showed 67.67 and 68.40 wt% Ni and 30.82 and 32.06 wt% As. Antimony constitutes the highest proportion of the impurities, with a maximum value of ~3.37 and a minimum of 2.64 wt% Sb. Orcelite contains from 0.34 to 0.11 wt% Fe with a median of 0.22 Fe wt%, and from 0.088 to 0.098 wt% S with a median of 0.09 S wt%. Silica, magnesium and water were not measured due to the microprobe analysis package used for the analyses. The elevated Sb content in these analyses is most likely due to the presence of tiny inclusions of breithauptite NiSb that were verified by the scanning electron microscopy.

In the harzburgite, IMK – 05156, which comprises a disseminated chromite zone with Ni arsenide minerals, contrary to the initial identification through TIMA, the Ni arsenides are represented not by maucherite but instead by orcelite according to the microprobe results. Out of the 24 total analyses done, ten were classified as orcelite, as the other analyses had bad totals, either by being too much above or too much below 100%. The reliable analyses (Appendix V)

show variations of Ni values between 63.05 and 68.79 wt% Ni with a median value of 65.20 wt% Ni, as for arsenic, values were slightly more homogeneous between 33.80 and 37.43 wt% As with a median of 34.72 wt% As. Therefore, the Ni values are on the higher end and slightly above the standard compositions shown in the handbook of mineralogy (Anthony, et al., 2001-2005), however, the As content is well within the expected values. In terms of impurities, orcelite contains from 0.46 and 1.00 wt% Sb with a median of 0.68 Sb wt%, and traces of Te with a median value of 0.12 wt% Te. Overall, the observed Ni enrichment and deficiency of impurities, with the exception of Sb, can be explained by the fact that Si, Mg and water values are not accounted for in these analyses.

Two analyses in the sample 05149 (Appendix V) show the presence of Ni arsenide with 63.40 - 63.36 wt% Ni and 24.44 - 28.24 wt% As. These values are similar to the Ni value of orcelite, however, the arsenic content is well below the expected values. The total of the components in the first analysis only adds up to 92.62 wt% whereas the second analysis has a total of 98.25 wt%. This suggest that some grains of orcelite or other Ni arsenide do occur in this sample although the analytical results on its composition are unreliable.

7.3.10. Unknown/Unnamed Nickel Antimonide

Seven analyses of Ni antimonides were obtained for the studied samples. Out of these, only four of them in the sample IMK – 05153 have had results that coincide to known Ni antimonide. This mineral contains 58.52 to 60.77 wt% Ni and 38.56 to 40.89 wt% Sb (Appendix V), that fit the known, but unnamed, Ni antimonide with the chemical formula (IMA): Ni_3Sb.

In sample IMK – 05149, four other analyses yielded Ni and antimony, however, three of those also had a significant arsenic value that was nearly equal to the antimony value. The compositions with only antimony and Ni had a near ~90 wt% total, which made them difficult to interpret. Most of antimonides are present as tiny inclusions 1-20 microns in size in orcelite and maucherite, therefore the contamination is unavoidable and the compositions reflect the mixes of Ni antimonides and Ni arsenides.

7.3.11. Parkerite

The rarest mineral is a nickel-bismuth-lead-sulphide that was classified as parkerite. The IMA-approved formula (IMA) for this mineral is $Ni_3(Bi,Pb)_2S_2$ (Anthony, et al., 2001-2005). The mineral consists of ~30 wt% Ni, 50 to 60 wt% Bi, 0 - 9.5 wt% Pb and ~9-10 wt% S. Three analyses (Appendix V) show a relatively homogeneous composition with ~9-10 wt% S and 27.2-28.36 wt% Ni, however, ~30-32 wt% Bi are slightly lower, whereas ~24-25 wt% Pb are slightly higher than expected values. Taking into account the possible isomorphism between Bi and Pb, these compositions are compatible with the IMA formula. In addition to parkerite, small grains, less than 20 microns in size, in the sample IKM – 05149 were diagnosed as shandite $Pb_2Ni_3S_2$ according to energy-dispersive analysis by TIMA.

7.3.12. Chromite

Chromite is a common mineral in ultramafic rocks and can form economically significant layers in the Bushveld Complex and other layered intrusions.

Chromite is the principal member of the spinel series, alongside magnesiochromite. The spinel-group minerals are divided into three series, where the trivalent ion is the defining factor, as it can be Al, Fe^{3+} or Cr (Deer, et al., 1992). The mineral group is divided into the spinel series if Al is the trivalent ion, the magnetite series if Fe^{3+} is the trivalent ion and the chromite series if Cr is the trivalent ion. In total, there are eight important endmembers in respect to the different spinel group series: chromite, magnesiochromite, spinel, magnesioferrite, magnesium titanate, magnetite and ulvospinel. These minerals also constitute the endmembers of the spinel compositional prism, as shown in Figure 36. The chromite formula is $(Fe,Mg)(Cr,Fe,Al)_3O_4$.

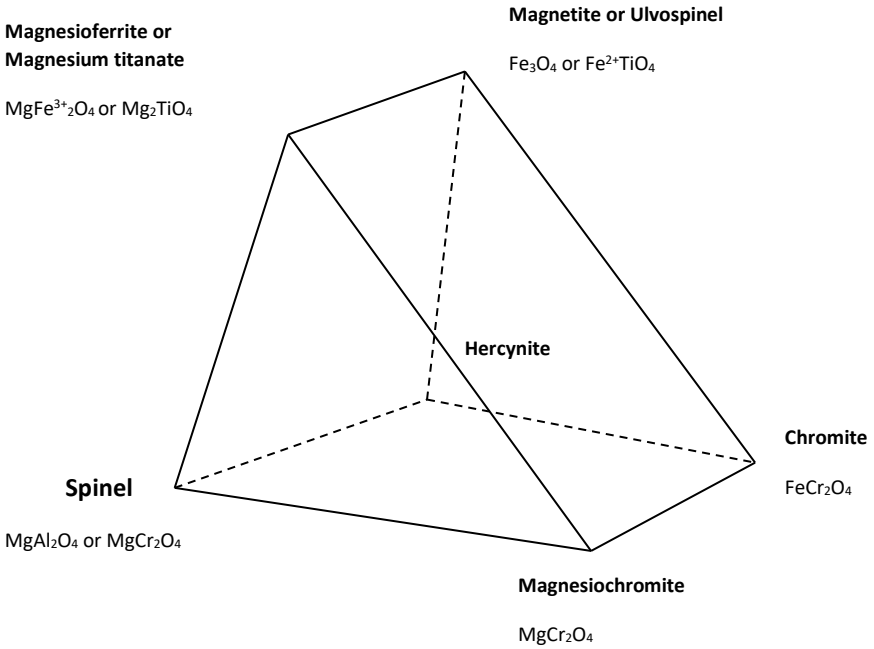

Figure 36: Compositions of the spinel group minerals represented on the spinel prism. The apices are defined by Fe^{3+}, Cr^{3+} and Al^{3+}, after Deer et al., (1992).

Samples IMK – 05139 and IMK – 05149 contain disseminated chromite, whereas for sample IMK – 05156, it contains a chromite rich zone that is up to 5 cm thick.

A total of twelve chromite analyses were made on sample IMK – 05139. The compositional ranges (Appendix V) are wide: 49.72 - 65.14 wt% Cr_2O_3 with a median of 55.83 wt% Cr_2O_3, from 15.46 to 28.40 wt% FeO with a median of 25.79 wt% FeO, while calculated values of Fe_2O_3 varies from 0 to 1.02 wt% Fe_2O_3 with a median of 0.26 wt% Fe_2O_3. In all the samples, the chromite formula and proportions of divalent and trivalent Fe were calculated based on the spinel stoichiometry and using the spreadsheet provided by *S.J. Barnes (pers com)*. Similarly, Mg and Al also show some variations: from 2.6 to 12.15 wt% MgO with a median of 4.63 wt% MgO, and from 1.94 to 18.99 wt% Al_2O_3 with a median of 8.87 wt% Al_2O_3. Nickel content varies from below the detection limit to 0.13 wt% NiO with a median of 0.03 wt% NiO. The other elements vary within the following compositional ranges: 0.18 to 0.31 wt% V_2O_3, 0.17 to 0.72 wt% TiO_2 and 0.11 to 0.48 wt% ZnO. Manganese is regularly below the detection limit. These results show the existence of a continuous series of the chromite compositions from Mg-poor Cr to Mg-enriched and Cr-depleted (Figure 37). The magnesium-Fe molecular ratio or Mg# by the formula: Mg# = $\frac{100 \times Mg}{Mg + Fe2+}$, and Cr-Al molecular ratio or Cr# by the formula: #Cr = $\frac{100 \times Cr}{Cr + Al}$ correlate negatively so that a higher Mg# corresponds to a lower Cr# and vice versa.

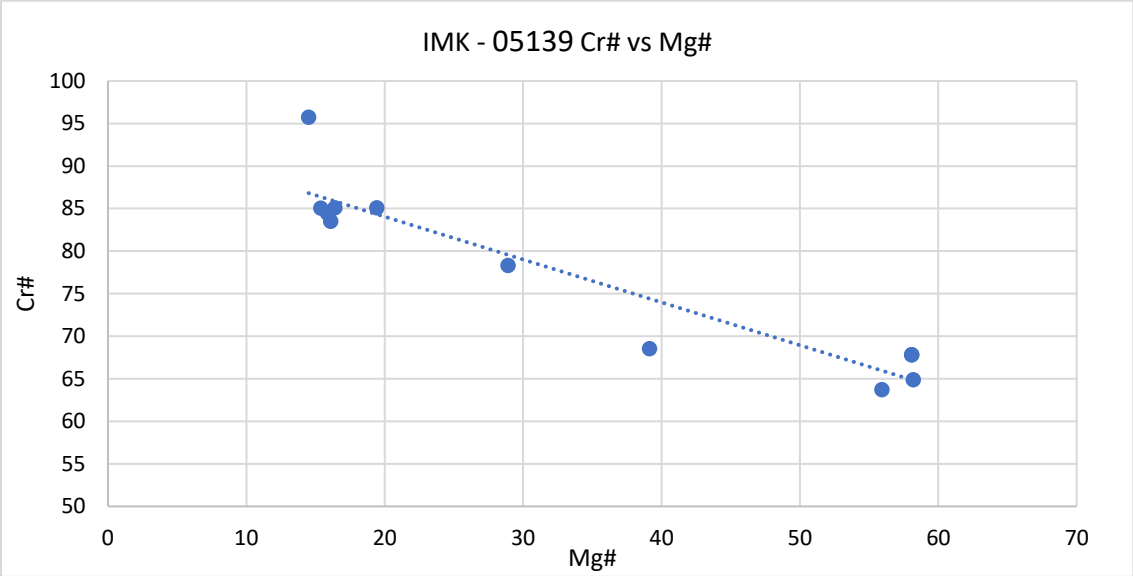

Figure 37: Chromium variation in chromites from sample IMK – 05139, with Cr# Vs Mg#, where Cr# is the Cr-Al molecular ratio and Mg# is the Mg-Fe molecular ratio.

A total of six chromites were analysed in sample IMK – 05149 which show very little compositional variation compared to sample IMK – 05139. Chromites from sample IMK – 05149 contain 53.39 - 42.94 wt% Cr_2O_3 with a median of 49.62 wt% Cr_2O_3, from 25.79 to 28.30 wt% FeO with a median of 27.91 wt% FeO, and also calculated Fe_2O_3 values are between 4.98 and 7.14 with a median of 5.57 wt% Fe_2O_3 (Appendix V). NiO values are between 0.12 and 0.56 with a median of 0.29 wt% NiO. These values show an Fe enrichment and a Cr deficiency in these chromites with respect to chromite in the sample IMK – 05139 whilst Ti shows a slight enrichment. The compositional ranges of the remaining elements are: 5.83 to 15.21 wt% Al_2O_3, 2.41 to 5.06 wt% MgO, 0.28 to 0.40 wt% V_2O_3, 0.62 to 1.12 wt% TiO_2 and 0.21 to 0.42 wt% ZnO. Manganese is regularly below detection limit. The calculated Mg# and Cr# values (Figure 38) show a negative correlation similar to the trend in the sample IMK – 05139.

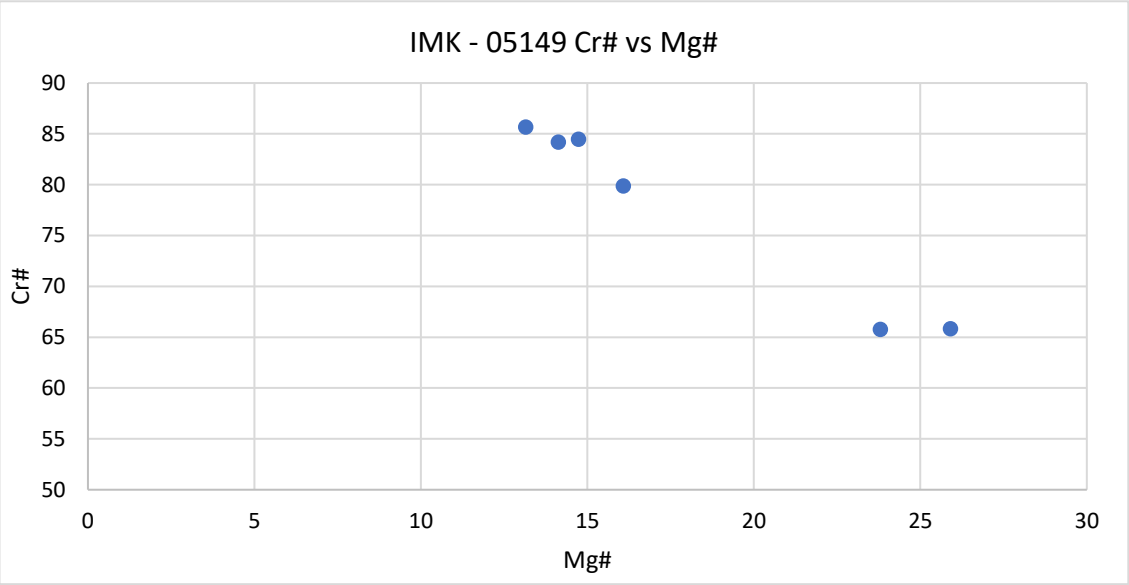

Figure 38: Chromium variation in chromites from sample IMK – 05149, with Cr# Vs Mg#, where Cr# is the Cr-Al molecular ratio and Mg# is the Mg-Fe molecular ratio.

A total of 47 chromites were analysed in sample IMK – 05156. Chromite contains 16.87-29.82 wt% FeO with a median of 20.94 wt% FeO, additionally, Fe_2O_3 content was calculated at a maximum of 25.16 and a minimum of 0.22 wt% Fe_2O_3, with a median of 0.91 wt% Fe_2O_3 (Appendix V). Chromite analyses show a maximum of 57.52 wt% Cr_2O_3 a minimum of 38.10 wt% Cr_2O_3 and a median of 47.90 wt% Cr_2O_3.

The maximum Fe values coincided with the minimum Cr values denoting outliers of an Fe-rich spinel. Excluding the outliers, the maximum Cr values also coincided, generally, with higher Fe values.

Aluminium and Mg values show wide variations from 2.50 to 21.01 wt% Al_2O_3, with a median of 18.55 wt% Al_2O_3, and from 1.51 to 11.02 wt% MgO, with a median of 8.63 wt% MgO. A positive correlation between these two elements is observable, as two spinel compositions are distinguishable. One composition has high-Al, low-Cr and high-Mg, while a second one has a low-Al, high-Cr and low-Mg. The calculated Mg# and Cr# values were plotted in Figure 39, where two distinct clusters of points occur that correlate to two different compositional groups and further corroborate the data obtained in the previous samples (Figure 37 & Figure 38).

The compositional ranges of the remaining elements are: 0.12 to 0.38 wt% V_2O_3, 0.29 to 0.93 wt% TiO_2 and 0.10 to 0.71 wt% ZnO. All Mn concentrations are below the detection limit. The Ni values observed were from below the detection limit up to 0.20 wt% NiO, with a median value of 0.06 wt% NiO.

Chromite occurs as the remnant grains of the primary cumulus assemblage in most samples, as evidenced by elevated Cr content, with the median of 3725 ppm Cr in orthopyroxenite and the median of 5428 ppm Cr in harzburgites thus indicating the higher Cr enrichment of harzburgites. As visualised in the TIMA map of the sample IMK – 05156 (Figure 44), this harzburgite is characterised by the highest Cr enrichment due to a heavily disseminated chromite zone. The chromite analyses correspond to two different compositional groups, most clearly visible in sample IMK – 05156 where there are also a higher number of points. It is less clear for sample IMK – 05139, where some analyses appear to have some transitional characteristics. The Ni values are low, where IMK – 05149 chromite shows the highest median

values at 0.29 NiO, whilst chromite from the samples IMK – 05149 and IMK - 05156 had 0.03 and 0.06 NiO wt%, respectively. The majority of the Ni values denote a very low level of nickel enrichment of spinels. The Fe-rich and the Cr-rich reflect the formation of Fe-rich rims and domains. The formation of the Fe-rich rims is generally assumed to indicate alteration of chromite through the hydrothermal processes (Yudovskaya & Kinnaird, 2010), which might also have resulted in the formation of the secondary sulphide-alloy-arsenide assemblages.

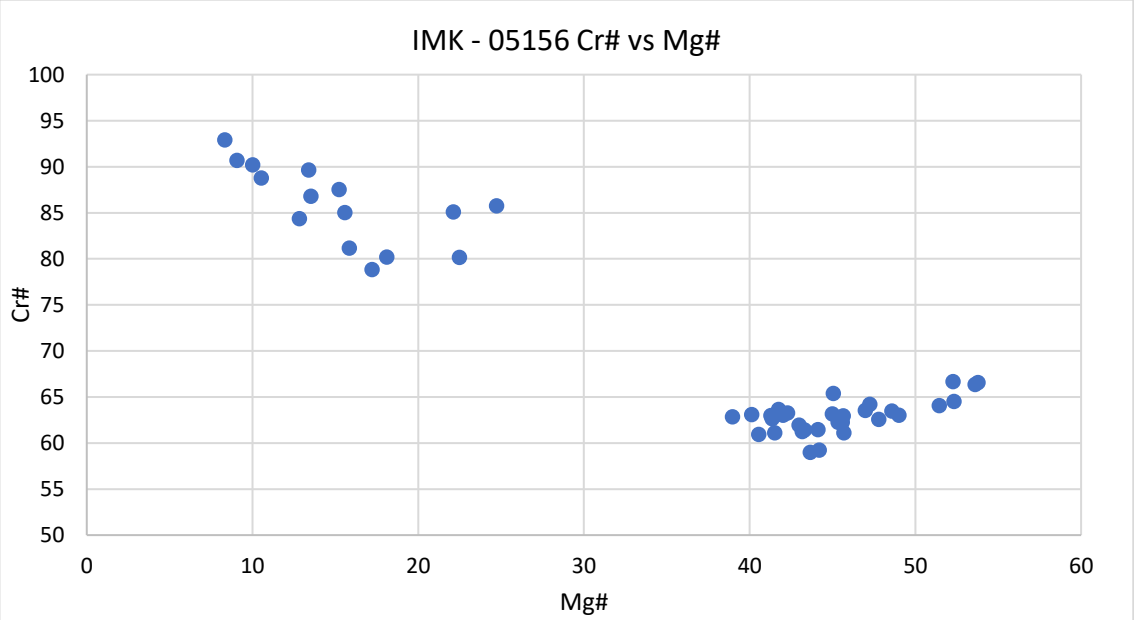

Figure 39: Chromium variation in chromites from sample IMK – 05156, with Cr# Vs Mg#, where Cr# is the Cr-Al molecular ratio and Mg# is the Mg-Fe molecular ratio.

The compositions of Molopo Farms Complex chromite form two clusters on the diagrams: High-Mg (~39 to ~54 Mg#) and low-Mg (~8 to ~25 wt% Mg#) types (Figure 37; Figure 38, Figure 39 & Figure 40). High-Mg chromite compositions are very similar to the compositions of chromite in the Lower Zone of the Bushveld Complex (Hulbert & Gruenewaldt, 1985) and massive chromitites of the Uitkomst satellite intrusion of the Bushveld LIP (Yudovskaya, et al., 2015). These high-Mg chromites are also distinguished by similar elevated Cr content up to ~53 wt% Cr_2O_3 in Molopo Farms Complex, 57 wt% Cr_2O_3 in the Lower Zone and up to 55 wt% Cr_2O_3 in Uitkomst satellite intrusion, that is notably higher than the Cr_2O_3 wt% content in chromite of the Critical Zone of the Bushveld Complex (Naldrett, et al., 2009). This similarity likely reflects a common chemically primitive composition of their Mg- and Cr-rich parental magmas of the komatiitic lineage.

The Molopo Farm Complex low-Mg chromite (Figure 37; Figure 38, Figure 39 & Figure 40) is a result of element redistribution during superimposed alteration that is induced by serpentinisation-related fluid activity. The low-Mg chromite is characterised by the elevated Cr content (up to ~65 wt% Cr2O3) and the very low content of trivalent Fe (locally below the detection limit of the microprobe analysis, Appendix V). The secondary origin of low-Mg chromite is supported by the widespread chemical heterogeneity of Molopo Farms altered chromite that is seen in the polished sections as the variably coloured domains in the grain under reflected light.

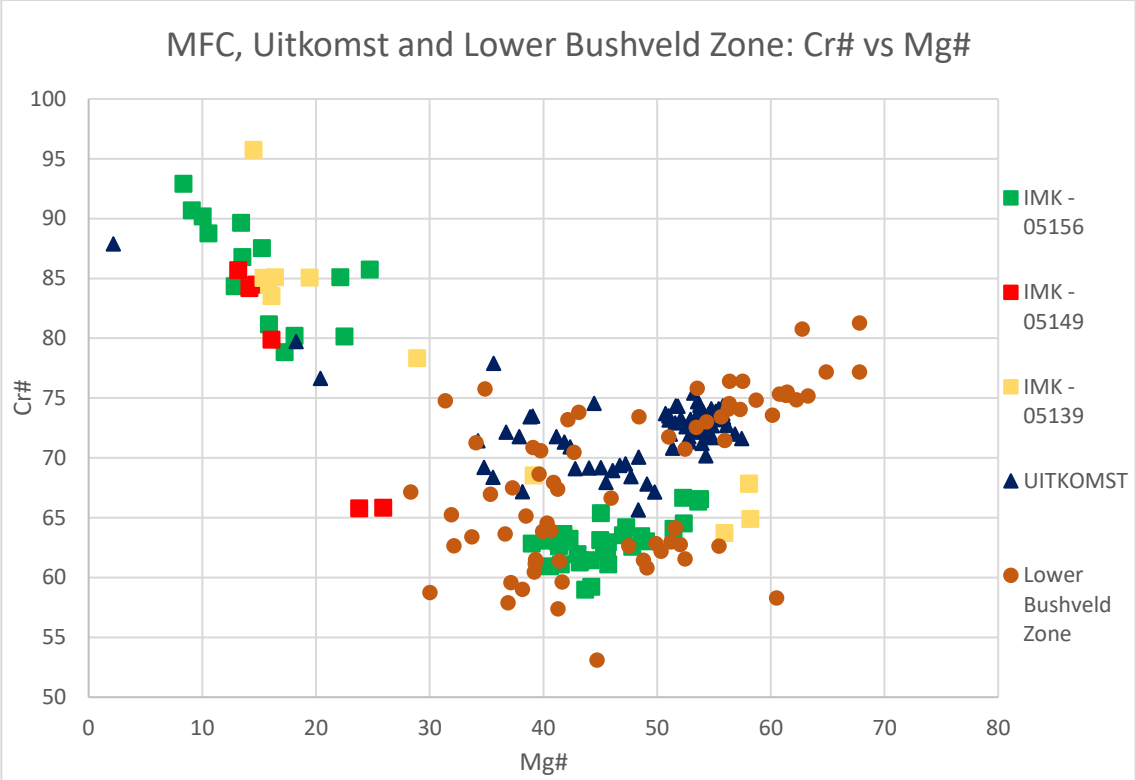

Figure 40: Comparison of Cr variation in chromites from samples IMK – 05156, IMK – 05149, IMK – 05139, Uitkomst intrusion (Yudovskaya, et al., 2015) and Lower Bushveld Zone (Hulbert & Gruenewaldt, 1985). Values as Cr# Vs Mg#, where Cr# is the Cr-Al molecular ratio and Mg# is the Mg-Fe molecular ratio.

Chapter 8

TESCAN Integrated Mineral Analyser

8.1. Description of the TIMA approach and its limitations

This method of automated mineralogy was used in order to produce statistical data. It was also used to obtain graphic representation and visual illustrations of the mineral and element distribution in the studied samples through the available TIMA software and through some processing. The samples used were IMK – 05139, IMK – 05149, IMK – 05153 and IMK – 05156, the same set that was also selected for the microprobe analysis based on the occurrence of visible Ni sulphide minerals.

As outlined in chapter 3.4, the statistical data provided by the software can be prone to significant error margins and requires manual correction. The software assumes an equal elemental percent weight within a specific mineral phase and can therefore induce statistical errors for compositionally zoned mineral phases and for minerals not considered by the software library to contain certain elements. Nickel is the element of interest in this work but is not a major component of most minerals present in the samples. Ni was detected and is known to be present in all the analysed silicates in low and variable amounts. The majority of the mineral phases, especially the silicates, do not have information on their Ni content in the software library, thus the protocol was modified in order to introduce Ni data.

The protocol consists, firstly, of collecting the percent amount of each mineral present in the sample, which is provided by the software. Secondly, in order to introduce Ni data that are representative of each mineral phase, an attentive manual selection of a group of analyses, per mineral phase, per sample, was performed. After this selection, the variable compositions (including Ni content) of each analysed point, are obtained through the program, which are then transferred into an excel sheet. The third step required the calculation of the median values of the Ni elemental percentages gathered for the mineral phase, then, the fourth and final step consists of introducing the calculated median Ni value into the program, which will now consider the newly introduced Ni value as the value present in the mineral phase. This method is then repeated in the four samples for each mineral phase that comprises over 0.1% of the sample (data provided by the software, step one) and does not include Ni as the major component in its formula. In Appendix VI the mineral phases' partition in the samples are given, as well as the Ni median and average values used in the workaround and the Ni deportment per mineral. Additional statistical graphics produced in TIMA software are also provided in Appendix VI.

Although relevant and necessary in order to provide useful statistical data, this method suffers from obvious flaws. These flaws are introduced within the selection of points, which no matter how time-consuming and thorough the work is performed, is always somewhat imprecise as the studied minerals are highly heterogeneous in composition that reflect the variable degree of fluid-induced alteration of the primary magmatic matrix.

After this process, it was possible to gather TIMA data that is vital to the understanding of the Ni distribution within the samples.

8.2. TIMA maps

TIMA produced graphical and statistical information of the four samples studied: IMK – 05139, IMK – 05149, IMK – 05153 and IMK - 05156. Examples of TIMA mineral imagery are shown in Figure 41 to Figure 44.

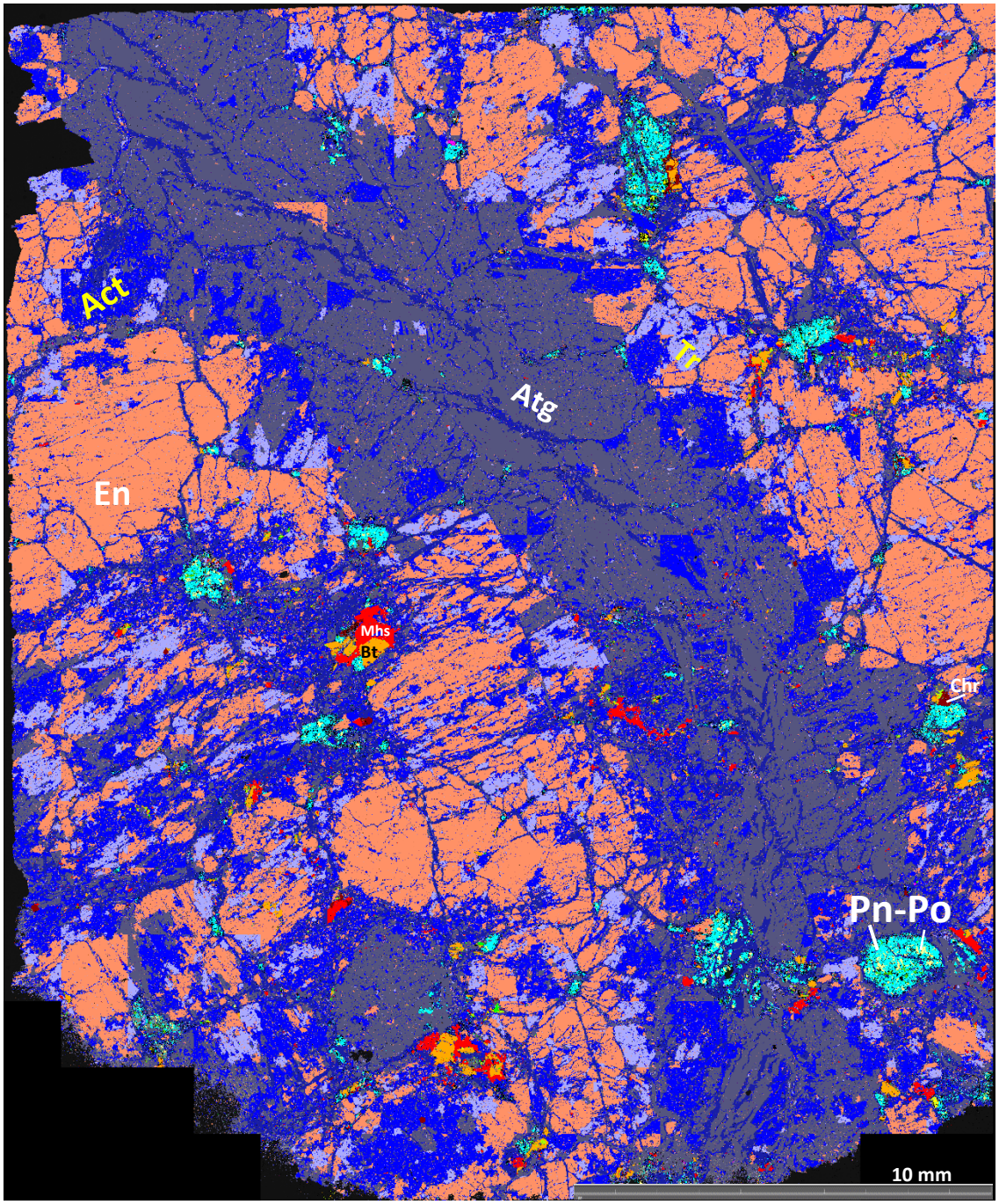

Figure 41: TIMA map for coarse-grained orthopyroxenite, sample IMK – 05139. Pn-Po = pentlandite-pyrrhotite; Bt = biotite; Mhs = magnesiohastingsite; En = enstatite; Atg = antigorite; Act = actinolite; Tr = tremolite; Chr = chromite.

In the image of coarse grained orthopyroxenite (Figure 41) in sample IMK – 05139, it is possible to observe coarse enstatite grains (pink-orange) that appear fractured and cut by amphiboles of the actinolite-tremolite series, shown as blue and light purple, respectively. Amphiboles also appear to replace the enstatite along the grains and in their boundaries; the alteration pattern seems to represent the most typical alteration of orthopyroxene by amphiboles. The intimate intergrowths between enstatite and replacive amphiboles show the gradational grain boundaries reflecting diffusive replacements that are far from equilibrium. In a darker grey-purple colour, a large antigorite vein cuts the sample, with some amphiboles associated, while antigorite also occurs throughout the sample.

Ore minerals occur as pentlandite blebs, shown as light blue, with minor pyrrhotite, shown as bright yellow, and maucherite grains in darker yellow (relative to pyrrhotite). The Ni mineralisation occurs in the large antigorite vein and is associated with a highly altered portions of enstatite.

Pyrrhotite solely occurs as small grains, within, or in the border of, larger pentlandite blebs, suggesting the formation of a more Ni-rich sulphide exsolved from a pyrrhotite with MSS-like composition. Maucherite is rare and occurs in a very close association with the large pentlandite blebs. The Ni mineralisation appears to be altered with the larger pentlandite-pyrrhotite-(local) maucherite blebs corroded and crosscut by the amphibole crystals and aggregates.

Chromite generally occurs in a close association with sulphides and is locally characterised by Fe-rich rims, indicative of alteration. Furthermore, most chromite grains are locally accompanied by biotite, and to a lesser extent chlorite, which appear to replace the chromite grains along the margins.

In the pyroxenite sample IMK – 05149, the majority of the sample (Figure 42) is comprised of fine-grained antigorite (dark-purple colour). Magnesiohastingsite (bright red) is superimposed on enstatite (pink-orange), this larger magnesiohastingsite grain appears to be bordering a large heazlewoodite-pentlandite bleb, both in shades of blue. Phlogopite flakes and plates (orange) are locally altered to chlorite in green. At the top, a horizontal cross-cutting veinlet of clinopyroxene (diopside and hedenbergite) with sporadic local amphibole occurs.

Clinopyroxenes in this samples are associated with veining cutting the predominant matrix, indicating their crystallisation after the serpentinisation event. In this sample, the TIMA map demonstrates the predominance of alteration minerals in association with disseminated sulphides and the existence of the relatively large sulphide blebs, which may inherit the texture of the primary magmatic sulphides.

Mineralisation is predominantly present as heazlewoodite (light blue), intergrowing with pentlandite (darker blue). Pentlandite appears to occur mostly in the border of the sulphide bleb whilst the heazlewoodite is more central, which may imply an initial Ni-rich and Fe-poor composition that gradually became more Fe-rich and Ni-poor.

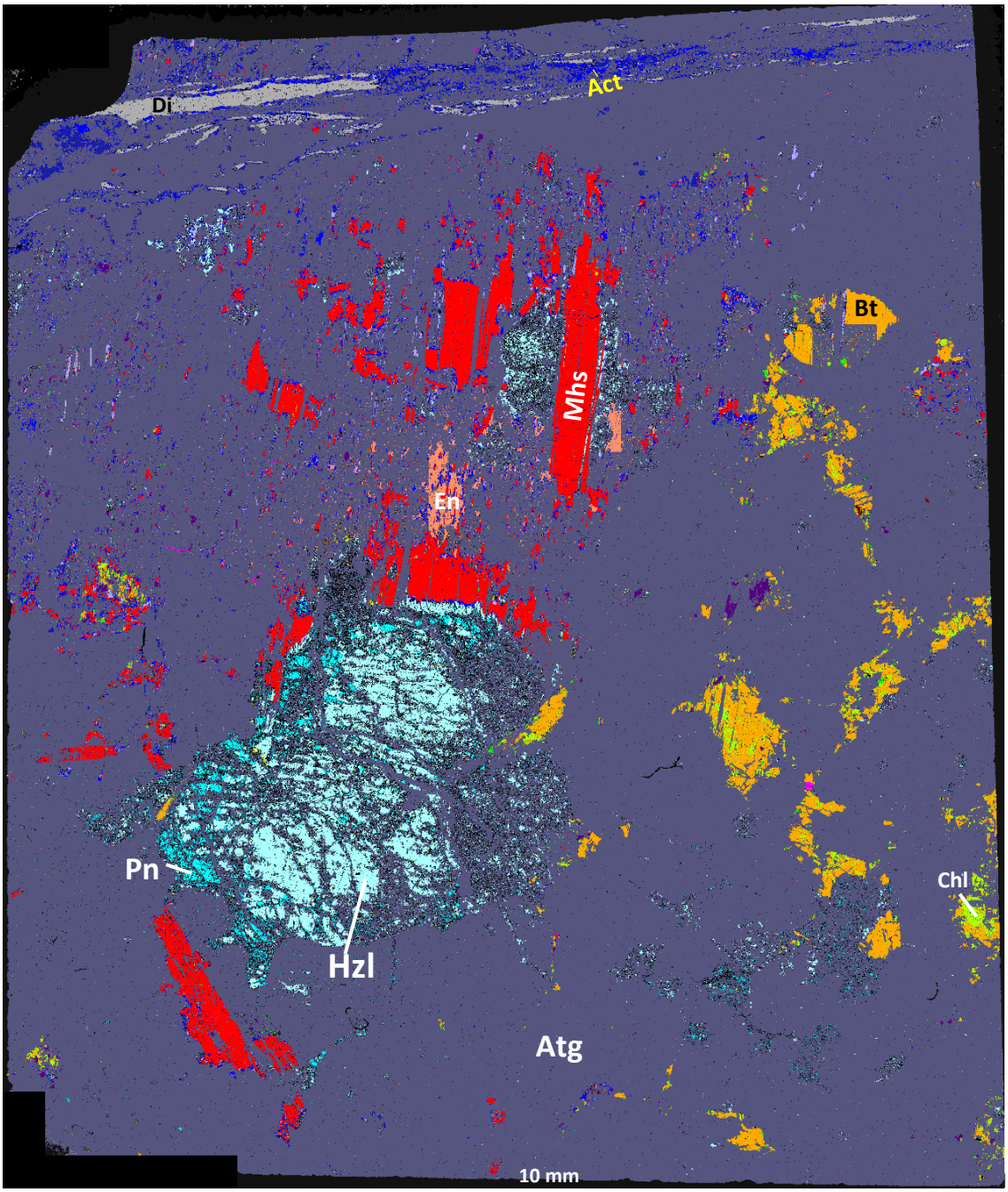

Figure 42: TIMA map for heavily altered orthopyroxenite, sample IMK – 05149. Pn = pentlandite; Hzl = heazlewoodite; Mhs = magnesiohastingsite; En = enstatite; Atg = antigorite; Act = actinolite; Bt = biotite; Chl = chlorite; Di = diopside.

Sample IMK – 05153 (Figure 43) is characterised by predominant enstatite (pink-orange), altered to amphiboles (dark and lighter-blue) in an antigorite matrix (in grey). Local phlogopite (bright orange), is intergrown with replacive amphiboles of the actinolite-tremolite series whereas magnesiohastingsite occurs in altered enstatite. Chlorite (bright green) occurs locally replacing biotite and amphiboles. As with sample IMK – 05139 (Figure 41) a few unrecognised blocks are present at the margins of the enstatite grains where they are replaced by serpentine (bastite), chlorite and amphibole (circled in Figure 43). These indicate locations where the TIMA software was unable to separate certain minerals due to their similar compositions and gradational diffusive boundaries between minerals in the intimate fine-grained intergrowths. Ore minerals occur as disseminated heazlewoodite-predominant and awaruite grains. This

indicates a Ni-rich and S-poor environment where the sulphide is Ni-rich whereas Fe sulphides are absent but instead Ni-Fe alloy is developed.

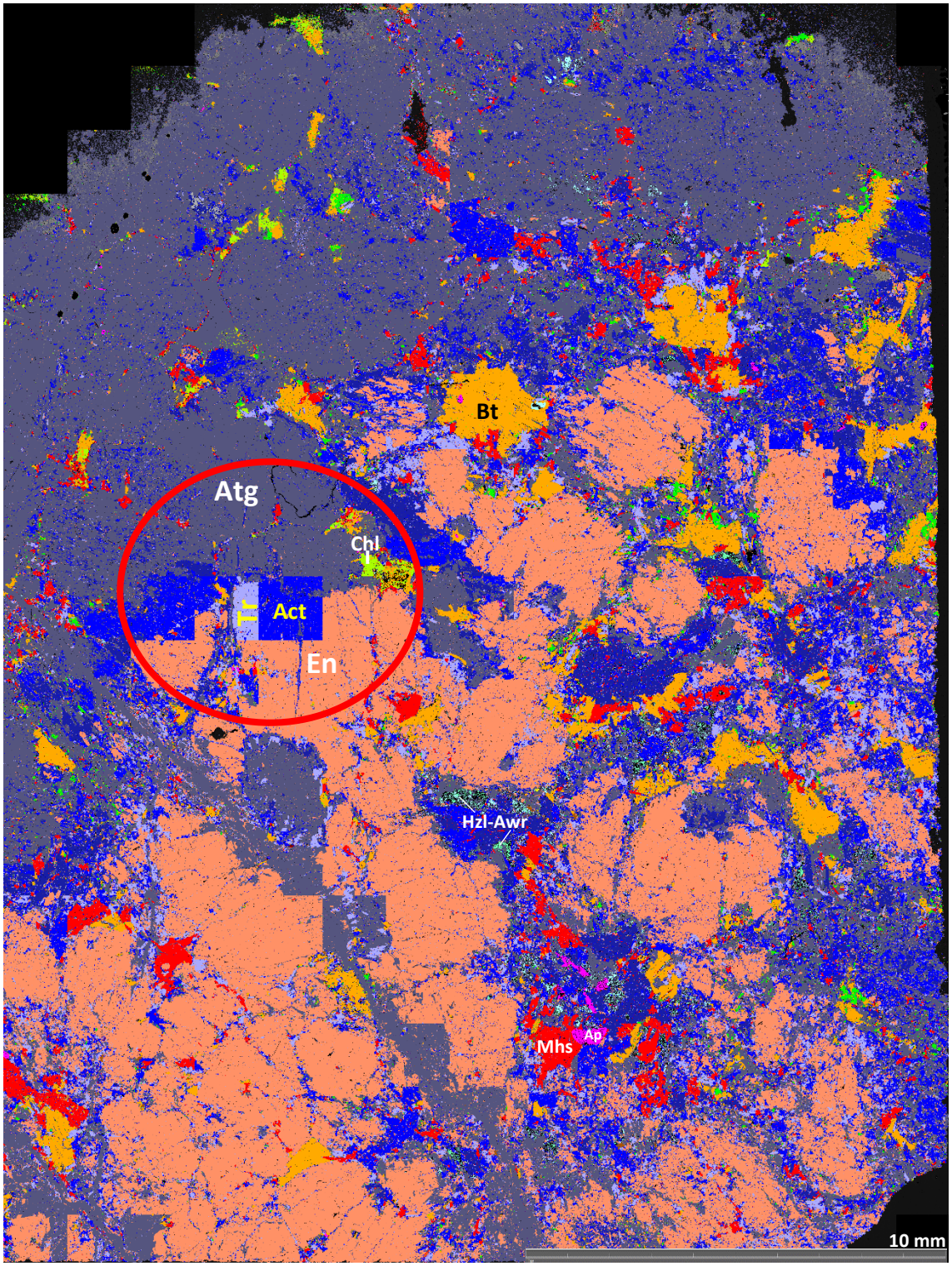

Figure 43: TIMA map for altered orthopyroxenite, sample IMK – 05153. Within the red circle is an example of the graphical glitches that occur due to the similar compositions of the various phases in those patches. Hzl-Awr = heazlewoodite-awaruite Mhs = magnesiohastingsite; En = enstatite; Atg = antigorite; Act = actinolite; Tr = tremolite; Bt = biotite; Chl = chlorite; Ap = apatite.

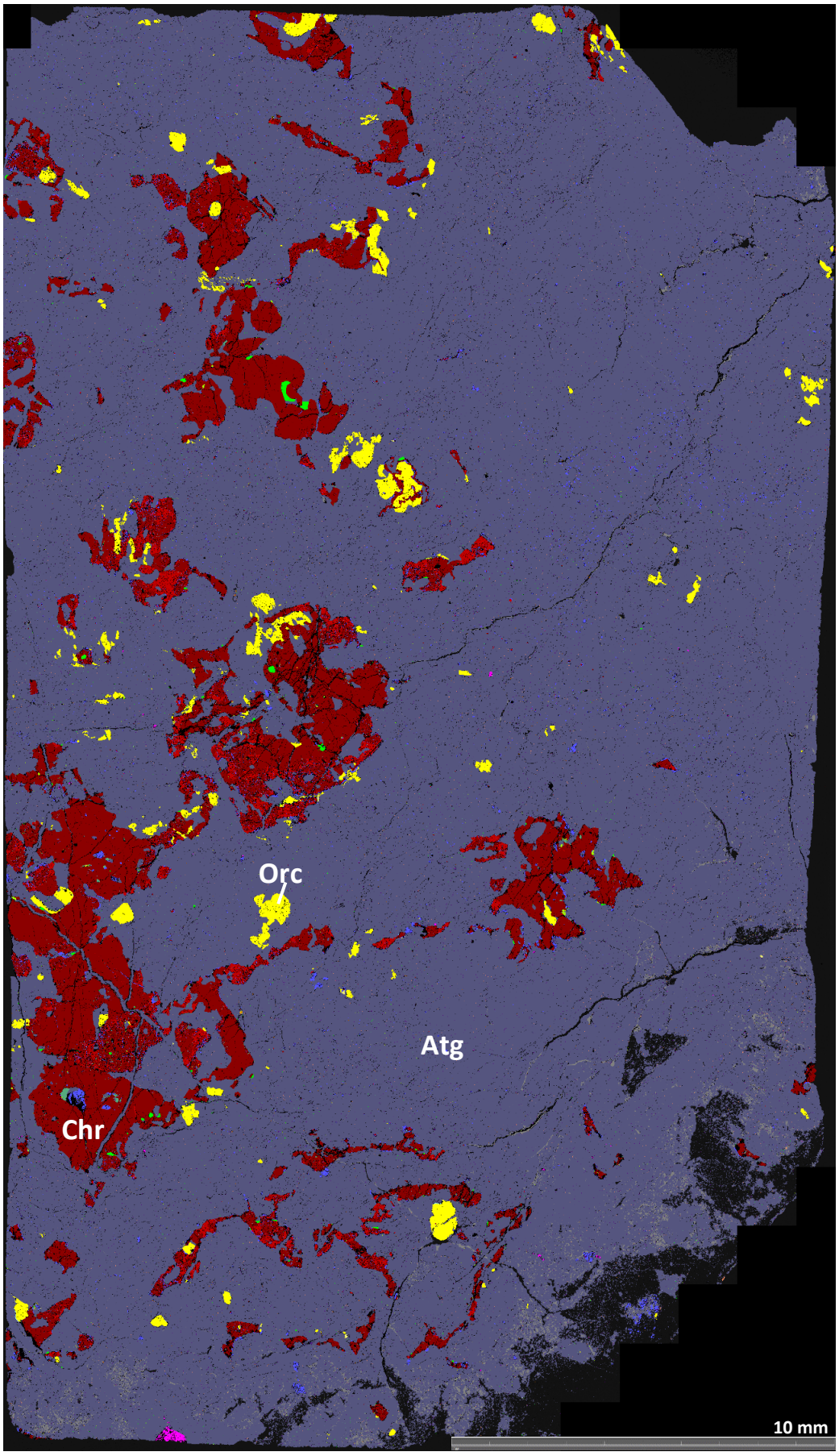

Figure 44: TIMA map for serpentinised harzburgite with chromite zone, sample IMK – 05156. Atg = antigorite; Chr = chromite; Orc = orcelite.

In sample IMK – 05156 (Figure 44) serpentinised harzburgite, is characterised by a predominance of antigorite, shown in purple-grey, with relatively large chromite aggregates, in dark and bright-red, and sporadic arsenide (orcelite) blebs. The chromite demonstrates Fe-rich rims which are indicative of alteration related to serpentinisation. The formation of orcelite could be related to the same process since this mineral occurs in the spatial association with altered chromite and also belongs to the secondary sulphide assemblages.

8.3. TIMA quantitative estimates of the mineral proportions

In sample IMK – 05149, a highly serpentinised pyroxenite, with slightly compositionally variable varieties of serpentine-group minerals (antigorite) dominate the sample comprising around 81.17 wt%. Secondary amphiboles account for 6.55 wt%, with the heazlewoodite proportion 3.19 wt%, followed by pyroxenes at 1.81 wt%. Minor pentlandite accounts for 1.19 wt%, phlogopite for 1.18 wt% and all chlorite varieties for 0.37 wt%. These mineral phases account for 95.67 wt% of the sample IMK – 05149, of which 91.29 % are silicates and 4.38 wt% are Ni-rich sulphides, namely pentlandite and heazlewoodite (Appendix VI and Figure 42).

The results are shown in Figure 45, Table 1 and Appendix VI. Out of the total Ni present in the sample, 90.5 wt% is present in the sulphides of this sample, of which, 75.25 wt% are in heazlewoodite and 15.25 wt% in pentlandite. The secondary silicates contain 9.02 wt% of the Ni present in this sample, followed by primary silicates accommodating 0.14 % of the total Ni. Accessory Ni-Fe alloys contribute an additional 0.34 wt% of the total Ni in the sample. In summary, in the sample IMK – 05149, approximately ~91 wt% of the total Ni is hosted in sulphides and alloys whereas the remaining ~9 wt% is incorporated in secondary silicates and, to the much lesser extent, primary silicates.

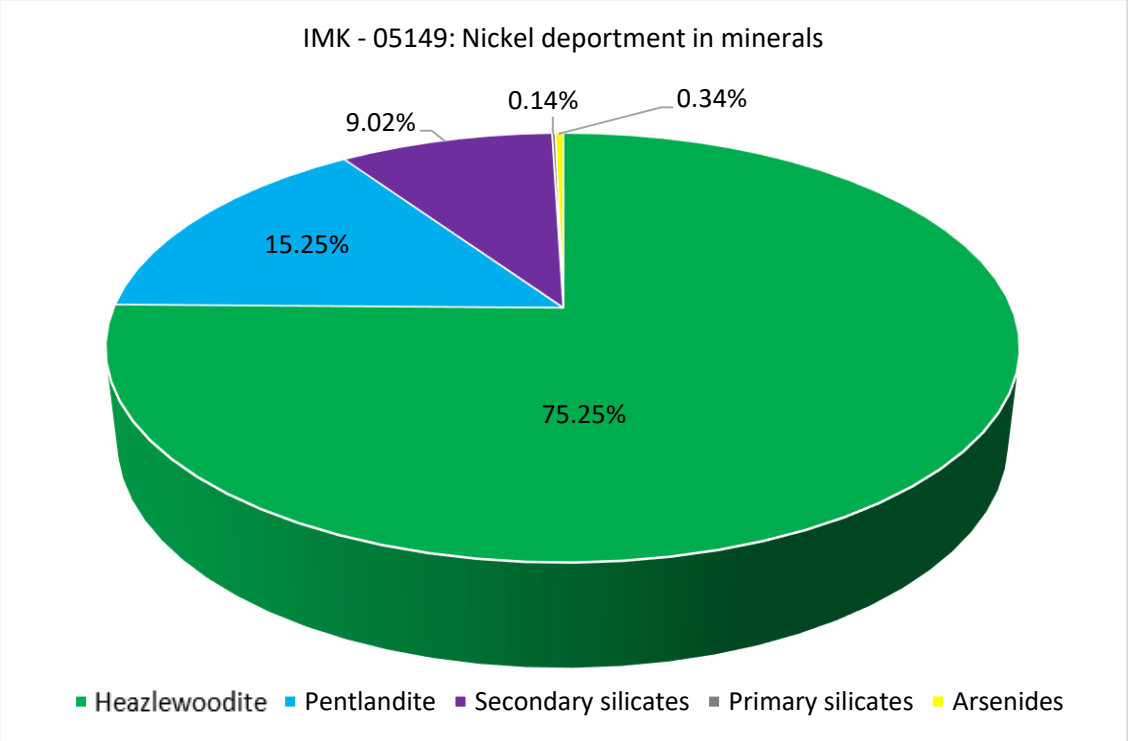

Figure 45: Pie chart of the Ni deportment in minerals of sample IMK – 05149.

Table 1: Mineral groupings, their Ni deportment and proportions (wt%) in sample IMK – 05149.

Grouping	Ni deportment in minerals	Mineral phases wt%
Heazlewoodite	75.25%	3.19%
Pentlandite	15.25%	1.19%
Secondary silicates	9.02%	90.81%
Primary silicates	0.14%	3.19%
Arsenides	0.34%	0.017%
Total	100%	~99%

Sample IMK – 05153, also a highly serpentinised pyroxenite, consists of 36.54 wt% serpentines of slightly variable composition (antigorite), 27.50 wt% pyroxenes and 27.29 wt% secondary amphiboles. With an additional 5.16 wt% of phlogopite and 0.69 wt% chlorites, the silicates account for 97.18 wt% of the sample. Accessory sulphides are composed of heazlewoodite at 0.19 wt% and awaruite at 0.1 wt% of the sample, totalling at 0.29 wt%. Rare apatite grains account for 0.12 wt% (Appendix VI and Figure 43).

As shown in Figure 46, Table 2 and Appendix VI, 48.04 wt% of the total Ni is present in the secondary silicates and 5.92 wt% is in primary silicates, which adds up to ~54 wt% of the total Ni. For Ni-rich minerals, heazlewoodite accounts for 28.4 wt% and awaruite for 16.50 wt% total Ni with trace amount of Ni arsenides incorporating 0.90 wt% of the total Ni, adding up to 45.80 wt%. These results demonstrate that over 50 wt% of the total Ni is hosted in the silicates. In this sample, the proportion of accessory minerals is 0.29 wt%, although these trace sulphide and alloys contribute 45.80 wt% of the overall Ni.

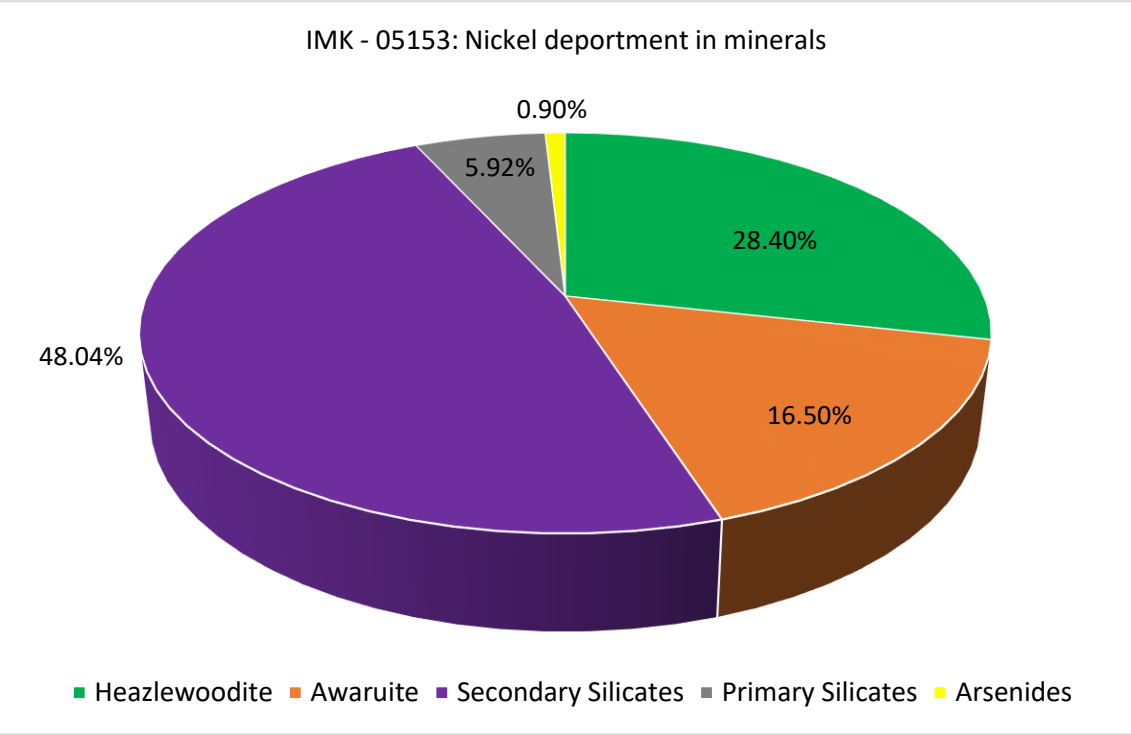

Figure 46: Pie chart of the Ni deportment in minerals of sample IMK – 05153.

Table 2: Mineral groupings, their Ni deportment and proportions (wt%) in sample IMK – 05153.

Grouping	Ni deportment in minerals	Mineral phases wt%
Heazlewoodite	28.40 %	0.19%
Awaruite	16.50 %	0.10%
Secondary Silicates	48.04 %	69.69%
Primary Silicates	5.92 %	27.50%
Arsenides	0.90 %	<0.1%
Total	99.75 %	~97.6%

Sample IMK – 05156, which is a completely serpentinised harzburgite that hosts the chromite segregation, consists of 78.62 wt% serpentine-group minerals, whilst pyroxenes only add up to 0.12 wt%, thus, the silicates correspond to 78.74 wt% of the sample. Coarse-grained chromite accounts for 14.45 wt%, other oxides such as secondary hematite or magnetite were also present contributing 1.52 wt%. The only Ni mineral present is in the form of an Ni arsenide, orcelite ($Ni_{5-x}As_2$ *(x=~0.25)*), which corresponds to 1.17 wt% of the total (Appendix VI and Figure 44).

The TIMA statistics (Figure 47, Table 3 and Appendix VI), show that the silicates amount to 13.71 wt% of the total Ni in the sample, followed by chromite with 5.11 wt% and the secondary oxides with 1.22 wt%. Orcelite accounts for 79.77 wt% of the total Ni in this sample, plus several small Ni-Fe sulphide (heazlewoodite and pentlandite) grains detected by the software. These host 0.18 wt% of the total Ni. These results show that Ni is mostly hosted in Ni arsenides, contributing nearly ~80 wt% of the overall Ni, whilst the secondary silicates, although comprising nearly 80 wt% of the sample, are very minor contributors with a much lower portion of the total Ni present.

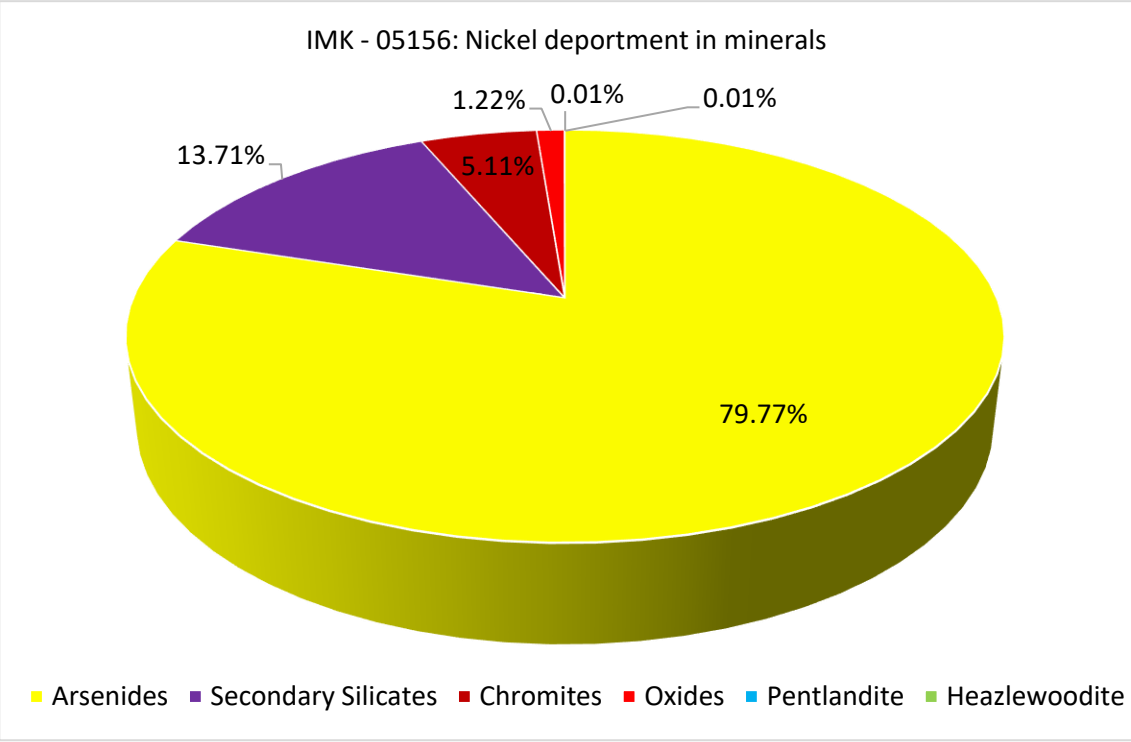

Figure 47: Pie chart of the Ni deportment in minerals of sample IMK – 05156.

Table 3: Mineral groupings, their Ni deportment and proportions (wt%) in sample IMK – 05156.

Grouping	Ni deportment in minerals	Mineral phases wt%
Arsenides	79.77%	1.17%
Secondary Silicates	13.71%	78.72%
Chromites	5.11%	14.45%
Oxides	1.22%	1.52%
Pentlandite	0.01%	<0.1%
Heazlewoodite	0.01%	<0.1%
TOTAL	99.83%	~96.06%

Finally, in the sample IMK – 05139 a slightly different approach was taken. The first step of gathering the information regarding the distribution of the various mineral phases was the same. Serpentines account for 29.51 wt% of the sample, pyroxenes 27.23 wt% and the proportion of amphiboles is <38.09 wt%. Silicates sum up to 95.41 wt%, out of which 27.23 wt% are primary silicates (pyroxenes) and 67.60 wt% are secondary silicates (antigorite, actinolite and tremolite). Sulphide minerals occur mostly as pentlandite, which corresponds to 2.17 wt% of the total rock, whilst small grains of chalcopyrite at 0.09 wt% and pyrrhotite + mackinawite at 0.06 wt% were also detected. Finally, chromite accounts for 0.16 wt% of the sample (Appendix VI and Figure 41).

In the process of the selection of the representative points for Ni data extraction, high variations of Ni contents were noticed which later influenced the decision of using the median values instead of the averages. This heterogeneity of Ni distribution was attributed to the apparent proximity of the selected points to Ni enriched mineral intergrowths. To verify the impact of the Ni enrichment in silicates in their proximity to mineralisation, it was decided to use two different average values of Ni content in sample IMK – 05139. The first Ni value was calculated according to the average maximum values detected in silicates adjacent to mineralisation, implying further relevance on the influence of Ni mineralisation on the Ni concentration in adjacent silicates. The second Ni value was calculated by disregarding the portions used for the first value, where the Ni values appeared enriched due to their proximity with Ni minerals. This secondary Ni value would reflect the real Ni content in silicates are not influenced by the occurrence of nearby Ni-bearing Ni minerals. By verifying the difference in the statistical calculations using both values, it is possible to observer the maximum and minimum Ni values present in silicates of sample IMK – 05139. This demonstrates how the Ni values are influenced by the location of the chosen points for analyses and how the Ni concentrations in silicates can be inflated due to their proximity with Ni sulphides.

As seen in Table 4 and Appendix VI, the different average minimum and average maximum Ni values can vary by a factor of 2 or more. The variation is then reproduced for the Ni deportment in minerals as shown in Figure 48 and Table 5, as well as in Figure 49 and Table 6.

Table 4: All minerals with >~0.1 wt% Ni, their average minimum Ni values and their average maximum Ni values for sample IMK – 05139.

PHASES/MINERALS	wt% of mineral in sample	Average minimum Ni value (wt%)	Average maximum Ni value (wt%)
Enstatite	27.23	0.04	0.06
Antigorite_HighAl_1	25.2	0.05	0.1
Actinolite_1_low_Ca_high_Mg	17.82	0.08	0.14
Actinolite	12.63	0.07	0.26
Tremolite_1	6.92	0.05	0.09
Pentlandite	2.17	26.39	28.55
Antigorite_8	2.02	0.08	0.3 (0.54)
Antigorite_6 (low-Al)	1.39	0.01	0.01
Biotite	0.58	0.18	0.42
Magnesiohastingsite	0.58	0.13	0.35 (0.6)
Antigorite_9 (9-Fe)	0.54	0.11	1
Antigorite_HighAl_2	0.24	0.11	0.35 (0.68)
Pyrrhotite	0.2	6.05	11.3
Chromite	0.16	0.15	0.8
Magnesiohastingsite_2	0.14	0.15	0.4
Antigorite_2	0.12		
Chalcopyrite	0.09	0.36	4.22
Pyrrhotite_2 or mackinawite	0.06	6.33	10.07

Using the average minimum values (Table 4) accounts for 2.39 wt% and chalcopyrite for 0.15 wt%, with a total of 90.47 wt% of the Ni in the sample hosted in sulphides. Accessory Ni arsenide contributes up to 0.98 wt% and oxides up to 0.088 wt% (Figure 48 and Table 5).

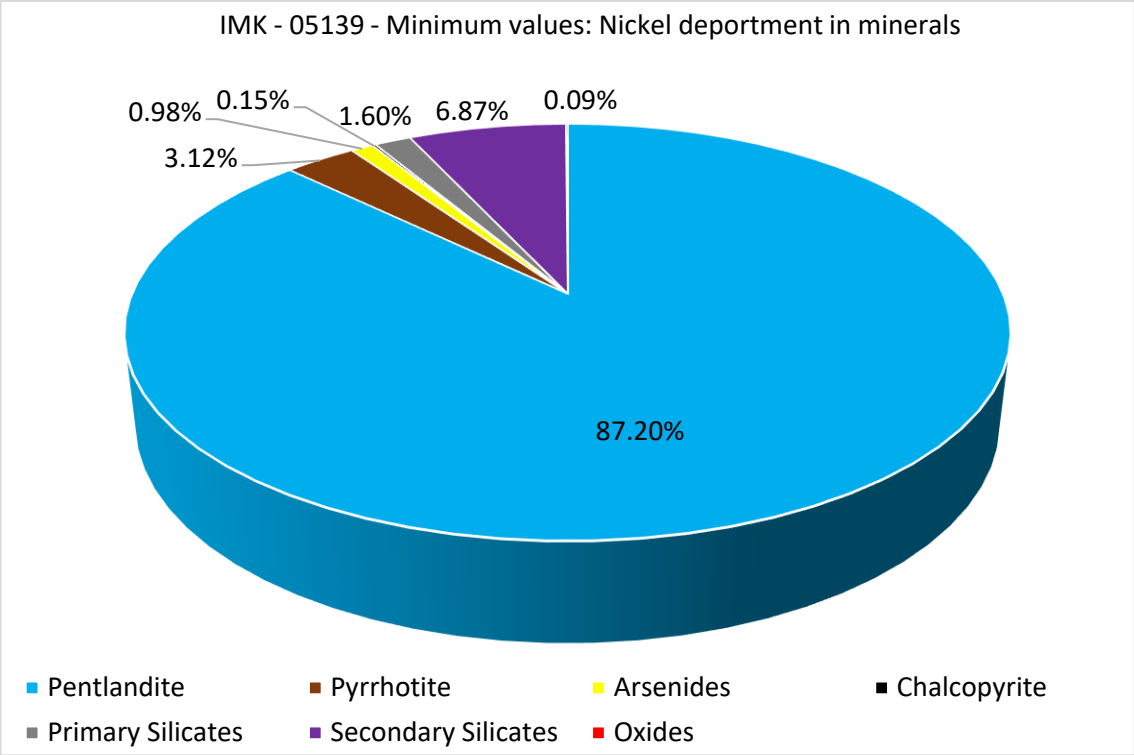

Figure 48: Pie chart of the Ni deportment in minerals of sample IMK – 05139 using the minimum average Ni values.

Table 5: Mineral groupings, their Ni deportment and proportions (wt%) in sample IMK – 05139, using the minimum average Ni values.

Grouping	Ni deportment in minerals	Mineral phases wt%
Pentlandite	87.20%	2.17%
Pyrrhotite and mackinawite	3.12%	0.2%
Arsenides	0.98%	0.01%
Chalcopyrite	0.15%	0.09%
Primary Silicates	1.60%	27.27%
Secondary Silicates	6.87%	68.36%
Oxides	0.09%	0.16%
Total	100%	98.26%

By using the average maximum values, as seen in Table 4, the results differ with an increase of the Ni proportion in silicates, culminating in 15.83 wt% of the Ni in this sample, which is 7.36 wt% higher than by the previous calculations above. As for the sulphides, the value is lowered to 83.2 wt% of the total Ni, with pentlandite contributing 80.18 wt%. Arsenides host ~0.90 wt% and oxides ~0.081 wt% of the total Ni (Figure 49 and Table 6).

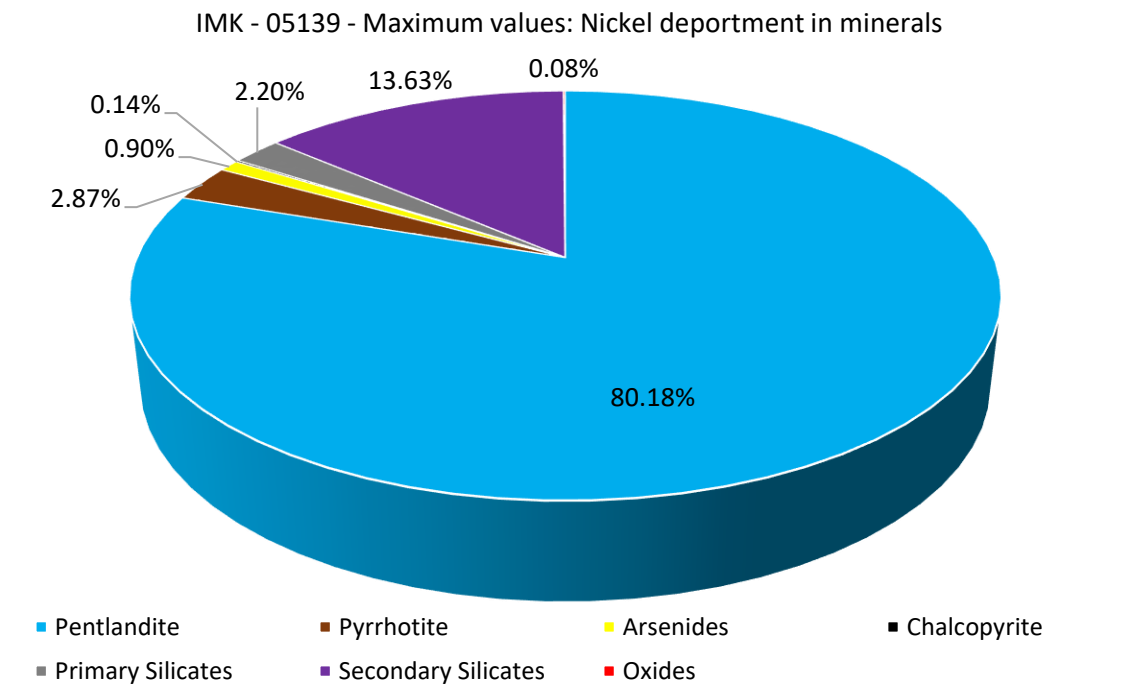

Figure 49: Pie chart of the Ni deportment in minerals of sample IMK – 05139 using the maximum average Ni values.

Table 6: Mineral groupings, their Ni deportment and proportions (wt%) in sample IMK – 05139, using the maximum average Ni values.

Grouping	Ni deportment in minerals	Mineral phases wt%
Pentlandite	80.18%	2.17%
Pyrrhotite and mackinawite	2.87%	0.2%
Arsenides	0.90%	0.01%
Chalcopyrite	0.14%	0.09%
Primary Silicates	2.20%	27.27%
Secondary Silicates	13.63%	68.36%
Oxides	0.08%	0.16%
Total	100%	98.26%

The difference in these two scenarios suggests that, although relevant, the variation observed still demonstrates that Ni sulphides are the main Ni contributor. However, the difference of nearly 7% of the total Ni allocated to silicates, is important for the economic viability repercussions.

Also, it is important to note that the relevance of the results obtained by using the average maximum Ni values is dependent of the quantity and geometry of the sulphide minerals, hence, less mineralised samples will not have much of the silicates enriched in Ni at contacts with sulphides minerals. In contrast, highly mineralised samples will have a higher proportion of Ni-enriched silicates at contacts with Ni phases.

Overall, in samples that have a higher percentage of Ni minerals such as IMK – 05139, IMK – 05149 and IMK – 05156, the sulphides, arsenides and alloys are the main Ni contributors ranging from nearly 80 wt% to about 91 wt% of the total Ni in the samples. Conversely, the Ni-rich minerals in the sample IMK – 05153 only amount to 0.29 wt% whereas nearly 55 wt% of the total Ni was calculated to be hosted mostly in silicates.

Table 7, compares the XRF whole rock Ni content data for the four studied samples, IMK – 05139, IMK – 05149, IMK – 05153 and IMK – 05156 (Appendix VI), in ppm, with the TIMA-based Ni deportment data. Assuming that the four thin sections used in TIMA are representative of the four mineralised intervals in the borehole KKME 1-6, it is possible to calculate the whole rock percentages of so-called recoverable Ni (ppm) hosted in Ni-rich minerals (sulphides, alloys and arsenides) by multiplying the whole rock Ni (ppm) by the percentage of Ni in mineralisation according to TIMA.

Table 7: Comparison of XRF whole rock data and TIMA Ni deportment with the calculation of unrecoverable and recoverable Ni in the samples.

SAMPLE	**IMK - 05139**	**IMK - 05149**	**IMK - 05153**	**IMK - 05156**
Whole rock Ni (ppm) content	10154	28175	2022	7484
Total Ni (%) in ore minerals (TIMA)	85	90.5	45.8	79.8
Total Ni (ppm) in ore minerals	8630.9	25498.38	926,076	5969.99
Proportion of ore minerals (%)	2.32	4.38	0.29	1.17
Unrecoverable total Ni (%) in silicates and oxides (TIMA)	15	9.5	54.2	20.23
Total unrecoverable Ni (ppm)	1523.1	2676.63	1095.92	1514.01

The results are plotted in Figure 50, which shows a correlation between the higher Ni grade (ppm) and the higher recoverable Ni share (that is hosted in ore minerals as silicate Ni is commonly unrecoverable). The content of unrecoverable Ni varies from 0.11 to 0.28 wt% Ni which should be considered if economic grades are encountered in future drilling. Likewise, the provisional Ni losses during the processing of minerals correlates with a future Ni grade and are expected to be higher for a possible high-grade mineralisation if it is found.

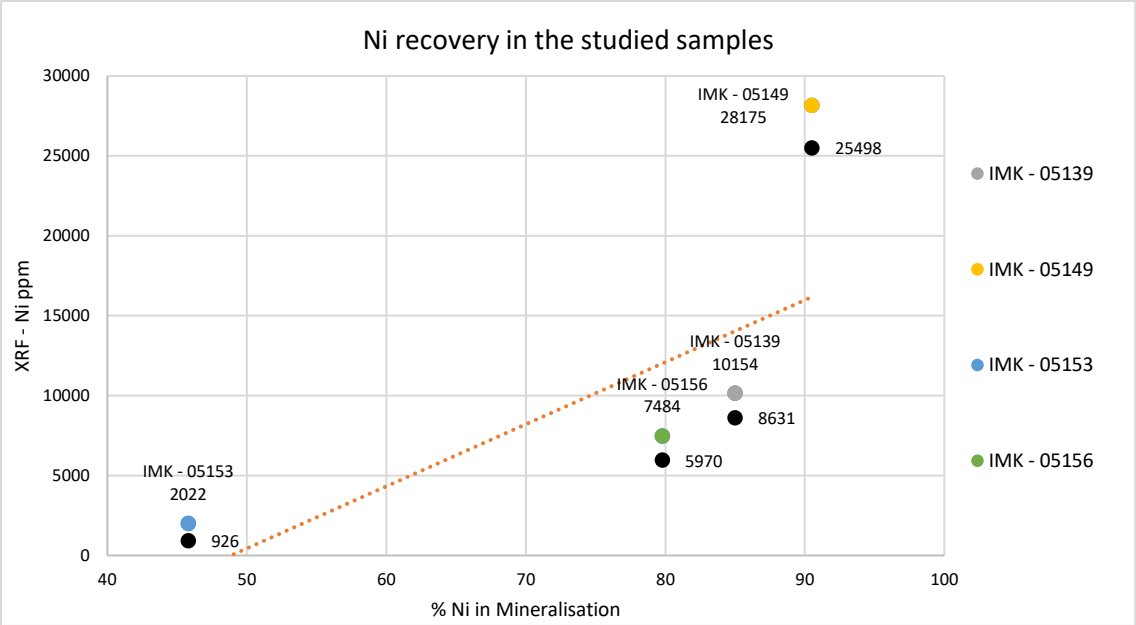

Figure 50: Proportion of recoverable Ni ppm per sample (black) and total Ni ppm in those samples.

Similarly, the proportions of unrecoverable Ni in silicates and oxides against the whole rock Ni grade are shown in Figure 51. The highest amount and proportion of unrecoverable Ni is observed in the Ni richest sample IMK – 05149, where secondary silicates are characterised by the overall elevated Ni content. The other 3 samples, despite the varied Ni proportions in the silicates and the different Ni grade show a consistent trend of a negative correlation between the two values.

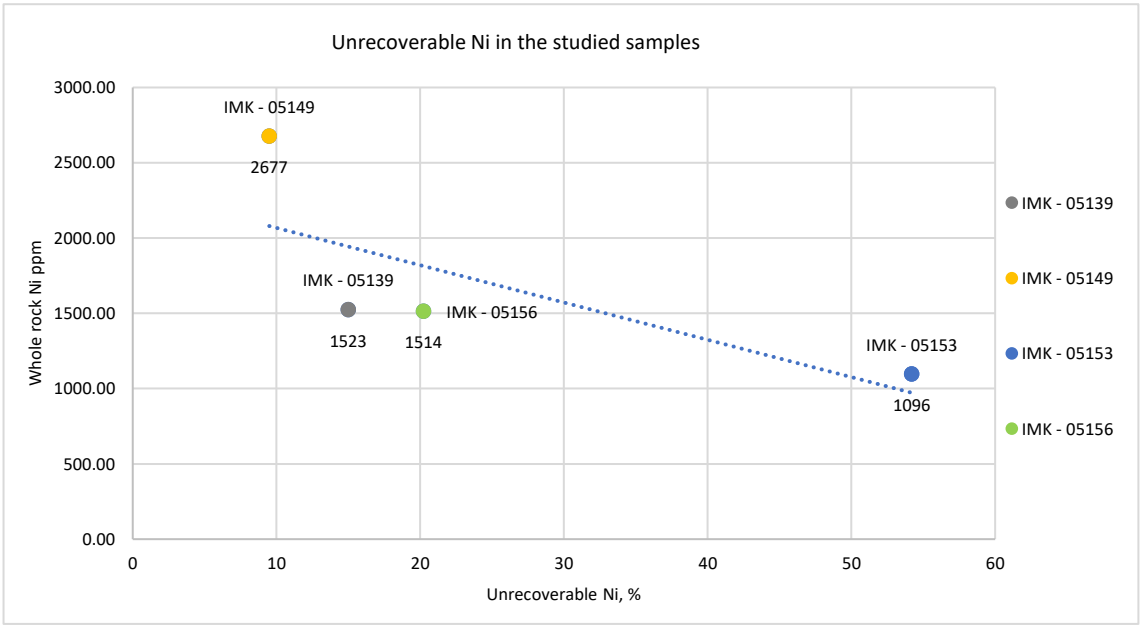

Figure 51: Proportion of unrecoverable Ni ppm per sample and total Ni in those samples.

Chapter 9

Discussion

9.1. Mineral Associations

9.1.1. General features of the main rock-forming processes

As described in the geological setting chapter, the studied portion of borehole KKME - 1/6 intercepted ultramafic rocks of the Molopo Farms Complex (MFC). Although only four mineralised samples were analysed, they are representative for the identified ore intervals and their mineralogy indicates a complex history of secondary alteration. Understanding the chemistry and relationships between the minerals, including the secondary silicates and the various sulphides, is crucial in determining the processes of their formation.

The primary minerals are those associated with the magmatic processes controlling the formation of the Molopo Farms Complex. In ultramafic rocks, the primary minerals are olivine, orthopyroxene and chromite. The former two minerals comprise most of the peridotite and orthopyroxenite in variable proportions that determine their classification. The relic textures, observed in a few polished sections, indicate the cumulus nature of olivine and chromite that formed as liquidus phases in all rock types. A frequently observed poikilitic texture composed of olivine and chromite chadacrysts within orthopyroxene oikocrysts indicates later growth of orthopyroxene in harzburgite. An equigranular to granoblastic texture of orthopyroxene in orthopyroxenite indicates liquidus crystallisation of orthopyroxene and later recrystallisation. Interstitial minerals are represented by phlogopite and very rare plagioclase. Accessory primary minerals include zircon and apatite, which occur as euhedral crystals in the interstitial assemblage. These observations corroborate with data in the literature on the petrography of the ultramafic units of the MFC in other places (Reichhardt (1994), Kaavera, et al., (2018) and Kaavera, et al., (2020)) that allow correlating this zone across the complex. The high proportion of cumulus minerals and very minor proportion of the interstitial minerals is consistent with the earlier identification of this sequence as ultramafic cumulates (Reichhardt, 1994); (Kaavera, et al., 2018); and (Kaavera, et al., 2020). The proportion of the primary interstitial minerals in the mineralised samples may be underestimated because of the widespread and intensive alteration.

Secondary minerals are those that occurred through later stage processes indicating a change in conditions and a specific environment that induced alteration of the protolith. Pyroxene and olivine are not the most abundant minerals in the studied mineralised samples of the borehole KKME – 1/6. Instead, serpentine-group and amphibole-group minerals dominate the mineral assemblage. Serpentine is a common secondary mineral during alteration of mafic and ultramafic rocks and forms by hydrothermal process. Serpentinisation implies the alteration of olivine and pyroxene to a serpentine-group mineral in a hydrous environment by the reactions (Adreani, et al., 2007):

1. $6\ (Mg,Fe)_2SiO_4 + 7\ H_2O = 3\ (Mg,Fe)_3\ Si_2O_5\ (OH)_4 + Fe_3O_4 + H_2$
   Olivine + water = serpentine (mesh) + magnetite + hydrogen

2. $3\ (Mg,Fe)SiO_4 + 2\ H_2O = (Mg,Fe)_3\ Si_2O_5\ (OH)_4 + SiO_{2(aq)}$
   Orthopyroxene + water = serpentine(bastite) + silica released in the fluid phase

The accompanying reactions with water also favour formation of talc, chlorite and brucite. Serpentinisation is an exothermic reaction with energy released mostly in the form of heat (Adreani, et al., 2007).

Secondary amphibole supergroup minerals in ultramafic rocks cannot form during relatively low temperature serpentinisation (50-300 ^{o}C according to (Evans, 2010) and require a higher temperature metasomatic process (Ridolfi, 2021) with significant redistribution or input of Ca and Al.

9.1.2. Observations in hand samples and polished sections

The logging undertaken in Botswana provided the general macroscopic characterisation of borehole KKME – 1/6. The most common minerals that were visually observed included pyroxenes, phlogopite, a fine-grained serpentine-amphibole matrix, talc, chlorite, asbestos, magnetite and sulphides. It was also possible to observe very high degrees of alteration and define the mineralised intervals at the depths of ~294-319m, 446.3-451m, 506-520.7m, ~531m, 547-561m and 589-598m. Olivine was not visually observed as it was altered into serpentine with secondary magnetite within the serpentine-amphibole matrix. The relic poikilitic texture of the serpentinised olivine chadacrysts included in the orthopyroxene oikocrysts was the best indicator to distinguish between heavily serpentinised peridotite and pyroxenite. Although variably altered, pyroxene was the predominant primary mineral that occurred in less altered samples.

During the petrographic study, very rare olivine was detected in some of the samples, while fresh orthopyroxene was more common. The fine-grained serpentine-matrix has replaced both olivine and orthopyroxene to an almost complete pseudomorphic replacement. The coarser grained to fibrous serpentine occurs in veins cross-cutting both the primary magmatic minerals and the secondary fine-grained matrix. Secondary magnetite occurs as dusty disseminations associated with fine-grained serpentine and also forms magnetite veinlets with or without serpentine and chlorite

Amphibole-group minerals do not form pseudomorphic replacement of primary olivine and orthopyroxene but mostly occur as fine-grained locally radiating aggregates replacing the serpentine matrix. Also, coarse-grained amphibole needles up to 1 cm long crosscut all minerals including the sulphide aggregates. Locally, the amphibole needles replace interstitial phlogopite that is seen in their mutual intergrowths and reflected in the K-enriched compositions of this amphibole. Fine-grained amphiboles replace pentlandite, pyrrhotite and heazlewoodite grains along the margins. Also, fine needles of amphiboles and chlorite corrode and replace the margins of the chromite grains. Therefore, the petrographic observations indicate that amphiboles are among the latest minerals to form in the studied rocks.

The cross-cutting and replacive nature of the serpentine and amphibole-group minerals is indicative of their secondary origin. The Ni-rich mineral assemblage described in the studied samples, including Ni sulphides and alloys, is associated with the serpentine-talc-chlorite parageneses and predates the crystallisation of the amphibole-group minerals. Nevertheless, some of Ni arsenides may be formed later than the main sulphide assemblage as discussed below.

As a conclusion, three main stages are revealed by the rock petrography and supported by TIMA mapping data:

1. The magmatic stage, during which the ultramafic cumulates were separated from their parental magmatic liquid and deposited. The primary interstitial sulphide associations, which were described in the other areas of the MFC (Reichhardt (1994), Kaavera, et al., (2018) and Kaavera, et al., (2020)) were not observed in the studied rocks although the textural evidence of an interstitial nature of some sulphide blebs and the elevated whole-rock PGE content (Power Metal Resources, 2022) indicate that primary sulphide precursors did exist in these ultramafic rocks.
2. The serpentinisation stage, when the primary silicates were replaced by serpentine, talc and chlorite occurred under lower temperature water-rich conditions; cumulus chromite was modified. The primary magmatic sulphides were replaced by the secondary Ni-rich assemblage that includes pentlandite, Ni-rich pyrrhotite to mackinawite, heazlewoodite and awaruite. The change from Ni sulphides to alloys suggest changing redox conditions within the stage.
3. During the third stage, secondary amphiboles locally replaced the previously serpentinised assemblage. Replacement of phlogopite, the serpentine-talc-chlorite matrix and the intergrowths of secondary sulphides occurred. A source of energy and fluid for this higher temperature process is not obvious. It is possible that the replacive amphiboles are coeval with the formation of the crosscutting asbestos, magnetite and clinopyroxene veins and veinlets, that are tectonically controlled and crosscut all the assemblages of the first two stages although this is an entirely speculative hypothesis so far.

9.2. Nickel deportment

One of the main objectives of this thesis was to understand the Ni distribution in Ni-bearing rocks since this affects the economic parameters of all Ni-Cu-PGE occurrences associated with ultramafic rocks.

Whole rock geochemistry (Chapter 6) through XRF analyses was able to provide the valuable information regarding the whole rock chemical composition for the borehole KKME – 1/6. Data indicates (Chapter 6 and Appendix IV) the slightly higher median Ni enrichment in harzburgites (that is related to the Ni contribution from magmatic olivine), whereas orthopyroxenites have the highest Ni content in the sample IMK – 05149 (that is related to the presence of sulphides). Harzburgites have, on average, the higher LOI value indicating the higher level of alteration, while Ni also appears to have a weak positive correlation with the higher LOI values corroborating the link between the higher Ni enrichment in harzburgites with the former presence of olivine. Overall, Ni appears enriched in the studied samples, with a minimum value of 745 ppm Ni and a maximum value of 28 174 ppm Ni, both in orthopyroxenite, while the

median is 2150 ppm Ni, and a weak correlation between the degree of alteration and the Ni grade is observed. Taking into consideration the high proportion of olivine in harzburgite (up to 90 modal %), the correlation between the higher average Ni values with Ni-enriched olivine precursor is obvious, however, the anomalous Ni enrichment in olivine-free orthopyroxenite is not due to the primary silicate Ni enrichment but instead stems from Ni sulphide (or alloy/arsenide) mineralisation.

The microprobe data provided accurate Ni concentrations for each mineral. Among the primary silicates, pyroxenes are generally Ni-poor and contain on average less than 0.1 wt% NiO. As for the secondary silicates, the predominant mineral is serpentine with an average NiO value below 0.5 wt% NiO, indicating no Ni enrichment in these silicates during alteration. However, chlorite contains slightly more Ni compared to the other secondary silicates with the median value of ~0.28 wt% NiO. Chlorite is suggested to be formed, at least partly, during the third stage of alteration postdating the main serpentinisation event. The main serpentinisation event is likely to correlate with the formation of Ni-rich minerals. This suggests that Ni in chlorite is enriched due to Ni remobilisation from the adjacent primary sulphides as the source of Ni.

Amphiboles are characterised by a variable Ni enrichment, where the hornblende-group amphiboles have a median of ~0.15 wt% NiO while the actinolite-tremolite series amphiboles have the median of 0.09 wt% NiO and the Mg-Fe-Mn amphiboles have a median of 0.07 wt% NiO. Therefore, the hornblende-group amphiboles occur slightly more enriched in Ni, however, they are more abundant in the Ni-rich rocks as represented by the sample IMK-05149.

All major ore minerals were classified with high-quality microprobe data, including Ni sulphides, Cu(-Ni) sulphide, a Ni-Fe alloy, Ni arsenides, a rare Ni antimonide and parkerite. Among the major Ni sulphides: pentlandite, pyrrhotite, mackinawite and heazlewoodite, there is a gradual increase in Ni enrichment from pyrrhotite to mackinawite then to pentlandite and to heazlewoodite which has the highest Ni enrichment. Pentlandite in association with heazlewoodite in sample IMK – 05149 has a higher Ni enrichment than pentlandite in association with pyrrhotite and mackinawite in the sample IMK – 05139. Different Ni sulphides may indicate different conditions of formation and the fact the some may coexist whilst others don't, also has implications.

Orcelite is the Ni arsenide responsible for the majority of Ni present in sample IMK – 05156. This mineral comprises almost all of the total Ni in the sample IMK – 05156. The presence of Ni arsenides is indicative of a hydrothermal process. Although the textural relationships between orcelite and other Ni-phases has not been observed. Based on the mineral assemblage, orcelite could be formed by replacing the earlier secondary Ni sulphides, primarily pentlandite, pyrrhotite, mackinawite and heazlewoodite, as a result of an increase in As fugacity. Heazlewoodite was detected by microprobe analysis in the sample IMK – 05156 whereas maucherite was not found in the association with orcelite.

The TIMA-derived data helped to provide the Ni deportment in the four studied samples. This was a major contribution of this thesis. The TIMA data confidently showed that in Ni mineralised rocks, the principal Ni contributors are the ore minerals (Figure 52 and Table 8). The Ni concentrations in silicates and oxides was quantitatively evaluated.

Overall, with the studied type of mineralisation up to ~1000 – 1500 ppm Ni are hosted in silicates and oxides and would not be recovered. Sulphides, alloys and arsenides are the

dominant hosts of Ni in samples IMK – 05139, IMK- 05149 and IMK – 05156. If we use the four studied samples as representative of the mineralised zones between 294-319m (IMK – 05139, IMK- 05149 and IMK – 05153) and 446.3-451m (IMK – 05156), these results indicate a potential economic viability, Figure 4. These zones are between 5 and 15 m thick, as such, the representativeness of the four samples must be taken with a grain of salt, where the Ni enrichment is over ~1000 – 1500 ppm or ~0.3 NiO wt%. Furthermore, sample IMK – 05149 and sample IMK – 05153 are very near to each other at 294.7 and 296.9m, respectively, indicating a high variance of Ni enrichment in a short amount of length. This also would raise the Ni cut-off grade by at least 0.3% due to the unrecoverable Ni present in silicates and oxides.

Table 8: Comparison of XRF whole rock data and TIMA Ni deportment with the calculation of unrecoverable and recoverable Ni in the samples.

SAMPLE	**IMK - 05139**	**IMK - 05149**	**IMK - 05153**	**IMK - 05156**
Whole rock Ni (ppm) content	10154	28175	2022	7484
Total Ni (%) in ore minerals (TIMA)	85	90.5	45.8	79.8
Total Ni (ppm) in ore minerals	8630.9	25498.38	926.08	5969.99
Proportion of ore minerals (%)	2.32	4.38	0.29	1.17
Unrecoverable total Ni (%) in silicates and oxides (TIMA)	15	9.5	54.2	20.23
Total unrecoverable Ni (ppm)	1523.1	2676.63	1095.92	1514.01

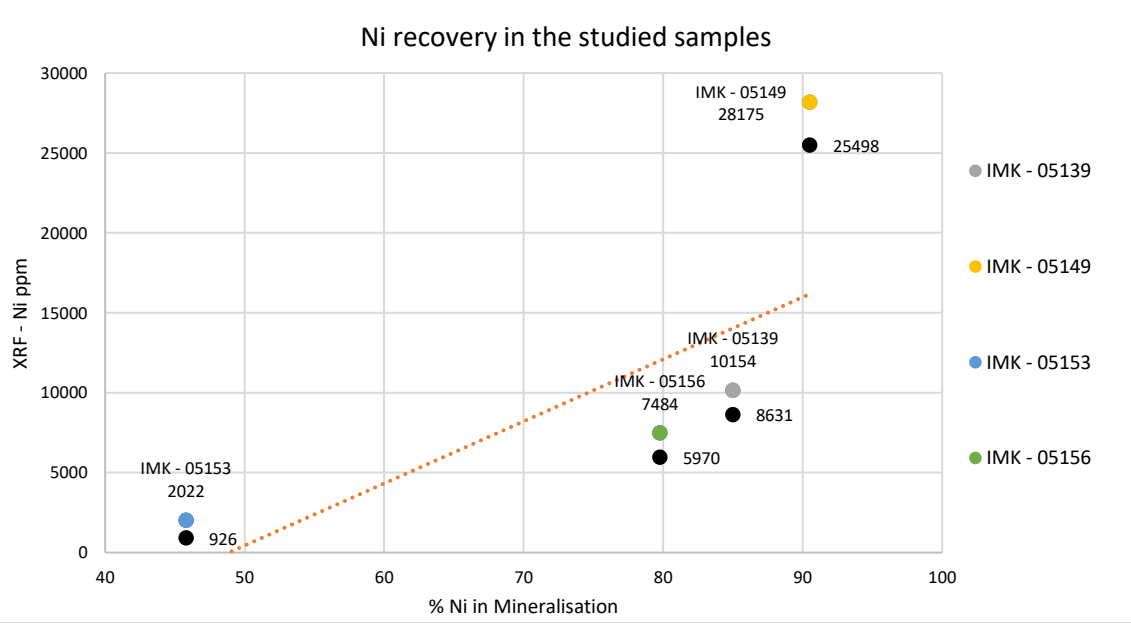

Figure 52: Proportion of recoverable Ni ppm per sample (black) and total Ni ppm in those samples.

9.3. Hydrothermal Ni in serpentines

The study provides textural and mineralogical evidence on the secondary nature of the Ni minerals rather than a magmatic origin. Hydrothermal Ni-sulphide deposits are rare but they do exist as summarised by González-Álvarez, et al., (2013). These authors suggested that the possible mobilisation of Ni at low temperatures (<250ºC) is a reason for potentially more wide spread occurrences of the hydrothermal Ni deposits. Some cases of hydrothermal Ni deposits include the Avebury deposit in Tasmania, Australia (Kamenetsky, et al., 2016), Enterprise Ni deposit in the Zambian Copperbelt (Capistrant, et al., 2015), and some disputable cases such as the upper zone of the Waterberg deposit in South Africa (McCreesh, et al., 2018), hydrothermal Ni dissemination in the Cenozoic(?) Papuan Ultramafic Belt (I.González-Álvarez, et al., 2013) and reclassification of the Epoch Ni deposit, Zimbabwe (Pirajno & González-Álvarez, 2013), as a hydrothermal Ni deposit.

Nickel is generally thought not to be mobile under most conditions, however, the experimental work by Liu, et al., (2012) indicated Ni mobilisation under acidic and oxidised environments. Furthermore, Le Vaillant et al., (2015) also showed that some hydrothermal fluids including those that are As-rich are able to mobilise Ni, as well as Cu and PGEs.

According to Frost (1984), heazlewoodite, a S-poor sulphide, occurs in carbonate-free serpentinites, also, Ni-Fe alloys are preferentially found in partially serpentinised peridotites which are thought to be highly reduced. Furthermore, in metamorphic environment of upper greenschist facies or higher, a SO_2 fluid in the carbonate bearing portion of an ultramafic body may lead to remobilisation of the metal, which might then be transported to carbonate-free serpentines in a reduced environment (Frost, 1984). Frost (1984) indicated that serpentinisation occurs under conditions of low oxygen fugacity and in a reduced environment, furthermore, the formation and composition of Ni-Fe alloys are indicative of the temperature and oxygen fugacity conditions of the serpentinisation.

The formation of awaruite could be associated with high H_2 concentrations, prevailing during serpentinisation and the desulphurisation of pentlandite (Schwarzenbach, et al., 2021). Awaruite occurs only in sample IMK – 05153, where ore minerals are comprised of heazlewoodite-awaruite grains that implies a complete replacement of pre-existent pentlandite with awaruite and the S-poor heazlewoodite.

The plot by Frost (1984), indicates the specific temperature, oxygen fugacity and presence of H_2 (reduced environment) for awaruite formation, which would imply that pyroxenite IMK – 05153 underwent serpentinisation under similar conditions of approximately 400ºC.

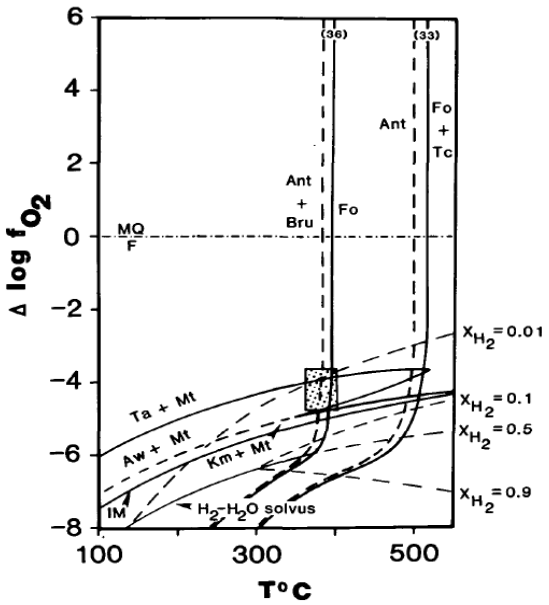

Figure 53: Plot of log fO_2 Vs T showing the equilibrium in Fe and Ni-bearing serpentines at $PH_2O + PH_2$ = 2 kb, after Frost (1984). Heavy lines separate the reaction temperatures for XMg olivine = 0.80. The box indicates the approximate fO_2 conditions for the antigorite-olivine-brucite-magnetite assemblage, inferred by the presence of awaruite, after Frost (1984). Ant = antigorite, Bru = brucite, Fo = forsterite, Tc = talc, Ta = taenite, Mt = magnetite, Aw = awaruite, Km = kamacite, IM = iron-magnetite, MQ = magnetite-quartz and F = fayalite.

The study by Oen et al., (1980), on orcelite from Ni-Fe-As-S mineralisation in chromitites and orthopyroxenite of Nebral, Málaga, Spain, indicates that orcelite was formed through serpentinisation of the pre-existing maucherite-pentlandite-heazlewoodite assemblage. This may be compared to the harzburgite IMK – 05156, that is host to a chromite zone with disseminated orcelite grains (Figure 44). Rare heazlewoodite grains were detected by microprobe analyses in this polished section. Orcelite has likely replaced possible maucherite - or pentlandite or heazlewoodite as a product of the serpentinisation event that also produced Fe-rich rims in chromite, which appear spatially adjacent to the orcelite disseminations. This harzburgite sample is characterised by the absence of amphiboles, which are very common in all other studied orthopyroxenite samples, whereas the secondary assemblage of IMK – 05156 harzburgite is dominated by serpentine.

Chapter 10

Conclusions and recommendations

The findings of the study support several conclusions:

1. Firstly, the highly altered rocks hosting Ni mineralisation can be divided into peridotites and pyroxenites that are distinguishable in core and polished sections based on the poikilitic and granular relic textures, whereas the granoblastic texture of their recrystallisation can only be identified under a microscope. These rocks are hard to distinguish by their chemistry as their compositions are largely overlapping due to intense alteration. The SiO_2 and MgO contents of harzburgite and orthopyroxenite also vary within the same range. Mineralised harzburgite is richer in Cr, Ca and Zr whereas mineralised orthopyroxenite is richer in chalcophile elements such as Ni, Cu and Zn. Ni mineralisation occurs in a wide-ranging assemblage in orthopyroxenite.
2. Orthopyroxenes, chromite and phlogopite comprise the only primary minerals present in the studied rocks which are dominated by the secondary minerals as serpentine (bastite), amphibole-group minerals, chlorite and biotite, as well as, Ni-sulphide minerals as pyrrhotite, mackinawite, pentlandite and heazlewoodite, Ni-Fe alloy (awaruite), arsenides (maucherite and orcelite), minor chalcocite, samaniite, parkerite and Ni antimonide.
3. Any primary ore minerals were not preserved but can be inferred from textural evidence as some pyrrhotite has an MSS composition. The majority of Ni-Cu-rich minerals present are associated with the serpentinisation stage where the primary sulphides were replaced by Ni-rich sulphides and Ni-Fe alloys. Late alteration most likely formed the Ni arsenides observed in sample IMK – 05156 and replaced the earlier formed Ni-Cu-rich minerals by secondary silicates (serpentine and amphibole).
4. The Ni deportment in the studied samples indicates a general Ni enrichment where a relevant portion (~1000 – 1500 ppm Ni) is hosted by silicate and/or oxide minerals. Furthermore, orthopyroxenite IMK – 05153, according to the XRF trace data, contains 2022 Ni ppm, which is near a calculated median of 2213 Ni ppm for all the XRF-analysed samples (Appendix IV). Sample IMK – 05153 has the lowest modal amount of Ni-bearing minerals (0.29 wt%) among the four samples studied by TIMA. With whole rock Ni ppm of approximately 1100 Ni ppm (ppm) in silicates, this sample should be representative of the Ni deportment for all altered and weakly mineralised orthopyroxenite. This indicates that orthopyroxenite enriched in Ni, to close to, or above 2000 ppm Ni, would have at least, ~1000 – 1500 ppm of unrecoverable Ni hosted in silicates and oxides. If the whole rock Ni grade is higher, the amount of Ni present in the silicates would not increase, but rather will be predominantly concentrated in ore minerals. This is confirmed by the Ni deportment for samples IMK – 05139 (10154 ppm Ni) and IMK – 05156 (7484 ppm Ni), both corresponding to approximately 1520 ppm of calculated unrecoverable Ni.

An S-isotope study would be required to get a better understanding of the exact origin of the Ni mineralisation. Additionally, a more in-depth correlation with other Ni hydrothermal deposits may lead to a better understanding of Ni mineralisation found in the KKME – 1/6 sequence of the MFC.

In conclusion, the occurrence of Ni-Cu bearing minerals in strongly altered ultramafic rocks of borehole KKME-1/6 is a result of several stages of hydrothermal and mineralogical alteration. This was most likely related to serpentinisation at relatively a lower temperature of <400ºC in a reducing environment, as evidenced by the presence of awaruite, a Ni-Fe alloy. The heazlewoodite-awaruite assemblage in sample IMK – 05153, implies involvement of a S-poor and Ni-rich fluid whereas the heazlewoodite-pentlandite assemblage suggests a fluid composition rich in Ni and more enriched in S and Fe with respect to the fluid that precipitated the assemblage with awaruite. The formation of orcelite indicates an elevated As activity that could have been caused by the incorporation of sedimentary wall-rock during hydrothermal fluid circulation. The Ni deportment study shows that approximately 1000 – 1500 ppm Ni of the total Ni content is hosted in the silicates and oxides. This Ni cannot be extracted during recovery of Ni from the Ni-bearing sulphides, alloys and arsenides.

References

Adreani, M., Mével, C., Boullier, A. & Escarín, J., 2007. Dynamic control on serpentine crystallization in veins: Constraints on hydration processes in oceanic peridotites. *Geochemistry, Geophysics, Geosystems,* 8(2).

Anthony, J. W., Bideaux, R. A., Bladh, K. W. & Nichols, a. M. C., 2001-2005. Handbook of Mineralogy. In: *Handbook of Mineralogy.* s.l.:Mineral Publishing.

Beukes, N. et al., 2019. The age and country rock provenance of the Molopo Farms Complex: implications for Transvaal Supergroup correlation in southern Africa. *March Geological Society of South Africa,* pp. 39-56.

Capistrant, P. L. et al., 2015. Geology of the Enterprise Hydrothermal Nickel Deposit, North-Western Province, Zambia. *Geology of the Enterprise Hydrothermal Nickel Deposit, North-Western Province, Zambia*, 01 01, pp. 9-38.

Deer, W. A., Howie, R. A. & Zussman, J., 1992. *An introduction to the rock-forming minerals.* 2nd ed ed. Harlow, Essex, England : New York, NY : Longman Scientific & Technical.

Evans, B. W., 2010. Lizardite versus antigorite serpentinite: Magnetite, hydrogen, and life(?). In: *Geology.* s.l.:s.n., pp. 879-882.

Frost, B. R., 1984. On the Stability of Sulfides, Oxides, and Native Metals in Serpentinite. *On the Stability of Sulfides, Oxides, and Native Metals in Serpentinite*, 10 06, p. 33.

González-Álvarez, I., Pirajno, F. & Kerrich, R., 2013. Hydrothermal nickel deposits: Secular variation and diversity. *Ore Geology Reviews,* Volume 52, pp. 1-3.

Gould, D., Rathbone, P. & Kimbell, G., 1987. The geology of the Molopo Farms Complex, southern Botswana. In: G. S. o. Botswana, ed. *Bulletin of the Geological Survey of Botswana.* Lobatse: Geological Survey of Botswana, p. 178.

Hawthorne, F. C. et al., 2012. Nomenclature of the amphibole supergroup. *American Mineralogist,* Volume 97, pp. 2031-2048.

HrsTka, T. et al., 2018. Automated mineralogy and petrology – applications of TESCAN Integrated Mineral Analyzer (TIMA). *Journal of Geosciences,* Volume 63, pp. 47-63.

Hulbert, L. J. & Gruenewaldt, G. V., 1985. Textural and compositional features of chromite in the lower and critical zones of the Bushveld Complex south of Potgietersrus. *Economic Geology,* 80(4), p. 872–895.

I.González-Álvarez, M.Sweetapple, I.D.Lindley & J.Kirakar, 2013. Hydrothermal Ni: Doriri Creek, Papua New Guinea. *Ore Geology Reviews,* Volume 52, pp. 37-57.

JEOL, 2006. *Features of Electron Probe Micro Analyzers, JXA-8100 and JXA-8200.* [Online] Available at: https://www.jeol.com/applications/pdf/xm/856_en.pdf
[Accessed 25 11 2022].

Kaavera, J. et al., 2020. Controls on the disseminated Ni-Cu-PGE sulfide mineralization at the Tubane section, northern Molopo Farms Complex, Botswana: Implications for the formation of conduit style magmatic sulfide ores. *Ore Geology Reviews,* Volume 126, pp. 1-23.

Kaavera, J., Rajesh, H., Tsunogae, T. & Belyanin, G., 2018. Marginal facies and compositional equivalents of Bushveld parental sills from the Molopo Farms Complex layered intrusion, Botswana: Petrogenetic and mineralization implications. *Ore Geology Reviews,* Volume 92, pp. 506-528.

Kamenetsky, V. S. et al., 2016. A story of olivine from the McIvor Hill complex (Tasmania, Australia). *A story of olivine from the McIvor Hill complex (Tasmania, Australia): Clues to the origin of the Avebury metasomatic Ni sulfide deposit* , 01 06, pp. 1321-1331.

Key, R., 2021. *Completion of the first phase of drilling.* [Online]
Available at: https://www.kalaharikey.co.uk/news/
[Accessed 20 06 2022].

Liu, W., Migdisov, A. & Williams-Jones, A., 2012. The stability of aqueous nickel(II) chloride complexes in hydrothermal solutions: Results of UV–Visible spectroscopic experiments. *Geochimica et Cosmochimica Acta,* Volume 94, pp. 276-290.

Mapeo, R. et al., 2004. Bushveld-age magmatism in southeastern Botswana: evidence from U-Pb zircon and titanite geochronology of the Moshaneng Complex. *SOUTH AFRICAN JOURNAL OF GEOLOGY,* pp. vol 107, 219-232.

McCreesh, M. J. G., Yudovskaya, M. A., Kinnaird, J. A. & Reinke, C., 2018. *Platinum-group minerals of the F and T zones, Waterberg Project, far northern Bushveld Complex: implication for the formation of the PGE mineralization*, 01 01, pp. 539-575.

Naldrett, A. J. et al., 2009. Chromite composition and PGE content of Bushveld chromitites: Part 1 – the Lower and Middle Groups. *Applied Earth Science,* 118(3-4), pp. 131-161.

Oen, I. S., Kieft, C., Burke, E. A. J. & Westerhof, A. E., 1980. Orcelite and associated minerals in the Ni — Fe — As — S system in chromitites and orthopyroxenites of Nebral, Málaga, Spain. *Bulletin de Minéralogie,* Volume 103-2, pp. 198-208.

Pirajno, F. & González-Álvarez, I., 2013. A re-appraisal of the Epoch nickel sulphide deposit, Filabusi Greenstone Belt, Zimbabwe: A hydrothermal nickel mineral system?. *Ore Geology Reviews,* Volume 52, pp. 58-65.

Power Metal Resources, 2022. *MOLOPO FARMS COMPLEX.* [Online]
Available at: https://www.powermetalresources.com/project/molopo-farms-complex/
[Accessed 15 11 2022].

Prendergast, M., 2012. The Molopo Farms Complex, southern Botswana - A reconsideration of structure, evolution and the Bushveld connection. *SOUTH AFRICAN JOURNAL OF GEOLOGY,* pp. 77-90.

Reichhardt, F., 1994. The Molopo Farms Complex, Botswana: History, Stratigraphy, Petrography, Petrochemistry and Ni-Cu-PGE Mineralization. In: *Explor. Mining Geol.*. Gold Fields Botswana, Box 271 Gaborone, Botswana: Pergamon, pp. 263-284.

Ridolfi, F., 2021. *Amp-TB2: An Updated Model for Calcic Amphibole Thermobarometry.* [Online] Available at: https://doi.org/10.3390/min11030324
[Accessed 27 12 2022].

Schwarzenbach, E. M. et al., 2021. *Sulfide Dissolution and Awaruite Formation in Continental Serpentinization Environments and Its Implications to Supporting Life*, 31 03.

Scoates, J. S. et al., 2021. Dating the Bushveld Complex: Timing of Crystallization, Duration of Magmatism, and Cooling of the World's Largest Layered Intrusion and Related Rocks. *Journal of Petrology,* 62(2).

Vaillant, M. L. et al., 2015. A Hydrothermal Ni-As-PGE Geochemical Halo Around the Miitel Komatiite-Hosted Nickel Sulfide Deposit, Yilgarn Craton, Western Australia. *Economic Geology,* Volume 110, pp. 505-530.

Yudovskaya, M. A. & Kinnaird, J. A., 2010. Chromite in the Platreef (Bushveld Complex, South Africa): Occurrence and evolution of its chemical composition. *Mineralium Deposita,* Volume 45, pp. 369-391.

Yudovskaya, M. A. et al., 2015. Reverse Compositional Zoning in the Uitkomst Chromitites as an Indication of Crystallization in a Magmatic Conduit. *Journal of Petrology,* 56(12), pp. 2373-2394.

Appendix I. -

I. Thin section descriptions

SAMPLE	Depth (m)	Mineralogy	Ore minerals	Textures	Alteration	% of alteration	Rock Name	Thin Section Image
IMK - 05147	293	Pyroxenes(OPX) - 80%; Olivine - 5%; Serpentine - 10%; Magnetite - 1-5%; Sulphides - <0,1%	Very small disseminated sulphides, not classified	Phaneritic, homogenous, with serpentine and magnetite veining	Serpentinisation	Low - 20%	Granular harzburgite	Thin section image - IMK - 05147
IMK - 05149	295	Pyroxenes(OPX) - 15%; Serpentine - 75%; Amphiboles - 5%; Sulphides – 4-5%	Polymineralic sulphide bleb (1 cm), Heazlewoodite-pentlandite	Phaneritic, heterogeneous, Vein with clinopyroxenes, altered orthopyroxenes	Serpentinisation and replacement to Amphibolites	High – 85%	Serpentinised orthopyroxenite	
IMK - 05153	297	Serpentine - 40% Orthopyroxene - 35%; Amphiboles - 20%; Mica - 1-5%; Sulphides - <1%	Small disseminated sulphide blebs, heazlewoodite-awaruite	Phaneritic, heterogeneous, serpentine veining and disseminated sulphides	Serpentinisation	Mod - 50%	Serpentinised orthopyroxenite	Thin section image – IMK - 05153
IMK - 05139	309,61	Pyroxenes(OPX) - 85%; Serpentine - 10-15%; Sulphides - <1%	Polymineralic sulphide blebs (0,2-4 mm) of pentlandite and pyrrhotite. Minor chromite	Phaneritic, heterogenous, serpentine veining	Serpentinisation	Mod - 40%	Altered/Serpentinised orthopyroxenite	Thin section image – IMK - 05139
1/6 - 310	310	Pyroxenes(OPX) - 90%; Olivine - 2%; Serpentine - 8%; Magnetite - 2%; Sulphides - <0,1%	Very small disseminated sulphides associated with veins, not classified	Phaneritic, heterogeneous, serpentine and magnetite veining	Serpentinisation	Low - 10-15%	Harzburgite	Thin section image – 1/6 - 310

II. Thin section description

SAMPLE	Depth (m)	Mineralogy	Ore minerals	Textures	Alteration	% of alteration	Rock Name	Thin Section Image
1/6 - 312	312	Pyroxenes(OPX) - 55%; Serpentine - 35%; Oxides - 5%; Amphibole - 1-5%; Chlorite 1-5%	Sulphides up to 1mm, associated with alteration	Phaneritic, heterogenous, serpentine veining, mica and chlorite replacing	Serpentinisation (major 90%) and chloritisation (minor 10%)	Mod - 50%	Altered pyroxenite	Thin section image – 1/6 - 312
IMK - 05156	446	Serpentine - 85%; Chromite - 10-15%; Chlorite - 1-5%; Mica - <1%; Ore mineral (orcelite/arsenide) - <1%	Large chromite blebs with associated arsenide (orcelite) minerals	Aphanitic, heterogenous; chromite rich horizon with all primary silicate altered	Serpentinisation (major 90%) and chloritisation (minor 10%)	Nearly full - 95-100%	Serpentinite after harzburgite	
IMK - 05136	502	Pyroxenes(OPX) - 90%; Serpentine - 8-10%; Oxides - 1-2%	Minor opaques/oxides, possibly chromite	Phaneritic, homogeneous, relic olivine textures	Serpentinisation	Low - 10%	Orthopyroxenite	
IMK - 05134	504	Serpentine - 90%; Olivine - 8-10%; Opaques/Oxides - <1%	None	Phaneritic, homogeneous, serpentine veining and relic olivine	Serpentinisation	High - 90%	Serpentinite after Ol-bearing pyroxenite	
IMK - 05132	506	Serpentine - 90%; Amphiboles - 8-10%%; Opaques/Oxides - <1%	None	Aphanitic, heterogeneous, large serpentine vein and relic opx	Serpentinisation	Nearly full - 95-100%	Serpentinite after pyroxenite	
IMK - 05125	512,5	Serpentine - 95-100%; Oxides - 1-5%;	None	Aphanitic, heterogeneous, minor relic texture of olivine and opx	Serpentinisation	Nearly full - 95-100%	Serpentinite after pyroxenite	

III. Thin section description

SAMPLE	Depth (m)	Mineralogy	Ore minerals	Textures	Alteration	% of alteration	Rock Name	Thin Section Image
1/6 - 515	515	Pyroxenes(OPX) - 70%; Serpentine -25%; Chlorite - 1-5%; Sulphides - <1%	Polymineralic sulphide blebs (up to 2mm), possible pentlandite and pyrrhotite	Phaneritic, heterogenous, serpentine and/or chlorite veining	Serpentinisation (major - 80-90%) and Cholitisation	Mod - 30%	Orthopyroxenite	Thin section image – 1/6 - 515
IMK - 05117	520	Serpentine - 90%; Chromite - 10%; Sulphides - <1%	Euhedral Chromite grains; very rare possible arsenide (IMK - 05156)	Aphanitic, homogeneous, magnetite veining	Serpentinisation	Nearly full - 95-100%	Massive serpentinite after harzburgite	
IMK - 05116	521	Serpentine - 85%; Chromite - 10%; Chlorite - <5%; Sulphides - <1%	Euhedral Chromite grains; very rare possible arsenide (IMK - 05156)	Aphanitic, homogeneous, magnetite veining	Serpentinisation and minor chloritisation	Nearly full - 95-100%	Massive serpentinite after harzburgite	
IMK - 05108	527	Serpentine - 85%, Mica - 15%; Oxides - <1%	None	Phaneritic, heterogenous, large crystals of phlogopite,	Serpentinisation	Nearly full - 95-100%	Serpentinite after harzburgite	
IMK - 05106	528.5	Pyroxenes(OPX) - 80%; Serpentine -15-20%; Olivine - 1-5%; Opaques - <1%	None	Phaneritic, heterogenous, variable degrees of alteration, relic olivine	Serpentinisation	Mod - 30%	Altered Ol-bearing orthopyroxenite	
1/6 - 531	531	Pyroxenes(OPX) - 70%; Serpentine -20%; Olivine - 5%; Mica - 1-5%; Amphiboles - 1-5%; Opaques - <1%	Micrometric sulphide specs, disseminated in veins and interstitial	Phaneritic, heterogeneous, serpentine and talc veining.	Serpentinisation	Mod - 40%	Altered Ol-bearing orthopyroxenite	Thin section image – 1/6 - 531
1/6 - 547	547	Pyroxenes(OPX) - 85%; Olivine - 10%; Serpentine - 1-5%; Mica - 1-5%; Opaques - <1%	None	Phaneritic, homogeneous, minor serpentine and mica veining.	serpentinisation and minor mica	Low - 5%	Ol-bearting orthopyroxenite	Thin section image – 1/6 - 547

IV. Thin section description

SAMPLE	Depth (m)	Mineralogy	Ore minerals	Textures	Alteration	% of alteration	Rock Name	Thin Section Image
1/6 - 555	555	Serpentine - 95%; Oxides - 1-5%; Olivine - <1%	Sporadic, sub millimetric, possible heazlewoodite	Aphanitic, homogeneous, talc alteration	Serpentinisation	Nearly full - 95-100%	Serpentinite after poikilitic harzburgite	Thin section image – 1/6 - 555
1/6 - 561	561	Serpentine - 70%; Amphibole - 15%; Mica - 5%; Olivine - 5%; Oxides - 1-5%; sulphides - <1%	Generally broken and altered sulphides, possible heazlewoodite	Aphanitic, heterogeneous, talc and chlorite alteration	Serpentinisation and minor chlrotisation	Nearly full - 95-100%	Serpentinite after harzburgite	Thin section image – 1/6 - 561
1/6 - 591	591	Serpentine - 95%; Oxides - 1-5%; Mica - <1%; Sulphides - <1%	Sporadic, polymineralic, possible heazlewoodite awaruite	Aphanitic, heterogeneous, talc alteration	Serpentinisation	Nearly full - 95-100%	Serpentinite after harzburgite	Thin section image – 1/6 - 591
IMK - 05101	597,5	Serpentine - 90%; Pyroxenes(OPX) - 5-10%; Oxides - <1%; olivine - 1-5%; Sulphides - <1%	Sulphides, generally inside oikocrysts, up to 1mm, anhedral.	Aphanitic, homogeneous, relic Opx and Ol textures	Serpentinisation	High - 90%	Serpentinite after harzburgite	

Appendix II. Thin section images

i. Thin section image - IMK - 05147

ii. Thin section image – IMK -05153

iii. Thin section image – IMK -05139

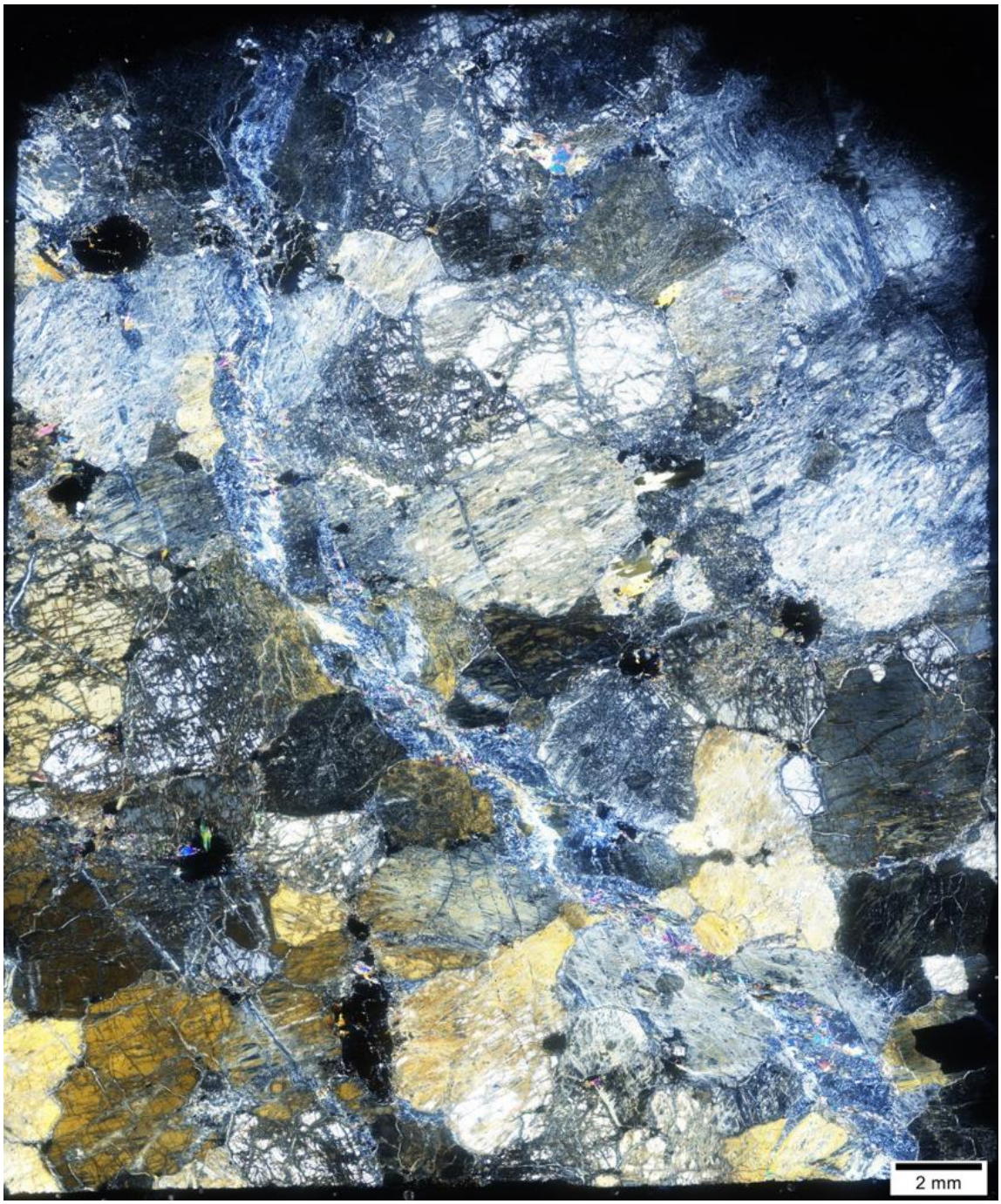

iv. Thin section image – 1/6 - 310

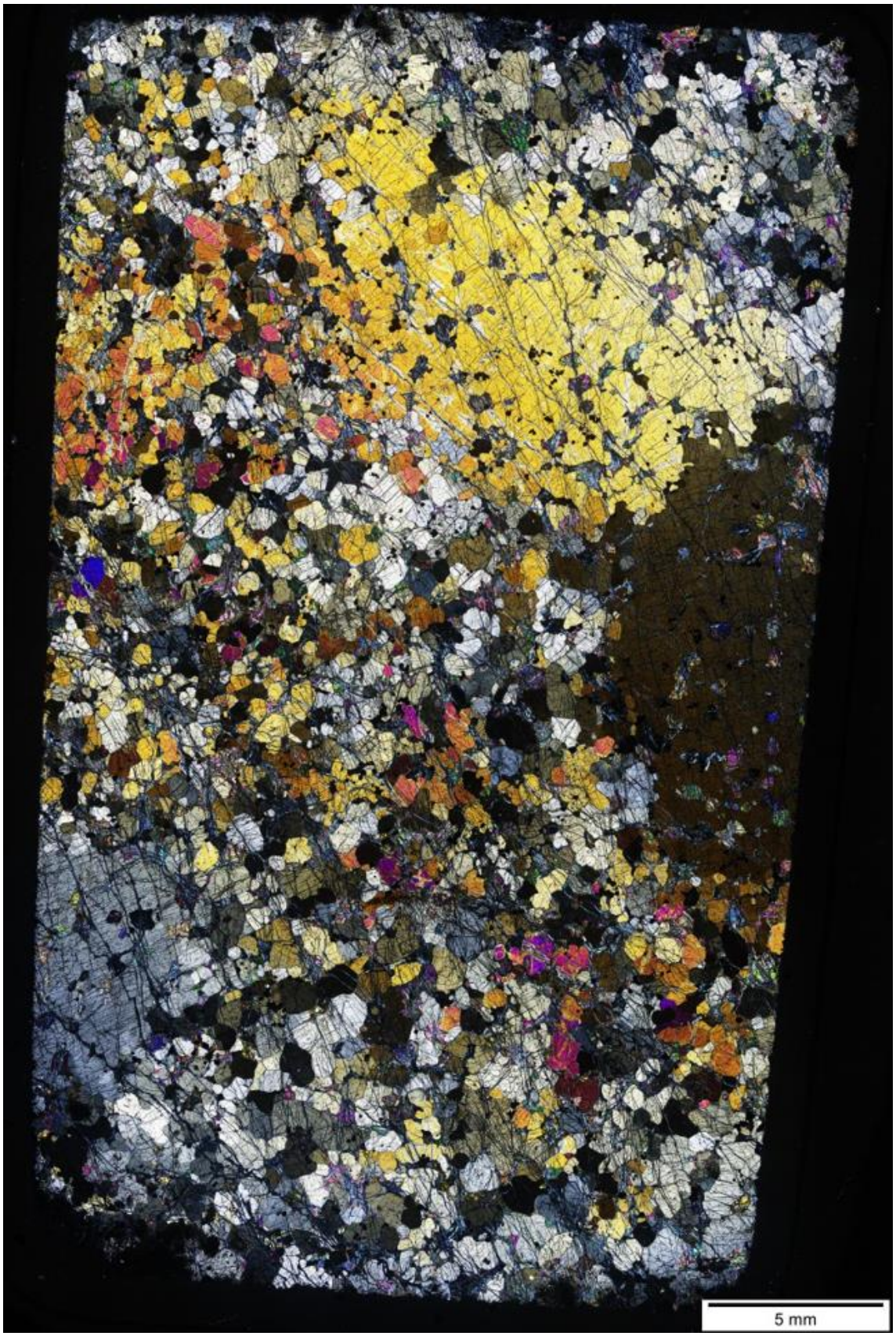

v. Thin section image – 1/6 - 312

vi. Thin section image – 1/6 - 515

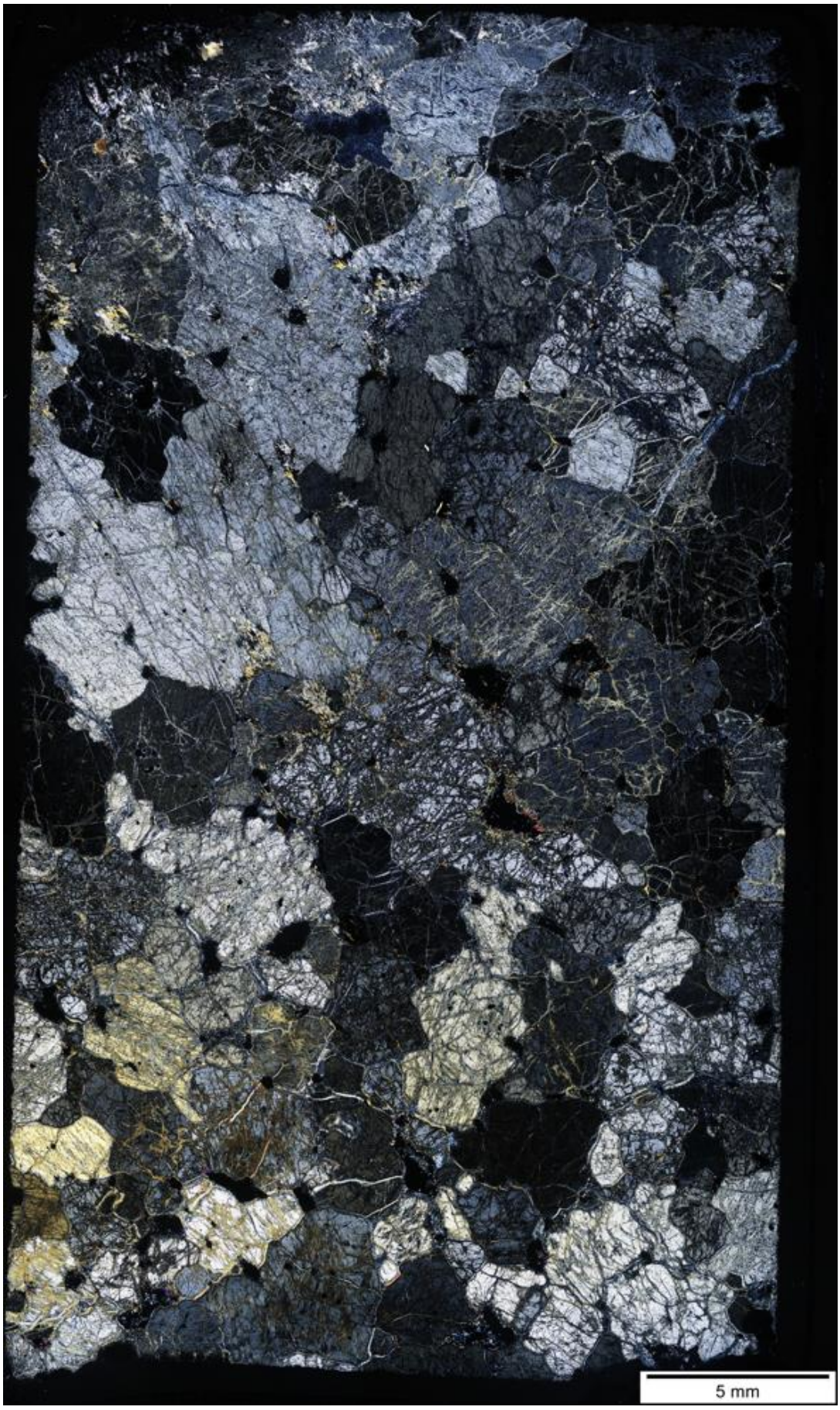

vii. Thin section image – 1/6 - 531

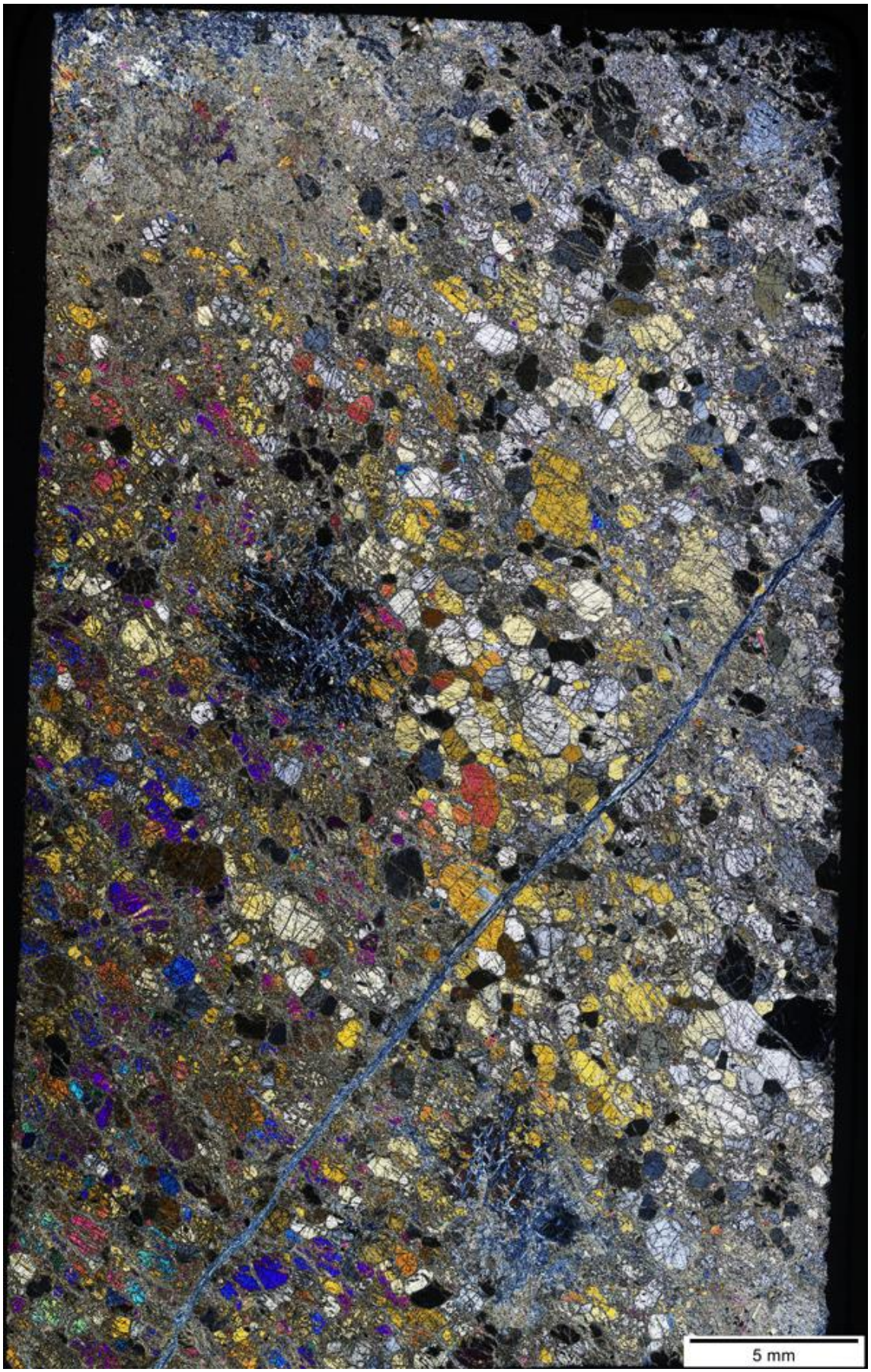

viii. Thin section image – 1/6 - 547

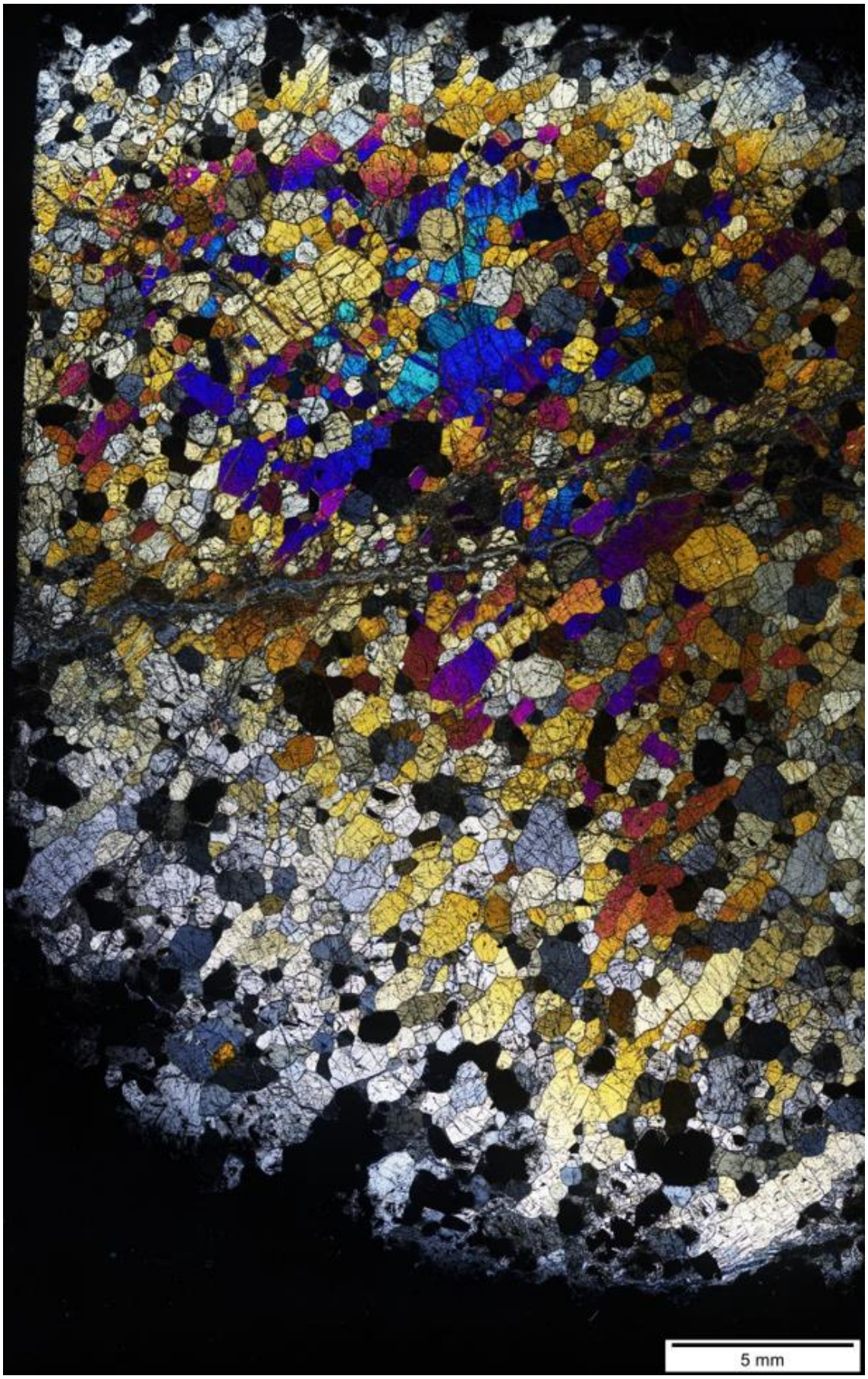

ix. Thin section image – 1/6 - 555

x. Thin section image – 1/6 - 561

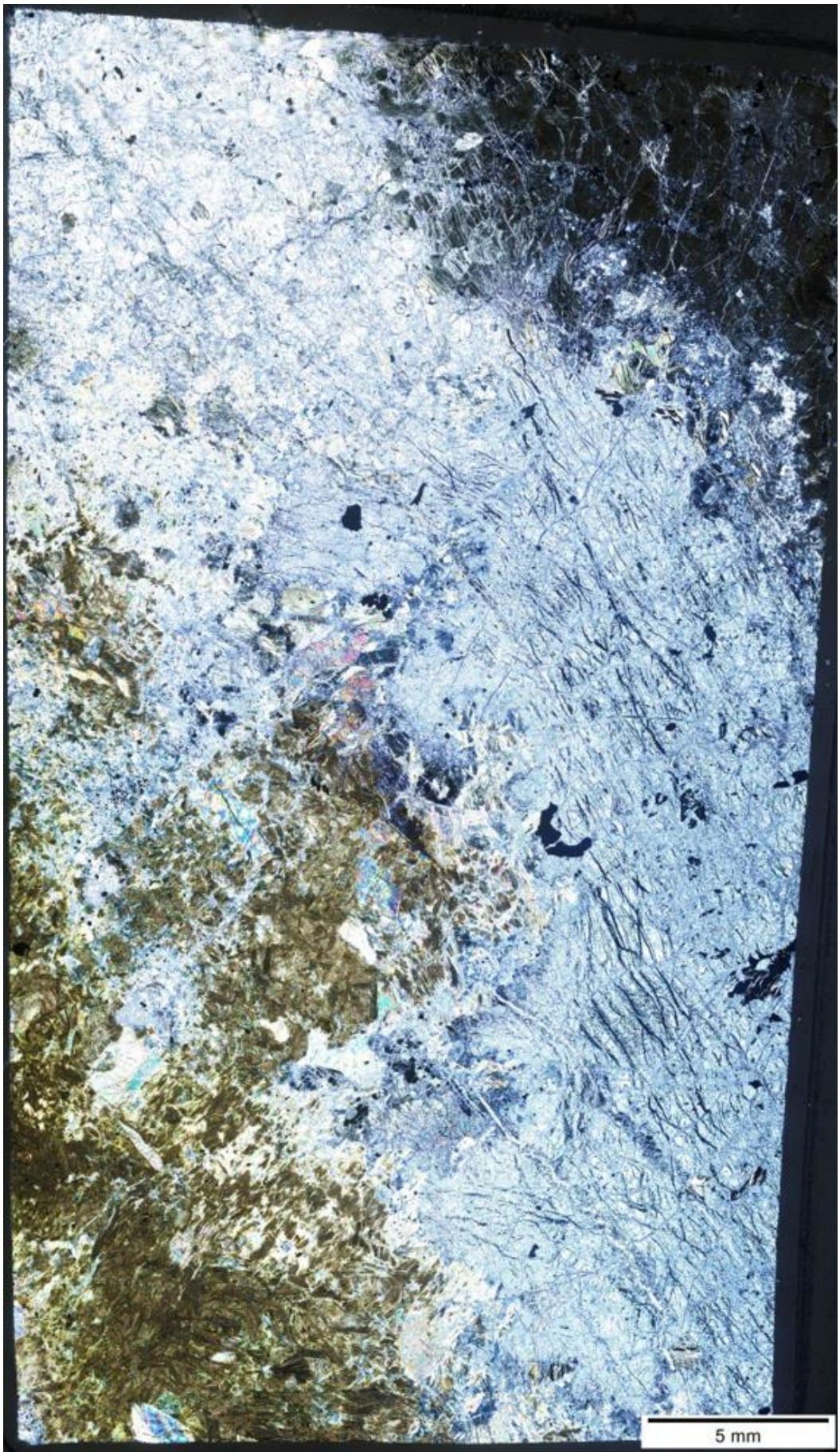

xi. Thin section image – 1/6 - 591

Appendix III. Hand sample descriptions

I. Hand sample description

SAMPLE	Depth (m)	Rock name	Hand Sample Description
IMK - 05117	520	Massive serpentinite	Massive dark coloured aphanitic rock, homogenous, heavily altered with abundant sulphides and opaques (5-10%), 90-95% fine grained serpentine.
IMK - 05116	521	Massive Serpentinite	Massive dark-green coloured aphanitic rock, homogeneous, heavily altered, some opaques, chlorite, and dominant serpentine.
IMK - 05139	309.61	Pyroxenite	Phaneritic rock, greyish coloured with green tint, altered pyroxenite, pyroxenes of 1-5 mm, somewhat euhedral, dominant, about 90-100% in less altered portions, 70-80% in more altered, alteration is serpentine, fine grained, about 20%. Interstitial sulphides blebs 0.2 mm to 4mm.
IMK - 05108	527	Serpentinised pyroxenite	Phaneritic to aphanitic, altered pyroxenite, greyish with green tint, pyroxenes of 1-5 mm, somewhat euhedral, mostly altered. Alteration in grains and veining as serpentine and large grains of phlogopite, up to 4 mm, especially associated with veining. Vein has up to 6 mm.
IMK - 05125	512.5	Serpentinised Harzburgite	Massive dark coloured to small greenish tint, aphanitic rock, serpentine replacing pyroxenes and olivines, preserving grains shapes, with interstitial dark coloured material (magnetite/oxide), grains up to 2 mm, most are smaller.
IMK - 05147	294	Granular harzburgite	Fresh dominant OPX, bright grey with some green patches on alteration, coarse grained, 2-4 mm. Serpentine veining, green coloured, up to 1.8 cm and apparent parallel distribution between each other and inclined to the core axis, with later magnetite veining, black coloured, smaller, 0.2 to 3 mm, sub parallel with each other and apparent interstitial.
IMK - 05134	504	Orthopyroxenite	Altered pyroxenite, dominant orthopyroxene, coarse grained, greyish with green tint, up to 4mm, more altered near vein. Serpentine vein (alteration zone, greener), up to 2 cm with antigorite/asbestos/chlorite. Vein of 1–3mm, some phlogopite specs.
IMK - 05132	506	Serpentinite	Massive black to dark green coloured, aphanitic rock with some opaque/oxides specs. Mostly fine-grained matrix after pyroxenite, common antigorite and serpentine veining, up to 2mm, and sparse diss oxides.
IMK - 05136	502	Orthopyroxenite	Massive, grey coloured, orthopyroxenite, phaneritic, coarse grained orthopyroxene, up to 5 mm. Local inclined veins of alteration (talc), 2mm, with alterations zone of serpentine alteration, up to 7 mm.
IMK - 05101	597.5	Poikilitic Harzburgite	Poikilitic Harzburgite, highly altered. Massive, dark coloured with green tint, aphanitic matrix of serpentine with large 1cm long orthopyroxene oikocrysts, also altered into serpentine. Opaque veining, 0.2-0.5 mm, common and sulphide spec inside orthopyroxene oikocrysts
IMK - 05106	528.5	Altered Pyroxenite	Heavily altered olivine bearing orthopyroxenite. Massive, aphanitic, grey to green coloured rock. Serpentinisation is major in some darker spots with more olivine. Some serpentine veining, up to 1 mm.
1/6 - 310	310	Pyroxenite	Dark homogeneous phaneritic rock, small, up to 2mm and average 1mm, grey to black grains. Interstitial black and fine-grained material, not to common. Green tint as alteration across sample, probable over 90% alteration, serpentine and or chlorite.

II. Hand sample description

SAMPLE	Depth (m)	Rock name	Hand Sample Description
1/6 - 312	312	Pyroxenite	Dark to grey, heterogeneous phaneritic rock, large pyroxene grains, coarser than sample 1/6 - 310, up to 4 mm, larger dark fine-grained matrix, altered portion meaning probable larger olivine proportion and alteration of them. Sulphide grains, up to 1mm, +-10 grains
1/6 - 515	515	Magnetite lens in Harzburgite	Massive dark-coloured magnetite lens
1/6 - 531	531	Pyroxenite	Grey coloured with black veins, large pyroxene grains, up to 1-2 cm with alteration and veining of serpentine, up to 6mm. Phaneritic, heterogeneous. Serpentine alteration common
1/6 - 547	547	Pyroxenite	Fine grained pyroxenite, grey with green tint, phaneritic, homogeneous. Serpentine vein, 1mm, dark coloured. Local pyroxenes up to 1mm. Serpentine grains up to 2mm. No sulphides
1/6 - 555	555	Serpentinised Harzburgite	Poikilitic Harzburgite, highly altered. Massive, dark coloured with green tint, aphanitic matrix of serpentine with large 1cm long orthopyroxene oikocrysts, also altered into serpentine
1/6 - 561	561	Harzburgite	Grey coloured phaneritic rock, fine to medium grained pyroxenes, plenty alteration. Sulphide blebs, up to 1mm. Dark alteration matrix and veins
1/6 - 591	591	Harzburgite	Poikilitic Harzburgite, highly altered. Massive, dark coloured with green tint, aphanitic matrix of serpentine with large, up to 3cm long orthopyroxene oikocrysts, also altered into serpentine. Sulphide specs in oikocrysts

Appendix IV. XRF

i. XRF Major elements data 1

			Major oxides proportions in wt%													
Sample ID	**Lithology**	**Depth (m)**	**SiO_2**	**Al_2O_3**	**Fe_2O_3**	**MnO**	**MgO**	**CaO**	**Na_2O**	**K2O**	**TiO_2**	**P_2O_5**	**Cr_2O_3**	**NiO**	**LOI**	**TOTAL**
1-6 / 310	Harzburgite	310,6	48,96	1,7	9,14	0,21	29,16	3,72	0,08	0,1	0,09	0,02	0,63	1,12	4,8	99,72
1-6 / 312	Orthopyroxenite	312	45,69	1,01	4,76	0,24	36,6	0,78	0,09	0,04	0,05	0,02	0,43	0,31	9,83	99,84
IMK-05139	Orthopyroxenite	309,8	49,39	1,55	10,11	0,18	28,68	3,7	0,07	0,08	0,08	0,02	0,64	1,35	4,22	100,06
IMK-05149	Orthopyroxenite	295	41,7	1,48	11,33	0,29	29,9	2,27	0,11	0,11	0,05	0,03	0,13	3,67	9,16	100,22
IMK-05153	Orthopyroxenite	297	47,22	2,45	8,39	0,3	31,22	2,45	0,11	0,23	0,1	0,03	0,46	0,28	6,74	99,99
IMK-05101	Harzburgite	597	36,1	0,78	10,74	0,11	37,22	0,06	0,05	0	0,02	0,02	1,66	0,38	12,9	100,06
IMK-05132	Orthopyroxenite	506	40,38	1,33	10,51	0,37	35,2	0,05	0,04	0,02	0,05	0,01	0,67	0,13	11,72	100,5
IMK-05147	Harzburgite	293,7	49,57	0,94	7,94	0,17	34,62	0,61	0,06	0,01	0,06	0,02	0,61	0,19	5,55	100,35
1-6 / 551	Orthopyroxenite	551	49,94	1,49	9,43	0,2	33,8	0,88	0,06	0,02	0,06	0,02	1,1	0,28	3,22	100,5
1-6 / 531	Orthopyroxenite	531	53,02	1,13	9,47	0,17	30,9	1,14	0,07	0,1	0,06	0,01	0,42	0,1	3,5	100,08
1-6 / 547	Orthopyroxenite	547	54,73	1,47	9,56	0,19	31,36	1,33	0,06	0,02	0,07	0,01	0,63	0,1	0,93	100,44
1-6 / 555	Harzburgite	555	36,75	0,87	10,85	0,13	36,67	0,07	0,04	0	0,03	0,02	1,65	0,35	12,43	99,85
1-6 / 561	Harzburgite	561	44,03	0,96	9,93	0,26	35,34	0,5	0,06	0,01	0,04	0,02	0,75	0,28	8,28	100,46
1-6 / 589	Harzburgite	589	37,45	0,83	8,3	0,1	38,34	0,08	0,05	0	0,03	0,02	1,33	0,34	13,12	99,98
1-6 / 515	Magnetite Vein	515	14,19	0,32	65,38	0,13	14,69	0,09	-0,14	0,02	0,03	0,02	0,37	0,13	3,37	98,58
IMK-05117	Harzburgite	520	42,58	3,16	12,51	0,26	29,41	0,45	0,17	0,54	0,15	0,03	0,85	0,2	10,21	100,51

	Secondary standards in wt%														
	SiO_2	**Al_2O_3**	**Fe_2O_3**	**FeO**	**MnO**	**MgO**	**CaO**	**Na_2O**	**K_2O**	**TiO_2**	**P_2O_5**	**Cr_2O_3**	**NiO**	**TOTAL**	**LOI**
NIM-P	51,38	4,3	1,28	10,36	0,23	25,35	2,65	0,36	0,1	0,19	0,03	3,55	0,08	99,84	-0,23
NIM-D	39,04	0,33	1,72	13,91	0,22	43,98	0,33	0,03	0,01	0,03	0,01	0,42	0,26	100,3	-0,51
W2	53,08	15,59	1,09	8,85	0,17	6,42	10,93	2,24	0,66	1,07	0,13	0,02	0,01	100,3	0,19
NIM-S	63,99	17,31	0,14	1,12	0,01	0,47	0,61	0,38	15,41	0,05	0,12	0	0	99,62	0,42
GSP2	67,44	15,09	0,5	4,03	0,04	1	2,12	2,82	5,48	0,68	0,29	0	0	99,49	0,87
BCR2	54,4	13,6	1,39	11,3	0,19	3,62	7,17	3,18	1,79	2,29	0,36	0,01	0	99,3	0,1
NIM-N	53,03	16,72	0,91	7,33	0,18	7,53	11,54	2,45	0,25	0,2	0,02	0,01	0,02	100,2	0,04
NIM-G	76,28	12,22	0,2	1,6	0,02	0,07	0,79	3,34	5,06	0,1	0,02	0	0	99,67	0,73
PCC1	44,35	0,75	0,87	7,06	0,12	45,86	0,63	0,07	0	0,01	0,01	0,43	0,33	100,5	5,09
BHVO2	50,25	13,73	1,25	10,11	0,17	7,31	11,5	2,24	0,51	2,77	0,27	0,05	0,02	100,2	-0,48
AGV2	60,64	17,26	0,69	5,56	0,1	1,83	5,32	4,27	2,94	1,06	0,48	0,01	0	100,1	1,8
G2	69,76	15,41	0,27	2,18	0,04	0,78	1,94	4,08	4,5	0,49	0,14	0	0	99,6	0,64
DTS1	40,99	0,28	0,87	7,07	0,12	50	0,19	0,06	0	0,02	0,01	0,6	0,31	100,5	-0,02

ii. XRF Major elements data 2

			Major oxides proportions in wt%												
Sample ID	**Lithology**	**Depth (m)**	**SiO_2**	**Al_2O_3**	**Fe_2O_3**	**MnO**	**MgO**	**CaO**	**Na_2O**	**K_2O**	**TiO_2**	**P_2O_5**	**Cr_2O_3**	**NiO**	**LOI**	**TOTAL**
IMK - 05156	Harzburgite	446,9	35,33	4,46	4,5	0,1	37,21	0,09	0,04	0,04	0,1	0,03	2,44	1,4	13,28	99,04

	Secondary standards in wt%														
	SiO_2	**Al_2O_3**	**Fe_2O_3**	**FeO**	**MnO**	**MgO**	**CaO**	**Na_2O**	**K_2O**	**TiO_2**	**P_2O_5**	**Cr_2O_3**	**NiO**	**TOTAL**	**LOI**
NIM-P	51,23	4,27	1,28	10,4	0,22	25,39	2,63	0,36	0,1	0,2	0,03	3,52	0,07	99,71	-0,23
NIM-D	39,06	0,32	1,72	13,94	0,22	44,05	0,32	0,02	0,01	0,03	0,01	0,41	0,27	100,4	-0,51
W2	53,1	15,56	1,1	8,87	0,16	6,43	10,96	2,23	0,66	1,08	0,13	0,02	0,01	100,3	0,19
NIM-S	64,1	17,34	0,14	1,14	0,01	0,49	0,62	0,37	15,46	0,05	0,12	0	0	99,83	0,42
GSP2	67,73	15,12	0,5	4,04	0,04	1,01	2,12	2,83	5,51	0,68	0,29	0	0	99,86	0,87
BCR2	54,53	13,64	1,4	11,3	0,2	3,63	7,15	3,18	1,78	2,29	0,36	0,01	0	99,46	0,1
NIM-N	53,26	16,75	0,91	7,34	0,17	7,56	11,53	2,45	0,25	0,2	0,02	0,01	0,01	100,5	0,04
NIM-G	76,45	12,24	0,2	1,62	0,02	0,07	0,79	3,31	5,08	0,1	0,01	0	0	99,88	0,73
PCC1	44,57	0,74	0,87	7,04	0,12	45,92	0,62	0,08	0	0,01	0,01	0,43	0,33	100,7	5,09
BHVO2	50,28	13,73	1,25	10,12	0,17	7,33	11,51	2,2	0,52	2,76	0,27	0,06	0,02	100,2	-0,48
AGV2	60,62	17,34	0,69	5,56	0,1	1,85	5,3	4,22	2,94	1,06	0,48	0,01	0	100,2	1,8
G2	69,7	15,42	0,27	2,18	0,04	0,79	1,94	4,07	4,5	0,49	0,14	0	0	99,54	0,64
DTS1	40,71	0,28	0,87	7,07	0,13	50,08	0,19	0,05	0	0,01	0,01	0,59	0,31	100,3	-0,02
SIO2	98,36	0,24	0	0	0	0,16	0,04	-0,03	0,01	0,01	0,02	0	0	98,81	0

d.l. - detection limit

iii. XRF Minor elements data 2

			Trace elements proportions in wt%																
Sample ID	**Lithology**	**Depth (m)**	Sc	V	Cr	Co	Ni	Cu	Zn	Ga	Rb	Sr	Y	Zr	Nb	Mo	Ba	Pb	Th	U
1-6 / 310,6	Harzburgite	310,6	15,57	56,4	4127,29	238,47	*7541,49*	649,5	53,39	1,34	5,76	25,51	1,38	9,27	0,15	5,39	11,48	4,69	d.l.	d.l.
1-6 / 312,8	Orthopyroxenite	312	12,17	30,05	2693,19	124,89	1902,23	d.l.	47,96	0,08	1,62	3,08	0,8	2,47	0,56	0,62	15,45	3,61	0,13	d.l.
IMK-05139	Orthopyroxenite	309,8	18,63	69,37	4514,77	303,24	*10153,64*	526,32	51,63	1,72	5,94	29,18	1,91	6,3	d.l.	5,92	14,87	5,34	d.l.	d.l.
IMK-05149	Orthopyroxenite	295	6,25	19,45	1048,86	416,47	*28174,83*	1407,3	91,87	1,85	1,94	13,2	3,69	11,29	d.l.	9,6	30,57	8,84	d.l.	d.l.
IMK-05153	Orthopyroxenite	297	18,79	54,53	3266,34	91,28	*2022,44*	d.l.	63,93	2,57	12,57	15,74	2,74	11,18	d.l.	d.l.	44,33	6,27	d.l.	d.l.
IMK-05101	Harzburgite	597	8,93	45,01	*9970,38*	65,8	2891,18	d.l.	58,06	2,34	d.l.	0,56	0,68	d.l.	d.l.	d.l.	8,62	8,67	d.l.	d.l.
IMK-05132	Orthopyroxenite	506	17,17	51,82	4350,6	207,23	1061,3	d.l.	54,95	1,82	0,2	0,65	1,46	1,36	d.l.	0,31	6,76	2,14	d.l.	d.l.
IMK-05147	Harzburgite	293,7	10,71	46,22	3675,43	101,84	1545,44	d.l.	47,34	1,95	3,87	2,61	0,6	0,86	d.l.	d.l.	11,47	2,52	d.l.	d.l.
1-6 / 551	Orthopyroxenite	551	9,05	53,53	7469,83	145,5	3015,04	d.l.	57,78	1,41	d.l.	1,35	0,78	0,24	d.l.	0,58	2,42	2,73	d.l.	d.l.
1-6 / 531	Orthopyroxenite	531	18,56	106,58	2786,25	88,84	745,72	2,78	52,52	1,27	3,47	3,38	0,86	0,02	0,09	d.l.	11,2	3,7	d.l.	d.l.
1-6 / 547	Orthopyroxenite	547	22,8	59,94	4184,8	87,4	819,47	d.l.	63,87	2,6	d.l.	2,15	0,69	1,23	0,8	0,34	7,25	3,13	d.l.	d.l.
1-6 / 555	Harzburgite	555	17,64	66,7	6481,64	118,42	2277,39	d.l.	62,82	0,34	1,28	1,51	2,04	0,97	d.l.	d.l.	7,66	0,74	d.l.	d.l.
1-6 / 561	Harzburgite	561	15,07	78,96	4071,62	112,02	2150,19	d.l.	46,53	1,78	2,14	2,54	1,75	1	d.l.	0,33	5,94	2,78	d.l.	d.l.
1-6 / 589	Harzburgite	589	8,3	36,5	7291,33	85,52	2627,64	d.l.	45,69	0,06	d.l.	2,01	1,65	0,76	d.l.	d.l.	5,91	2,52	d.l.	d.l.
1-6 / 515	Magnetite Vein	515	6,56	31,18	4772	177	1805	60,8	62,00	1,48		3,05	0,73	0,28	1,84	1,01	25,00	36,76		
IMK-05117	Harzburgite	520	12,05	94,72	4375,14	139,56	1616,81	d.l.	60,54	5,25	21,38	10,89	4,47	26,16	1,23	0,5	88,22	1,88	d.l.	d.l.

	Secondary Standards																	
	Sc	V	Cr	Co	Ni	Cu	Zn	Ga	Rb	Sr	Y	Zr	Nb	Mo	Ba	Pb	Th	U
BR	28,94	225,29	332,47	49,91	281,32	80,28	156	18	47,7	1389	29,1	280,2	102	3,45	1255	5,07	8,58	2,5
NIM-N	42,71	211,28	29,27	58,6	109,46	16,63	58,42	18,1	4,15	252,8	6,3	12,8	0,15	d.l.	76,07	5,58	d.l.	d.l.
AGV2	16,49	106,94	18,49	13,66	14,02	55,13	85,61	22,2	67,77	640,9	20	239,5	12,8	3,07	1208	15,1	4,75	d.l.
GSP2	6,06	53,48	30,92	6,03	17,78	46,19	114,3	22,2	241,9	232,6	27,4	550,7	24,9	2,13	1395	46,9	115	3,9
NIM-D	4,11	46,03	2492,75	191,74	2160,44	1,53	91,38	0,64	d.l.	3,04	1,05	2,04	d.l.	0,43	6	2,47	d.l.	d.l.
NIM-S	5,18	5,24	9,05	4,59	3,71	16,65	6,93	12,2	522	61,91	3,25	14,85	0,02	0,47	2621	3,59	d.l.	2
BHVO2	34,91	311,24	284,23	43,25	119,61	131,42	101,1	21,8	7,35	381,7	26,9	177,1	16,5	3,15	140,1	4	d.l.	d.l.
NIM-G	0,3	1,82	17,21	0,35	2,74	11,61	45,93	29,2	316,2	10,75	131	276,1	51,3	2,67	113,7	40,2	49,1	18

d.l. - detection limit

iv. XRF Minor elements data 2

			Trace elements proportions in wt%																
Sample ID	**Lithology**	**Depth (m)**	Sc	V	Cr	Co	Ni	Cu	Zn	Ga	Rb	Sr	Y	Zr	Nb	Mo	Ba	Pb	Th	U
IMK - 05156	Harzburgite	446,9	12,76	69,03	9898,58	571,4	*7484,02*	d.l.	58.69	3.44	3.05	2.07	1.11	27.95	1.65	0.67	10.17	64.78	d.l.	d.l.

Appendix V. Microprobe data

a. Orthopyroxene 1

Sample - IMK - 05139

Lithology	Coarse-grained orthopyroxenite											
File	Z1	Z1	Z1	Z1	Z1	Z1	Z1	Z1	Z1	Z1	Z1	Z1
Analyses ID	14	16	17	18	19	20	23	25	27	28	29	31
Mineral name	Enstatite	Enstatite	Enstatite	Enstatite	Enstatite	Enstatite	Enstatite	Enstatite	Enstatite	Enstatite	Enstatite	Enstatite
SiO2	56,42	56,61	57,13	57,19	56,24	57,28	55,08	57,09	56,62	55,70	57,31	56,74
TiO2	0,07	0,07	0,08	0,03	0,04	0,08	0,04	0,05	0,04	0,14	0,04	0,08
Al2O3	1,23	1,21	1,25	1,19	1,08	1,23	1,21	1,17	1,06	1,07	1,09	1,38
Cr2O3	0,84	0,77	0,86	0,72	0,74	0,80	0,77	0,75	0,70	0,62	0,70	0,95
MgO	31,40	32,80	32,41	32,79	32,18	33,10	30,81	32,03	31,78	30,51	33,15	32,40
CaO	1,97	1,47	1,22	1,19	1,27	1,13	0,98	2,27	2,56	1,06	1,00	1,29
MnO	0,11	0,08	0,07	0,11	0,11	0,08	0,12	0,08	0,14	0,13	0,09	0,04
FeO	7,02	6,51	6,88	6,34	6,19	6,37	7,59	6,16	6,24	9,25	6,26	6,58
NiO	0,04	0,01	0,04	b.d.l	b.d.l	0,01	0,04	0,00	0,08	0,06	0,06	0,06
Total (wt%)	99,23	99,55	99,99	99,69	98,05	100,17	96,71	99,75	99,28	98,55	99,81	99,53
Atomic proportions (apfu) in the base of 6 O												
Si	1,969	1,961	1,971	1,975	1,976	1,969	1,972	1,974	1,972	1,972	1,976	1,964
Ti	0,002	0,002	0,002	0,001	0,001	0,002	0,001	0,001	0,001	0,004	0,001	0,002
Al	0,069	0,067	0,069	0,066	0,061	0,068	0,070	0,065	0,059	0,061	0,060	0,077
Cr	0,023	0,021	0,023	0,020	0,020	0,022	0,022	0,021	0,019	0,017	0,019	0,026
Mg	1,634	1,694	1,667	1,688	1,686	1,696	1,644	1,651	1,650	1,611	1,703	1,672
Ca	0,074	0,055	0,045	0,044	0,048	0,042	0,037	0,084	0,096	0,040	0,037	0,048
Mn	0,003	0,002	0,002	0,003	0,003	0,002	0,004	0,002	0,004	0,004	0,003	0,001
Fe2+	0,205	0,189	0,199	0,183	0,182	0,183	0,227	0,178	0,182	0,274	0,180	0,190
FE3+	0,000	0,000	0,000	0,000	0,000	0,000	0,000	0,000	0,000	0,000	0,000	0,000
Ni	0,001	0,000	0,001	0,000	0,000	0,000	0,001	0,000	0,002	0,002	0,002	0,002
Total (apfu)	3,984	3,993	3,981	3,983	3,984	3,986	3,982	3,983	3,988	3,985	3,985	3,983

b. Orthopyroxene 2

Sample - IMK - 05139

Lithology	Coarse-grained orthopyroxenite												
File	Z1	Z1	Z1	Z1	Z1	Z1	Z1	Z1	Z2	Z2	Z2	Z2	Z2
Analyses ID	33	35	36	37	40	41	42	44	3	5	7	8	11
Mineral name	Enstatite	Enstatite	Enstatite	Enstatite	Enstatite	Enstatite	Enstatite	Enstatite	Enstatite	Enstatite	Enstatite	Enstatite	Enstatite
SiO2	57,44	56,97	56,85	57,06	56,24	56,89	56,37	56,83	57,51	57,48	57,74	56,71	57,48
TiO2	0,02	0,05	b.d.l	0,04	0,09	0,03	0,10	0,09	0,08	0,03	0,07	0,04	0,05
Al2O3	1,16	1,02	1,14	1,22	1,31	1,40	1,48	1,24	1,16	1,15	1,23	1,19	1,06
Cr2O3	0,78	0,66	0,74	0,77	0,87	0,87	0,91	0,77	0,77	0,77	0,76	0,78	0,65
MgO	33,36	32,69	33,12	32,97	32,29	32,83	31,93	33,16	33,04	33,55	33,28	33,67	33,44
CaO	0,94	0,94	0,98	1,03	1,13	1,09	1,41	1,01	1,25	1,23	1,19	1,02	1,17
MnO	0,09	0,12	0,10	0,08	0,10	0,09	0,07	0,10	0,06	0,09	0,11	0,11	0,12
FeO	6,30	7,22	6,34	6,32	6,94	6,44	6,86	6,41	6,80	6,59	6,42	6,69	6,45
NiO	b.d.l	b.d.l	0,03	0,02	b.d.l	b.d.l	0,06	b.d.l	0,06	0,02	0,01	b.d.l	0,04
Total (wt%)	100,14	99,69	99,44	99,54	99,00	99,74	99,24	99,71	100,76	100,91	100,89	100,29	100,58
Atomic proportions (apfu) in the base of 6 O													
Si	1,972	1,974	1,968	1,971	1,961	1,964	1,960	1,962	1,969	1,964	1,970	1,950	1,970
Ti	0,001	0,001	0,000	0,001	0,002	0,001	0,003	0,002	0,002	0,001	0,002	0,001	0,001
Al	0,064	0,056	0,063	0,067	0,073	0,077	0,083	0,068	0,063	0,063	0,067	0,065	0,058
Cr	0,021	0,018	0,020	0,021	0,024	0,024	0,025	0,021	0,021	0,021	0,020	0,021	0,018
Mg	1,707	1,689	1,709	1,698	1,678	1,689	1,655	1,707	1,686	1,708	1,692	1,726	1,709
Ca	0,034	0,035	0,036	0,038	0,042	0,040	0,052	0,037	0,046	0,045	0,043	0,038	0,043
Mn	0,003	0,004	0,003	0,002	0,003	0,003	0,002	0,003	0,002	0,002	0,003	0,003	0,004
Fe2+	0,181	0,209	0,183	0,182	0,202	0,186	0,200	0,185	0,195	0,188	0,183	0,180	0,185
FE3+	0,000	0,000	0,000	0,000	0,000	0,000	0,000	0,000	0,000	0,000	0,000	0,012	0,000
Ni	0,000	0,000	0,001	0,001	0,000	0,000	0,002	0,000	0,002	0,000	0,000	0,000	0,001
Total (apfu)	3,985	3,988	3,991	3,984	3,988	3,986	3,984	3,991	3,987	3,994	3,985	4,000	3,992

c. Orthopyroxene 3

Sample - IMK - 05139

Lithology	Coarse-grained orthopyroxenite												
File	Z2	Z2	Z2	Z2	Z2	Z2	Z3	Z3	Z3	Z3	Z3	Z3	Z3
Analyses ID	13	14	15	17	19	24	1	3	4	7	8	10	13
Mineral name	Enstatite	Enstatite	Enstatite	Enstatite	Enstatite	Enstatite	Enstatite	Enstatite	Enstatite	Enstatite	Enstatite	Enstatite	Enstatite
SiO2	57,70	57,49	56,71	57,03	57,87	56,46	57,55	57,14	57,31	57,34	57,49	57,40	57,17
TiO2	0,07	0,05	0,07	0,06	0,06	0,08	0,05	0,07	0,01	0,07	0,05	0,04	0,08
Al2O3	1,05	1,14	1,19	1,19	1,10	1,06	1,16	1,21	1,17	1,09	1,13	1,17	1,20
Cr2O3	0,68	0,75	0,78	0,73	0,72	0,74	0,75	0,69	0,71	0,66	0,72	0,78	0,73
MgO	33,21	33,79	32,61	32,97	33,76	33,39	33,05	31,83	33,42	33,50	32,74	33,13	32,38
CaO	1,29	1,01	1,85	1,14	1,01	2,06	1,11	1,23	1,02	0,98	1,03	1,10	1,25
MnO	0,13	0,10	0,08	0,10	0,10	0,12	0,08	0,10	0,09	0,08	0,10	0,11	0,13
FeO	6,22	6,33	6,74	7,13	6,24	6,40	6,52	8,41	6,43	6,30	6,38	6,52	7,37
NiO	b.d.l	b.d.l	b.d.l	0,04	b.d.l	0,00	0,02	b.d.l	0,02	0,02	0,04	b.d.l	0,02
Total (wt%)	100,35	100,71	100,17	100,41	100,96	100,33	100,32	100,76	100,30	100,08	99,69	100,25	100,38

Atomic proportions (apfu) in the base of 6 O

Si	1,978	1,965	1,959	1,963	1,971	1,942	1,974	1,970	1,968	1,971	1,982	1,971	1,970
Ti	0,002	0,001	0,002	0,001	0,002	0,002	0,001	0,002	0,000	0,002	0,001	0,001	0,002
Al	0,058	0,062	0,066	0,065	0,060	0,058	0,064	0,067	0,064	0,060	0,062	0,064	0,066
Cr	0,018	0,020	0,021	0,020	0,019	0,020	0,020	0,019	0,019	0,018	0,020	0,021	0,020
Mg	1,697	1,721	1,679	1,691	1,714	1,712	1,690	1,636	1,710	1,716	1,683	1,696	1,663
Ca	0,047	0,037	0,068	0,042	0,037	0,076	0,041	0,045	0,037	0,036	0,038	0,040	0,046
Mn	0,004	0,003	0,002	0,003	0,003	0,003	0,002	0,003	0,003	0,002	0,003	0,003	0,004
Fe2+	0,178	0,181	0,195	0,205	0,178	0,149	0,187	0,243	0,185	0,181	0,184	0,187	0,212
FE3+	0,000	0,000	0,000	0,000	0,000	0,035	0,000	0,000	0,000	0,000	0,000	0,000	0,000
Ni	0,000	0,000	0,000	0,001	0,000	0,000	0,000	0,000	0,000	0,000	0,001	0,000	0,000
Total (apfu)	3,983	3,993	3,998	3,994	3,988	4,000	3,982	3,986	3,992	3,989	3,975	3,985	3,986

d. Orthopyroxene 4

Sample - IMK - 05139

Lithology	Coarse-grained orthopyroxenite										
File	Z3	Z3	Z3	Z3	Z3	Z4	Z4	Z4	Z4	Z4	Z4
Analyses ID	14	17	18	20	26	1	8	9	13	15	28
Mineral name	Enstatite	Enstatite	Enstatite	Enstatite	Enstatite	Enstatite	Enstatite	Enstatite	Enstatite	Enstatite	Enstatite
SiO2	57,16	57,23	57,25	57,57	57,25	56,99	57,00	57,13	57,20	57,15	57,19
TiO2	0,07	0,07	0,04	0,06	0,01	0,03	0,02	0,05	0,05	0,05	0,03
Al2O3	1,14	1,28	1,16	1,11	1,18	1,16	1,16	1,10	1,23	1,28	1,07
Cr2O3	0,77	0,75	0,71	0,74	0,75	0,75	0,78	0,76	0,77	0,81	0,72
MgO	32,69	33,19	33,32	33,38	32,85	33,30	32,57	32,90	33,13	33,23	33,18
CaO	1,12	1,13	1,09	1,18	1,53	0,96	1,07	1,18	0,99	1,08	0,98
MnO	0,08	0,09	0,08	0,11	0,09	0,10	0,14	0,13	0,11	0,05	0,08
FeO	6,36	6,34	6,50	6,48	6,34	6,32	7,07	6,64	6,43	6,48	6,35
NiO	0,04	0,04	b.d.l	0,01	0,01	0,05	b.d.l	0,08	0,04	0,06	b.d.l
Total (wt%)	99,54	100,21	100,23	100,71	100,07	99,75	99,84	100,02	100,01	100,20	99,74
Atomic proportions (apfu) in the base of 6 O											
Si	1,977	1,966	1,967	1,970	1,971	1,967	1,971	1,971	1,969	1,963	1,973
Ti	0,002	0,002	0,001	0,002	0,000	0,001	0,000	0,001	0,001	0,001	0,001
Al	0,063	0,071	0,064	0,061	0,065	0,064	0,065	0,061	0,068	0,071	0,059
Cr	0,021	0,020	0,019	0,020	0,020	0,020	0,021	0,021	0,021	0,022	0,020
Mg	1,685	1,699	1,707	1,702	1,686	1,714	1,679	1,692	1,700	1,702	1,706
Ca	0,042	0,042	0,040	0,043	0,056	0,036	0,039	0,044	0,036	0,040	0,036
Mn	0,002	0,003	0,002	0,003	0,002	0,003	0,004	0,004	0,003	0,001	0,002
Fe2+	0,184	0,182	0,187	0,185	0,183	0,182	0,204	0,192	0,185	0,186	0,183
FE3+	0,000	0,000	0,000	0,000	0,000	0,000	0,000	0,000	0,000	0,000	0,000
Ni	0,001	0,001	0,000	0,000	0,000	0,001	0,000	0,002	0,001	0,002	0,000
Total (apfu)	3,980	3,988	3,991	3,989	3,987	3,991	3,986	3,988	3,987	3,989	3,988

e. Orthopyroxene 5

Sample - IMK - 05153

Lithology	Serpentinised pyroxenite											
File	Z1	Z1	Z1	Z1	Z1	Z1	Z2	Z2	Z2	Z2	Z2	Z2
Analyses ID	23	24	29	35	36	40	2	4	6	8	14	15
Mineral name	Enstatite	Enstatite	Enstatite	Enstatite	Enstatite	Enstatite	Enstatite	Enstatite	Enstatite	Enstatite	Enstatite	Enstatite
SiO2	57,27	56,95	57,03	56,44	57,05	56,90	56,14	56,65	56,95	56,77	56,91	56,76
TiO2	0,02	0,07	0,02	0,06	0,05	0,08	0,15	0,09	0,06	0,05	0,06	0,05
Al2O3	1,07	1,06	0,98	1,18	0,92	1,14	1,15	1,16	1,09	1,09	0,94	1,10
Cr2O3	0,49	0,53	0,51	0,53	0,54	0,53	0,52	0,46	0,59	0,50	0,54	0,55
MgO	32,99	32,97	33,41	32,13	33,17	32,55	31,60	32,08	32,68	33,26	33,07	32,38
CaO	0,89	0,91	0,73	0,95	0,79	0,98	1,12	0,98	0,85	0,78	0,74	0,76
MnO	0,15	0,12	0,16	0,15	0,10	0,13	0,17	0,11	0,08	0,18	0,17	0,13
FeO	7,35	7,26	7,20	7,72	7,18	8,08	8,50	7,74	7,35	7,43	7,17	7,25
NiO	0,04	b.d.l	0,09	0,02	0,11	0,05	0,14	0,06	0,06	0,04	b.d.l	0,05
Total (wt%)	100,30	99,92	100,30	99,24	99,98	100,47	99,48	99,35	99,80	100,11	99,70	99,11
Atomic proportions (apfu) in the base of 6 O												
Si	1,972	1,969	1,967	1,969	1,972	1,964	1,964	1,973	1,972	1,961	1,973	1,977
Ti	0,001	0,002	0,000	0,002	0,001	0,002	0,004	0,002	0,001	0,001	0,001	0,001
Al	0,059	0,059	0,054	0,066	0,051	0,063	0,064	0,065	0,060	0,060	0,052	0,061
Cr	0,013	0,015	0,014	0,015	0,015	0,014	0,014	0,013	0,016	0,014	0,015	0,015
Mg	1,694	1,699	1,718	1,671	1,709	1,675	1,648	1,665	1,687	1,713	1,709	1,681
Ca	0,033	0,034	0,027	0,036	0,029	0,036	0,042	0,036	0,032	0,029	0,027	0,028
Mn	0,004	0,004	0,005	0,004	0,003	0,004	0,005	0,003	0,002	0,005	0,005	0,004
Fe2+	0,212	0,210	0,208	0,225	0,207	0,233	0,249	0,226	0,213	0,212	0,208	0,211
FE3+	0,000	0,000	0,000	0,000	0,000	0,000	0,000	0,000	0,000	0,002	0,000	0,000
Ni	0,001	0,000	0,003	0,001	0,003	0,001	0,004	0,002	0,002	0,001	0,000	0,001
Total (apfu)	3,991	3,993	4,000	3,990	3,994	3,995	3,993	3,986	3,989	4,000	3,994	3,984

f. Orthopyroxene 6

Sample - IMK - 05153

Lithology	Serpentinised pyroxenite					
File	Z2	Z2	Z2	Z2	Z2	Z2
Analyses ID	17	18	20	21	23	25
Mineral name	Enstatite	Enstatite	Enstatite	Enstatite	Enstatite	Enstatite
SiO2	56,89	56,67	56,03	57,31	56,66	55,89
TiO2	b.d.l	0,03	0,05	0,07	0,05	0,03
Al2O3	0,33	1,07	1,09	1,00	1,15	0,53
Cr2O3	0,15	0,54	0,49	0,52	0,50	0,22
MgO	32,11	32,76	32,12	33,06	32,33	32,25
CaO	0,15	0,85	1,71	0,86	0,50	0,38
MnO	0,20	0,15	0,14	0,11	0,11	0,15
FeO	9,49	7,45	7,48	7,15	7,90	9,23
NiO	0,05	0,02	b.d.l	0,10	b.d.l	0,17
Total (wt%)	99,39	99,59	99,15	100,18	99,24	98,90
Atomic proportions (apfu) in the base of 6 O						
Si	1,997	1,968	1,959	1,975	1,974	1,970
Ti	0,000	0,001	0,001	0,002	0,001	0,001
Al	0,018	0,060	0,061	0,055	0,064	0,030
Cr	0,004	0,015	0,013	0,014	0,014	0,006
Mg	1,680	1,696	1,674	1,698	1,679	1,695
Ca	0,006	0,032	0,064	0,032	0,019	0,014
Mn	0,006	0,004	0,004	0,003	0,003	0,004
Fe2+	0,279	0,216	0,213	0,206	0,230	0,250
FE3+	0,000	0,000	0,006	0,000	0,000	0,022
Ni	0,002	0,000	0,000	0,003	0,000	0,005
Total (apfu)	3,992	3,994	3,999	3,989	3,986	4,000

a. Clinopyroxene 1

Sample - IMK - 05139					
Lithology	Coarse-grained orthopyroxenite				
File	Z2	Z2	Z2	Z1	Z1
Analyses ID	18	23	27	4	12
Mineral name	Pigeonite	Pigeonite	Diopside	Augite	Augite
SiO2	56,56	55,47	55,32	57,97	57,62
TiO2	0,03	b.d.l	0,03	b.d.l	b.d.l
Al2O3	1,09	0,60	b.d.l	0,09	0,10
Cr2O3	0,78	0,24	0,04	0,07	0,09
MgO	31,96	28,90	16,04	22,19	21,39
CaO	2,81	4,62	25,27	12,44	14,27
MnO	0,14	0,21	0,12	0,14	0,04
FeO	6,23	9,33	4,61	4,84	3,90
NiO	0,04	0,02	0,13	0,03	0,14
Total (wt%)	99,76	99,47	101,64	97,95	97,67
Atomic proportions (apfu) in the base of 6 O					
Si	2,002	2,083	2,079	1,963	1,967
Ti	0,001	0,000	0,000	0,001	0,000
Al	0,000	0,005	0,006	0,061	0,034
Cr	0,001	0,002	0,002	0,022	0,007
Mg	0,865	1,188	1,151	1,654	1,528
Ca	0,980	0,479	0,552	0,105	0,175
Mn	0,004	0,004	0,001	0,004	0,006
Fe2+	0,139	0,145	0,118	0,181	0,249
FE3+	0,000	0,000	0,000	0,000	0,028
Ni	0,004	0,001	0,004	0,001	0,001
Total (apfu)	3,998	3,915	3,918	3,996	3,999

b. Clinopyroxene 2

Sample - IMK - 05149

Lithology	Serpentinised pyroxenite												
File	Z4	Z4	Z4	Z4	Z4	Z4	Z4	Z4	Z4	Z4	Z4	Z4	Z4
Analyses ID	1	2	3	4	5	6	7	9	10	11	12	13	15
Mineral name	Hedenbergite	Hedenbergite	Hedenbergite	Hedenbergite	Hedenbergite	Diopside	Augite	Augite	Diopside	Hedenbergite	Diopside	Diopside	Hedenbergite
SiO2	51,99	50,75	51,57	50,98	52,78	51,18	54,98	54,31	52,92	51,97	54,91	55,06	52,41
TiO2	b.d.l	b.d.l	b.d.l	b.d.l	b.d.l	b.d.l	b.d.l	0,06	0,01	0,01	0,02	b.d.l	0,00
Al2O3	b.d.l	b.d.l	b.d.l	b.d.l	0,01	b.d.l	0,02	0,09	0,43	0,01	0,02	0,04	0,01
Cr2O3	0,07	0,08	0,10	0,08	0,07	0,09	0,09	0,07	0,13	0,01	0,05	0,06	0,07
MgO	7,72	4,70	7,63	4,95	8,92	8,95	17,19	18,44	16,63	8,82	15,91	15,75	8,47
CaO	24,25	23,63	23,08	23,81	22,17	23,80	22,51	18,37	24,07	22,36	24,07	23,45	24,35
MnO	0,70	1,44	0,84	1,19	1,15	0,98	0,18	0,14	0,13	0,71	0,12	0,19	0,47
FeO	16,06	20,01	16,86	20,16	15,82	14,77	5,12	6,39	4,73	16,98	5,90	6,19	15,15
NiO	b.d.l	0,02	0,01	b.d.l	0,03	0,01	0,03	0,06	0,01	b.d.l	0,05	0,05	0,00
Total (wt%)	100,80	100,70	100,20	101,20	101,01	99,88	100,18	98,13	99,12	101,07	101,07	100,81	100,92
Atomic proportions (apfu) in the base of 6 O													
Si	2,005	2,004	2,006	2,001	2,016	1,980	2,007	2,013	1,953	1,995	2,002	2,010	2,007
Ti	0,000	0,000	0,000	0,000	0,000	0,000	0,000	0,002	0,000	0,000	0,001	0,000	0,000
Al	0,000	0,000	0,000	0,000	0,001	0,000	0,001	0,006	0,025	0,000	0,001	0,003	0,000
Cr	0,002	0,002	0,003	0,003	0,002	0,003	0,003	0,002	0,004	0,000	0,001	0,002	0,002
Mg	0,444	0,276	0,442	0,289	0,508	0,516	0,936	1,019	0,915	0,505	0,865	0,857	0,483
Ca	1,002	1,000	0,962	1,001	0,908	0,987	0,881	0,730	0,952	0,920	0,940	0,917	0,999
Mn	0,023	0,048	0,028	0,040	0,037	0,032	0,006	0,005	0,004	0,023	0,004	0,006	0,015
Fe2+	0,518	0,661	0,549	0,662	0,505	0,438	0,156	0,198	0,080	0,530	0,180	0,189	0,485
FE3+	0,000	0,000	0,000	0,000	0,000	0,039	0,000	0,000	0,066	0,015	0,000	0,000	0,000
Ni	0,000	0,000	0,000	0,000	0,001	0,000	0,001	0,002	0,000	0,000	0,001	0,002	0,000
Total (apfu)	3,994	3,996	3,994	3,998	3,983	4,000	3,992	3,983	4,001	3,999	3,996	3,987	3,992

c. Clinopyroxene 3

Sample - IMK - 05149

Lithology	Serpentinised pyroxenite												
File	Z4	Z4	Z4	Z4	Z4	Z4	Z4	Z4	Z4	Z4	Z5	Z5	Z5
Analyses ID	16	17	18	19	20	21	23	24	25	28	5	6	7
Mineral name	Diopside	Hedenbergite	Diopside	Diopside	Augite	Augite	Diopside	Augite	Augite	Diopside	Augite	Augite	Hedenbergite
SiO2	51,58	50,10	54,89	54,77	55,29	55,91	54,51	55,35	55,10	54,79	54,70	52,04	51,45
TiO2	b.d.l	b.d.l	0,01	0,02	0,01	b.d.l	b.d.l	0,06	0,03	0,01	0,03	b.d.l	b.d.l
Al2O3	b.d.l	0,01	0,02	0,09	0,03	0,05	0,02	0,08	0,05	0,07	0,09	b.d.l	b.d.l
Cr2O3	0,02	0,06	0,08	0,11	0,08	0,10	0,06	0,07	0,06	0,12	0,10	0,03	0,07
MgO	9,02	4,22	16,66	16,86	16,43	18,03	16,12	17,29	16,05	16,82	18,20	7,76	8,11
CaO	24,17	23,58	23,91	23,89	22,20	21,42	22,92	19,43	22,01	22,63	21,36	20,38	23,79
MnO	0,77	1,45	0,20	0,18	0,20	0,17	0,17	0,24	0,23	0,18	0,14	0,90	0,80
FeO	14,19	20,17	4,36	4,78	5,31	4,51	5,26	6,27	6,10	5,04	5,13	18,05	16,03
NiO	0,03	b.d.l	0,04	b.d.l	0,08	0,03	b.d.l	0,03	b.d.l	0,04	b.d.l	b.d.l	b.d.l
Total (wt%)	99,91	99,73	100,22	100,72	99,73	100,28	99,10	98,89	99,69	99,75	99,77	99,36	100,33

Atomic proportions (apfu) in the base of 6 O

Si	1,990	2,001	2,005	1,993	2,025	2,023	2,015	2,035	2,024	2,008	1,998	2,032	1,993
Ti	0,000	0,000	0,000	0,000	0,000	0,000	0,000	0,002	0,001	0,000	0,001	0,000	0,000
Al	0,000	0,001	0,001	0,005	0,002	0,003	0,001	0,005	0,003	0,004	0,005	0,000	0,000
Cr	0,001	0,002	0,002	0,003	0,002	0,003	0,002	0,002	0,002	0,003	0,003	0,001	0,002
Mg	0,519	0,251	0,907	0,914	0,897	0,972	0,888	0,948	0,879	0,919	0,991	0,452	0,468
Ca	0,999	1,009	0,936	0,931	0,871	0,830	0,908	0,766	0,866	0,888	0,836	0,853	0,987
Mn	0,025	0,049	0,006	0,005	0,006	0,005	0,005	0,008	0,007	0,005	0,004	0,030	0,026
Fe2+	0,434	0,670	0,133	0,140	0,163	0,136	0,163	0,193	0,187	0,155	0,157	0,589	0,505
FE3+	0,023	0,003	0,000	0,005	0,000	0,000	0,000	0,000	0,000	0,000	0,000	0,000	0,014
Ni	0,001	0,000	0,001	0,000	0,002	0,001	0,000	0,001	0,000	0,001	0,000	0,000	0,000
Total (apfu)	3,999	3,997	3,994	4,000	3,974	3,975	3,984	3,961	3,973	3,989	3,997	3,969	4,000

d. Clinopyroxene 4

Sample - IMK - 05149				
Lithology	Serpentinised pyroxenite			
File	Z5	Z5	Z5	Z5
Analyses ID	8	9	10	19
Mineral name	Augite	Hedenbergite	Hedenbergite	Diopside
SiO2	54,87	51,28	51,55	54,26
TiO2	0,02	0,03	b.d.l	0,01
Al2O3	0,11	b.d.l	b.d.l	0,02
Cr2O3	0,07	0,09	0,09	0,12
MgO	18,38	7,80	7,78	14,49
CaO	19,29	24,07	23,90	24,77
MnO	0,19	1,55	1,59	0,16
FeO	5,28	14,94	14,92	6,38
NiO	0,01	b.d.l	0,00	b.d.l
Total (wt%)	98,39	99,77	99,94	100,32
Atomic proportions (apfu) in the base of 6 O				
Si	2,021	1,998	2,004	2,004
Ti	0,001	0,001	0,000	0,000
Al	0,006	0,000	0,000	0,001
Cr	0,002	0,003	0,003	0,004
Mg	1,009	0,453	0,451	0,798
Ca	0,761	1,005	0,996	0,981
Mn	0,006	0,051	0,052	0,005
Fe2+	0,163	0,487	0,485	0,197
FE3+	0,000	0,000	0,000	0,000
Ni	0,000	0,000	0,000	0,000
Total (apfu)	3,976	3,999	3,996	3,994

e. Clinopyroxene 5

Sample - IMK - 05153

Lithology	Serpentinised pyroxenite		
File	Z1	Z1	Z1
Analyses ID	1	2	3
Mineral name	Augite	Diopside	Augite
SiO2	52,02	52,17	51,89
TiO2	b.d.l	0,01	b.d.l
Al2O3	0,46	0,09	0,34
Cr2O3	0,49	0,26	0,79
MgO	15,38	9,85	15,64
CaO	21,59	23,20	21,68
MnO	1,05	1,72	1,00
FeO	9,81	12,43	9,62
NiO	0,01	b.d.l	0,03
Total (wt%)	100,85	99,84	101,06
	Atomic proportions (apfu) in the base of 6 O		
Si	1,920	2,002	1,910
Ti	0,000	0,000	0,000
Al	0,027	0,006	0,020
Cr	0,014	0,008	0,023
Mg	0,846	0,564	0,858
Ca	0,854	0,954	0,855
Mn	0,033	0,056	0,031
Fe2+	0,181	0,399	0,155
FE3+	0,121	0,000	0,141
Ni	0,000	0,000	0,001
Total (apfu)	3,999	3,992	3,999

a. Serpentines 1

Sample - IMK - 05139

Lithology	Coarse-grained orthopyroxenite												
File	Z1	Z1	Z1	Z1	Z1	Z1	Z1	Z1	Z1	Z1	Z1	Z1	Z1
Analyses ID	1	5	6	7	8	9	10	13	21	26	30	32	34
TiO2	0,01	0,03	0,04	0,04	0,02	0,05	0,06	0,08	b.d.l	0,03	0,01	0,01	b.d.l
CaO	1,28	0,66	0,14	0,74	0,82	2,38	4,54	0,09	0,23	0,60	1,05	0,53	0,64
SiO2	42,68	42,14	43,54	44,22	42,02	44,91	48,46	41,37	42,71	44,89	45,19	44,05	44,35
Cr2O3	1,29	0,91	0,89	0,92	1,30	0,99	0,83	1,98	1,19	0,49	0,94	0,90	0,90
MnO	0,07	0,07	0,30	0,32	0,06	0,13	0,12	0,03	0,22	0,33	0,30	0,28	0,28
MgO	33,66	34,57	31,53	30,90	33,51	33,12	29,05	38,74	31,11	31,09	31,16	31,44	31,36
FeO	8,39	7,68	11,52	11,23	8,36	7,18	6,94	4,15	11,66	10,88	9,93	10,63	10,72
Al2O3	3,15	2,81	1,33	1,18	3,07	1,65	1,89	0,76	1,70	1,31	1,41	1,57	1,39
NiO	b.d.l	0,06	0,09	0,01	b.d.l	b.d.l	b.d.l	0,05	0,09	0,13	b.d.l	b.d.l	b.d.l
Total (wt%)	90,79	89,14	89,56	89,71	89,24	90,55	92,22	87,31	89,07	89,89	90,17	89,58	89,88
Atomic proportions (apfu) in the base of 14 O													
Ti	0,000	0,002	0,003	0,003	0,001	0,004	0,004	0,005	0,000	0,002	0,001	0,000	0,000
Ca	0,127	0,067	0,014	0,075	0,083	0,234	0,438	0,009	0,023	0,060	0,105	0,054	0,064
Si	3,950	3,952	4,125	4,175	3,949	4,133	4,359	3,915	4,079	4,210	4,210	4,149	4,166
Cr	0,095	0,068	0,067	0,069	0,097	0,072	0,059	0,148	0,090	0,036	0,069	0,067	0,067
Mn	0,005	0,006	0,024	0,026	0,004	0,010	0,009	0,003	0,018	0,026	0,024	0,022	0,022
Mg	4,643	4,832	4,453	4,349	4,695	4,543	3,896	5,464	4,430	4,347	4,328	4,414	4,393
Al	0,343	0,311	0,149	0,131	0,340	0,179	0,200	0,085	0,192	0,145	0,155	0,174	0,154
Ni	0,000	0,004	0,007	0,001	0,000	0,000	0,000	0,004	0,007	0,010	0,000	0,000	0,000
Fe2+	0,649	0,602	0,913	0,886	0,657	0,552	0,522	0,328	0,931	0,853	0,773	0,837	0,842
Fe3+	0,000	0,000	0,000	0,000	0,000	0,000	0,000	0,000	0,000	0,000	0,000	0,000	0,000
Total (apfu)	9,842	9,864	9,769	9,730	9,836	9,745	9,520	9,965	9,789	9,706	9,684	9,734	9,733

b. Serpentines 2

Sample - IMK - 05139

Lithology	Coarse-grained orthopyroxenite												
File	Z1	Z1	Z2	Z2	Z2	Z2	Z2	Z2	Z3	Z3	Z3	Z3	Z3
Analyses ID	38	39	2	4	20	21	25	28	9	11	12	15	16
TiO2	0,07	0,03	0,03	0,05	0,04	0,06	0,02	0,03	b.d.l	b.d.l	0,07	b.d.l	b.d.l
CaO	0,29	0,55	2,13	1,22	0,63	2,13	0,83	2,64	0,77	0,55	0,25	0,95	0,73
SiO2	43,69	44,99	45,54	45,14	44,23	44,24	43,57	44,90	44,43	46,50	43,73	43,71	44,28
Cr2O3	1,01	0,83	0,95	1,02	0,74	1,03	1,10	0,87	1,06	0,85	1,00	0,99	0,79
MnO	0,34	0,31	0,24	0,32	0,32	0,25	0,09	0,15	0,28	0,22	0,33	0,10	0,06
MgO	31,18	30,52	31,09	31,28	31,64	30,23	34,50	33,01	31,65	32,68	31,27	34,42	35,51
FeO	10,92	10,69	10,01	11,31	10,63	10,40	7,22	8,05	10,40	9,38	11,51	6,78	6,49
Al2O3	1,43	1,34	1,19	1,12	1,76	1,01	1,69	2,06	1,36	1,45	1,18	1,90	1,60
NiO	0,05	0,05	0,04	0,04	0,06	0,07	0,04	b.d.l	0,03	0,02	0,02	b.d.l	b.d.l
Total (wt%)	89,24	89,49	91,42	91,62	90,25	89,58	89,22	92,04	90,21	91,75	89,63	89,04	89,58
Atomic proportions (apfu) in the base of 14 O													
Ti	0,005	0,002	0,002	0,003	0,003	0,004	0,002	0,002	0,000	0,000	0,005	0,000	0,000
Ca	0,029	0,055	0,211	0,120	0,063	0,216	0,083	0,258	0,077	0,053	0,025	0,094	0,072
Si	4,143	4,231	4,202	4,176	4,136	4,184	4,066	4,091	4,156	4,227	4,141	4,075	4,089
Cr	0,076	0,062	0,069	0,074	0,055	0,077	0,081	0,063	0,078	0,061	0,075	0,073	0,058
Mn	0,028	0,025	0,018	0,025	0,026	0,020	0,007	0,012	0,022	0,017	0,027	0,008	0,005
Mg	4,407	4,280	4,276	4,314	4,411	4,262	4,799	4,483	4,414	4,429	4,415	4,784	4,888
Al	0,159	0,149	0,129	0,122	0,194	0,113	0,186	0,221	0,150	0,155	0,131	0,209	0,175
Ni	0,004	0,004	0,003	0,003	0,005	0,005	0,003	0,000	0,002	0,002	0,002	0,000	0,000
Fe2+	0,866	0,841	0,772	0,875	0,831	0,823	0,564	0,613	0,813	0,713	0,911	0,529	0,501
Fe3+	0,000	0,000	0,000	0,000	0,000	0,000	0,000	0,000	0,000	0,000	0,000	0,000	0,000
Total (apfu)	9,744	9,668	9,707	9,728	9,749	9,723	9,806	9,779	9,737	9,670	9,761	9,789	9,801

c. Serpentines 3

Sample - IMK - 05139

Lithology	Coarse-grained orthopyroxenite												
File	Z3	Z3	Z3	Z3	Z4	Z4	Z4	Z4	Z4	Z4	Z4	Z4	Z4
Analyses ID	19	24	25	28	2	4	6	7	12	17	18	23	24
TiO2	b.d.l	0,03	0,03	0,02	0,02	0,03	0,01	0,05	0,05	0,10	0,04	b.d.l	0,03
CaO	0,92	3,71	0,95	2,45	2,12	0,36	1,00	6,01	1,32	3,43	1,96	0,63	5,43
SiO2	44,72	45,18	49,47	44,78	45,23	44,59	44,13	49,25	44,14	46,08	45,21	42,18	48,63
Cr2O3	0,83	0,62	0,92	1,08	0,90	0,89	0,92	0,73	0,96	0,86	0,87	0,94	0,95
MnO	0,24	0,15	0,18	0,08	0,11	0,33	0,32	0,08	0,12	0,28	0,42	0,02	0,04
MgO	31,81	28,33	31,43	28,77	33,69	30,86	30,49	27,92	34,23	28,12	29,79	35,39	29,64
FeO	9,45	7,05	8,08	7,41	6,48	11,28	10,96	5,96	6,87	10,08	11,24	6,82	6,06
Al2O3	1,36	2,49	1,22	2,90	1,74	1,27	1,29	1,73	1,98	1,07	0,81	3,15	1,91
NiO	b.d.l	b.d.l	b.d.l	b.d.l	0,03	b.d.l	0,06	b.d.l	0,02	0,09	b.d.l	0,04	0,01
Total (wt%)	89,42	87,80	92,51	87,64	90,47	89,82	89,37	91,95	89,82	90,23	90,55	89,34	92,89
Atomic proportions (apfu) in the base of 14 O													
Ti	0,000	0,002	0,002	0,001	0,001	0,002	0,001	0,003	0,003	0,007	0,003	0,000	0,002
Ca	0,092	0,376	0,091	0,248	0,208	0,036	0,101	0,578	0,131	0,344	0,197	0,063	0,519
Si	4,190	4,275	4,406	4,239	4,145	4,195	4,180	4,427	4,082	4,311	4,238	3,928	4,335
Cr	0,062	0,046	0,065	0,081	0,065	0,066	0,069	0,052	0,070	0,063	0,065	0,069	0,067
Mn	0,019	0,012	0,013	0,006	0,008	0,026	0,026	0,006	0,009	0,023	0,033	0,002	0,003
Mg	4,444	3,996	4,173	4,060	4,603	4,329	4,305	3,741	4,718	3,922	4,162	4,913	3,939
Al	0,150	0,278	0,128	0,324	0,188	0,141	0,144	0,183	0,216	0,118	0,090	0,346	0,201
Ni	0,000	0,000	0,000	0,000	0,002	0,000	0,004	0,000	0,001	0,007	0,000	0,003	0,001
Fe2+	0,741	0,558	0,602	0,586	0,496	0,888	0,868	0,448	0,531	0,789	0,881	0,531	0,452
Fe3+	0,000	0,000	0,000	0,000	0,000	0,000	0,000	0,000	0,000	0,000	0,000	0,000	0,000
Total (apfu)	9,710	9,578	9,500	9,568	9,731	9,707	9,722	9,465	9,778	9,600	9,687	9,871	9,537

d. Serpentines 4

Sample - IMK - 05139			
Lithology	Coarse-grained orthopyroxenite		
File	Z4	Z4	Z4
Analyses ID	25	26	27
TiO2	0,04	0,04	0,04
CaO	6,07	5,33	5,54
SiO2	47,90	47,47	47,28
Cr2O3	0,85	0,81	1,14
MnO	0,16	0,12	0,18
MgO	28,71	29,02	27,28
FeO	7,64	7,44	7,47
Al2O3	2,16	2,19	1,53
NiO	b.d.l	0,05	0,03
Total (wt%)	93,81	92,69	90,91
	Atomic proportions (apfu) in the base of 14 O		
Ti	0,002	0,002	0,003
Ca	0,581	0,515	0,547
Si	4,279	4,278	4,354
Cr	0,060	0,058	0,083
Mn	0,012	0,009	0,014
Mg	3,823	3,898	3,745
Al	0,228	0,233	0,166
Ni	0,000	0,003	0,003
Fe2+	0,570	0,560	0,576
Fe3+	0,000	0,000	0,000
Total (apfu)	9,588	9,588	9,532

e. Serpentines 5

Sample - IMK - 05149

Lithology	Serpentinised pyroxenite												
File	Z1	Z1	Z1	Z1	Z1	Z1	Z1	Z1	Z1	Z2	Z2	Z2	Z2
Analyses ID	1	2	3	1	2	3	4	5	6	1	2	4	5
TiO2	b.d.l	b.d.l	0,05	b.d.l	0,03	0,01	b.d.l	b.d.l	0,02	b.d.l	0,01	0,02	b.d.l
CaO	0,09	0,17	0,33	0,07	0,12	0,07	0,07	0,05	0,08	0,15	0,06	0,03	0,04
SiO2	43,51	45,41	42,40	44,30	43,78	44,02	43,99	43,97	43,25	44,83	43,41	43,79	43,93
Cr2O3	0,08	0,20	0,20	0,07	0,11	0,08	0,10	0,03	0,05	0,10	0,07	0,07	0,04
MnO	0,40	0,07	0,08	0,43	0,45	0,42	0,40	0,38	0,33	0,33	0,38	0,31	0,38
MgO	33,78	32,17	34,24	33,85	32,45	33,28	33,70	33,47	32,75	32,71	33,68	33,22	32,99
FeO	11,32	6,34	5,39	11,83	11,87	11,60	11,45	11,57	12,44	11,12	11,26	11,40	11,47
Al2O3	0,23	1,40	1,54	0,18	0,18	0,16	0,14	0,18	0,20	0,23	0,26	0,23	0,20
NiO	0,06	0,19	0,29	0,11	0,26	0,07	0,06	0,08	1,27	0,15	0,04	0,06	0,08
Total (wt%)	89,71	86,20	84,85	90,94	89,41	89,88	89,99	89,85	90,59	89,65	89,22	89,25	89,44
Atomic proportions (apfu) in the base of 14 O													
Ti	0,000	0,000	0,003	0,000	0,002	0,000	0,000	0,000	0,002	0,000	0,001	0,001	0,000
Ca	0,009	0,018	0,034	0,007	0,012	0,007	0,007	0,005	0,008	0,015	0,006	0,003	0,004
Si	4,117	4,315	4,114	4,137	4,165	4,154	4,142	4,148	4,100	4,218	4,122	4,155	4,166
Cr	0,006	0,015	0,015	0,005	0,008	0,006	0,007	0,002	0,004	0,007	0,005	0,005	0,003
Mn	0,032	0,006	0,006	0,034	0,036	0,034	0,032	0,031	0,026	0,026	0,031	0,025	0,031
Mg	4,765	4,557	4,952	4,712	4,602	4,682	4,731	4,707	4,628	4,587	4,767	4,699	4,665
Al	0,026	0,156	0,176	0,020	0,021	0,018	0,016	0,020	0,022	0,025	0,029	0,026	0,023
Ni	0,004	0,014	0,022	0,009	0,020	0,005	0,005	0,006	0,096	0,012	0,003	0,005	0,006
Fe2+	0,896	0,503	0,437	0,924	0,944	0,915	0,902	0,913	0,986	0,875	0,894	0,904	0,910
Fe3+	0,000	0,000	0,000	0,000	0,000	0,000	0,000	0,000	0,000	0,000	0,000	0,000	0,000
Total (apfu)	9,891	9,619	9,808	9,866	9,825	9,834	9,847	9,843	9,886	9,776	9,862	9,830	9,849

f. Serpentines 6

Sample - IMK - 05149

Lithology	Serpentinised pyroxenite												
File	Z2	Z2	Z2	Z3	Z3	Z3	Z3	Z3	Z3	Z3	Z3	Z3	Z3
Analyses ID	6	7	8	1	2	3	4	5	1	2	3	4	5
TiO2	0,03	b.d.l	b.d.l	0,01	b.d.l	b.d.l	b.d.l	0,01	b.d.l	0,02	0,01	0,01	b.d.l
CaO	0,04	0,02	0,02	0,31	0,58	0,07	0,05	0,05	0,29	0,07	0,24	0,08	0,07
SiO2	43,89	43,72	43,96	44,34	44,45	43,91	44,07	43,76	49,03	46,82	44,24	46,38	47,72
Cr2O3	0,10	0,07	0,06	0,09	0,07	0,07	0,14	0,06	0,32	0,20	0,06	0,19	0,19
MnO	0,35	0,39	0,36	0,35	0,40	0,36	0,37	0,37	0,06	0,23	0,36	0,07	0,13
MgO	33,69	33,52	33,36	33,02	32,99	33,64	33,80	33,70	34,63	34,20	33,56	34,22	34,02
FeO	11,00	11,32	11,47	11,16	11,52	11,54	11,51	11,20	5,91	7,64	11,28	5,52	6,44
Al2O3	0,18	0,18	0,17	0,26	0,23	0,21	0,22	0,32	1,71	1,83	0,35	1,95	1,87
NiO	0,09	0,06	0,05	0,09	0,04	0,07	b.d.l	0,10	0,19	0,05	0,09	0,10	0,28
Total (wt%)	89,35	89,38	89,54	89,86	90,39	90,07	90,32	89,62	92,41	91,14	90,42	88,94	90,96

Atomic proportions (apfu) in the base of 14 O

Ti	0,002	0,000	0,000	0,001	0,000	0,000	0,000	0,001	0,000	0,001	0,001	0,001	0,000
Ca	0,004	0,002	0,002	0,031	0,058	0,007	0,005	0,005	0,027	0,007	0,024	0,008	0,006
Si	4,149	4,142	4,158	4,177	4,169	4,138	4,136	4,132	4,324	4,232	4,145	4,257	4,292
Cr	0,007	0,005	0,005	0,007	0,005	0,005	0,010	0,004	0,022	0,014	0,004	0,013	0,013
Mn	0,028	0,031	0,029	0,028	0,032	0,029	0,029	0,029	0,004	0,017	0,028	0,006	0,010
Mg	4,748	4,736	4,703	4,637	4,612	4,725	4,727	4,744	4,554	4,608	4,688	4,683	4,562
Al	0,020	0,020	0,018	0,029	0,025	0,024	0,025	0,036	0,178	0,195	0,038	0,211	0,198
Ni	0,007	0,004	0,004	0,007	0,003	0,005	0,000	0,007	0,013	0,004	0,007	0,007	0,020
Fe2+	0,870	0,897	0,907	0,879	0,903	0,909	0,903	0,884	0,436	0,578	0,884	0,424	0,484
Fe3+	0,000	0,000	0,000	0,000	0,000	0,000	0,000	0,000	0,000	0,000	0,000	0,000	0,000
Total (apfu)	9,835	9,846	9,834	9,840	9,825	9,881	9,848	9,847	9,585	9,669	9,843	9,679	9,610

g. Serpentines 7

Sample - IMK - 05149

Lithology	Serpentinised pyroxenite												
File	Z3	Z4	Z4	Z4	Z4	Z4	Z4	Z4	Z4	Z4	Z4	Z4	Z4
Analyses ID	6	1	2	3	4	5	6	7	8	9	10	11	12
TiO2	0,03	0,02	0,01	0,01	b.d.l	0,02	b.d.l	0,01	b.d.l	0,01	b.d.l	b.d.l	b.d.l
CaO	0,05	0,02	0,02	0,03	0,04	0,00	0,01	0,02	0,04	0,03	0,03	0,02	0,07
SiO2	47,90	43,55	43,62	43,73	43,29	43,66	43,32	43,64	43,86	43,81	43,28	43,87	43,39
Cr2O3	0,17	0,07	0,05	0,06	0,07	0,02	0,07	0,07	0,07	0,06	0,07	0,05	0,06
MnO	0,07	0,39	0,35	0,38	0,39	0,35	0,37	0,34	0,31	0,48	0,41	0,37	0,46
MgO	34,80	33,76	33,16	33,02	33,45	33,05	33,26	32,94	33,24	32,67	33,13	33,23	33,15
FeO	5,24	12,37	12,24	11,91	11,84	11,87	12,01	12,14	11,80	12,26	12,11	11,89	12,16
Al2O3	1,24	0,33	0,44	0,26	0,31	0,27	0,33	0,32	0,24	0,26	0,60	0,36	0,29
NiO	0,29	0,02	0,07	0,12	0,09	0,09	0,08	0,06	0,13	0,17	0,07	0,04	0,09
Total (wt%)	89,93	90,63	90,07	89,55	89,76	89,42	89,66	89,73	89,80	89,88	89,90	90,09	89,90
Atomic proportions (apfu) in the base of 14 O													
Ti	0,002	0,002	0,001	0,000	0,000	0,001	0,000	0,001	0,000	0,001	0,000	0,000	0,000
Ca	0,005	0,002	0,002	0,003	0,004	0,000	0,001	0,002	0,004	0,003	0,003	0,002	0,007
Si	4,328	4,095	4,120	4,147	4,105	4,145	4,113	4,137	4,145	4,151	4,100	4,137	4,115
Cr	0,012	0,005	0,004	0,004	0,006	0,001	0,005	0,005	0,005	0,005	0,005	0,004	0,005
Mn	0,005	0,031	0,028	0,030	0,031	0,028	0,030	0,028	0,025	0,038	0,033	0,030	0,037
Mg	4,687	4,732	4,669	4,667	4,730	4,678	4,707	4,655	4,683	4,615	4,678	4,672	4,686
Al	0,132	0,037	0,049	0,029	0,034	0,030	0,036	0,035	0,027	0,029	0,067	0,040	0,032
Ni	0,021	0,002	0,005	0,009	0,007	0,007	0,006	0,004	0,010	0,013	0,005	0,003	0,007
Fe2+	0,396	0,972	0,967	0,945	0,939	0,942	0,954	0,962	0,932	0,971	0,960	0,937	0,964
Fe3+	0,000	0,000	0,000	0,000	0,000	0,000	0,000	0,000	0,000	0,000	0,000	0,000	0,000
Total (apfu)	9,606	9,886	9,853	9,837	9,877	9,842	9,869	9,843	9,839	9,852	9,870	9,842	9,868

h. Serpentines 8

Sample - IMK - 05149

Lithology	Serpentinised pyroxenite												
File	Z4	Z4	Z4	Z4	Z4	Z4	Z4	Z4	Z4	Z4	Z4	Z4	Z4
Analyses ID	13	14	15	16	17	18	19	20	21	22	23	24	25
TiO2	b.d.l	b.d.l	b.d.l	b.d.l	b.d.l	b.d.l	b.d.l	0,02	b.d.l	0,02	b.d.l	b.d.l	b.d.l
CaO	0,03	0,06	0,04	0,05	0,02	0,03	0,03	0,02	0,00	0,04	0,01	0,02	0,04
SiO2	43,73	42,10	43,81	43,79	43,36	43,33	43,26	43,62	43,69	43,53	43,41	43,57	43,49
Cr2O3	0,08	0,18	0,07	0,07	0,07	0,08	0,11	0,15	0,04	0,05	0,11	0,07	0,04
MnO	0,35	0,45	0,39	0,40	0,37	0,33	0,39	0,35	0,30	0,34	0,39	0,37	0,40
MgO	33,64	31,98	33,31	32,75	33,17	33,05	33,07	33,21	33,42	33,13	33,33	33,13	33,42
FeO	11,54	12,82	11,91	12,16	12,01	11,70	12,13	11,39	11,69	11,71	11,85	12,00	11,77
Al2O3	0,59	0,25	0,23	0,24	0,39	0,35	0,23	0,26	0,27	0,32	0,43	0,26	0,49
NiO	0,03	1,91	0,02	0,02	0,02	0,08	0,03	0,08	0,00	0,06	0,09	0,09	0,12
Total (wt%)	90,06	90,16	89,90	89,59	89,52	89,07	89,49	89,14	89,60	89,28	89,74	89,65	89,90
Atomic proportions (apfu) in the base of 14 O													
Ti	0,000	0,000	0,000	0,000	0,000	0,000	0,000	0,001	0,000	0,001	0,000	0,000	0,000
Ca	0,003	0,006	0,004	0,005	0,002	0,003	0,003	0,002	0,000	0,004	0,001	0,002	0,004
Si	4,114	4,052	4,140	4,155	4,118	4,130	4,121	4,145	4,138	4,136	4,112	4,132	4,111
Cr	0,006	0,014	0,006	0,005	0,005	0,006	0,008	0,011	0,003	0,004	0,008	0,005	0,003
Mn	0,027	0,036	0,031	0,032	0,029	0,026	0,031	0,028	0,024	0,027	0,031	0,029	0,032
Mg	4,718	4,589	4,692	4,632	4,697	4,697	4,696	4,704	4,718	4,692	4,707	4,684	4,710
Al	0,066	0,029	0,026	0,027	0,043	0,039	0,026	0,029	0,030	0,036	0,047	0,029	0,054
Ni	0,002	0,148	0,001	0,002	0,002	0,006	0,002	0,006	0,000	0,004	0,007	0,007	0,009
Fe2+	0,908	1,032	0,941	0,965	0,954	0,933	0,966	0,905	0,926	0,930	0,939	0,952	0,930
Fe3+	0,000	0,000	0,000	0,000	0,000	0,000	0,000	0,000	0,000	0,000	0,000	0,000	0,000
Total (apfu)	9,853	9,951	9,856	9,831	9,858	9,849	9,887	9,834	9,869	9,844	9,873	9,853	9,871

i. Serpentines 9

Sample - IMK - 05149

Lithology	Serpentinised pyroxenite												
File	Z4	Z4	Z4	Z4	Z4	Z4	Z4	Z4	Z4	Z4	Z4	Z4	Z4
Analyses ID	2	3	4	5	6	7	8	9	10	11	12	13	14
TiO2	0,02	b.d.l	b.d.l	b.d.l	b.d.l	b.d.l	b.d.l	b.d.l	b.d.l	0,01	b.d.l	b.d.l	b.d.l
CaO	0,04	0,04	0,02	0,01	0,01	0,03	0,05	0,02	0,00	0,04	0,01	0,01	0,03
SiO2	41,24	43,42	43,57	43,64	43,60	43,50	43,55	43,48	43,84	43,58	43,60	43,36	43,58
Cr2O3	0,36	0,07	0,07	0,05	0,06	0,09	0,04	0,03	0,05	0,05	0,04	0,06	0,08
MnO	0,11	0,37	0,42	0,38	0,31	0,39	0,43	0,35	0,35	0,38	0,36	0,35	0,38
MgO	37,21	33,44	32,70	33,36	33,45	32,84	32,86	33,31	33,31	32,85	33,27	33,14	33,64
FeO	7,12	11,98	12,18	12,02	11,78	12,11	12,13	11,95	12,00	11,79	12,48	12,05	11,84
Al2O3	2,16	0,27	0,27	0,23	0,28	0,32	0,31	0,32	0,26	0,27	0,28	0,34	0,29
NiO	0,04	0,04	0,06	0,05	0,09	0,04	0,09	0,19	0,09	b.d.l	0,08	0,09	0,13
Total (wt%)	88,55	89,76	89,33	89,81	89,71	89,38	89,53	89,71	89,99	89,25	90,42	89,53	90,02
	Atomic proportions (apfu) in the base of 14 O												
Ti	0,001	0,000	0,000	0,000	0,000	0,000	0,000	0,000	0,000	0,001	0,000	0,000	0,000
Ca	0,004	0,004	0,002	0,001	0,001	0,003	0,005	0,002	0,000	0,004	0,001	0,001	0,003
Si	3,888	4,115	4,147	4,130	4,126	4,138	4,137	4,121	4,139	4,149	4,117	4,119	4,114
Cr	0,027	0,005	0,005	0,004	0,005	0,007	0,003	0,002	0,004	0,004	0,003	0,005	0,006
Mn	0,009	0,030	0,034	0,030	0,025	0,031	0,035	0,028	0,028	0,031	0,028	0,028	0,030
Mg	5,229	4,724	4,640	4,707	4,720	4,656	4,655	4,705	4,687	4,662	4,683	4,694	4,734
Al	0,240	0,030	0,031	0,025	0,032	0,036	0,035	0,035	0,028	0,030	0,031	0,038	0,032
Ni	0,003	0,003	0,005	0,004	0,007	0,003	0,007	0,014	0,007	0,000	0,006	0,007	0,010
Fe2+	0,561	0,950	0,969	0,951	0,932	0,963	0,964	0,947	0,948	0,939	0,986	0,958	0,935
Fe3+	0,000	0,000	0,000	0,000	0,000	0,000	0,000	0,000	0,000	0,000	0,000	0,000	0,000
Total (apfu)	9,986	9,868	9,836	9,856	9,856	9,843	9,844	9,862	9,846	9,852	9,910	9,863	9,868

j. Serpentines 10

Sample - IMK - 05149

Lithology	Serpentinised pyroxenite												
File	Z4	Z4	Z4	Z4	Z4	Z4	Z4	Z4	Z4	Z4	Z4	Z4	Z4
Analyses ID	15	16	17	18	19	20	21	22	23	24	25	26	27
TiO2	0,01	0,01	0,02	b.d.l	b.d.l	0,02	0,02	b.d.l	b.d.l	0,02	b.d.l	b.d.l	b.d.l
CaO	0,18	0,04	0,06	0,03	0,05	0,02	0,05	0,02	0,04	0,02	0,02	0,01	0,01
SiO2	43,28	42,50	43,51	41,73	42,12	41,14	43,63	43,24	43,39	43,10	43,48	43,33	43,77
Cr2O3	0,03	0,11	0,09	0,12	0,05	0,17	0,05	0,05	0,09	0,07	0,07	0,06	0,07
MnO	0,38	0,18	0,47	0,03	0,11	0,08	0,36	0,37	0,42	0,46	0,41	0,39	0,35
MgO	32,00	38,17	32,56	37,33	37,80	37,36	33,43	33,40	33,11	32,96	33,47	33,16	33,16
FeO	12,57	7,14	12,24	6,37	7,61	6,81	11,79	12,11	12,03	12,04	11,95	12,03	11,94
Al2O3	0,32	0,76	0,30	1,88	0,48	2,71	0,42	0,32	0,34	0,42	0,30	0,32	0,33
NiO	0,20	0,13	0,08	0,03	0,04	0,10	b.d.l	0,05	0,05	0,07	0,09	0,08	0,07
Total (wt%)	89,10	89,14	89,50	87,82	88,38	88,76	89,79	89,80	89,70	89,26	89,91	89,58	89,89
Atomic proportions (apfu) in the base of 14 O													
Ti	0,001	0,000	0,001	0,000	0,000	0,001	0,001	0,000	0,000	0,001	0,000	0,000	0,000
Ca	0,018	0,004	0,006	0,003	0,005	0,002	0,005	0,002	0,004	0,002	0,002	0,001	0,001
Si	4,146	3,974	4,141	3,942	3,981	3,863	4,122	4,104	4,119	4,111	4,113	4,118	4,137
Cr	0,002	0,008	0,007	0,009	0,004	0,013	0,003	0,004	0,006	0,005	0,005	0,004	0,005
Mn	0,031	0,015	0,038	0,003	0,009	0,006	0,029	0,030	0,034	0,037	0,033	0,031	0,028
Mg	4,569	5,321	4,620	5,257	5,327	5,231	4,708	4,726	4,685	4,686	4,720	4,698	4,673
Al	0,036	0,084	0,033	0,209	0,054	0,300	0,047	0,036	0,038	0,047	0,033	0,036	0,037
Ni	0,015	0,010	0,006	0,002	0,003	0,007	0,000	0,004	0,004	0,005	0,007	0,006	0,006
Fe2+	1,007	0,558	0,974	0,503	0,601	0,534	0,932	0,961	0,955	0,960	0,945	0,956	0,944
Fe3+	0,000	0,000	0,000	0,000	0,000	0,000	0,000	0,000	0,000	0,000	0,000	0,000	0,000
Total (apfu)	9,837	9,982	9,843	9,961	9,992	10,000	9,853	9,902	9,869	9,862	9,869	9,876	9,843

k. Serpentines 11

Sample - IMK - 05149

Lithology	Serpentinised pyroxenite												
File	Z4	Z4	Z4	Z4	Z4	Z4	Z4	Z4	Z4	Z4	Z4	Z4	Z4
Analyses ID	28	29	30	31	32	33	34	35	36	37	38	39	40
TiO2	b.d.l	0,01	b.d.l	b.d.l	b.d.l	0,01	b.d.l	0,01	b.d.l	b.d.l	0,01	0,01	b.d.l
CaO	0,01	0,04	0,04	0,03	0,01	0,04	0,03	0,04	0,00	0,01	0,03	0,01	0,01
SiO2	43,81	43,40	43,52	43,28	43,37	43,59	43,61	43,52	43,55	43,31	43,35	43,42	43,40
Cr2O3	0,03	0,07	0,07	0,04	0,05	0,06	0,03	0,07	0,05	0,07	0,06	0,08	0,06
MnO	0,35	0,31	0,38	0,34	0,37	0,38	0,39	0,41	0,35	0,33	0,40	0,35	0,33
MgO	32,92	33,72	33,49	33,31	33,38	33,22	33,24	33,11	34,01	33,22	33,07	33,11	33,02
FeO	11,77	11,35	11,94	12,13	11,99	11,49	11,88	12,01	11,21	12,20	11,93	11,78	12,12
Al2O3	0,30	0,32	0,34	0,37	0,34	0,47	0,45	0,38	0,30	0,31	0,33	0,31	0,30
NiO	0,09	0,04	0,08	0,02	0,00	0,06	0,07	0,07	0,07	0,10	0,19	0,06	0,04
Total (wt%)	89,48	89,41	89,94	89,71	89,64	89,44	89,77	89,76	89,67	89,66	89,43	89,27	89,46

Atomic proportions (apfu) in the base of 14 O

Ti	0,000	0,000	0,000	0,000	0,000	0,000	0,000	0,001	0,000	0,000	0,001	0,001	0,000
Ca	0,001	0,004	0,004	0,003	0,001	0,004	0,003	0,004	0,000	0,001	0,003	0,001	0,001
Si	4,156	4,115	4,114	4,108	4,114	4,131	4,125	4,124	4,114	4,113	4,123	4,132	4,127
Cr	0,002	0,005	0,005	0,003	0,004	0,005	0,003	0,005	0,004	0,005	0,005	0,006	0,005
Mn	0,028	0,024	0,030	0,027	0,030	0,030	0,031	0,033	0,028	0,026	0,032	0,029	0,027
Mg	4,656	4,766	4,719	4,713	4,720	4,693	4,687	4,678	4,790	4,704	4,688	4,697	4,681
Al	0,034	0,035	0,038	0,041	0,038	0,053	0,051	0,042	0,033	0,035	0,037	0,034	0,033
Ni	0,007	0,003	0,006	0,001	0,000	0,004	0,005	0,005	0,005	0,007	0,014	0,005	0,003
Fe2+	0,933	0,900	0,944	0,963	0,951	0,911	0,940	0,952	0,886	0,969	0,949	0,938	0,964
Fe3+	0,000	0,000	0,000	0,000	0,000	0,000	0,000	0,000	0,000	0,000	0,000	0,000	0,000
Total (apfu)	9,834	9,866	9,867	9,884	9,874	9,841	9,849	9,856	9,869	9,870	9,857	9,870	9,856

I. Serpentines 12

Sample - IMK - 05149

Lithology	Serpentinised pyroxenite												
File	Z5	Z5	Z5	Z5	Z5	Z5	Z5	Z5	Z5	Z5	Z5	Z5	Z5
Analyses ID	2	3	4	5	6	7	8	9	10	11	12	13	14
TiO2	0,05	b.d.l	0,05	b.d.l	b.d.l	0,02	b.d.l	b.d.l	0,01	0,02	b.d.l	0,01	b.d.l
CaO	0,03	0,03	0,01	0,04	0,03	0,02	0,01	0,04	0,03	0,04	0,08	0,04	0,01
SiO2	40,71	41,70	39,30	47,15	39,97	43,48	43,46	43,86	43,85	43,80	43,53	43,66	43,68
Cr2O3	0,30	0,35	0,74	0,19	0,90	0,07	0,05	0,09	0,03	0,07	0,04	0,06	0,08
MnO	0,10	0,00	0,02	0,16	0,03	0,33	0,37	0,36	0,37	0,33	0,18	0,37	0,34
MgO	37,71	39,50	37,57	35,09	36,24	33,25	33,49	33,60	33,75	33,63	38,52	33,29	33,41
FeO	7,21	5,81	5,49	6,64	6,72	11,36	12,09	11,39	10,98	11,71	6,35	11,42	11,78
Al2O3	2,95	1,93	5,08	1,32	3,90	0,43	0,55	0,24	0,23	0,22	0,40	0,29	0,23
NiO	0,02	0,08	0,18	0,14	0,21	0,12	0,08	0,09	0,06	0,05	0,10	0,02	0,10
Total (wt%)	89,46	89,46	88,54	91,01	88,06	89,17	90,19	89,78	89,60	89,88	89,27	89,19	89,73
Atomic proportions (apfu) in the base of 14 O													
Ti	0,004	0,000	0,003	0,000	0,000	0,002	0,000	0,000	0,001	0,001	0,000	0,000	0,000
Ca	0,003	0,003	0,001	0,003	0,003	0,002	0,001	0,004	0,003	0,004	0,008	0,004	0,001
Si	3,808	3,864	3,683	4,252	3,785	4,130	4,100	4,139	4,143	4,132	4,038	4,145	4,132
Cr	0,022	0,026	0,055	0,014	0,068	0,005	0,004	0,007	0,002	0,005	0,003	0,004	0,006
Mn	0,008	0,000	0,001	0,012	0,002	0,027	0,030	0,029	0,029	0,026	0,014	0,030	0,027
Mg	5,258	5,456	5,249	4,718	5,117	4,709	4,709	4,727	4,753	4,729	5,327	4,711	4,712
Al	0,325	0,211	0,561	0,141	0,435	0,048	0,061	0,026	0,025	0,025	0,044	0,032	0,026
Ni	0,002	0,006	0,014	0,010	0,016	0,009	0,006	0,007	0,005	0,004	0,008	0,001	0,007
Fe2+	0,564	0,450	0,430	0,501	0,532	0,903	0,954	0,899	0,868	0,924	0,493	0,906	0,932
Fe3+	0,000	0,000	0,000	0,000	0,000	0,000	0,000	0,000	0,000	0,000	0,000	0,000	0,000
Total (apfu)	10,033	10,025	10,008	9,677	9,964	9,843	9,878	9,845	9,871	9,851	9,946	9,837	9,855

m. Serpentines 13

Sample - IMK - 05149

Lithology	Serpentinised pyroxenite												
File	Z5	Z5	Z5	Z5	Z5	Z5	Z5	Z5	Z5	Z5	Z5	Z5	Z5
Analyses ID	16	17	18	19	20	21	22	23	24	25	26	27	28
TiO2	0,01	b.d.l	b.d.l	0,01	b.d.l	b.d.l	b.d.l	0,03	b.d.l	b.d.l	b.d.l	0,01	b.d.l
CaO	0,03	0,02	0,06	0,12	0,02	0,04	0,01	0,03	0,04	0,05	0,05	0,09	0,01
SiO2	43,30	43,29	43,59	43,58	43,57	43,13	43,72	43,55	43,46	43,05	42,30	43,50	43,65
Cr2O3	0,08	0,18	0,05	0,10	0,06	0,07	0,04	0,07	0,08	0,19	0,23	0,05	0,05
MnO	0,34	0,36	0,39	0,37	0,31	0,34	0,37	0,39	0,39	0,12	0,13	0,39	0,34
MgO	33,42	33,31	33,34	30,27	33,53	33,62	33,63	33,23	33,47	38,55	37,44	33,26	33,50
FeO	11,50	11,56	11,49	13,66	11,70	11,60	11,53	11,74	11,48	6,20	7,08	11,96	11,61
Al2O3	0,30	0,36	0,35	0,36	0,32	0,65	0,36	0,37	0,38	0,69	1,40	0,62	0,39
NiO	0,05	0,02	0,08	1,00	0,03	0,08	0,11	0,09	0,05	0,18	0,04	0,06	0,14
Total (wt%)	89,12	89,20	89,39	89,62	89,67	89,70	89,84	89,70	89,50	89,15	88,85	90,22	89,91
Atomic proportions (apfu) in the base of 14 O													
Ti	0,000	0,000	0,000	0,000	0,000	0,000	0,000	0,002	0,000	0,000	0,000	0,001	0,000
Ca	0,003	0,002	0,006	0,012	0,002	0,004	0,001	0,003	0,004	0,005	0,005	0,009	0,001
Si	4,122	4,119	4,133	4,183	4,123	4,085	4,125	4,126	4,119	4,003	3,965	4,103	4,122
Cr	0,006	0,013	0,004	0,008	0,004	0,005	0,003	0,005	0,006	0,014	0,017	0,004	0,004
Mn	0,027	0,029	0,031	0,030	0,025	0,028	0,030	0,031	0,031	0,009	0,010	0,031	0,027
Mg	4,743	4,725	4,713	4,333	4,731	4,747	4,731	4,693	4,729	5,343	5,232	4,678	4,715
Al	0,034	0,040	0,039	0,040	0,035	0,073	0,040	0,041	0,042	0,076	0,154	0,069	0,044
Ni	0,004	0,001	0,006	0,077	0,003	0,006	0,008	0,007	0,004	0,013	0,003	0,005	0,011
Fe2+	0,916	0,920	0,911	1,097	0,926	0,919	0,910	0,930	0,910	0,482	0,555	0,943	0,916
Fe3+	0,000	0,000	0,000	0,000	0,000	0,000	0,000	0,000	0,000	0,000	0,000	0,000	0,000
Total (apfu)	9,861	9,869	9,848	9,794	9,859	9,877	9,854	9,864	9,859	9,954	9,963	9,862	9,855

n. Serpentines 14

Sample - IMK - 05149						
Lithology	Serpentinised pyroxenite					
File	Z5	Z5	Z5	Z4	Z5	Z5
Analyses ID	29	30	32	8	11	12
TiO2	b.d.l	b.d.l	b.d.l	b.d.l	0,03	b.d.l
CaO	0,04	0,04	0,04	0,05	0,07	3,65
SiO2	41,56	43,08	41,92	41,83	41,89	46,29
Cr2O3	0,28	0,06	0,14	0,09	0,11	0,10
MnO	0,10	0,24	0,04	0,38	0,38	0,42
MgO	37,10	36,43	38,41	32,39	32,20	26,89
FeO	7,13	8,62	5,69	11,33	11,31	8,36
Al2O3	1,71	0,39	1,53	0,28	0,36	0,82
NiO	0,11	0,09	b.d.l	0,07	0,05	0,07
Total (wt%)	88,24	89,10	87,91	86,50	86,57	86,80
Atomic proportions (apfu) in the base of 14 O						
Ti	0,000	0,000	0,000	0,000	0,002	0,000
Ca	0,004	0,004	0,004	0,005	0,007	0,376
Si	3,928	4,052	3,941	4,110	4,112	4,448
Cr	0,021	0,005	0,011	0,007	0,008	0,007
Mn	0,008	0,019	0,003	0,031	0,031	0,034
Mg	5,227	5,107	5,384	4,743	4,713	3,851
Al	0,190	0,043	0,169	0,032	0,042	0,093
Ni	0,008	0,007	0,000	0,006	0,004	0,005
Fe2+	0,563	0,678	0,448	0,931	0,929	0,672
Fe3+	0,000	0,000	0,000	0,000	0,000	0,000
Total (apfu)	9,971	9,926	9,970	9,872	9,862	9,510

o. Serpentines 15

Sample - IMK - 05153

Lithology	Serpentinised pyroxenite												
File	Z1	Z1	Z1	Z1	Z1	Z1	Z1	Z1	Z1	Z1	Z1	Z1	Z1
Analyses ID	1	2	4	5	6	8	9	15	17	18	19	20	30
TiO2	0,03	0,02	0,02	b.d.l	0,02	0,02	0,03	0,01	b.d.l	0,03	0,03	0,02	b.d.l
CaO	0,34	0,44	0,06	0,34	2,42	1,73	3,78	0,17	0,45	0,02	0,37	0,37	0,06
SiO2	42,89	42,70	43,41	43,32	43,54	44,77	46,45	42,88	42,04	42,87	42,88	43,03	43,87
Cr2O3	0,72	0,69	0,05	0,11	0,76	0,80	0,74	0,62	0,71	0,17	0,78	0,43	0,10
MnO	0,52	0,44	0,74	0,54	0,38	0,73	0,85	0,65	0,55	0,55	0,87	0,76	0,45
MgO	32,86	33,66	33,02	33,16	31,43	30,93	29,14	31,54	34,40	33,11	31,69	32,21	35,18
FeO	11,40	8,53	11,45	10,86	8,14	9,62	10,34	11,63	8,07	11,34	10,74	10,95	8,86
Al2O3	1,35	2,48	0,54	0,67	3,17	1,62	1,21	1,17	1,93	0,94	1,58	1,38	0,51
NiO	0,23	0,38	0,25	0,10	0,17	0,22	0,36	0,15	0,21	0,09	0,17	0,15	0,39
Total (wt%)	90,43	89,50	89,70	89,41	90,19	90,71	93,15	89,00	88,60	89,29	89,26	89,46	89,56
Atomic proportions (apfu) in the base of 14 O													
Ti	0,002	0,001	0,001	0,000	0,002	0,001	0,002	0,001	0,000	0,002	0,002	0,001	0,000
Ca	0,034	0,045	0,007	0,034	0,241	0,173	0,370	0,017	0,046	0,002	0,038	0,037	0,006
Si	4,040	4,006	4,116	4,111	4,052	4,168	4,242	4,104	3,987	4,079	4,080	4,085	4,110
Cr	0,054	0,051	0,004	0,009	0,056	0,059	0,053	0,047	0,053	0,013	0,059	0,032	0,007
Mn	0,042	0,035	0,060	0,043	0,030	0,058	0,066	0,053	0,044	0,045	0,070	0,061	0,036
Mg	4,614	4,709	4,667	4,691	4,360	4,292	3,967	4,500	4,863	4,696	4,495	4,557	4,914
Al	0,149	0,275	0,060	0,075	0,348	0,178	0,130	0,131	0,215	0,105	0,177	0,154	0,057
Ni	0,018	0,029	0,019	0,008	0,013	0,017	0,026	0,012	0,016	0,007	0,013	0,012	0,029
Fe2+	0,898	0,669	0,908	0,862	0,634	0,749	0,790	0,931	0,640	0,902	0,855	0,869	0,695
Fe3+	0,000	0,000	0,000	0,000	0,000	0,000	0,000	0,000	0,000	0,000	0,000	0,000	0,000
Total (apfu)	9,866	9,834	9,856	9,876	9,751	9,718	9,672	9,810	9,882	9,865	9,806	9,826	9,871

p. Serpentines 16

Sample - IMK - 05153

Lithology	Serpentinised pyroxenite						
File	Z1	Z1	Z2	Z2	Z2	Z2	Z2
Analyses ID	31	32	1	9	11	16	22
TiO2	b.d.l	0,03	0,04	0,04	0,02	0,01	b.d.l
CaO	0,36	0,22	0,34	2,29	0,07	0,27	0,13
SiO2	43,13	42,08	42,85	44,84	43,72	49,19	42,28
Cr2O3	0,69	0,60	0,54	0,25	0,15	0,19	0,70
MnO	0,92	0,31	0,58	0,22	0,36	0,09	0,80
MgO	30,01	35,33	34,29	32,75	35,84	33,32	34,03
FeO	12,42	7,27	8,27	6,45	8,43	4,07	8,37
Al2O3	1,28	1,69	1,65	2,81	0,64	1,75	1,91
NiO	0,21	0,21	0,18	0,33	0,58	0,33	0,08
Total (wt%)	89,24	87,99	88,86	90,21	89,95	89,48	88,52

Atomic proportions (apfu) in the base of 14 O

Ti	0,000	0,002	0,003	0,002	0,001	0,001	0,000
Ca	0,037	0,023	0,034	0,226	0,007	0,026	0,013
Si	4,137	3,994	4,041	4,123	4,076	4,426	4,012
Cr	0,052	0,045	0,040	0,018	0,011	0,013	0,053
Mn	0,074	0,025	0,047	0,017	0,029	0,007	0,065
Mg	4,291	5,000	4,821	4,489	4,982	4,469	4,814
Al	0,144	0,189	0,183	0,305	0,070	0,185	0,213
Ni	0,016	0,016	0,013	0,024	0,043	0,024	0,006
Fe2+	0,997	0,577	0,652	0,496	0,657	0,306	0,664
Fe3+	0,000	0,000	0,000	0,000	0,000	0,000	0,000
Total (apfu)	9,775	9,899	9,849	9,723	9,902	9,488	9,860

q. Serpentines 17

Sample - IMK - 05156

Lithology	Serpentinised harzburgite												
File	Z1	Z1	Z1	Z1	Z1	Z1	Z1	Z1	Z1	Z1	Z1	Z1	Z1
Analyses ID	1	3	5	6	8	9	10	11	12	13	14	15	16
TiO2	b.d.l	b.d.l	0,03	b.d.l	0,01	0,04	b.d.l	b.d.l	b.d.l	0,04	0,00	0,05	0,02
CaO	0,02	b.d.l	0,01	b.d.l	b.d.l	0,01	0,02	b.d.l	0,04	0,02	0,01	b.d.l	0,02
SiO2	41,30	41,97	40,41	44,38	41,45	41,55	41,82	41,45	44,09	41,33	41,32	40,39	41,61
Cr2O3	1,10	1,18	0,91	0,30	0,82	0,70	0,73	1,08	0,45	0,64	1,16	0,30	0,97
MnO	b.d.l	b.d.l	b.d.l	0,01	0,01	0,04	0,04	0,03	0,01	0,05	0,00	0,07	0,06
MgO	41,14	41,10	41,34	39,37	40,65	42,26	42,25	40,08	41,23	42,38	41,61	41,29	37,99
FeO	3,19	2,43	1,59	4,28	3,87	1,62	1,63	3,59	2,67	1,74	2,34	1,95	5,34
Al2O3	1,89	1,36	0,97	0,39	1,60	1,20	1,21	1,63	0,71	1,51	1,33	0,87	1,79
NiO	0,63	0,55	2,17	0,13	0,03	0,04	0,00	0,03	0,02	0,06	0,04	b.d.l	0,01
Total (wt%)	89,28	88,60	87,53	88,94	88,49	87,46	87,83	87,96	89,28	87,90	87,94	85,11	87,85

Atomic proportions (apfu) in the base of 14 O

Ti	0,000	0,000	0,002	0,000	0,000	0,003	0,000	0,000	0,000	0,003	0,000	0,004	0,001
Ca	0,002	0,000	0,001	0,000	0,000	0,001	0,001	0,000	0,004	0,002	0,001	0,000	0,002
Si	3,810	3,878	3,811	4,081	3,853	3,864	3,874	3,871	4,014	3,833	3,844	3,872	3,916
Cr	0,080	0,086	0,068	0,022	0,060	0,052	0,053	0,080	0,032	0,047	0,085	0,023	0,072
Mn	0,000	0,000	0,000	0,001	0,001	0,003	0,003	0,002	0,000	0,004	0,000	0,006	0,005
Mg	5,657	5,662	5,813	5,398	5,633	5,858	5,835	5,579	5,596	5,859	5,771	5,900	5,330
Al	0,205	0,148	0,108	0,042	0,176	0,132	0,132	0,179	0,077	0,165	0,146	0,098	0,199
Ni	0,047	0,041	0,165	0,010	0,003	0,003	0,000	0,002	0,002	0,004	0,003	0,000	0,000
Fe2+	0,246	0,188	0,125	0,329	0,301	0,126	0,126	0,281	0,203	0,135	0,182	0,156	0,420
Fe3+	0,000	0,000	0,000	0,000	0,000	0,000	0,000	0,000	0,000	0,000	0,000	0,000	0,000
Total (apfu)	10,047	10,006	10,101	9,888	10,028	10,041	10,035	9,999	9,932	10,066	10,040	10,088	9,950

r. Serpentines 18

Sample - IMK - 05156

Lithology	Serpentinised harzburgite												
File	Z1	Z1	Z1	Z1	Z1	Z1	Z1	Z1	Z1	Z1	Z1	Z1	Z1
Analyses ID	19	21	23	24	25	26	29	32	33	34	35	37	38
TiO2	0,02	b.d.l	0,01	b.d.l	0,02	0,06	b.d.l	0,04	b.d.l	0,02	0,07	0,03	0,01
CaO	0,01	0,02	0,01	b.d.l	0,01	0,01	b.d.l	b.d.l	b.d.l	b.d.l	b.d.l	b.d.l	b.d.l
SiO2	41,21	38,11	41,70	42,65	41,22	42,25	43,53	41,10	41,00	42,05	41,67	41,39	39,91
Cr2O3	0,82	3,27	0,47	0,25	0,74	0,35	0,42	0,74	1,31	0,43	1,10	0,75	1,65
MnO	b.d.l	0,08	0,06	0,03	0,00	0,08	0,07	0,04	0,00	0,03	0,03	0,04	0,07
MgO	40,72	35,05	42,09	42,99	41,31	42,34	38,64	41,85	40,90	42,30	40,13	41,96	36,36
FeO	2,80	8,20	1,72	1,78	1,36	1,99	4,16	1,88	2,60	1,68	2,45	1,66	6,96
Al2O3	1,46	3,80	0,89	0,37	0,88	0,90	1,04	1,32	1,35	0,83	2,51	0,90	2,94
NiO	0,01	0,04	0,06	0,01	0,04	0,09	0,05	0,09	0,12	b.d.l	0,05	0,02	0,15
Total (wt%)	87,21	88,61	87,10	88,15	85,67	88,14	88,03	87,19	87,44	87,36	88,05	86,97	88,17
Atomic proportions (apfu) in the base of 14 O													
Ti	0,002	0,000	0,000	0,000	0,001	0,004	0,000	0,003	0,000	0,001	0,005	0,002	0,000
Ca	0,001	0,002	0,001	0,000	0,001	0,001	0,000	0,000	0,000	0,000	0,000	0,000	0,000
Si	3,867	3,653	3,895	3,931	3,908	3,902	4,045	3,846	3,844	3,909	3,860	3,878	3,794
Cr	0,061	0,247	0,034	0,018	0,055	0,026	0,031	0,054	0,097	0,032	0,081	0,055	0,124
Mn	0,000	0,006	0,005	0,002	0,000	0,006	0,005	0,003	0,000	0,002	0,002	0,003	0,006
Mg	5,697	5,009	5,860	5,907	5,838	5,830	5,353	5,838	5,717	5,862	5,542	5,862	5,153
Al	0,162	0,429	0,098	0,040	0,099	0,098	0,114	0,145	0,149	0,091	0,274	0,099	0,329
Ni	0,001	0,003	0,004	0,001	0,003	0,007	0,004	0,006	0,009	0,000	0,004	0,001	0,012
Fe2+	0,220	0,657	0,135	0,137	0,108	0,153	0,323	0,147	0,204	0,130	0,190	0,130	0,553
Fe3+	0,000	0,000	0,000	0,000	0,000	0,000	0,000	0,000	0,000	0,000	0,000	0,000	0,000
Total (apfu)	10,020	10,010	10,040	10,041	10,039	10,032	9,883	10,053	10,032	10,029	9,958	10,061	9,980

s. Serpentines 19

Sample - IMK - 05156

Lithology	Serpentinised harzburgite										
File	40	41	43	44	45	50	52	54	56	58	60
Analyses ID	40	41	43	44	45	50	52	54	56	58	60
TiO2	0,01	0,02	b.d.l	b.d.l	b.d.l	0,02	0,02	0,02	b.d.l	0,02	b.d.l
CaO	b.d.l	b.d.l	0,01	b.d.l	0,00	0,00	0,00	0,03	b.d.l	0,01	0,03
SiO2	43,52	40,51	44,81	43,52	43,97	41,43	44,63	41,76	44,24	41,62	43,04
Cr2O3	0,38	0,69	0,12	0,60	0,45	0,76	0,18	0,72	0,32	0,58	0,45
MnO	0,06	b.d.l	0,06	0,05	0,03	0,09	0,07	0,05	0,02	0,04	0,07
MgO	38,73	39,28	38,92	40,88	40,14	42,51	38,75	42,11	38,59	41,57	41,75
FeO	3,92	2,91	4,92	2,62	3,26	1,38	4,90	1,34	4,61	1,66	2,27
Al2O3	0,80	4,92	0,65	0,61	0,69	0,67	0,74	0,72	0,89	1,00	0,62
NiO	0,05	0,49	0,10	0,01	0,10	b.d.l	0,10	0,04	0,02	b.d.l	0,02
Total (wt%)	87,69	88,87	89,70	88,40	88,65	86,96	89,59	86,87	88,79	86,61	88,36
Atomic proportions (apfu) in the base of 14 O											
Ti	0,001	0,001	0,000	0,000	0,000	0,001	0,001	0,001	0,000	0,001	0,000
Ca	0,000	0,000	0,001	0,000	0,000	0,000	0,000	0,003	0,000	0,001	0,003
Si	4,058	3,731	4,094	4,006	4,040	3,876	4,087	3,904	4,077	3,905	3,963
Cr	0,028	0,051	0,009	0,043	0,033	0,056	0,013	0,054	0,023	0,043	0,032
Mn	0,005	0,000	0,004	0,004	0,002	0,007	0,005	0,004	0,002	0,003	0,006
Mg	5,382	5,394	5,301	5,611	5,499	5,929	5,290	5,870	5,301	5,815	5,731
Al	0,087	0,534	0,070	0,066	0,075	0,074	0,080	0,079	0,096	0,111	0,068
Ni	0,004	0,036	0,007	0,001	0,007	0,000	0,007	0,003	0,001	0,000	0,001
Fe2+	0,305	0,224	0,376	0,202	0,250	0,108	0,375	0,105	0,356	0,130	0,175
Fe3+	0,000	0,000	0,000	0,000	0,000	0,000	0,000	0,000	0,000	0,000	0,000
Total (apfu)	9,894	9,976	9,876	9,940	9,906	10,060	9,889	10,029	9,864	10,017	9,989

a. Chlorite 1

Sample - IMK - 05149				
Lithology	Serpentinised pyroxenite			
File	Z5	Z5	Z5	Z4
Analyses ID	1	15	31	1
TiO2	0,03	0,03	0,05	0,02
CaO	0,03	0,02	0,03	0,05
SiO2	33,14	32,47	35,45	40,45
Cr2O3	0,30	1,97	0,39	0,14
K2O	b.d.l	0,01	0,03	1,66
MnO	b.d.l	b.d.l	0,03	0,07
MgO	33,31	32,83	33,71	34,24
FeO	5,27	4,34	6,87	6,70
Al2O3	14,95	15,12	10,50	5,32
NiO	0,30	0,39	0,22	0,17
Total (wt%)	87,41	87,33	87,46	89,02
	Atomic proportions (apfu) in the base of 14 O			
Ti	0,002	0,002	0,004	0,001
Ca	0,003	0,002	0,003	0,005
Si	3,145	3,091	3,391	3,811
Cr	0,022	0,148	0,029	0,011
K	0,000	0,001	0,004	0,199
Mn	0,000	0,000	0,002	0,006
Mg	4,714	4,659	4,806	4,808
Al	1,673	1,696	1,183	0,591
Ni	0,023	0,030	0,017	0,013
Fe2+	0,418	0,345	0,549	0,528
Fe3+	0,000	0,000	0,000	0,000
Total (apfu)	6,006	5,986	6,004	5,989

b. Chlorite 2

Sample - IMK - 05153

Lithology	Serpentinised pyroxenite											
File	Z1	Z1	Z1	Z1	Z1	Z1	Z1	Z1	Z1	Z1	Z2	Z2
Analyses ID	3	7	10	11	13	26	28	33	37	39	3	24
TiO2	0,01	b.d.l	b.d.l	0,01	0,01	0,03	0,12	0,08	0,24	0,15	0,07	b.d.l
CaO	0,14	0,06	0,01	0,03	0,08	0,04	0,93	0,09	0,01	0,01	0,27	0,45
SiO2	39,77	37,99	32,81	33,36	32,99	41,30	43,70	39,95	43,13	41,20	38,02	34,30
Cr2O3	0,55	0,06	0,75	0,92	0,94	0,41	0,69	0,33	0,87	0,23	1,47	0,78
K2O	0,93	0,04	b.d.l	0,01	0,01	3,53	3,69	1,90	7,23	7,02	0,00	0,01
MnO	0,10	0,24	b.d.l	b.d.l	b.d.l	0,06	0,02	0,09	0,00	0,06	0,00	0,00
MgO	31,76	33,71	33,26	33,68	32,82	28,91	26,56	31,11	25,50	26,42	34,10	33,08
FeO	7,97	8,09	4,25	4,89	4,39	8,16	6,70	7,30	6,04	6,03	4,61	4,92
Al2O3	8,06	7,56	15,43	14,35	15,39	8,75	9,38	8,07	10,05	11,45	6,81	14,69
NiO	0,36	0,11	0,59	0,63	0,72	0,20	0,39	0,24	0,47	0,45	0,17	0,55
Total (wt%)	89,83	88,03	87,10	87,88	87,55	91,50	92,35	89,35	93,64	93,17	85,66	88,97
Atomic proportions (apfu) in the base of 14 O												
Ti	0,000	0,000	0,000	0,001	0,001	0,002	0,008	0,006	0,017	0,010	0,005	0,000
Ca	0,014	0,006	0,001	0,003	0,008	0,004	0,090	0,009	0,001	0,001	0,027	0,045
Si	3,719	3,621	3,116	3,155	3,127	3,826	3,973	3,758	3,932	3,781	3,667	3,202
Cr	0,041	0,004	0,056	0,069	0,070	0,030	0,050	0,025	0,063	0,017	0,112	0,057
K	0,111	0,005	0,000	0,001	0,001	0,418	0,428	0,228	0,840	0,822	0,000	0,001
Mn	0,008	0,020	0,000	0,000	0,000	0,005	0,002	0,007	0,000	0,005	0,000	0,000
Mg	4,427	4,790	4,709	4,749	4,636	3,993	3,600	4,362	3,466	3,615	4,904	4,603
Al	0,888	0,849	1,727	1,599	1,718	0,956	1,005	0,895	1,080	1,239	0,774	1,616
Ni	0,027	0,008	0,045	0,048	0,055	0,015	0,028	0,018	0,035	0,033	0,013	0,041
Fe2+	0,623	0,645	0,338	0,387	0,348	0,633	0,509	0,574	0,460	0,463	0,372	0,384
Fe3+	0,000	0,000	0,000	0,000	0,000	0,000	0,000	0,000	0,000	0,000	0,000	0,000
Total (apfu)	9,873	9,984	9,992	10,011	9,979	9,889	9,716	9,904	9,903	9,998	9,886	9,964

c. Chlorite 3

Sample - IMK - 05156

Lithology	Serpentinised harzburgite												
File	Z1	Z1	Z1	Z1	Z1	Z1	Z1	Z1	Z1	Z1	Z1	Z1	Z1
Analyses ID	2	4	7	17	18	20	22	27	28	30	31	36	39
TiO2	0,01	0,01	0,04	0,03	0,02	0,02	0,03	0,16	0,03	b.d.l	b.d.l	0,04	0,05
CaO	b.d.l	b.d.l	b.d.l	b.d.l	0,01	0,01	0,02	0,01	0,01	0,01	0,02	0,02	0,02
SiO2	34,79	36,60	34,97	34,98	34,89	34,04	34,85	34,50	35,51	34,31	34,98	38,09	34,96
Cr2O3	0,90	1,18	0,97	0,99	1,08	1,06	0,88	1,07	1,28	0,84	0,96	1,04	0,93
K2O	0,41	0,34	0,18	0,30	0,34	0,17	0,19	0,20	0,11	0,46	0,32	0,25	0,36
MnO	b.d.l	b.d.l	0,01	b.d.l	b.d.l	b.d.l	b.d.l	b.d.l	b.d.l	b.d.l	b.d.l	b.d.l	b.d.l
MgO	34,76	35,91	36,33	35,30	34,88	34,28	35,02	36,89	35,14	34,89	34,92	37,06	35,91
FeO	5,12	4,10	5,33	5,06	4,76	4,54	4,55	4,43	4,29	4,45	4,54	3,76	5,12
Al2O3	11,44	10,46	9,49	10,90	10,96	11,07	11,73	9,44	10,87	10,96	11,39	5,94	8,74
NiO	0,28	0,35	0,12	0,17	0,28	0,32	0,30	0,03	0,31	0,33	0,39	0,21	0,06
Total (wt%)	87,75	88,97	87,53	87,81	87,38	85,60	87,72	86,74	87,63	86,38	87,62	86,54	86,26
	Atomic proportions (apfu) in the base of 14 O												
Ti	0,000	0,001	0,003	0,002	0,001	0,002	0,002	0,011	0,002	0,000	0,000	0,003	0,004
Ca	0,000	0,000	0,000	0,000	0,001	0,001	0,002	0,001	0,001	0,001	0,002	0,002	0,002
Si	3,302	3,403	3,335	3,316	3,323	3,303	3,296	3,307	3,355	3,304	3,316	3,633	3,382
Cr	0,068	0,087	0,073	0,074	0,081	0,081	0,066	0,081	0,096	0,064	0,072	0,078	0,071
K	0,050	0,040	0,022	0,036	0,041	0,021	0,022	0,024	0,014	0,056	0,039	0,031	0,044
Mn	0,000	0,000	0,001	0,000	0,000	0,000	0,000	0,000	0,000	0,000	0,000	0,000	0,000
Mg	4,917	4,977	5,165	4,989	4,952	4,959	4,938	5,271	4,950	5,008	4,935	5,269	5,178
Al	1,280	1,146	1,066	1,218	1,231	1,266	1,307	1,066	1,210	1,244	1,273	0,667	0,996
Ni	0,021	0,026	0,009	0,013	0,021	0,025	0,023	0,002	0,024	0,026	0,030	0,016	0,005
Fe2+	0,406	0,319	0,425	0,401	0,379	0,368	0,360	0,355	0,339	0,358	0,360	0,300	0,414
Fe3+	0,000	0,000	0,000	0,000	0,000	0,000	0,000	0,000	0,000	0,000	0,000	0,000	0,000
Total (apfu)	10,048	10,002	10,104	10,055	10,041	10,034	10,031	10,123	9,998	10,070	10,031	10,008	10,105

d. Chlorite 4

Sample - IMK - 05156

Lithology	Serpentinised harzburgite									
File	Z1	Z1	Z1	Z1	Z1	Z1	Z1	Z1	Z1	Z1
Analyses ID	42	46	47	48	49	51	53	55	57	59
TiO2	0,21	b.d.l	0,15	0,14	b.d.l	0,23	0,05	b.d.l	b.d.l	0,01
CaO	0,01	b.d.l	0,02	0,00	0,02	0,01	0,01	0,03	0,01	0,00
SiO2	34,18	34,78	36,47	33,58	35,62	34,43	34,82	34,91	35,03	34,13
Cr2O3	0,96	1,06	1,27	0,87	0,95	0,95	0,66	0,89	1,39	1,07
K2O	0,11	0,19	0,09	0,06	0,22	0,09	0,05	0,18	0,08	0,20
MnO	b.d.l	b.d.l	b.d.l	b.d.l	b.d.l	b.d.l	b.d.l	b.d.l	b.d.l	b.d.l
MgO	36,47	34,65	36,64	36,04	35,46	36,69	36,67	34,43	34,88	36,18
FeO	5,51	4,68	5,29	4,23	4,22	4,70	3,81	4,36	4,12	4,53
Al2O3	8,79	11,64	7,62	11,02	10,74	10,45	10,73	12,11	11,85	10,60
NiO	0,08	0,25	0,22	0,07	0,18	0,10	0,09	0,30	0,34	0,33
Total (wt%)	86,36	87,33	87,81	86,15	87,49	87,66	86,95	87,31	87,77	87,09
Atomic proportions (apfu) in the base of 14 O										
Ti	0,015	0,000	0,011	0,010	0,000	0,016	0,003	0,000	0,000	0,001
Ca	0,001	0,000	0,002	0,000	0,002	0,001	0,001	0,003	0,001	0,000
Si	3,311	3,305	3,462	3,235	3,367	3,266	3,306	3,309	3,302	3,263
Cr	0,074	0,079	0,095	0,066	0,071	0,071	0,049	0,067	0,104	0,081
K	0,014	0,023	0,011	0,007	0,026	0,011	0,005	0,022	0,010	0,024
Mn	0,000	0,000	0,000	0,000	0,000	0,000	0,000	0,000	0,000	0,000
Mg	5,267	4,908	5,185	5,175	4,997	5,189	5,189	4,864	4,903	5,157
Al	1,003	1,304	0,852	1,251	1,196	1,168	1,201	1,353	1,316	1,194
Ni	0,006	0,019	0,017	0,005	0,014	0,008	0,007	0,023	0,026	0,025
Fe2+	0,447	0,372	0,420	0,341	0,334	0,373	0,302	0,346	0,325	0,362
Fe3+	0,000	0,000	0,000	0,000	0,000	0,000	0,000	0,000	0,000	0,000
Total (apfu)	10,142	10,016	10,059	10,103	10,013	10,104	10,069	9,996	9,994	10,111

a. Amphiboles 1

Sample - IMK - 05139

Lithology	Coarse-grained orthopyroxenite												
File	Z1	Z1	Z1	Z1	Z1	Z2	Z2	Z2	Z2	Z2	Z2	Z2	Z2
Analyses ID	2	3	11	15	45	1	6	9	10	12	16	26	29
Mineral name	Hornblend	Hornblend	Hornblend	Actinolite-Tremolite	Hornblend	Hornblend	Hornblend	Actinolite-Tremolite	Actinolite-Tremolite	Hornblend	Actinolite-Tremolite	Hornblend	Ferro-Magnesian
TiO2	0,04	0,05	0,04	0,01	0,04	0,03	0,01	0,00	0,06	0,00	0,07	0,07	0,13
CaO	6,32	10,25	4,89	9,03	1,28	5,19	6,69	13,20	12,28	2,47	3,93	2,71	5,53
SiO2	47,29	52,27	50,07	52,47	51,99	48,30	49,04	58,70	55,49	50,70	54,41	51,12	56,07
Cr2O3	1,29	1,40	0,81	0,82	0,90	0,78	0,82	0,12	0,80	0,80	0,78	0,94	0,67
Na2O	0,14	0,16	0,07	0,09	0,03	0,09	0,04	0,07	0,10	0,04	0,08	0,11	0,50
K2O	0,09	0,06	0,07	0,08	0,03	0,06	0,03	0,03	0,04	0,05	0,08	0,10	0,04
MgO	29,81	23,81	31,02	25,08	31,20	30,25	28,57	22,05	23,08	31,42	28,22	30,24	23,80
FeO	6,73	5,82	6,67	6,22	7,82	6,81	6,02	4,31	4,78	8,29	8,39	7,52	7,61
Al2O3	2,87	1,75	2,05	0,65	1,23	1,65	1,51	0,08	0,60	1,46	0,91	1,36	3,19
NiO	0,01	0,03	0,00	0,05	0,00	0,00	0,07	0,01	0,07	0,01	0,03	b.d.l	0,12
Total (wt%)	94,67	95,73	95,95	94,59	94,76	93,26	93,04	98,78	97,51	95,54	97,19	94,45	97,79
Atomic proportions (apfu) in the base of 23 O													
Ti	0,004	0,006	0,004	0,001	0,005	0,003	0,001	0,000	0,006	0,000	0,007	0,007	0,013
Ca	0,983	1,569	0,742	1,394	0,195	0,815	1,051	1,930	1,835	0,376	0,587	0,416	0,814
Si	6,870	7,465	7,102	7,562	7,384	7,074	7,193	8,012	7,735	7,213	7,577	7,325	7,711
Cr	0,148	0,158	0,090	0,093	0,102	0,091	0,095	0,013	0,088	0,090	0,086	0,106	0,073
Na	0,040	0,045	0,019	0,025	0,007	0,024	0,013	0,018	0,027	0,010	0,021	0,030	0,134
K	0,016	0,010	0,012	0,014	0,005	0,012	0,005	0,005	0,007	0,009	0,014	0,018	0,006
Mg	6,456	5,069	6,560	5,388	6,606	6,605	6,246	4,487	4,796	6,664	5,860	6,459	4,880
Al	0,491	0,294	0,342	0,110	0,206	0,284	0,260	0,013	0,098	0,245	0,150	0,229	0,517
Ni	0,002	0,004	0,000	0,006	0,000	0,000	0,009	0,001	0,008	0,001	0,003	0,000	0,013
Fe2+	0,818	0,695	0,791	0,749	0,929	0,833	0,738	0,471	0,557	0,986	0,977	0,902	0,875
Fe3+	0,000	0,000	0,000	0,000	0,000	0,000	0,000	0,021	0,000	0,000	0,000	0,000	0,000
Total (apfu)	15,835	15,330	15,694	15,355	15,464	15,754	15,638	15,012	15,182	15,629	15,315	15,524	15,051

b. Amphiboles 2

Sample - IMK - 05139

Lithology	Coarse-grained orthopyroxenite												
File	Z2	Z3	Z3	Z3	Z3	Z3	Z3	Z4	Z4	Z4	Z4	Z4	Z4
Analyses ID	30	2	5	6	21	22	27	3	5	10	11	14	16
Mineral name	Actinolite-Tremolite	Actinolite-Tremolite	Hornblend	Actinolite-Tremolite	Actinolite-Tremolite	Actinolite-Tremolite	Ferro-Magnesian	Hornblend	Actinolite-Tremolite	Actinolite-Tremolite	Hornblend	Ferro-Magnesian	Ferro-Magnesian
TiO2	0,04	0,02	0,04	0,07	0,00	0,01	0,08	0,07	0,05	0,04	0,08	0,03	0,06
CaO	9,43	9,37	6,58	7,69	13,32	2,00	6,62	3,69	3,12	14,03	11,41	1,68	3,05
SiO2	52,72	53,45	51,75	55,23	58,38	54,81	49,13	52,81	54,40	57,08	52,43	55,62	53,40
Cr2O3	0,58	0,46	0,42	0,70	0,13	0,83	0,90	0,75	0,71	0,28	1,03	0,84	0,70
Na2O	0,05	0,09	0,10	0,07	0,03	0,04	0,11	0,11	0,05	0,10	0,88	0,03	0,09
K2O	0,02	0,05	0,08	0,05	0,01	0,03	0,07	0,08	0,05	0,03	0,07	0,02	0,05
MgO	25,34	24,59	28,04	27,43	21,60	31,13	27,39	28,16	29,37	21,03	19,65	29,69	31,39
FeO	5,90	6,28	9,65	5,96	4,20	7,07	7,81	8,45	7,07	4,60	5,41	5,89	6,52
Al2O3	0,58	0,71	0,82	0,96	0,02	1,15	1,69	1,17	1,34	0,08	5,25	1,14	1,36
NiO	0,05	0,02	b.d.l	0,03	0,02	0,04	0,07	0,04	0,05	b.d.l	0,11	0,07	0,07
Total (wt%)	94,91	95,41	97,79	98,39	97,81	97,37	94,09	95,53	96,41	97,60	96,42	95,11	96,85
Atomic proportions (apfu) in the base of 23 O													
Ti	0,004	0,002	0,004	0,008	0,000	0,001	0,008	0,008	0,005	0,004	0,009	0,003	0,006
Ca	1,449	1,433	0,996	1,131	1,964	0,294	1,038	0,561	0,465	2,093	1,730	0,250	0,452
Si	7,566	7,631	7,310	7,584	8,038	7,531	7,184	7,497	7,566	7,945	7,417	7,732	7,401
Cr	0,065	0,052	0,047	0,076	0,014	0,090	0,104	0,084	0,078	0,031	0,115	0,092	0,077
Na	0,015	0,025	0,026	0,020	0,007	0,011	0,030	0,030	0,015	0,026	0,240	0,008	0,025
K	0,004	0,009	0,014	0,009	0,002	0,005	0,012	0,014	0,009	0,004	0,013	0,003	0,008
Mg	5,421	5,234	5,905	5,615	4,432	6,375	5,972	5,959	6,088	4,365	4,145	6,152	6,487
Al	0,098	0,119	0,136	0,156	0,003	0,187	0,292	0,196	0,220	0,013	0,875	0,186	0,222
Ni	0,006	0,003	0,000	0,003	0,002	0,005	0,008	0,005	0,005	0,000	0,013	0,008	0,008
Fe2+	0,708	0,749	1,139	0,684	0,398	0,813	0,955	1,003	0,822	0,435	0,424	0,685	0,755
Fe3+	0,000	0,000	0,000	0,000	0,085	0,000	0,000	0,000	0,000	0,100	0,216	0,000	0,000
Total (apfu)	15,358	15,298	15,614	15,307	14,958	15,340	15,631	15,392	15,293	15,084	15,206	15,132	15,460

c. Amphiboles 3

Sample - IMK - 05139				
Lithology	Coarse-grained orthopyroxenite			
File	Z4	Z4	Z4	Z4
Analyses ID	19	20	21	22
Mineral name	Ferro-Magnesian	Hornblend	Hornblend	Hornblend
TiO2	0,07	0,01	0,05	b.d.l
CaO	1,12	1,05	0,89	0,97
SiO2	56,32	50,05	53,41	54,40
Cr2O3	0,75	0,75	0,84	0,72
Na2O	0,02	0,03	0,02	0,05
K2O	0,00	0,02	0,03	0,03
MgO	31,99	31,87	32,32	32,74
FeO	6,45	7,67	7,77	6,92
Al2O3	1,20	1,58	1,29	1,49
NiO	0,02	0,08	0,01	0,00
Total (wt%)	98,07	93,44	96,93	97,45
Atomic proportions (apfu) in the base of 23 O				
Ti	0,007	0,001	0,006	0,000
Ca	0,162	0,162	0,132	0,142
Si	7,612	7,232	7,397	7,444
Cr	0,080	0,085	0,092	0,078
Na	0,004	0,008	0,006	0,012
K	0,000	0,004	0,005	0,005
Mg	6,446	6,864	6,673	6,678
Al	0,191	0,269	0,210	0,240
Ni	0,002	0,009	0,001	0,000
Fe2+	0,729	0,927	0,899	0,792
Fe3+	0,000	0,000	0,000	0,000
Total (apfu)	15,248	15,596	15,452	15,406

d. Amphiboles 4

Sample - IMK - 05149

Lithology	Serpentinised pyroxenite												
File	Z1	Z1	Z1	Z1	Z1	Z1	Z1	Z2	Z2	Z2	Z3	Z3	Z3
Analyses ID	1	2	3	1	2	3	4	1	2	3	1	2	3
Mineral name	Hornblend	Hornblend	Hornblend	Hornblend	Hornblend	Hornblend	Hornblend	Hornblend	Hornblend	Hornblend	Hornblend	Hornblend	Hornblend
TiO2	0,11	0,06	0,16	0,12	0,09	0,06	0,15	0,17	0,21	0,14	0,19	0,15	0,08
CaO	11,80	11,50	11,45	11,73	11,66	11,37	11,66	11,47	11,67	11,52	12,05	11,76	11,42
SiO2	50,77	47,58	47,28	46,37	46,67	49,24	47,97	47,30	47,56	50,61	50,84	51,82	47,79
Cr2O3	0,65	0,67	0,84	0,56	0,59	0,52	0,42	0,92	0,86	1,04	0,68	0,74	0,58
Na2O	1,42	2,06	2,04	2,03	2,04	1,63	1,81	1,85	1,95	1,37	1,29	1,19	2,07
K2O	0,06	0,08	0,07	0,10	0,10	0,09	0,10	0,08	0,09	0,05	0,06	0,05	0,13
MgO	19,88	18,56	18,88	18,38	18,36	19,30	19,09	19,07	18,79	20,49	20,97	20,93	19,12
FeO	4,05	4,74	4,43	5,08	4,89	5,09	4,21	4,04	4,44	4,07	4,20	3,71	4,83
Al2O3	8,19	11,96	11,42	12,48	12,38	9,46	10,75	11,19	11,58	7,45	8,37	7,11	11,11
NiO	0,18	0,14	0,18	0,19	0,14	0,14	0,11	0,13	0,18	0,16	0,16	0,18	0,17
Total (wt%)	97,19	97,36	96,75	97,13	96,99	96,98	96,35	96,23	97,32	96,90	98,88	97,68	97,35
Atomic proportions (apfu) in the base of 23 O													
Ti	0,011	0,006	0,017	0,013	0,009	0,006	0,016	0,019	0,022	0,015	0,020	0,015	0,008
Ca	1,771	1,736	1,738	1,783	1,770	1,720	1,773	1,747	1,761	1,736	1,781	1,750	1,726
Si	7,109	6,701	6,701	6,579	6,617	6,951	6,806	6,724	6,701	7,114	7,013	7,198	6,741
Cr	0,072	0,075	0,095	0,063	0,066	0,058	0,047	0,104	0,096	0,115	0,074	0,082	0,064
Na	0,384	0,563	0,561	0,558	0,560	0,447	0,497	0,510	0,532	0,374	0,346	0,321	0,566
K	0,011	0,015	0,012	0,018	0,017	0,017	0,018	0,014	0,017	0,010	0,010	0,009	0,024
Mg	4,151	3,896	3,990	3,887	3,881	4,060	4,038	4,041	3,947	4,293	4,312	4,335	4,020
Al	1,352	1,984	1,908	2,087	2,069	1,574	1,797	1,875	1,922	1,235	1,361	1,164	1,847
Ni	0,020	0,016	0,020	0,022	0,016	0,016	0,013	0,015	0,020	0,018	0,018	0,020	0,019
Fe2+	0,475	0,558	0,525	0,603	0,580	0,601	0,499	0,481	0,523	0,478	0,484	0,431	0,570
Fe3+	0,000	0,000	0,000	0,000	0,000	0,000	0,000	0,000	0,000	0,000	0,000	0,000	0,000
Total (apfu)	15,365	15,552	15,568	15,622	15,595	15,459	15,514	15,530	15,542	15,388	15,427	15,329	15,590

e. Amphiboles 5

Sample - IMK - 05149

Lithology	Serpentinised pyroxenite												
File	Z3	Z3	Z3	Z3	Z3	Z3	Z3	Z3	Z4	Z4	Z4	Z5	Z5
Analyses ID	4	5	1	2	3	4	5	6	22	26	27	2	3
Mineral name	Hornblend	Hornblend	Hornblend	Hornblend	Hornblend	Hornblend	Hornblend	Hornblend	Hornblend	Hornblend	Hornblend	Hornblend	Hornblend
TiO2	0,10	0,18	0,10	0,12	0,09	0,10	0,04	0,07	0,48	0,51	0,40	0,16	0,31
CaO	11,86	11,79	11,89	11,75	11,70	11,58	11,62	11,71	12,67	10,60	11,55	11,19	11,55
SiO2	49,54	48,84	46,69	46,53	46,82	46,56	46,59	46,75	52,93	44,79	46,23	46,00	46,21
Cr2O3	0,50	0,88	0,54	0,57	0,61	0,73	0,59	0,68	1,53	1,23	1,17	0,91	1,20
Na2O	1,71	1,75	2,20	2,24	2,22	2,45	2,33	2,18	0,46	2,23	2,37	2,21	2,25
K2O	0,12	0,10	0,12	0,11	0,11	0,13	0,11	0,11	0,01	0,15	0,12	0,11	0,18
MgO	19,50	19,14	18,79	18,86	18,80	18,80	18,83	18,88	20,26	18,96	18,59	18,61	18,57
FeO	4,93	4,67	4,63	4,39	4,42	4,24	4,62	4,37	2,68	5,69	4,36	4,60	4,01
Al2O3	9,49	10,54	12,28	12,36	12,46	12,35	12,48	12,40	5,93	10,56	11,31	12,44	11,77
NiO	0,19	0,15	0,18	0,09	0,20	0,13	0,13	0,17	0,09	0,10	0,15	0,15	0,11
Total (wt%)	98,00	98,10	97,44	97,06	97,57	97,12	97,38	97,39	97,08	94,90	96,23	96,47	96,17
Atomic proportions (apfu) in the base of 23 O													
Ti	0,010	0,019	0,010	0,012	0,010	0,011	0,004	0,007	0,050	0,056	0,043	0,017	0,034
Ca	1,777	1,764	1,799	1,782	1,765	1,756	1,759	1,769	1,887	1,661	1,772	1,710	1,768
Si	6,930	6,824	6,593	6,587	6,596	6,588	6,580	6,594	7,359	6,551	6,618	6,560	6,604
Cr	0,055	0,097	0,061	0,064	0,067	0,082	0,066	0,076	0,168	0,142	0,132	0,103	0,135
Na	0,464	0,473	0,603	0,615	0,607	0,673	0,637	0,597	0,124	0,633	0,658	0,611	0,624
K	0,021	0,017	0,021	0,020	0,020	0,023	0,020	0,019	0,002	0,028	0,022	0,020	0,033
Mg	4,067	3,986	3,956	3,979	3,949	3,966	3,964	3,970	4,198	4,135	3,968	3,955	3,957
Al	1,564	1,735	2,043	2,061	2,068	2,059	2,078	2,062	0,971	1,820	1,908	2,090	1,982
Ni	0,022	0,017	0,020	0,011	0,022	0,015	0,015	0,020	0,010	0,012	0,017	0,017	0,013
Fe2+	0,576	0,546	0,547	0,520	0,521	0,501	0,546	0,515	0,311	0,696	0,521	0,549	0,479
Fe3+	0,000	0,000	0,000	0,000	0,000	0,000	0,000	0,000	0,000	0,000	0,000	0,000	0,000
Total (apfu)	15,493	15,486	15,657	15,656	15,640	15,679	15,673	15,638	15,085	15,742	15,659	15,642	15,632

f. Amphiboles 6

Sample - IMK - 05149								
Lithology	Serpentinised pyroxenite							
File	Z5	Z5	Z5	Z5	Z5	Z5	Z5	Z5
Analyses ID	4	13	14	15	17	20	1	16
Mineral name	Hornblend	Hornblend	Hornblend	Hornblend	Hornblend	Hornblend	Tremolite	Actinolite
TiO2	0,37	0,08	0,18	0,16	0,11	0,08	0,05	0,06
CaO	11,29	11,38	11,86	11,78	11,70	11,62	12,26	10,90
SiO2	45,90	46,71	46,34	46,37	46,13	46,05	56,29	56,28
Cr2O3	1,29	0,70	0,98	0,91	1,15	0,71	0,27	0,14
Na2O	2,30	2,06	2,26	2,27	2,26	2,17	0,26	0,42
K2O	0,11	0,14	0,18	0,15	0,18	0,12	0,01	0,19
MgO	18,33	19,02	19,05	18,70	18,90	18,41	22,35	21,78
FeO	4,49	4,37	3,63	3,85	3,69	4,46	3,45	5,62
Al2O3	12,06	12,19	12,13	12,39	12,05	12,67	1,31	1,46
NiO	0,08	0,12	0,07	0,10	0,13	0,17	0,23	0,08
Total (wt%)	96,28	96,85	96,67	96,69	96,32	96,47	96,62	97,19
Atomic proportions (apfu) in the base of 23 O								
Ti	0,040	0,008	0,019	0,017	0,012	0,008	0,006	0,007
Ca	1,730	1,727	1,804	1,790	1,788	1,774	1,828	1,627
Si	6,566	6,617	6,577	6,581	6,577	6,562	7,837	7,843
Cr	0,146	0,078	0,110	0,102	0,130	0,080	0,029	0,016
Na	0,637	0,565	0,621	0,625	0,625	0,598	0,071	0,114
K	0,020	0,025	0,033	0,027	0,032	0,023	0,002	0,033
Mg	3,909	4,016	4,031	3,956	4,018	3,911	4,640	4,524
Al	2,032	2,035	2,030	2,072	2,025	2,128	0,215	0,239
Ni	0,009	0,013	0,008	0,012	0,014	0,019	0,025	0,009
Fe2+	0,537	0,518	0,431	0,456	0,440	0,531	0,402	0,655
Fe3+	0,000	0,000	0,000	0,000	0,000	0,000	0,000	0,000
Total (apfu)	15,634	15,613	15,662	15,641	15,662	15,636	15,071	15,096

g. Amphiboles 7

Sample - IMK - 05153

Lithology	Serpentinised pyroxenite												
File	Z1	Z1	Z1	Z1	Z1	Z1	Z1	Z1	Z2	Z2	Z2	Z2	Z2
Analyses ID	14	16	21	22	25	27	34	38	5	7	10	12	19
Mineral name	Tremolite	Actinolite	Tremolite	Tremolite	Actinolite	Tremolite	Actinolite	Actinolite	Actinolite	Actinolite	Actinolite	Hornblende	Hornblende
TiO2	b.d.l	b.d.l	0,05	0,08	0,01	0,03	b.d.l	0,08	0,02	0,00	0,02	0,34	0,10
CaO	10,44	9,28	11,40	10,44	10,20	9,54	7,42	7,77	5,18	9,00	3,35	10,02	10,24
SiO2	58,81	55,81	57,60	54,77	57,83	54,84	53,50	55,44	55,49	55,73	56,27	51,56	53,32
Cr2O3	0,23	0,56	0,20	0,62	0,49	0,52	0,52	0,59	0,37	0,43	0,26	1,34	0,76
Na2O	0,02	0,05	0,03	0,95	0,06	0,95	0,04	0,56	0,40	0,10	0,37	1,15	0,98
K2O	0,04	0,04	0,02	0,03	0,03	0,03	0,02	0,02	0,01	0,01	0,07	0,08	0,05
MgO	22,53	22,62	21,94	21,47	21,93	22,11	26,05	22,86	24,16	24,31	25,81	20,27	20,84
FeO	3,65	5,23	4,33	3,40	4,49	3,63	5,38	5,30	6,35	5,56	6,23	3,97	3,47
Al2O3	0,23	0,55	0,24	4,66	0,37	4,45	0,78	2,94	2,45	0,28	2,00	6,31	5,63
NiO	0,16	0,04	0,23	0,30	0,09	0,22	0,11	0,28	0,27	0,09	0,41	0,62	0,40
Total (wt%)	96,38	94,54	96,31	96,85	95,84	96,46	94,26	96,04	95,01	95,81	95,07	95,65	95,78

Atomic proportions (apfu) in the base of 23 O

Ti	0,000	0,000	0,005	0,009	0,001	0,003	0,000	0,008	0,002	0,000	0,002	0,036	0,011
Ca	1,545	1,415	1,703	1,550	1,526	1,419	1,137	1,162	0,780	1,357	0,502	1,521	1,539
Si	8,123	7,938	8,032	7,591	8,076	7,616	7,654	7,744	7,806	7,844	7,860	7,306	7,483
Cr	0,025	0,063	0,022	0,068	0,055	0,057	0,058	0,065	0,041	0,047	0,029	0,150	0,084
Na	0,006	0,013	0,009	0,256	0,015	0,257	0,010	0,150	0,109	0,027	0,100	0,316	0,266
K	0,007	0,007	0,004	0,005	0,006	0,006	0,004	0,004	0,002	0,002	0,012	0,014	0,009
Mg	4,640	4,796	4,561	4,437	4,565	4,576	5,556	4,761	5,066	5,101	5,375	4,283	4,360
Al	0,037	0,092	0,040	0,760	0,061	0,728	0,132	0,484	0,406	0,047	0,329	1,054	0,931
Ni	0,018	0,005	0,026	0,033	0,010	0,025	0,012	0,031	0,031	0,010	0,046	0,071	0,045
Fe2+	0,422	0,622	0,505	0,225	0,525	0,420	0,644	0,619	0,747	0,654	0,727	0,223	0,173
Fe3+	0,000	0,000	0,000	0,169	0,000	0,002	0,000	0,000	0,000	0,000	0,000	0,247	0,233
Total (apfu)	14,852	14,995	14,938	15,117	14,876	15,128	15,258	15,051	15,024	15,123	15,015	15,221	15,136

a. Pentlandite 1

Sample - IMK - 05139

Lithology	Coarse-grained orthopyroxenite												
File	A_Z1_Pent	A_Z1_Pent	A_Z1_Pent	A_Z1_Pent	A_Z1_Pent	A_Z1_Pent	A_Z1_Pent	A_Z1_Pent	A_Z1_Pent	A_Z1_Pent	A_Z1_Pent	A_Z1_Pent	A_Z1_Pent
Analyses ID	10	11	13	18	22	24	25	26	29	31	33	34	35
Au	0,01	0,04	b.d.l	b.d.l	0,01	b.d.l	b.d.l	0,03	b.d.l	0,02	0,02	b.d.l	b.d.l
Ag	b.d.l	0,03	0,01	0,02	0,01	0,01	b.d.l	b.d.l	b.d.l	0,02	b.d.l	0,03	b.d.l
Mo	0,02	0,09	0,07	0,06	0,06	0,09	0,11	0,11	0,11	0,08	0,05	0,10	0,07
S	33,57	33,77	33,66	33,95	34,15	33,80	33,57	33,68	33,81	33,23	33,76	33,59	33,75
Ni	30,22	29,43	29,38	29,61	29,46	27,11	29,10	28,71	28,85	28,63	28,96	29,48	29,44
Fe	34,78	35,13	36,07	36,09	36,04	36,17	35,81	36,25	35,84	35,37	36,00	35,86	35,23
Co	0,88	0,93	0,78	0,75	0,80	0,75	0,79	0,68	0,67	0,83	0,69	0,74	0,85
Cu	b.d.l	b.d.l	b.d.l	b.d.l	b.d.l	b.d.l	b.d.l	b.d.l	b.d.l	b.d.l	b.d.l	b.d.l	b.d.l
Total (wt%)	99,63	99,58	100,13	100,61	100,56	98,12	99,43	99,57	99,34	98,24	99,62	99,91	99,53
Atomic proportions (apfu) in the base of 17 atoms													
Au	0,000	0,002	0,000	0,000	0,001	0,000	0,000	0,001	0,000	0,001	0,001	0,000	0,000
Ag	0,000	0,002	0,000	0,001	0,000	0,001	0,000	0,000	0,000	0,001	0,000	0,002	0,000
Mo	0,002	0,007	0,005	0,005	0,004	0,007	0,009	0,009	0,009	0,006	0,004	0,008	0,006
S	8,086	8,131	8,071	8,093	8,131	8,222	8,095	8,107	8,144	8,108	8,119	8,071	8,127
Ni	3,975	3,871	3,848	3,854	3,831	3,603	3,833	3,775	3,797	3,815	3,804	3,869	3,873
Fe	4,809	4,857	4,965	4,938	4,926	5,052	4,957	5,010	4,957	4,954	4,970	4,948	4,870
Co	0,115	0,122	0,102	0,098	0,104	0,099	0,104	0,089	0,088	0,110	0,091	0,096	0,111
Cu	0,000	0,000	0,000	0,000	0,000	0,000	0,000	0,000	0,000	0,000	0,000	0,000	0,000
Total (apfu)	17	17	17	17	17	17	17	17	17	17	17	17	17

b. Pentlandite 2

Sample - IMK - 05139

Lithology	Coarse-grained orthopyroxenite												
File	A_Z2_Pent	A_Z2_Pent	A_Z2_Pent	A_Z2_Pent	A_Z2_Pent	A_Z2_Pent	A_Z2_Pent	A_Z2_Pent	A_Z2_Pent	A_Z3_Pent	A_Z3_Pent	A_Z3_Pent	A_Z3_Pent
Analyses ID	1	2	6	8	10	11	12	13	16	1	3	6	7
Au	b.d.l	b.d.l	b.d.l	0,02	b.d.l	0,04	b.d.l	b.d.l	b.d.l	0,01	b.d.l	0,04	b.d.l
Ag	b.d.l	0,02	b.d.l	b.d.l	b.d.l	0,01	0,00	b.d.l	0,03	0,00	0,02	0,02	b.d.l
Mo	0,09	0,10	0,10	0,14	0,06	0,06	0,10	0,12	0,11	0,12	0,07	0,06	0,10
S	33,93	33,92	33,76	33,59	33,73	33,93	33,97	33,88	33,86	34,07	33,95	33,82	33,70
Ni	29,25	29,53	28,88	28,44	28,70	29,35	29,22	29,26	29,08	30,18	29,04	29,68	29,42
Fe	35,50	35,37	35,47	35,86	36,50	35,98	36,63	36,21	36,30	35,28	36,35	35,83	35,85
Co	0,88	0,85	0,68	0,73	0,68	0,70	0,68	0,69	0,67	0,76	0,64	0,75	0,76
Cu	b.d.l	b.d.l	b.d.l	b.d.l	b.d.l	b.d.l	b.d.l	b.d.l	b.d.l	b.d.l	b.d.l	b.d.l	b.d.l
Total (wt%)	99,74	99,99	99,05	99,03	99,79	100,13	100,71	100,27	100,28	100,62	100,16	100,39	99,99
Atomic proportions (apfu) in the base of 17 atoms													
Au	0,000	0,000	0,000	0,001	0,000	0,001	0,000	0,000	0,000	0,000	0,000	0,001	0,000
Ag	0,000	0,002	0,000	0,000	0,000	0,000	0,000	0,000	0,002	0,000	0,001	0,001	0,000
Mo	0,007	0,008	0,008	0,011	0,005	0,005	0,008	0,009	0,009	0,009	0,005	0,005	0,008
S	8,144	8,133	8,158	8,132	8,101	8,119	8,089	8,101	8,104	8,123	8,120	8,086	8,086
Ni	3,835	3,867	3,812	3,760	3,765	3,836	3,800	3,821	3,801	3,930	3,793	3,876	3,856
Fe	4,892	4,868	4,921	4,983	5,032	4,942	5,007	4,970	4,987	4,828	4,990	4,918	4,937
Co	0,114	0,111	0,089	0,096	0,089	0,090	0,088	0,090	0,087	0,098	0,084	0,097	0,100
Cu	0,000	0,000	0,000	0,000	0,000	0,000	0,000	0,000	0,000	0,000	0,000	0,000	0,000
Total (apfu)	17	17	17	17	17	17	17	17	17	17	17	17	17

c. Pentlandite 3

Sample - IMK - 05139

Lithology	Coarse-grained orthopyroxenite												
File	A_Z3_Pent	A_Z3_Pent	A_Z3_Pent	A_Z3_Pent	A_Z3_Pent	A_Z3_Pent	A_Z3_Pent	A_Z3_Pent	A_Z3_Pent	A_Z3_Pent	A_Z4_Pent	A_Z4_Pent	A_Z4_Pent
Analyses ID	8	11	13	14	16	17	18	19	20	23	1	2	3
Au	b.d.l	b.d.l	0,01	b.d.l	0,01	b.d.l	b.d.l	b.d.l	0,03	b.d.l	b.d.l	0,02	b.d.l
Ag	0,02	b.d.l	0,03	0,04	b.d.l	0,04	b.d.l	0,05	b.d.l	b.d.l	0,00	b.d.l	0,02
Mo	0,08	0,07	0,10	0,14	0,09	0,11	0,07	0,09	0,06	0,10	0,09	0,08	0,10
S	33,84	33,97	33,90	33,91	33,86	33,96	33,79	33,82	33,43	34,18	33,58	33,26	33,29
Ni	29,89	29,28	28,91	29,60	29,57	30,04	30,33	30,71	29,95	27,61	28,37	28,67	28,24
Fe	35,80	36,03	36,41	36,63	36,32	35,80	35,85	35,24	35,01	35,15	35,56	35,15	35,71
Co	0,72	0,75	0,66	0,72	0,71	0,72	0,74	0,74	0,86	0,63	0,87	0,88	0,80
Cu	b.d.l	b.d.l	b.d.l	b.d.l	b.d.l	b.d.l	b.d.l	b.d.l	b.d.l	0,09	b.d.l	b.d.l	b.d.l
Total (wt%)	100,46	100,21	100,10	101,14	100,82	100,77	100,92	100,89	99,53	97,92	98,69	98,11	98,31
Atomic proportions (apfu) in the base of 17 atoms													
Au	0,000	0,000	0,000	0,000	0,000	0,000	0,000	0,000	0,001	0,000	0,000	0,001	0,000
Ag	0,001	0,000	0,002	0,003	0,000	0,003	0,000	0,003	0,000	0,000	0,000	0,000	0,001
Mo	0,006	0,006	0,008	0,011	0,007	0,009	0,006	0,007	0,005	0,008	0,007	0,007	0,008
S	8,082	8,122	8,114	8,053	8,069	8,086	8,045	8,060	8,069	8,312	8,148	8,120	8,117
Ni	3,900	3,824	3,780	3,840	3,849	3,907	3,945	3,997	3,948	3,667	3,761	3,823	3,761
Fe	4,908	4,944	5,004	4,993	4,969	4,894	4,900	4,821	4,851	4,907	4,954	4,927	4,998
Co	0,094	0,097	0,086	0,093	0,092	0,093	0,096	0,096	0,113	0,083	0,115	0,117	0,106
Cu	0,000	0,000	0,000	0,000	0,000	0,000	0,000	0,000	0,000	0,011	0,000	0,000	0,000
Total (apfu)	17	17	17	17	17	17	17	17	17	17	17	17	17

d. Pentlandite 4

Sample - IMK - 05139

Lithology	Coarse-grained orthopyroxenite											
File	A_Z4_Pent	A_Z4_Pent	A_Z4_Pent	A_Z4_Pent	A_Z4_Pent	A_Z4_Pent	A_Z4_Pent	A_Z4_Pent	A_Z4_Pent	A_Z4_Pent	A_Z4_Pent	A_Z4_Pent
Analyses ID	4	5	6	7	10	11	12	13	14	15	16	17
Au	b.d.l	0,02	0,01	b.d.l	0,00	0,01	0,05	b.d.l	b.d.l	b.d.l	b.d.l	0,03
Ag	b.d.l	b.d.l	b.d.l	b.d.l	b.d.l	0,04	b.d.l	0,03	b.d.l	b.d.l	b.d.l	0,03
Mo	0,11	0,14	0,11	0,06	0,10	0,12	0,04	0,08	0,10	0,14	0,06	0,13
S	33,11	33,72	33,50	33,60	33,63	33,43	33,55	33,50	33,66	33,50	33,51	33,66
Ni	28,56	28,64	28,53	29,50	28,65	28,35	28,97	29,71	28,56	28,43	28,91	28,79
Fe	35,66	35,79	36,11	35,33	35,92	35,92	35,71	34,85	35,41	35,83	35,20	35,77
Co	0,72	0,81	0,74	0,75	0,77	0,82	0,90	0,89	0,82	0,82	0,86	0,84
Cu	0,01	b.d.l	b.d.l	b.d.l	b.d.l	b.d.l	b.d.l	0,12	b.d.l	b.d.l	b.d.l	b.d.l
Total (wt%)	98,32	99,29	99,11	99,36	99,51	98,85	99,37	99,30	98,71	98,78	98,67	99,59
Atomic proportions (apfu) in the base of 17 atoms												
Au	0,000	0,001	0,000	0,000	0,000	0,000	0,002	0,000	0,000	0,000	0,000	0,001
Ag	0,000	0,000	0,000	0,000	0,000	0,003	0,000	0,002	0,000	0,000	0,000	0,002
Mo	0,009	0,011	0,009	0,005	0,008	0,010	0,003	0,007	0,008	0,011	0,005	0,010
S	8,080	8,138	8,103	8,108	8,115	8,110	8,099	8,095	8,161	8,122	8,132	8,116
Ni	3,807	3,776	3,769	3,888	3,776	3,757	3,820	3,921	3,782	3,766	3,833	3,792
Fe	4,995	4,960	5,014	4,894	4,976	5,002	4,949	4,834	4,929	4,988	4,904	4,951
Co	0,096	0,106	0,097	0,099	0,101	0,109	0,118	0,116	0,109	0,108	0,114	0,110
Cu	0,001	0,000	0,000	0,000	0,000	0,000	0,000	0,014	0,000	0,000	0,000	0,000
Total (apfu)	17	17	17	17	17	17	17	17	17	17	17	17

e. Pentlandite 5

Sample - IMK - 05149

Lithology	Serpentinised pyroxenite										
File	Z1_Heaz	Z1_Heaz	Z1_Heaz	Z4_Heaz	Z4_Heaz	Z4_Heaz	Z4_Pent	Z4_Pent	Z4_Pent	Z5_Heaz	Z5_Heaz
Analyses ID	1	2	3	15	16	17	1	2	4	12	20
Au	b.d.l	b.d.l	b.d.l	b.d.l	b.d.l	b.d.l	b.d.l	b.d.l	0,03	0,03	0,05
Ag	0,02	b.d.l	b.d.l	b.d.l	0,01	b.d.l	b.d.l	b.d.l	0,01	0,02	0,00
Mo	0,09	0,10	0,05	0,10	0,08	0,07	0,13	0,09	0,04	0,13	0,04
S	33,67	33,49	33,49	33,59	32,03	33,35	33,45	33,38	33,39	33,53	33,22
Ni	36,86	36,25	36,46	36,13	32,14	35,77	35,89	36,36	36,18	35,26	36,50
Fe	24,15	25,43	25,31	25,25	22,64	26,14	25,83	25,52	24,98	24,64	23,74
Co	4,72	3,70	3,78	4,26	4,43	3,73	3,67	3,86	3,98	4,88	3,08
Cu	b.d.l	b.d.l	b.d.l	b.d.l	0,87	b.d.l	b.d.l	b.d.l	0,01	b.d.l	0,28
Total (wt%)	99,66	99,52	99,47	99,48	92,41	99,22	99,13	99,42	98,78	98,67	97,03
Atomic proportions (apfu) in the base of 17 atoms											
Au	0,000	0,000	0,000	0,000	0,000	0,000	0,000	0,000	0,001	0,001	0,002
Ag	0,001	0,000	0,000	0,000	0,000	0,000	0,000	0,000	0,001	0,002	0,000
Mo	0,007	0,008	0,004	0,004	0,004	0,004	0,010	0,007	0,003	0,010	0,004
S	8,141	8,123	8,115	8,115	8,115	8,115	8,127	8,099	8,141	8,179	8,225
Ni	4,868	4,802	4,825	4,825	4,825	4,825	4,764	4,818	4,818	4,698	4,936
Fe	3,352	3,541	3,521	3,521	3,521	3,521	3,603	3,554	3,497	3,451	3,374
Co	0,621	0,488	0,499	0,499	0,499	0,499	0,485	0,509	0,528	0,648	0,415
Cu	0,000	0,000	0,000	0,000	0,000	0,000	0,000	0,000	0,001	0,000	0,035
Total (apfu)	17	17	17	17	17	17	17	17	17	17	17

a. Pyrrhotite 1

Sample - IMK - 05139

Lithology	Coarse-grained orthopyroxenite												
File	A_Z1_Pent	A_Z1_Pent	A_Z1_Pent	A_Z1_Pent	A_Z1_Pent	A_Z1_Pent	A_Z1_Pent	A_Z1_Pent	A_Z1_Pent	A_Z2_Pent	A_Z2_Pent	A_Z2_Pent	A_Z3_Pent
Analyses ID	2	4	5	7	14	16	17	19	23	3	4	14	10
Au	0,02	b.d.l	b.d.l	b.d.l	0,04	b.d.l	0,01	0,02	b.d.l	0,05	0,04	0,01	0,04
Ag	0,02	b.d.l	b.d.l	b.d.l	0,01	b.d.l	b.d.l	b.d.l	b.d.l	b.d.l	b.d.l	b.d.l	b.d.l
Mo	0,12	0,11	0,11	0,11	0,08	0,11	0,08	0,10	0,08	0,05	0,08	0,11	0,11
S	36,51	36,87	36,15	36,58	36,40	36,66	36,43	36,15	36,73	36,67	36,46	35,35	36,19
Ni	6,20	5,58	4,74	5,09	5,99	5,08	5,17	6,86	5,11	5,32	5,04	8,96	8,82
Fe	56,11	57,00	53,67	56,03	56,47	57,20	56,81	55,27	57,06	56,79	55,96	53,34	53,54
Co	0,76	0,67	0,61	0,65	0,41	0,54	0,66	0,65	0,60	0,75	0,51	0,58	0,52
Cu	b.d.l	b.d.l	4,21	0,69	0,11	b.d.l	b.d.l	b.d.l	b.d.l	b.d.l	0,36	b.d.l	b.d.l
Total (wt%)	99,83	100,41	99,54	99,26	99,60	99,89	99,25	99,29	99,82	99,73	98,52	98,53	99,33
Atomic proportions (apfu) in the base of 2 atoms													
Au	0,000	0,000	0,000	0,000	0,000	0,000	0,000	0,000	0,000	0,000	0,000	0,000	0,000
Ag	0,000	0,000	0,000	0,000	0,000	0,000	0,000	0,000	0,000	0,000	0,000	0,000	0,000
Mo	0,001	0,001	0,001	0,001	0,001	0,001	0,001	0,001	0,001	0,000	0,001	0,001	0,001
S	1,006	1,009	1,003	1,012	1,005	1,009	1,008	1,003	1,011	1,010	1,015	0,992	1,004
Ni	0,093	0,083	0,072	0,077	0,090	0,076	0,078	0,104	0,077	0,080	0,077	0,137	0,134
Fe	0,887	0,896	0,855	0,890	0,895	0,904	0,902	0,880	0,901	0,898	0,894	0,859	0,852
Co	0,011	0,010	0,009	0,010	0,006	0,008	0,010	0,010	0,009	0,011	0,008	0,009	0,008
Cu	0,000	0,000	0,059	0,010	0,001	0,000	0,000	0,000	0,000	0,000	0,005	0,000	0,000
Total (apfu)	2	2	2	2	2	2	2	2	2	2	2	2	2

b. Pyrrhotite 2

Sample - IMK - 05139

Lithology	Coarse-grained orthopyroxenite
File	A_Z3_Pent
Analyses ID	12
Au	b.d.l
Ag	b.d.l
Mo	0,08
S	36,29
Ni	8,63
Fe	53,84
Co	0,51
Cu	0,70
Total (wt%)	100,07

Atomic proportions (apfu) in the base of 2 atoms

Au	0,000
Ag	0,000
Mo	0,001
S	1,000
Ni	0,130
Fe	0,852
Co	0,008
Cu	0,010
Total (apfu)	2

a. Mackinawite 1

Sample - IMK - 05139

Lithology	Coarse-grained orthopyroxenite		
File	A_Z1_Pent	A_Z1_Pent	A_Z4_Pent
Analyses ID	1	12	8
Au	b.d.l	b.d.l	b.d.l
Ag	0,03	0,04	b.d.l
Mo	0,08	0,06	0,11
S	35,86	34,65	34,54
Ni	15,77	14,29	17,99
Fe	47,37	47,87	44,93
Co	0,94	0,96	0,84
Cu	b.d.l	b.d.l	b.d.l
Total (wt%)	100,15	97,95	98,47

Atomic proportions (apfu) in the base of 2 atoms

Au	0,000	0,000	0,000
Ag	0,000	0,000	0,000
Mo	0,001	0,001	0,001
S	0,993	0,983	0,977
Ni	0,238	0,221	0,278
Fe	0,753	0,779	0,730
Co	0,014	0,015	0,013
Cu	0,000	0,000	0,000
Total (apfu)	2	2	2

a. Heazlewoodite 1

Sample - IMK - 05149

Lithology	Serpentinised pyroxenite												
File	Z1_Heaz	Z1_Heaz	Z1_Heaz	Z4_Heaz	Z4_Heaz	Z4_Heaz	Z4_Heaz	Z4_Heaz	Z4_Heaz	Z4_Heaz	Z4_Heaz	Z4_Heaz	Z4_Heaz
Analyses ID	1	2	3	2	3	4	5	6	7	8	9	10	11
Au	b.d.l	b.d.l	0,01	b.d.l	b.d.l	b.d.l	0,03	0,04	b.d.l	b.d.l	b.d.l	b.d.l	0,04
Ag	0,00	0,02	0,01	0,06	0,01	0,07	b.d.l	0,03	b.d.l	b.d.l	b.d.l	b.d.l	b.d.l
Mo	0,10	0,16	0,08	0,09	0,08	0,05	0,08	0,09	0,07	0,10	0,05	0,09	0,11
S	27,49	27,43	27,51	27,53	27,40	27,54	27,43	27,47	27,72	27,74	27,66	27,82	27,43
Ni	70,91	70,96	71,56	70,20	72,16	71,90	70,82	71,36	70,92	71,35	71,45	71,89	71,50
Fe	0,03	0,04	0,01	0,21	0,65	0,62	0,30	0,22	0,18	0,11	0,08	0,16	0,14
Co	b.d.l	b.d.l	b.d.l	0,01	0,04	0,02	b.d.l	b.d.l	b.d.l	b.d.l	b.d.l	0,00	0,01
Te	0,10	0,12	0,10	0,17	0,09	0,17	0,13	0,07	0,13	0,11	0,14	0,12	0,16
Total (wt%)	98,77	98,87	99,51	98,35	100,49	100,51	98,89	99,32	99,12	99,57	99,37	100,28	99,54
Atomic proportions (apfu) in the base of 5 atoms													
Au	0,000	0,000	0,000	0,000	0,000	0,000	0,000	0,000	0,000	0,000	0,000	0,000	0,000
Ag	0,000	0,001	0,000	0,001	0,000	0,002	0,000	0,001	0,000	0,000	0,000	0,000	0,000
Mo	0,003	0,004	0,002	0,002	0,002	0,001	0,002	0,002	0,002	0,002	0,001	0,002	0,003
S	2,072	2,067	2,061	2,082	2,036	2,046	2,067	2,061	2,079	2,074	2,071	2,067	2,056
Ni	2,919	2,921	2,928	2,900	2,929	2,917	2,914	2,924	2,907	2,914	2,922	2,917	2,927
Fe	0,001	0,002	0,001	0,009	0,028	0,026	0,013	0,009	0,008	0,005	0,003	0,007	0,006
Co	0,000	0,000	0,000	0,000	0,001	0,001	0,000	0,000	0,000	0,000	0,000	0,000	0,000
Te	0,002	0,002	0,002	0,003	0,002	0,003	0,002	0,001	0,002	0,002	0,003	0,002	0,003
Total (apfu)	5	5	5	5	5	5	5	5	5	5	5	5	5

b. Heazlewoodite 2

Sample - IMK - 05139

Lithology	Coarse-grained orthopyroxenite												
File	Z4_Heaz	Z4_Heaz	Z4_Heaz	Z4_Heaz	Z4_Heaz	Z4_Heaz	Z4_Heaz	Z4_Heaz	Z4_Heaz	Z4_Heaz	Z4_Heaz	Z4_Heaz	Z4_Heaz
Analyses ID	12	13	14	18	19	20	22	23	24	24	3	2	4
Au	b.d.l	b.d.l	b.d.l	b.d.l	b.d.l	0,00	b.d.l	0,02	b.d.l	b.d.l	b.d.l	0,01	b.d.l
Ag	0,01	0,04	0,03	0,00	b.d.l	b.d.l	b.d.l	b.d.l	0,02	0,02	0,02	b.d.l	0,00
Mo	0,06	0,11	0,10	0,15	0,07	0,06	0,09	0,08	0,14	0,14	0,09	0,07	0,08
S	27,71	27,46	27,52	27,26	27,73	27,49	27,55	27,84	27,84	27,84	27,32	27,37	27,45
Ni	70,49	71,54	70,18	71,05	71,18	71,20	70,77	71,54	71,41	71,41	71,66	69,82	71,32
Fe	0,14	0,07	0,40	0,40	0,31	0,36	0,19	0,22	0,24	0,24	0,89	0,35	0,02
Co	0,02	b.d.l	0,01	b.d.l	b.d.l	b.d.l	b.d.l	b.d.l	0,01	0,01	0,01	b.d.l	b.d.l
Te	0,14	0,08	0,15	0,17	0,18	0,16	0,16	0,16	0,11	0,11	0,13	0,13	0,16
Total (wt%)	98,65	99,47	98,41	99,10	99,53	99,40	98,89	100,05	99,80	99,80	100,22	97,88	99,16
Atomic proportions (apfu) in the base of 5 atoms													
Au	0,000	0,000	0,000	0,000	0,000	0,000	0,000	0,000	0,000	0,000	0,000	0,000	0,000
Ag	0,000	0,001	0,001	0,000	0,000	0,000	0,000	0,000	0,000	0,000	0,000	0,000	0,000
Mo	0,001	0,003	0,002	0,004	0,002	0,001	0,002	0,002	0,003	0,003	0,002	0,002	0,002
S	2,087	2,059	2,079	2,052	2,073	2,061	2,073	2,072	2,075	2,075	2,036	2,080	2,063
Ni	2,900	2,930	2,896	2,922	2,907	2,916	2,909	2,909	2,908	2,908	2,917	2,898	2,928
Fe	0,006	0,003	0,018	0,017	0,013	0,015	0,008	0,009	0,010	0,010	0,038	0,015	0,001
Co	0,001	0,000	0,000	0,000	0,000	0,000	0,000	0,000	0,001	0,001	0,000	0,000	0,000
Te	0,003	0,002	0,003	0,003	0,003	0,003	0,003	0,003	0,002	0,002	0,002	0,002	0,003
Total (apfu)	5	5	5	5	5	5	5	5	5	5	5	5	5

c. Heazlewoodite 3

Sample - IMK - 05139

Lithology	Coarse-grained orthopyroxenite										
File	Z4_Heaz	Z4_Heaz	Z4_Heaz	Z4_Heaz	Z4_Heaz	Z4_Heaz	Z4_Heaz	Z4_Heaz	Z4_Heaz	Z4_Heaz	Z4_Heaz
Analyses ID	5	6	7	8	9	10	11	13	15	16	18
Au	b.d.l	b.d.l	b.d.l	b.d.l	b.d.l	b.d.l	0,01	0,04	b.d.l	0,03	0,00
Ag	0,00	b.d.l	0,01	0,01	0,05	0,02	0,03	b.d.l	0,04	0,02	b.d.l
Mo	0,09	0,11	0,08	0,05	0,10	0,09	0,08	0,13	0,12	0,06	0,11
S	27,25	27,46	27,38	27,52	27,45	27,37	27,63	27,56	27,37	27,36	27,49
Ni	70,83	70,65	70,23	70,96	70,64	70,82	70,62	70,35	70,03	69,91	70,30
Fe	0,09	0,07	0,22	0,12	0,30	0,02	0,05	0,09	0,05	0,17	0,36
Co	b.d.l	b.d.l	0,01	b.d.l	0,02	0,02	b.d.l	b.d.l	b.d.l	0,00	b.d.l
Te	0,11	0,08	0,10	0,12	0,12	0,19	0,16	0,14	0,11	0,10	0,13
Total (wt%)	98,59	98,49	98,13	98,88	98,95	98,65	98,66	98,36	97,90	97,78	98,50
Atomic proportions (apfu) in the base of 5 atoms											
Au	0,000	0,000	0,000	0,000	0,000	0,000	0,000	0,000	0,000	0,000	0,000
Ag	0,000	0,000	0,000	0,000	0,001	0,000	0,001	0,000	0,001	0,000	0,000
Mo	0,002	0,003	0,002	0,001	0,002	0,002	0,002	0,003	0,003	0,001	0,003
S	2,060	2,074	2,075	2,071	2,067	2,067	2,082	2,083	2,080	2,081	2,076
Ni	2,925	2,915	2,908	2,917	2,906	2,921	2,907	2,905	2,907	2,904	2,900
Fe	0,004	0,003	0,010	0,005	0,013	0,001	0,002	0,004	0,002	0,008	0,015
Co	0,000	0,000	0,000	0,000	0,001	0,001	0,000	0,000	0,000	0,000	0,000
Te	0,002	0,002	0,002	0,002	0,002	0,004	0,003	0,003	0,002	0,002	0,003
Total (apfu)	5	5	5	5	5	5	5	5	5	5	5

d. Heazlewoodite 4

Sample - IMK - 05153

Lithology	Serpentinised pyroxenite												
File	B_Z1_Heaz	B_Z1_Heaz	B_Z1_Heaz	B_Z1_Heaz	B_Z1_Heaz	B_Z1_Heaz	B_Z1_Heaz	B_Z1_Heaz	B_Z2_Heaz	B_Z2_Heaz	B_Z2_Heaz	B_Z2_Heaz	B_Z2_Heaz
Analyses ID	4	5	6	7	8	12	15	16	2	4	8	10	19
Au	b.d.l	0,03	b.d.l	0,03	b.d.l	0,01	b.d.l	b.d.l	b.d.l	b.d.l	0,02	b.d.l	b.d.l
Ag	b.d.l	b.d.l	b.d.l	0,04	0,02	b.d.l	0,03	0,03	0,02	b.d.l	b.d.l	b.d.l	b.d.l
Mo	0,09	0,08	0,06	b.d.l	0,07	0,06	0,07	0,08	0,10	0,10	0,10	0,03	0,04
S	27,34	27,63	27,65	26,93	27,70	27,45	27,86	27,39	27,59	27,58	26,79	27,33	27,72
Ni	70,66	72,30	72,93	69,53	72,75	71,37	71,85	72,13	72,43	72,40	71,42	72,64	72,63
Fe	0,02	0,03	0,12	4,18	1,18	0,71	0,33	0,04	0,54	0,17	1,11	0,31	0,65
Co	b.d.l	b.d.l	0,01	b.d.l	0,02	0,02	0,02	0,03	0,06	0,09	0,06	0,11	0,11
Te	0,12	0,12	0,18	0,13	0,14	0,15	0,05	0,15	0,12	0,17	0,13	0,12	0,18
Total (wt%)	98,31	100,38	101,04	100,99	102,05	99,90	100,24	100,00	100,89	100,69	99,69	100,57	101,50
Atomic proportions (apfu) in the base of 5 atoms													
Au	0,000	0,008	0,000	0,008	0,000	0,001	0,000	0,000	0,000	0,000	0,005	0,000	0,000
Ag	0,000	0,000	0,000	0,019	0,008	0,000	0,014	0,011	0,008	0,001	0,000	0,002	0,000
Mo	0,047	0,041	0,029	0,002	0,036	0,030	0,035	0,038	0,051	0,049	0,052	0,016	0,017
S	41,409	41,084	40,864	39,950	40,583	40,997	41,352	40,912	40,820	40,918	40,243	40,609	40,794
Ni	58,453	58,735	58,883	56,343	58,219	58,221	58,261	58,844	58,538	58,671	58,615	58,953	58,386
Fe	0,013	0,028	0,101	3,559	0,989	0,610	0,280	0,037	0,455	0,146	0,955	0,268	0,553
Co	0,000	0,000	0,009	0,000	0,013	0,012	0,015	0,027	0,048	0,076	0,052	0,085	0,089
Te	0,044	0,044	0,066	0,048	0,053	0,057	0,018	0,056	0,043	0,063	0,048	0,045	0,067
Total (apfu)	100	100	100	100	100	100	100	100	100	100	100	100	100

e. Heazlewoodite 5

Sample - IMK - 05153

Lithology	Serpentinised pyroxenite	
File	B_Z2_Heaz	B_Z2_Heaz
Analyses ID	21	25
Au	0,03	0,02
Ag	b.d.l	0,01
Mo	0,11	0,08
S	27,68	27,57
Ni	72,94	73,53
Fe	0,79	0,07
Co	0,14	0,05
Te	0,19	0,13
Total (wt%)	101,99	101,56

Atomic proportions (apfu) in the base of 5 atoms

Au	0,007	0,004
Ag	0,000	0,006
Mo	0,055	0,039
S	40,589	40,602
Ni	58,431	59,153
Fe	0,666	0,063
Co	0,111	0,040
Te	0,069	0,047
Total (apfu)	100	100

f. Heazlewoodite 6

Sample - IMK - 05156

Lithology	Serpentinised harzburgite	
File	05156_Mauch	05156_Mauch
Analyses ID	22	23
Au	b.d.l	b.d.l
Ag	b.d.l	0,01
Mo	0,08	0,12
S	26,42	27,13
Ni	70,06	69,84
Fe	0,25	0,16
Co	b.d.l	b.d.l
Te	0,18	0,16
Total (wt%)	97,08	97,50
Atomic proportions (apfu) in the base of 5 atoms		
Au	0,000	0,008
Ag	0,000	0,000
Mo	0,047	0,041
S	41,409	41,084
Ni	58,453	58,735
Fe	0,013	0,028
Co	0,000	0,000
Te	0,044	0,044
Total (apfu)	100	100

I. Chalcocite 1

Sample - IMK - 05149

Lithology	Serpentinised pyroxenite				
File	Z3_Cc	Z3_Cc	Z3_Cc	Z5_Heaz	Z5_Heaz
Analyses ID	1	2	3	19	21
Au	0,02	0,01	b.d.l	b.d.l	0,01
Ag	0,08	0,01	b.d.l	b.d.l	b.d.l
Mo	0,09	0,12	0,05	0,10	0,05
S	21,51	21,50	21,51	21,20	21,25
Ni	0,73	0,65	0,59	0,01	0,04
Fe	0,75	0,38	0,64	0,42	0,53
Co	0,39	0,13	0,15	b.d.l	0,02
Cu	77,34	77,80	77,03	76,71	77,29
Total (wt%)	101,14	100,98	100,40	98,51	99,37

Atomic proportions (apfu) in the base of 3 atoms

Au	0,000	0,000	0,000	0,000	0,000
Ag	0,001	0,000	0,000	0,000	0,000
Mo	0,001	0,002	0,001	0,002	0,001
S	1,046	1,047	1,052	1,056	1,051
Ni	0,019	0,017	0,016	0,000	0,001
Fe	0,021	0,011	0,018	0,012	0,015
Co	0,010	0,003	0,004	0,000	0,000
Cu	1,897	1,912	1,901	1,928	1,928
Total (apfu)	3	3	3	3	3

I. Samaniite 1

Sample - IMK - 05139	
Lithology	Coarse-grained orthopyroxenite
File	A_Z3_Pent
Analyses ID	21
Au	b.d.l
Ag	b.d.l
Mo	0,07
S	34,50
Ni	19,59
Fe	33,62
Co	0,53
Cu	11,32
Total (wt%)	99,78

	Atomic proportions (apfu) in the base of 17 atoms
Au	0,000
Ag	0,000
Mo	0,005
S	8,311
Ni	2,578
Fe	4,649
Co	0,069
Cu	1,375
Total (apfu)	17

I. Awaruite 1

Sample - IMK - 05153

Lithology	Serpentinised pyroxenite												
File	B_Z1_Heaz	B_Z1_Heaz	B_Z1_Heaz	B_Z2_Heaz	B_Z2_Heaz	B_Z2_Heaz	B_Z2_Heaz	B_Z2_Heaz	B_Z2_Heaz	B_Z2_Heaz	B_Z2_Heaz	B_Z2_Heaz	B_Z2_Heaz
Analyses ID	9	10	13	3	5	6	9	11	12	13	16	17	18
Au	0,02	b.d.l	b.d.l	0,02	0,01	b.d.l	b.d.l	b.d.l	b.d.l	b.d.l	b.d.l	0,02	b.d.l
Ag	b.d.l	b.d.l	b.d.l	b.d.l	b.d.l	b.d.l	0,07	0,01	0,04	b.d.l	b.d.l	b.d.l	0,04
Mo	b.d.l	0,03	b.d.l	b.d.l	b.d.l	b.d.l	b.d.l	b.d.l	0,02	b.d.l	b.d.l	b.d.l	b.d.l
S	1,69	1,05	0,00	0,01	0,14	0,74	0,04	0,01	0,01	0,10	0,04	0,03	0,03
Ni	74,51	74,68	74,95	74,37	74,59	75,18	74,05	75,04	75,62	75,62	74,93	75,74	75,27
Fe	23,00	24,04	24,11	24,00	24,57	24,10	24,50	24,73	24,58	24,87	24,66	24,35	23,98
Co	0,45	0,48	0,18	0,75	0,31	0,25	0,41	0,47	0,31	0,45	0,47	0,52	0,36
Te	0,11	0,09	0,08	0,16	0,14	0,12	0,13	0,11	0,14	0,08	0,09	0,15	0,09
Cu	0,43	0,55	0,58	0,65	0,42	0,48	0,53	0,60	0,20	0,72	0,60	0,45	0,49
Total (wt%)	100,29	101,06	100,01	100,25	100,43	101,00	99,79	101,18	101,04	102,10	100,97	101,42	100,40
Atomic proportions (apfu) in the base of 4 atoms													
Au	0,000	0,000	0,000	0,000	0,000	0,000	0,000	0,000	0,000	0,000	0,000	0,000	0,000
Ag	0,000	0,000	0,000	0,000	0,000	0,000	0,001	0,000	0,001	0,000	0,000	0,000	0,001
Mo	0,000	0,001	0,000	0,000	0,000	0,000	0,000	0,000	0,000	0,000	0,000	0,000	0,000
S	0,120	0,074	0,000	0,000	0,010	0,053	0,003	0,001	0,001	0,007	0,003	0,002	0,002
Ni	2,902	2,900	2,965	2,939	2,937	2,929	2,936	2,935	2,961	2,930	2,936	2,955	2,967
Fe	0,941	0,981	1,002	0,997	1,017	0,987	1,021	1,016	1,012	1,013	1,016	0,999	0,993
Co	0,017	0,019	0,007	0,030	0,012	0,010	0,016	0,018	0,012	0,017	0,018	0,020	0,014
Te	0,002	0,002	0,002	0,003	0,003	0,002	0,002	0,002	0,003	0,001	0,002	0,003	0,002
Cu	0,016	0,020	0,021	0,024	0,015	0,017	0,020	0,022	0,007	0,026	0,022	0,016	0,018
Total (apfu)	4	4	4	4	4	4	4	4	4	4	4	4	4

II. Awaruite 2

Sample - IMK - 05153

Lithology	Serpentinised pyroxenite					
File	B_Z2_Heaz	B_Z2_Heaz	B_Z2_Heaz	B_Z2_Heaz	B_Z2_Heaz	B_Z2_Heaz
Analyses ID	20	22	23	29	31	32
Au	b.d.l	b.d.l	0,00	b.d.l	b.d.l	0,05
Ag	0,02	b.d.l	0,05	b.d.l	0,03	b.d.l
Mo	0,01	b.d.l	0,03	b.d.l	b.d.l	0,01
S	0,01	b.d.l	0,01	0,02	0,01	0,01
Ni	74,87	75,25	75,11	74,83	74,83	74,79
Fe	25,09	24,31	24,88	24,47	24,41	25,25
Co	0,18	0,38	0,23	0,30	0,27	0,29
Te	0,12	0,11	0,08	0,13	0,13	0,12
Cu	0,48	0,54	0,49	0,52	0,50	0,36
Total (wt%)	100,96	100,80	101,17	100,69	100,45	101,06
	Atomic proportions (apfu) in the base of 4 atoms					
Au	0,000	0,000	0,000	0,000	0,000	0,001
Ag	0,000	0,000	0,001	0,000	0,001	0,000
Mo	0,000	0,000	0,001	0,000	0,000	0,000
S	0,001	0,000	0,001	0,002	0,001	0,001
Ni	2,933	2,954	2,937	2,943	2,949	2,928
Fe	1,033	1,003	1,023	1,011	1,011	1,039
Co	0,007	0,015	0,009	0,012	0,010	0,011
Te	0,002	0,002	0,001	0,002	0,002	0,002
Cu	0,017	0,020	0,018	0,019	0,018	0,013
Total (apfu)	4	4	4	4	4	4

I. Maucherite 1

Sample - IMK - 05139			
Lithology	Coarse-grained orthopyroxenite		
File	A_Z1_Pent	A_Z1_Pent	A_Z3_Pent
Analyses ID	28	30	22
Au	b.d.l	b.d.l	0,01
Ag	0,03	0,03	0,02
Mo	0,03	0,03	0,02
As	49,72	47,70	48,88
S	0,18	0,40	1,12
Ni	50,70	48,29	50,28
Fe	1,14	1,87	1,60
Sb	0,72	0,65	0,67
Co	0,70	0,70	0,91
Te	0,13	0,07	0,08
Cu	0,22	0,85	1,03
Total (wt%)	103,62	100,77	104,88
	Atomic proportions (apfu) in the base of 19 atoms		
Au	0,000	0,000	0,000
Ag	0,004	0,004	0,003
Mo	0,004	0,003	0,002
As	7,996	7,864	7,688
S	0,066	0,152	0,412
Ni	10,408	10,164	10,094
Fe	0,247	0,414	0,337
Sb	0,071	0,066	0,065
Co	0,144	0,147	0,181
Te	0,012	0,006	0,007
Cu	0,042	0,165	0,190
Total (apfu)	19	19	19

I. Orcelite 1

Sample - IMK - 05153

Lithology	Serpentinised pyroxenite	
File	B_Z2_Heaz	B_Z2_Heaz
Analyses ID	1	26
Au	b.d.l	b.d.l
Ag	b.d.l	b.d.l
Mo	0,02	b.d.l
As	30,82	32,06
S	0,10	0,09
Ni	67,67	67,73
Fe	0,11	0,34
Sb	3,37	2,64
Co	b.d.l	b.d.l
Te	0,12	0,05
Cu	b.d.l	b.d.l
Total (wt%)	102,21	102,93

Atomic proportions (apfu) in the base of 7 atoms

Au	0,000	0,000
Ag	0,000	0,000
Mo	0,001	0,000
As	1,802	1,857
S	0,013	0,012
Ni	5,050	5,008
Fe	0,008	0,026
Sb	0,121	0,094
Co	0,000	0,000
Te	0,004	0,002
Cu	0,000	0,000
Total (apfu)	7	7

II. Orcelite 2

Sample - IMK - 05156

Lithology	Serpentinised harzburgite									
File	05156_Mauch	05156_Mauch	05156_Mauch	05156_Mauch	05156_Mauch	05156_Mauch	05156_Mauch	05156_Mauch	05156_Mauch	05156_Mauch
Analyses ID	5	6	7	8	10	15	16	17	18	24
Au	0,04	0,05	b.d.l	b.d.l	b.d.l	0,09	0,04	b.d.l	b.d.l	0,01
Ag	b.d.l	b.d.l	0,02	b.d.l	b.d.l	b.d.l	0,01	0,02	b.d.l	0,01
Mo	0,02	b.d.l	b.d.l	b.d.l	b.d.l	b.d.l	0,03	b.d.l	b.d.l	0,01
As	33,82	34,87	33,84	37,21	33,94	34,56	36,09	33,80	37,43	36,88
S	0,03	0,03	0,02	0,03	0,01	0,03	0,02	0,01	0,02	0,02
Ni	68,79	65,92	64,39	64,09	66,07	66,16	64,48	66,22	63,97	63,05
Fe	b.d.l	0,05	0,01	0,01	0,04	0,06	b.d.l	0,02	0,01	b.d.l
Sb	1,00	0,97	0,64	0,60	0,84	0,67	0,48	0,68	0,47	0,90
Co	b.d.l	b.d.l	b.d.l	b.d.l	b.d.l	b.d.l	b.d.l	b.d.l	b.d.l	b.d.l
Te	0,01	0,18	0,15	0,04	0,16	0,13	0,12	0,17	0,10	0,11
Cu	b.d.l	b.d.l	b.d.l	b.d.l	b.d.l	b.d.l	b.d.l	b.d.l	b.d.l	b.d.l
Total (wt%)	103,76	102,13	99,23	102,00	101,16	101,77	101,32	100,96	102,05	101,15

Atomic proportions (apfu) in the base of 7 atoms

Au	0,001	0,001	0,000	0,000	0,000	0,002	0,001	0,000	0,000	0,000
Ag	0,000	0,000	0,001	0,000	0,000	0,000	0,000	0,001	0,000	0,000
Mo	0,001	0,000	0,000	0,000	0,000	0,000	0,002	0,000	0,000	0,000
As	1,934	2,036	2,031	2,180	1,996	2,020	2,124	1,989	2,192	2,185
S	0,004	0,004	0,002	0,004	0,002	0,004	0,002	0,001	0,002	0,002
Ni	5,023	4,913	4,932	4,792	4,959	4,937	4,846	4,975	4,782	4,768
Fe	0,000	0,004	0,000	0,001	0,003	0,005	0,000	0,002	0,001	0,000
Sb	0,035	0,035	0,024	0,022	0,031	0,024	0,017	0,025	0,017	0,033
Co	0,000	0,000	0,000	0,000	0,000	0,000	0,000	0,000	0,000	0,000
Te	0,000	0,006	0,005	0,002	0,006	0,004	0,004	0,006	0,003	0,004
Cu	0,000	0,000	0,000	0,000	0,000	0,000	0,000	0,000	0,000	0,000
Total (apfu)	7	7	7	7	7	7	7	7	7	7

I. Ni antimonide 1

Sample - IMK - 05153

Lithology	Serpentinised pyroxenite			
File	B_Z1_Heaz	B_Z1_Heaz	B_Z1_Heaz	B_Z2_Heaz
Analyses ID	1	2	3	7
Au	0,05	b.d.l	b.d.l	0,05
Ag	b.d.l	0,06	b.d.l	0,06
Mo	0,02	0,01	0,01	0,05
As	0,80	b.d.l	3,73	b.d.l
S	0,02	0,02	0,01	0,02
Ni	58,52	59,41	60,77	59,47
Fe	0,57	0,50	0,12	0,97
Sb	38,63	40,89	38,56	39,59
Co	b.d.l	b.d.l	b.d.l	b.d.l
Te	b.d.l	b.d.l	b.d.l	b.d.l
Cu	0,06	0,06	0,09	0,07
Total (wt%)	98,85	101,07	103,33	100,42

Atomic proportions (apfu) in the base of 4 atoms

Au	0,00	0,00	0,00	0,00
Ag	0,00	0,00	0,00	0,00
Mo	0,00	0,00	0,00	0,00
As	0,03	0,00	0,14	0,00
S	0,00	0,00	0,00	0,00
Ni	2,98	2,98	2,95	2,98
Fe	0,03	0,03	0,01	0,05
Sb	0,95	0,99	0,90	0,96
Co	0,00	0,00	0,00	0,00
Te	0,00	0,00	0,00	0,00
Cu	0,00	0,00	0,00	0,00
Total (apfu)	4,00	4,00	4,00	4,00

I. Parkerite 1

Sample - IMK - 05149

Lithology	Serpentinised pyroxenite		
File	05149_Z4_Mauc	05149_Z4_Mauc	05149_Z4_Mauc
Analyses ID	6	7	8
Bi	30,40	32,12	32,83
Pb	24,37	24,34	25,13
Au	b.d.l	b.d.l	b.d.l
Ag	0,11	b.d.l	b.d.l
S	9,10	9,53	10,17
Ni	27,20	27,86	28,36
Fe	0,46	0,29	0,46
Sb	6,00	2,63	0,74
Te	0,01	0,09	0,05
Cu	0,65	0,60	b.d.l
Total (wt%)	98,31	97,51	97,87

Atomic proportions (apfu) in the base of 19 atoms

Bi	0,943	0,995	1,004
Pb	0,763	0,761	0,775
Au	0,000	0,000	0,000
Ag	0,006	0,000	0,000
S	1,841	1,926	2,028
Ni	3,005	3,075	3,088
Fe	0,053	0,033	0,052
Sb	0,320	0,140	0,039
Te	0,001	0,004	0,003
Cu	0,066	0,061	0,000
Total (apfu)	7	7	7

I. Chromite 1

Sample - IMK - 05139

Lithology	Coarse-grained orthopyroxenite											
File	Z1_Chromite	Z1_Chromite	Z1_Chromite	Z1_Chromite	Z1_Chromite	Z3_Chromite	Z3_Chromite	Z3_Chromite	Z3_Chromite	Z4_Chromite	Z4_Chromite	Z4_Chromite
Analyses ID	1	2	3	4	5	1	2	3	3	1	2	3
Al2O3	6,87	7,40	7,15	6,82	6,98	15,78	10,34	16,66	16,66	1,94	18,29	18,99
MgO	2,89	2,96	2,98	3,03	3,64	7,81	5,62	12,02	12,02	2,65	12,15	11,69
MnO	b.d.l	b.d.l	b.d.l	b.d.l	b.d.l	b.d.l	b.d.l	b.d.l	b.d.l	b.d.l	b.d.l	b.d.l
V2O3	0,25	0,22	0,20	0,23	0,25	0,18	0,29	0,23	0,23	0,31	0,20	0,18
TiO2	0,69	0,52	0,72	0,51	0,42	0,17	0,61	0,17	0,17	0,36	0,23	0,18
ZnO	0,28	0,42	0,31	0,48	0,35	0,29	0,17	0,15	0,15	0,24	0,21	0,11
NiO	0,06	b.d.l	0,09	0,13	0,09	0,02	b.d.l	0,03	0,03	0,03	0,00	0,00
FeO	28,64	28,43	28,43	28,11	26,90	21,87	24,46	15,70	15,70	27,54	15,88	16,52
Cr2O3	58,24	55,90	57,88	58,02	59,30	51,21	55,76	52,38	52,38	65,14	50,41	49,72
Total (wt%)	97,93	95,86	97,77	97,33	97,93	97,32	97,25	97,33	97,33	98,20	97,36	97,39

Reconstitution with Fe partition

Al2O3	6,872	7,397	7,149	6,823	6,976	15,778	10,344	16,664	16,664	1,939	18,292	18,993
MgO	2,893	2,958	2,983	3,033	3,643	7,808	5,621	12,017	12,017	2,652	12,149	11,685
MnO	0,000	0,000	0,000	0,000	0,000	0,000	0,000	0,000	0,000	0,000	0,000	0,000
V2O3	0,246	0,220	0,203	0,232	0,254	0,178	0,292	0,232	0,232	0,314	0,195	0,175
TiO2	0,689	0,523	0,719	0,506	0,416	0,172	0,610	0,169	0,169	0,357	0,232	0,179
ZnO	0,282	0,421	0,309	0,475	0,351	0,287	0,165	0,147	0,147	0,241	0,205	0,110
NiO	0,060	0,002	0,094	0,129	0,085	0,021	0,000	0,025	0,025	0,025	0,000	0,000
FeO	28,396	27,517	28,219	27,584	26,924	21,645	24,653	15,463	15,463	27,873	15,558	16,420
Fe2O3	0,275	1,019	0,235	0,587	0,000	0,253	0,000	0,261	0,261	0,000	0,360	0,115
Cr2O3	58,240	55,901	57,882	58,024	59,301	51,206	55,760	52,376	52,376	65,137	50,405	49,721
Total (apfu)	97,953	95,958	97,793	97,393	97,950	97,348	97,445	97,354	97,354	98,538	97,396	97,397

II. Chromite 2

Sample - IMK - 05149

Lithology	Serpentinised pyroxenite					
File	Z3_Cromi	Z3_Cromi	Z3_Cromi	Z5_Cromi	Z5_Cromi	Z5_Cromi
Analyses ID	1	2	3	1	2	3
Al2O3	15,21	14,98	6,58	5,83	8,10	6,47
MgO	5,06	4,68	2,70	2,41	3,01	2,60
MnO	b.d.l	b.d.l	b.d.l	b.d.l	b.d.l	b.d.l
V2O3	0,31	0,28	0,31	0,40	0,35	0,39
TiO2	0,78	1,01	0,62	0,80	1,12	0,93
ZnO	0,23	0,21	0,32	0,39	0,42	0,31
NiO	0,42	0,38	0,56	0,12	0,19	0,13
FeO	30,57	32,07	32,33	33,53	34,39	32,97
Cr2O3	43,69	42,94	53,39	51,99	47,88	51,36
Total (wt%)	96,25	96,55	96,83	95,47	95,45	95,17
Reconstitution with Fe partition						
Al2O3	15,209	14,978	6,582	5,828	8,097	6,471
MgO	5,059	4,680	2,701	2,405	3,008	2,602
MnO	0,000	0,000	0,000	0,000	0,000	0,000
V2O3	0,305	0,281	0,314	0,396	0,353	0,394
TiO2	0,777	1,008	0,619	0,801	1,115	0,933
ZnO	0,227	0,213	0,323	0,393	0,415	0,308
NiO	0,419	0,380	0,564	0,122	0,190	0,132
FeO	25,791	26,710	27,847	28,302	27,966	28,178
Fe2O3	5,306	5,957	4,984	5,813	7,137	5,329
Cr2O3	43,688	42,938	53,393	51,991	47,882	51,358
Total (apfu)	96,782	97,145	97,327	96,050	96,163	95,705

III. Chromite 3

Sample - IMK - 05156

Lithology	Serpentinised harzburgite												
File	05156_chromite	05156_chromite	05156_chromite	05156_chromite	05156_chromite	05156_chromite	05156_chromite	05156_chromite	05156_chromite	05156_chromite	05156_chromite	05156_chromite	05156_chromite
Analyses ID	1	2	3	4	5	6	7	8	9	10	11	12	13
Al2O3	18,80	6,75	9,08	19,42	4,75	2,63	18,87	20,89	19,81	2,50	18,75	19,74	6,76
MgO	8,29	2,35	4,31	8,85	2,85	1,67	8,48	9,18	8,55	1,51	7,99	9,12	4,19
MnO	b.d.l	b.d.l	b.d.l	b.d.l	b.d.l	b.d.l	b.d.l	b.d.l	b.d.l	b.d.l	b.d.l	b.d.l	b.d.l
V2O3	0,16	0,20	0,24	0,13	0,38	0,21	0,18	0,17	0,15	0,23	0,15	0,14	0,28
TiO2	0,44	0,43	0,46	0,38	0,93	0,81	0,37	0,38	0,37	0,54	0,38	0,35	0,50
ZnO	0,24	0,63	0,39	0,33	0,54	0,42	0,33	0,39	0,30	0,71	0,20	0,30	0,21
NiO	0,05	0,00	0,09	0,05	0,20	0,11	0,09	0,06	0,08	0,15	0,03	0,03	0,13
FeO	22,63	32,15	29,06	21,53	38,34	52,46	22,09	21,69	22,22	43,51	23,14	21,24	28,34
Cr2O3	47,90	54,26	54,68	47,12	49,71	38,10	47,81	45,24	46,41	48,78	47,26	46,90	57,52
Total (wt%)	98,51	96,78	98,29	97,81	97,70	96,40	98,20	97,99	97,89	97,92	97,90	97,81	97,92
Reconstitution with Fe partition													
Al2O3	18,802	6,751	9,080	19,421	4,748	2,626	18,865	20,888	19,814	2,501	18,753	19,743	6,758
MgO	8,288	2,352	4,306	8,851	2,849	1,670	8,475	9,179	8,549	1,513	7,989	9,116	4,190
MnO	0,000	0,000	0,000	0,000	0,000	0,000	0,000	0,000	0,000	0,000	0,000	0,000	0,000
V2O3	0,163	0,201	0,235	0,126	0,382	0,211	0,176	0,167	0,151	0,226	0,145	0,136	0,277
TiO2	0,441	0,433	0,458	0,380	0,934	0,807	0,367	0,379	0,371	0,536	0,383	0,345	0,499
ZnO	0,240	0,634	0,385	0,330	0,540	0,420	0,332	0,389	0,300	0,714	0,204	0,301	0,210
NiO	0,047	0,000	0,088	0,047	0,196	0,110	0,086	0,057	0,076	0,151	0,025	0,034	0,131
FeO	22,040	28,461	26,449	20,914	28,249	29,817	21,476	20,651	21,459	29,668	22,304	20,568	26,280
Fe2O3	0,657	4,100	2,903	0,689	11,220	25,160	0,680	1,156	0,846	15,378	0,926	0,744	2,288
Cr2O3	47,899	54,259	54,678	47,123	49,705	38,097	47,813	45,243	46,406	48,778	47,261	46,898	57,520
Total (apfu)	98,577	97,191	98,582	97,881	98,822	98,918	98,270	98,109	97,973	99,465	97,991	97,886	98,153

IV. Chromite 4

Sample - IMK - 05156

Lithology	Serpentinised harzburgite												
File	05156_chromite	05156_chromite	05156_chromite	05156_chromite	05156_chromite	05156_chromite	05156_chromite	05156_chromite	05156_chromite	05156_chromite	05156_chromite	05156_chromite	05156_chromite
Analyses ID	14	15	16	17	18	20	21	22	23	24	25	26	27
Al2O3	18,94	4,50	18,60	19,95	3,64	19,93	18,61	18,32	5,75	18,55	19,56	17,58	18,39
MgO	9,37	1,94	9,66	9,44	1,85	8,32	8,63	8,51	2,49	8,52	8,83	9,22	10,62
MnO	b.d.l	b.d.l	b.d.l	b.d.l	b.d.l	b.d.l	b.d.l	b.d.l	b.d.l	b.d.l	b.d.l	b.d.l	b.d.l
V2O3	0,18	0,23	0,15	0,14	0,32	0,18	0,20	0,16	0,28	0,16	0,15	0,16	0,16
TiO2	0,33	0,74	0,30	0,38	0,89	0,36	0,33	0,36	0,47	0,33	0,37	0,32	0,29
ZnO	0,34	0,32	0,30	0,37	0,45	0,40	0,36	0,30	0,49	0,26	0,26	0,23	0,25
NiO	0,03	0,15	0,04	0,06	0,14	0,03	0,10	0,05	0,08	0,06	0,07	0,06	0,04
FeO	20,29	35,94	20,20	20,59	40,07	22,21	21,76	21,99	31,69	21,71	21,58	20,62	18,67
Cr2O3	47,96	53,06	48,30	46,70	49,80	46,33	47,73	47,80	56,18	47,11	46,10	49,48	48,87
Total (wt%)	97,44	96,88	97,55	97,62	97,15	97,75	97,70	97,48	97,43	96,68	96,91	97,66	97,29

Reconstitution with Fe partition

Al2O3	18,943	4,504	18,603	19,946	3,635	19,928	18,605	18,317	5,745	18,547	19,557	17,575	18,386
MgO	9,369	1,936	9,663	9,438	1,846	8,317	8,627	8,510	2,490	8,517	8,831	9,217	10,623
MnO	0,000	0,000	0,000	0,000	0,000	0,000	0,000	0,000	0,000	0,000	0,000	0,000	0,000
V2O3	0,181	0,225	0,151	0,140	0,322	0,180	0,203	0,162	0,280	0,159	0,147	0,162	0,157
TiO2	0,327	0,736	0,302	0,382	0,891	0,360	0,327	0,355	0,470	0,325	0,365	0,317	0,286
ZnO	0,335	0,324	0,298	0,372	0,453	0,396	0,355	0,297	0,489	0,257	0,260	0,234	0,254
NiO	0,034	0,153	0,035	0,061	0,137	0,032	0,098	0,052	0,083	0,059	0,070	0,060	0,040
FeO	19,878	29,288	19,435	19,987	29,546	21,723	20,978	21,165	28,373	20,936	20,712	20,032	17,867
Fe2O3	0,458	7,397	0,851	0,666	11,690	0,539	0,864	0,913	3,685	0,858	0,964	0,648	0,893
Cr2O3	47,956	53,059	48,300	46,699	49,800	46,329	47,729	47,796	56,184	47,108	46,095	49,478	48,869
Total (apfu)	97,482	97,622	97,638	97,691	98,320	97,804	97,787	97,566	97,799	96,766	97,002	97,723	97,375

V. Chromite 5

Sample - IMK - 05156

Lithology	Serpentinised harzburgite												
File	05156_chromite	05156_chromite	05156_chromite	05156_chromite	05156_chromite	05156_chromite	05156_chromite	05156_chromite	05156_chromite	05156_chromite	05156_chromite	05156_chromite	05156_chromite
Analyses ID	28	29	30	31	32	33	34	35	36	37	38	39	40
Al2O3	3,56	19,52	19,41	19,21	18,71	19,33	18,60	6,19	18,03	18,08	17,00	17,12	8,99
MgO	2,37	8,88	8,84	9,30	9,23	9,38	10,01	4,64	9,65	10,77	11,01	11,02	3,46
MnO	b.d.l	b.d.l	b.d.l	b.d.l	b.d.l	b.d.l	b.d.l	b.d.l	b.d.l	b.d.l	b.d.l	b.d.l	b.d.l
V2O3	0,37	0,19	0,17	0,15	0,13	0,15	0,16	0,35	0,17	0,14	0,12	0,15	0,30
TiO2	0,73	0,37	0,40	0,39	0,38	0,34	0,33	0,58	0,34	0,33	0,31	0,31	0,59
ZnO	0,60	0,22	0,32	0,32	0,29	0,17	0,19	0,23	0,20	0,15	0,30	0,10	0,34
NiO	0,10	0,07	0,08	0,08	0,05	0,07	0,04	0,10	0,03	0,02	0,02	0,09	0,13
FeO	39,78	21,70	21,53	20,55	20,74	20,15	19,64	28,86	20,04	18,04	17,55	17,64	30,21
Cr2O3	45,90	46,31	46,06	47,20	47,78	47,54	48,15	55,49	48,19	49,00	50,44	50,31	54,31
Total (wt%)	93,41	97,27	96,81	97,22	97,31	97,12	97,12	96,44	96,65	96,53	96,75	96,74	98,32

Reconstitution with Fe partition

Al2O3	3,561	19,522	19,408	19,214	18,713	19,334	18,604	6,187	18,027	18,082	17,001	17,117	8,993
MgO	2,373	8,883	8,838	9,301	9,225	9,378	10,012	4,639	9,651	10,773	11,013	11,022	3,457
MnO	0,000	0,000	0,000	0,000	0,000	0,000	0,000	0,000	0,000	0,000	0,000	0,000	0,000
V2O3	0,374	0,185	0,171	0,154	0,131	0,150	0,162	0,345	0,171	0,143	0,115	0,150	0,301
TiO2	0,734	0,373	0,404	0,394	0,381	0,339	0,328	0,582	0,336	0,327	0,305	0,312	0,590
ZnO	0,598	0,220	0,320	0,319	0,286	0,166	0,192	0,228	0,204	0,154	0,301	0,097	0,337
NiO	0,099	0,070	0,083	0,084	0,052	0,070	0,035	0,102	0,032	0,015	0,019	0,086	0,127
FeO	27,357	20,789	20,618	19,986	20,106	19,949	18,883	25,169	19,197	17,492	16,870	16,997	27,861
Fe2O3	13,801	1,013	1,015	0,627	0,703	0,218	0,840	4,105	0,936	0,607	0,758	0,712	2,609
Cr2O3	45,900	46,314	46,059	47,200	47,784	47,539	48,150	55,493	48,193	49,000	50,444	50,313	54,307
Total (apfu)	94,797	97,369	96,916	97,279	97,380	97,143	97,206	96,850	96,747	96,593	96,826	96,806	98,581

VI. Chromite 6

Sample - IMK - 05156

Lithology	Serpentinised harzburgite							
File	05156_chromite	05156_chromite	05156_chromite	05156_chromite	05156_chromite	05156_chromite	05156_chromite	05156_chromite
Analyses ID	41	42	43	44	45	46	47	48
Al2O3	16,96	6,41	19,11	18,82	8,55	21,01	18,71	9,38
MgO	10,71	2,88	9,87	10,07	2,97	9,07	8,46	3,25
MnO	b.d.l	b.d.l	b.d.l	b.d.l	b.d.l	b.d.l	b.d.l	b.d.l
V2O3	0,15	0,31	0,13	0,14	0,27	0,13	0,20	0,29
TiO2	0,30	0,54	0,33	0,29	0,48	0,38	0,52	0,59
ZnO	0,27	0,44	0,21	0,28	0,30	0,22	0,33	0,31
NiO	0,04	0,07	0,05	0,03	0,12	0,05	0,06	0,12
FeO	18,05	31,81	20,04	19,57	29,53	21,66	22,34	30,97
Cr2O3	50,56	54,22	47,61	47,82	54,86	45,03	46,73	52,09
Total (wt%)	97,02	96,66	97,35	97,02	97,07	97,55	97,35	97,00

Reconstitution with Fe partition

Al2O3	16,957	6,405	19,105	18,817	8,545	21,010	18,710	9,379
MgO	10,707	2,877	9,874	10,074	2,967	9,070	8,459	3,252
MnO	0,000	0,000	0,000	0,000	0,000	0,000	0,000	0,000
V2O3	0,148	0,306	0,128	0,139	0,272	0,130	0,200	0,289
TiO2	0,296	0,535	0,332	0,286	0,478	0,379	0,524	0,588
ZnO	0,267	0,435	0,210	0,282	0,299	0,219	0,334	0,312
NiO	0,038	0,068	0,045	0,031	0,115	0,048	0,060	0,121
FeO	17,421	27,783	19,225	18,676	28,055	20,851	21,379	27,865
Fe2O3	0,696	4,474	0,909	0,989	1,640	0,899	1,063	3,446
Cr2O3	50,560	54,220	47,610	47,823	54,863	45,031	46,725	52,093
Total (apfu)	97,090	97,103	97,438	97,117	97,233	97,637	97,453	97,344

Appendix VI. TIMA

I. Sample IMK – 05139 1

Sample IMK - 05139

Average maximum Ni deportment wt%	
Mineral phase names	**Ni deportment, wt%**
Pentlandite	80,18
Actinolite	4,40
Antigorite_HighAl_1	3,38
Actinolite_1_low_Ca_high_Mg	3,34
Pyrrhotite	2,20
Enstatite	2,19
Maucherite_3	0,85
Tremolite_1	0,84
Antigorite_8	0,81
Pyrrhotite_2	0,67
Antigorite_9 (9-Fe)	0,35
Biotite	0,20
Magnesiohastingsite	0,19
Chalcopyrite	0,14
Chromite	0,08
Antigorite_HighAl_2	0,08
Maucherite1	0,05
Magnesiohastingsite_2	0,04
Enstatite_3 (High Ca)	0,01
Maucherite_5	0,00
Total	100,00

Average minimum Ni deportment wt%	
Average minimum Ni deportment wt% per mineral groupings	
Grouping	**Ni deportment in grouping**
Pentlandite	87,20%
Pyrrhotite	3,12%
Arsenides	0,98%
Chalcopyrite	0,15%
Primary Silicates	1,60%
Secondary Silicates	6,87%
Oxides	0,09%
Total	100%

Average maximum Ni deportment wt%	
Average maximum Ni deportment wt% per mineral groupings	
Grouping	**Ni deportment in grouping**
Pentlandite	80,18%
Pyrrhotite	2,87%
Arsenides	0,90%
Chalcopyrite	0,14%
Primary Silicates	2,20%
Secondary Silicates	13,63%
Oxides	0,08%
Total	100%

II. Sample IMK – 05139 - 2

Sample IMK - 05139

Average maximum Ni deportment wt%	
Mineral phase names	**Ni deportment, wt%**
Pentlandite	80,18
Actinolite	4,40
Antigorite_HighAl_1	3,38
Actinolite_1_low_Ca_high_Mg	3,34
Pyrrhotite	2,20
Enstatite	2,19
Maucherite_3	0,85
Tremolite_1	0,84
Antigorite_8	0,81
Pyrrhotite_2	0,67
Antigorite_9 (9-Fe)	0,35
Biotite	0,20
Magnesiohastingsite	0,19
Chalcopyrite	0,14
Chromite	0,08
Antigorite_HighAl_2	0,08
Maucherite1	0,05
Magnesiohastingsite_2	0,04
Enstatite_3 (High Ca)	0,01
Maucherite_5	0,00
Total	100,00

Average minimum Ni deportment wt%	
Average minimum Ni deportment wt% per mineral groupings	
Grouping	**Ni deportment in grouping**
Pentlandite	87,20%
Pyrrhotite	3,12%
Arsenides	0,98%
Chalcopyrite	0,15%
Primary Silicates	1,60%
Secondary Silicates	6,87%
Oxides	0,09%
Total	100%

Average maximum Ni deportment wt%	
Average maximum Ni deportment wt% per mineral groupings	
Grouping	**Ni deportment in grouping**
Pentlandite	80,18%
Pyrrhotite	2,87%
Arsenides	0,90%
Chalcopyrite	0,14%
Primary Silicates	2,20%
Secondary Silicates	13,63%
Oxides	0,08%
Total	100%

III. Sample IMK – 05139 - 3

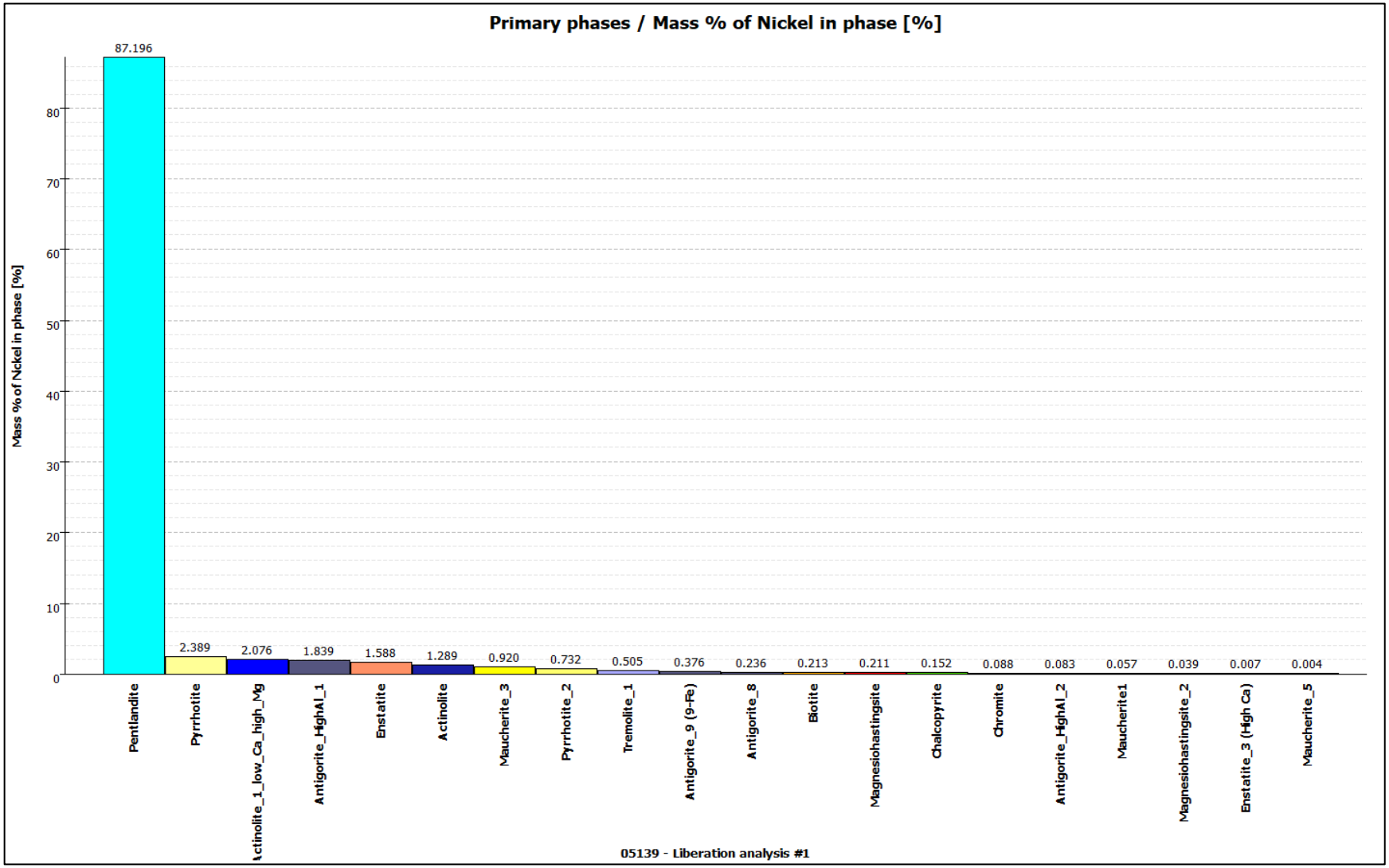

IV. Sample IMK – 05139 - 4

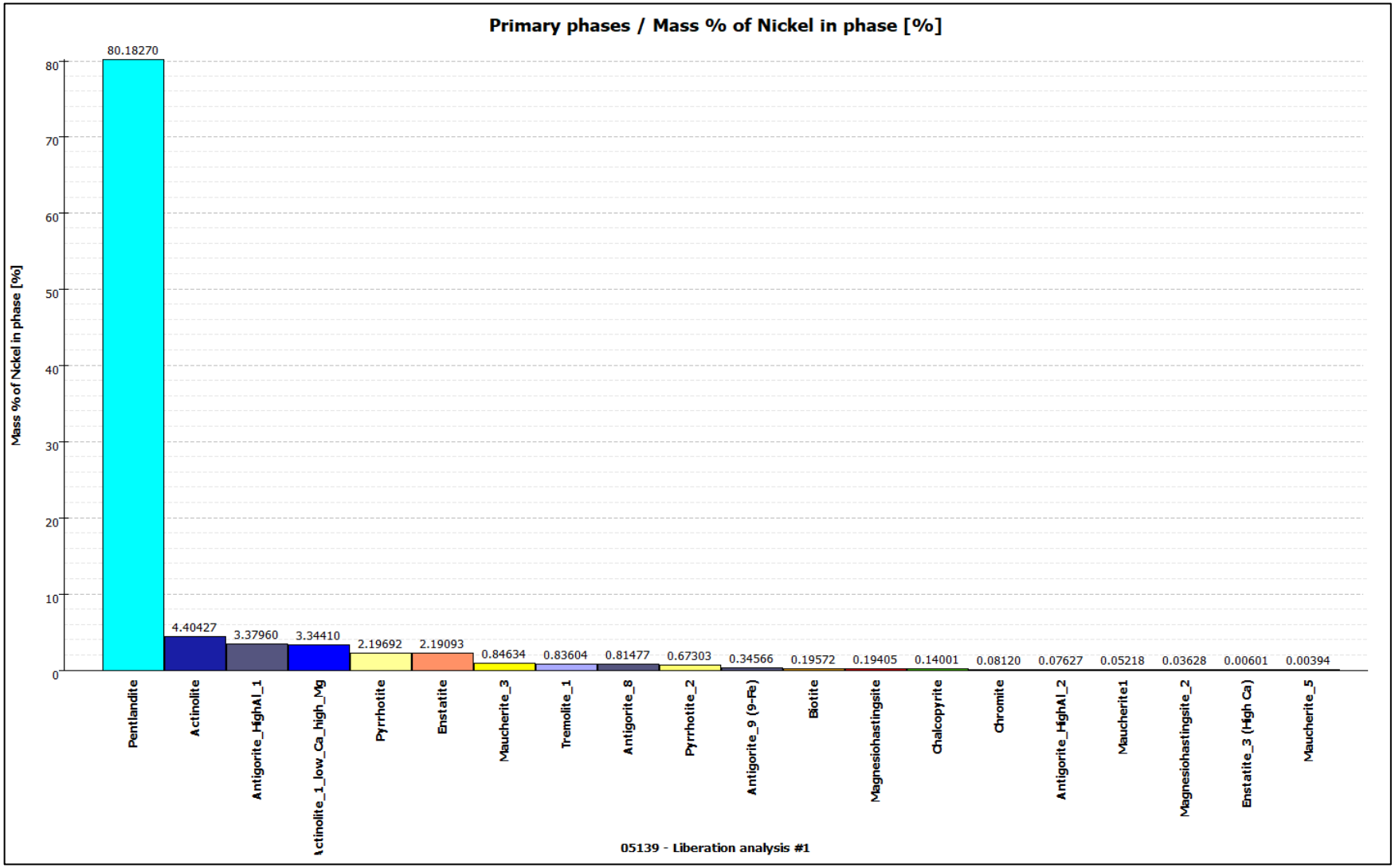

V. Sample IMK – 05139 -5

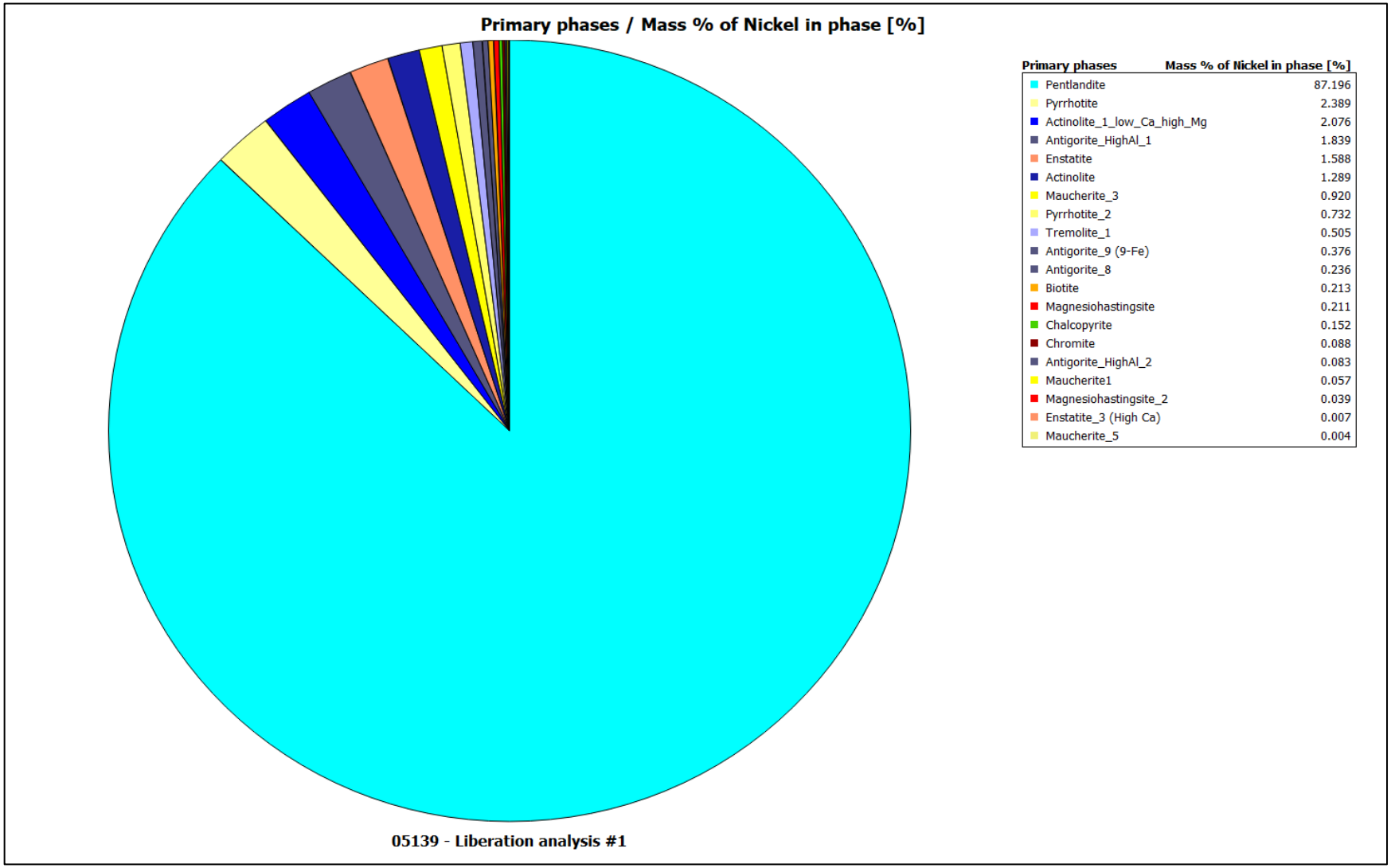

VI. Sample IMK – 05139 -6

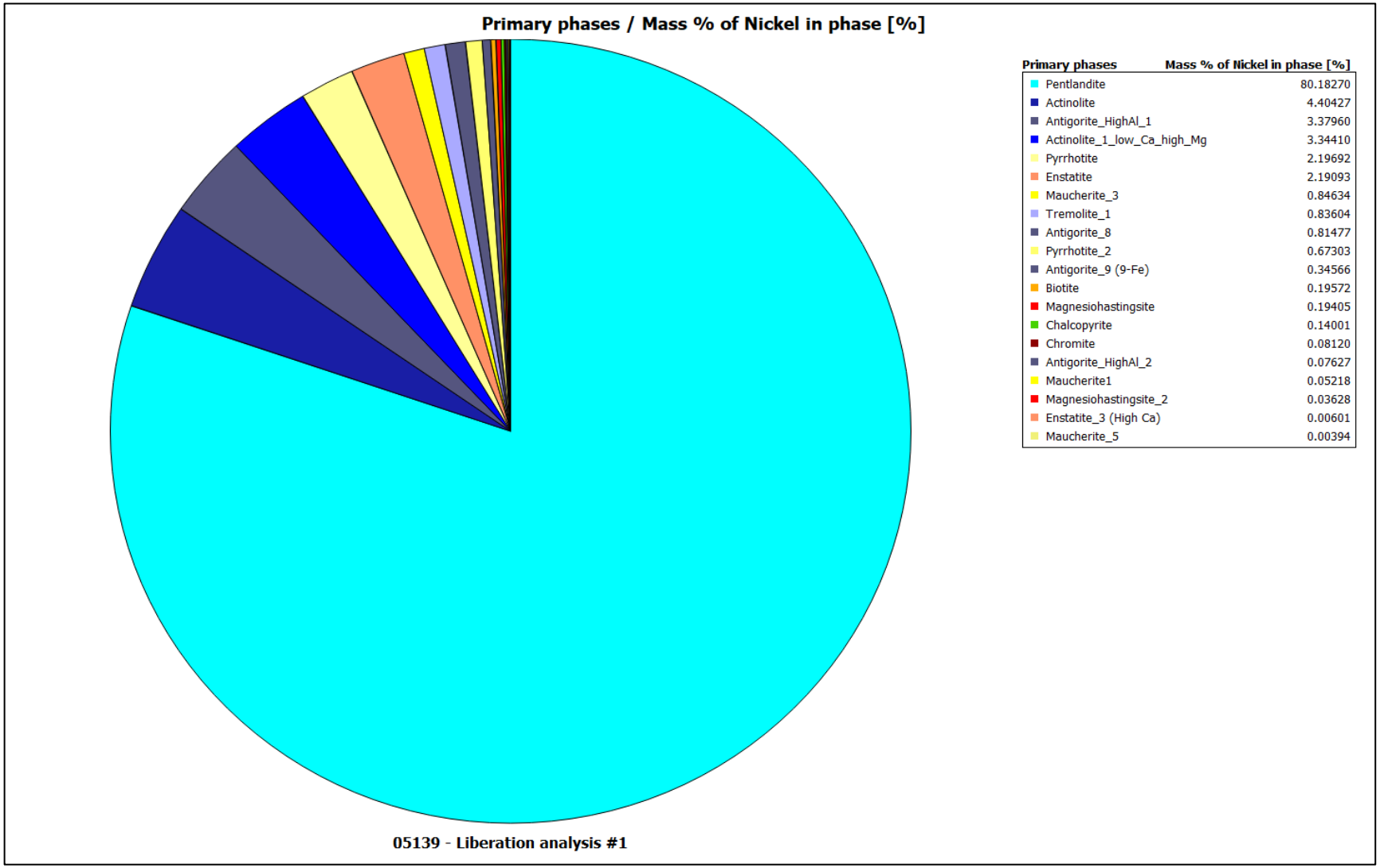

VII. Sample IMK – 05149 - 1

Sample IMK - 05149

Mineral phase names	wt% in sample	Average Ni wt%	Median Ni wt%	Number of points/analyses measured
Antigorite_6 (low-Al)	63,93	0.52	0.27	64
Antigorite_HighAl_1	12,71	0.33	0.24	53
Magnesiohastingsite	3,44	0.29	0.27	55
Heazlewoodite_1	3,19	62.18	62.36	24
Antigorite_9 (9-Fe)	3,04	0.19	0.33	31
Biotite	1,81		0.31	57
Actinolite_1_low_Ca_high_Mg	1,41	0.26	0.18	27
Actinolite	1,23	0.23	0.15	31
Pentlandite	1,19	34.18	33.93	50
Diopside_hedenbergite_1	0,71	0.22	0.165	40
Enstatite	0,67	0.46	0.395	30
Antigorite_8	0,66	0.1	0.09	36
Tremolite_1	0,46	0.52	0.235	34
Antigorite_HighAl_2	0,45	0.57	0.4	31
Antigorite_2	0,40	0.4	0.34	25
Chlorite - Clinochlore	0,37	0.3	0.295	30
Magnesiohastingsite_2	0,07			
Chlorite - Clinochlore_3	0,05			
Chalcocite	0,04			
Antigorite	0,04			
Chlorite - Chamosite	0,03			
Chromite	0,03			
Apatite	0,02			
Enstatite_3 (High Ca)	0,01			
Maucherite1	0,01			

VIII. Sample IMK – 05149 - 2

Sample IMK - 05149

Mineral phase names	Median Ni deportment, wt%
Heazlewoodite_1	75,25
Pentlandite	15,25
Antigorite_6 (low-Al)	6,53
Antigorite_HighAl_1	1,15
Antigorite_9 (9-Fe)	0,38
Magnesiohastingsite	0,35
Biotite	0,21
Maucherite1	0,21
Enstatite	0,10
Actinolite_1_low_Ca_high_Mg	0,10
Maucherite_3	0,08
Actinolite	0,07
Antigorite_HighAl_2	0,07
Maucherite_5	0,05
Antigorite_2	0,05
Diopside_hedenbergite_1	0,04
Chlorite - Clinochlore	0,04
Tremolite_1	0,04
Antigorite_8	0,02
Magnesiohastingsite_2	0,01
Chromite	0,00
Enstatite_3 (High Ca)	0,00
Pyrrhotite	0,00
Total	100,00

Grouping	Median Ni deportment in grouping, wt%
Heazlewoodite	75,25
Pentlandite	15,25
Secondary silicates	9,02
Primary silicates	0,14
Arsenides	0,34
Total	100,00

IX. Sample IMK – 05149 - 3

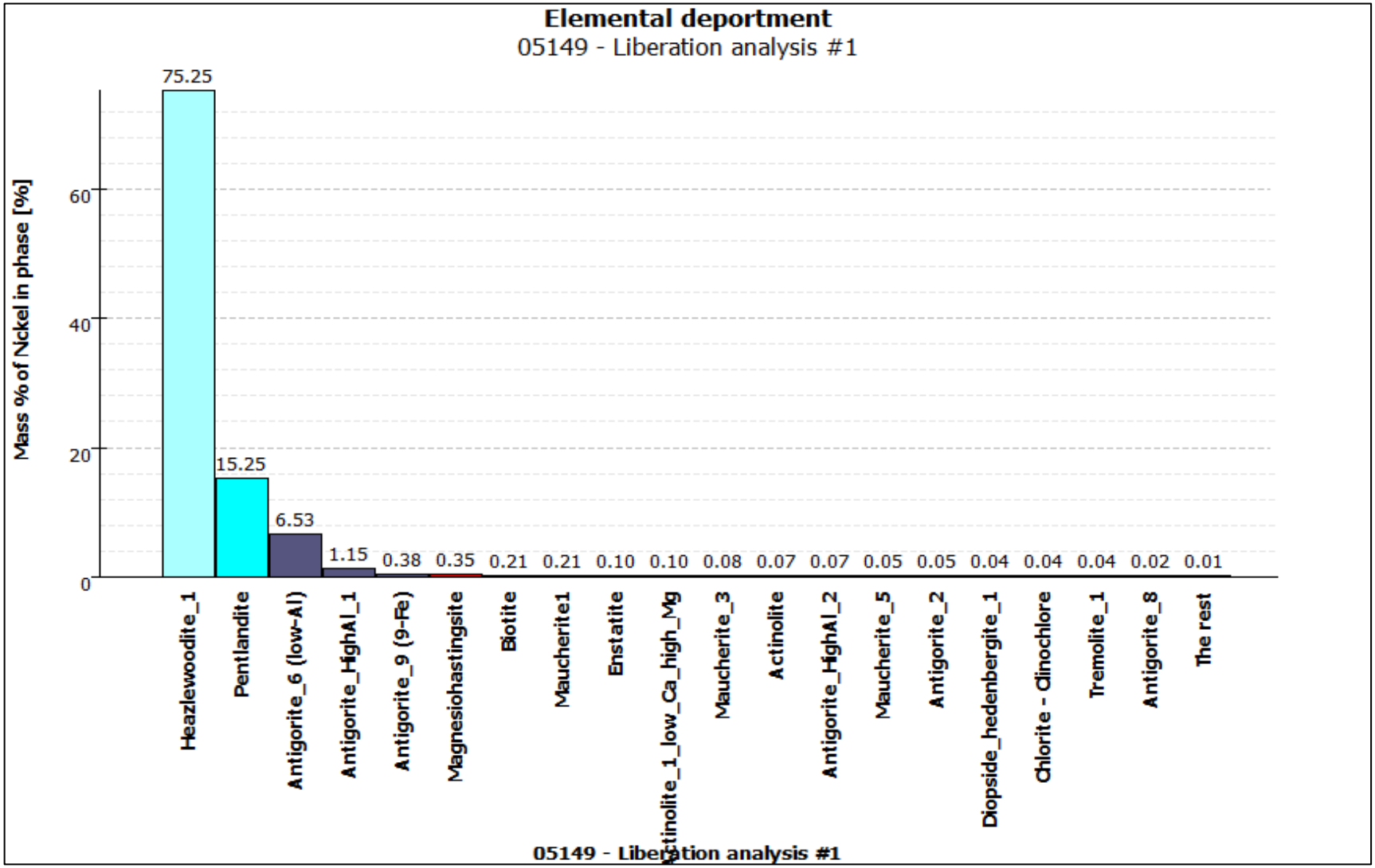

X. Sample IMK – 05149 - 4

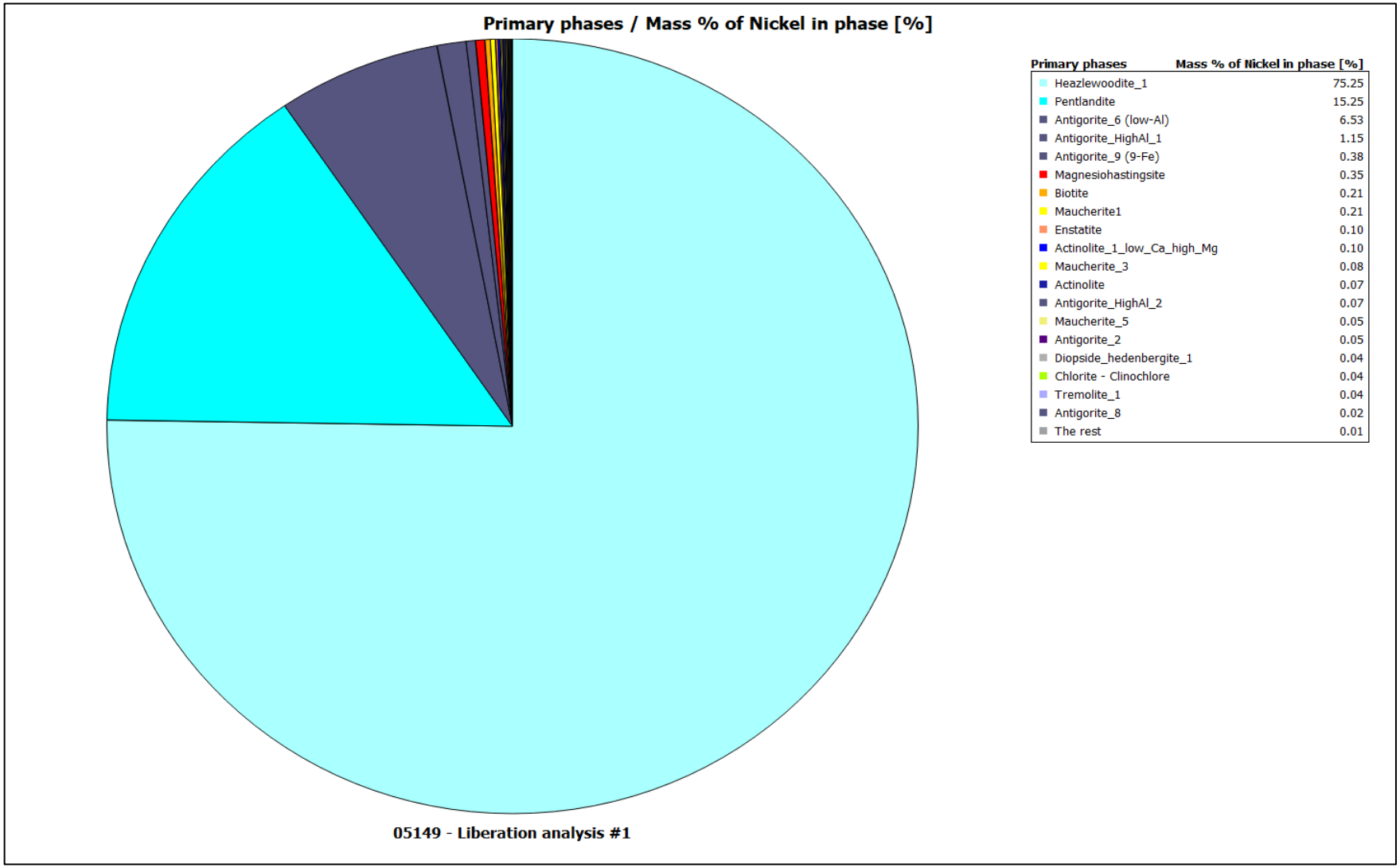

XI. Sample IMK – 05153 – 1

Sample IMK - 05153

Mineral phase names	wt% in sample	Average Ni wt%	Median Ni wt%	Number of points/analyses measured
Antigorite_HighAl_1	28,31	0.28	0.25	65
Enstatite	27,50	0.11	0.085	80
Actinolite_1_low_Ca_high_Mg	11,87	0.26	0.22	72
Actinolite	6,29	0.29	0.24	70
Tremolite_1	6,17	0.23	0.25	60
Biotite	5,16	0.44	0.45	73
Antigorite_6 (low-Al)	3,47	0.67	0.23	43
Antigorite_HighAl_2	2,09	0.66	0.54	40
Magnesiohastingsite	1,99	0.31	0.3	55
Antigorite_8	1,16	0.45	0.28	33
Magnesiohastingsite_2	0,97	0.31	0.29	50
Antigorite_2	0,92	0.53	0.51	40
Antigorite_9 (9-Fe)	0,46	1.4	0.23	20
Chlorite - Clinochlore_3	0,42	0.5	0.41	25
Chlorite - Clinochlore	0,27	0.34	0.37	24
Heazlewoodite_1	0,19	60.6	60.84	13
Antigorite	0,14	0.99	0.43	16
Apatite	0,12	0.86	0.81	25
Awaruite	0,10			
[Unclassified]	2,23			
The rest	0,18			
Total	100,00			

XII. Sample IMK – 05153 – 2

Sample IMK - 05153

Mineral phase names	Median Ni deportment, wt%
Heazlewoodite_1	28,40
Antigorite_HighAl_1	17,83
Awaruite	16,50
Actinolite_1_low_Ca_high_Mg	6,58
Enstatite	5,89
Biotite	5,85
Tremolite_1	3,81
Actinolite	3,80
Antigorite_HighAl_2	2,84
Antigorite_6 (low-Al)	2,01
Magnesiohastingsite	1,50
Antigorite_2	1,18
Antigorite_8	0,82
Magnesiohastingsite_2	0,71
Maucherite1	0,60
Chlorite - Clinochlore_3	0,44
Antigorite_9 (9-Fe)	0,27
Chlorite - Clinochlore	0,25
Apatite	0,24
Maucherite_5	0,18
Antigorite	0,15
Maucherite_3	0,12
Diopside_hedenbergite_1	0,01
Enstatite_3 (High Ca)	0,01
Chromite	0,01
Total	100,00

Grouping	Median Ni deportment in grouping, wt%
Heazlewoodite	28,40
Awaruite	16,50
Secondary Silicates	48,04
Primary Silicates	5,92
Arsenides	0,90
TOTAL	99,75

XIII. Sample IMK – 05153 – 3

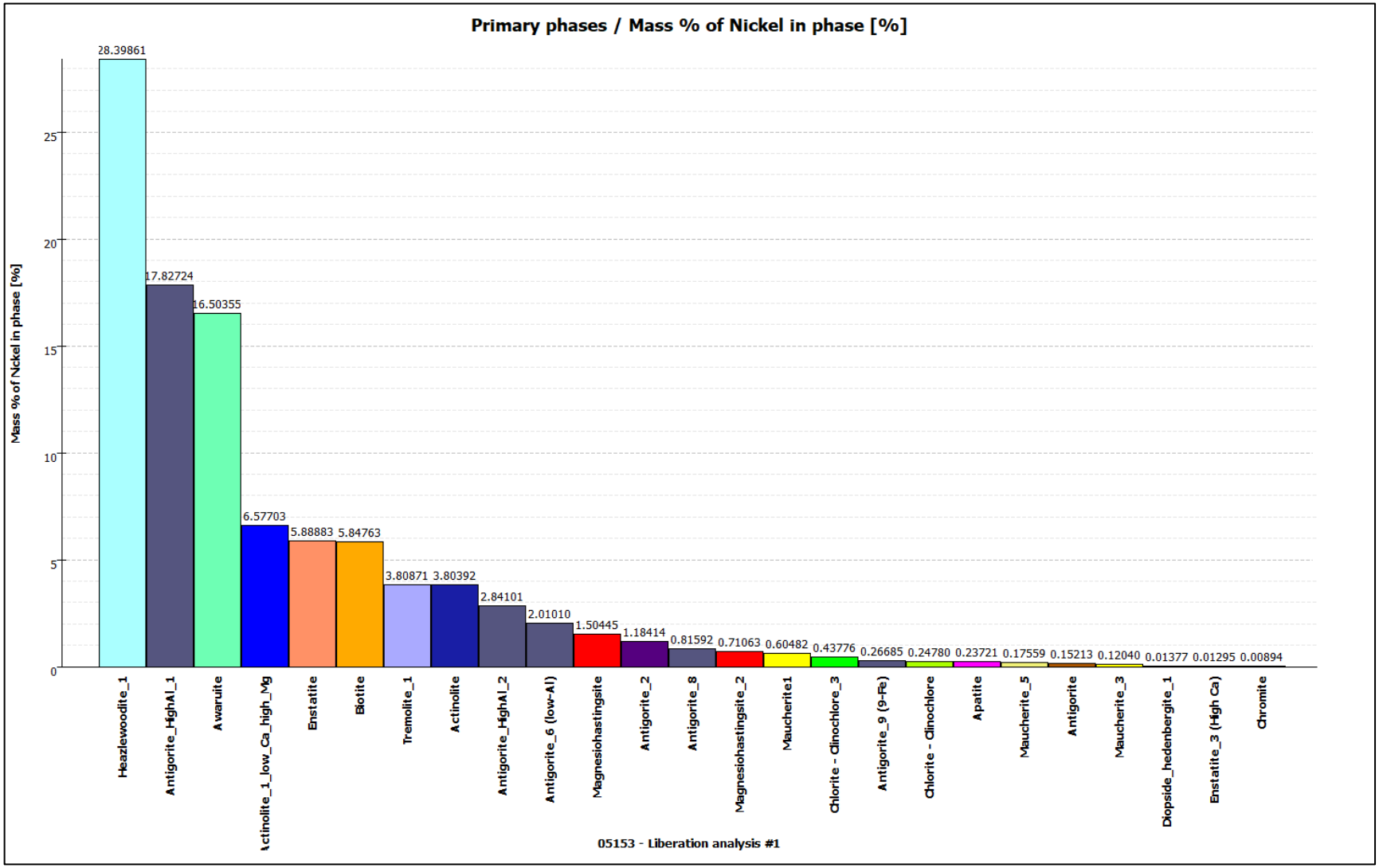

XIV. Sample IMK – 05153 – 4

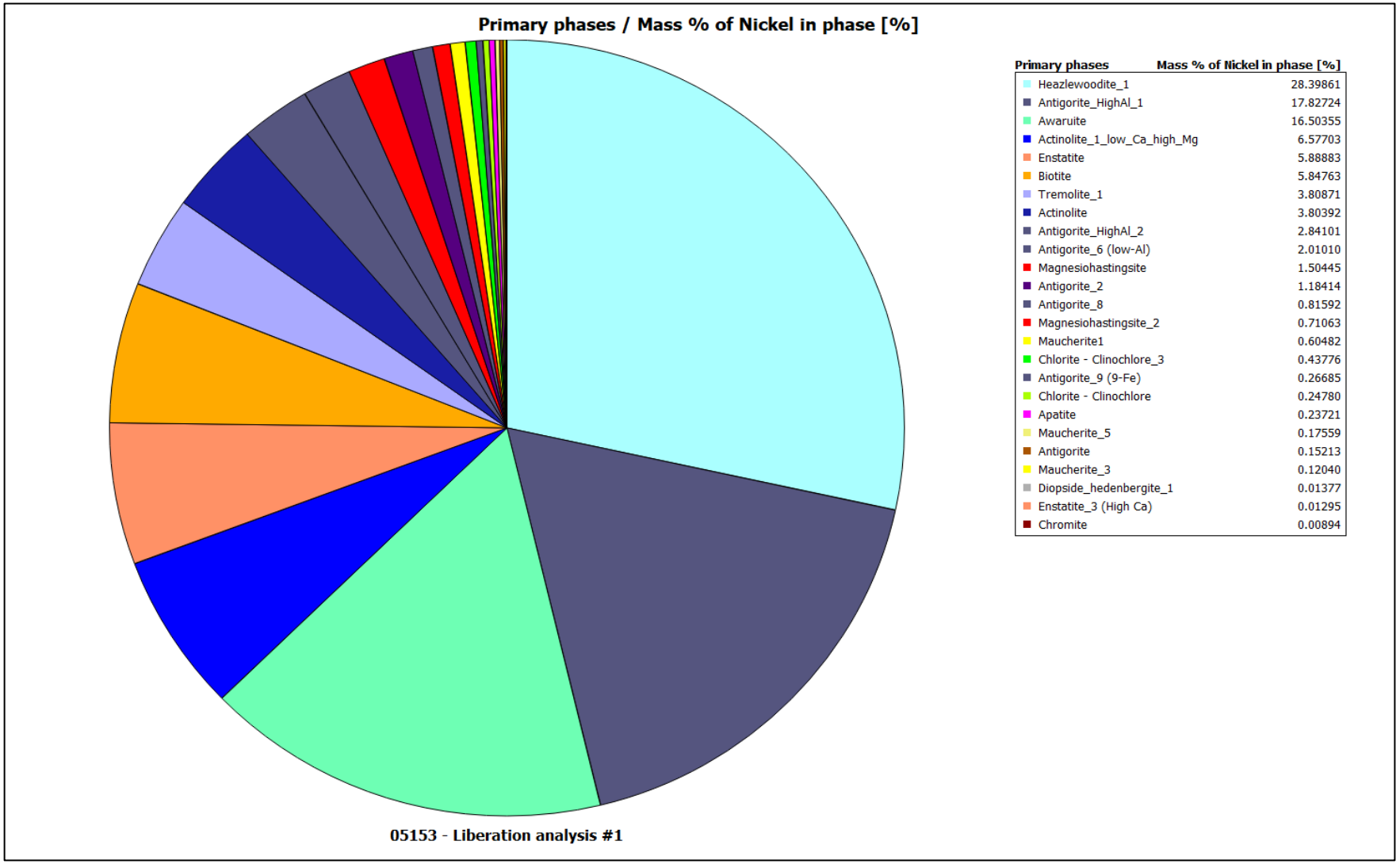

XV. Sample IMK – 05156 – 1

Sample IMK - 05156

Mineral phase names	wt% in sample	Average Ni wt%	Median Ni wt%	Number of points/analyses measured
Antigorite_HighAl_1	63,06	0.31	0.16	318
Antigorite_2	15,21	0.27	0.1	210
Chromite	13,41	0.34	0.3	190
Hematite/Magnetite	1,52	0.9	0.69	39
Maucherite1	1,17			
Chromite1_Fe-rich	1,04	0.35	0.35	70
Antigorite_HighAl_2	0,35	0.62	0.29	25
Enstatite	0,12			
[Unclassified]	3,72			
The rest	0,41			
Total	100			

XVI. Sample IMK – 05156 – 2

Sample IMK - 05156

Mineral phase names	Median Ni deportment, wt%
Maucherite1	78,13
Antigorite_HighAl_1	11,7
Chromite	4,69
Antigorite_2	1,77
Hematite/Magnetite	1,22
Maucherite_5	1,11
Maucherite_3	0,53
Chromite1_Fe-rich	0,42
Heazlewoodite_1	0,17
Antigorite_HighAl_2	0,12
Antigorite	0,04
Chlorite - Clinochlore_3	0,03
Apatite	0,03
Antigorite_6 (low-Al)	0,02
Pentlandite	0,01
The rest	0,02
Total	100

Grouping	Median Ni deportment in grouping, wt%
Arsenides	79,77
Secondary Silicates	13,71
Chromites	5,11
Oxides	1,22
Pentlandite	0,01
Heazlewoodite	0,01
TOTAL	99,83

XVII. Sample IMK – 05156 – 3

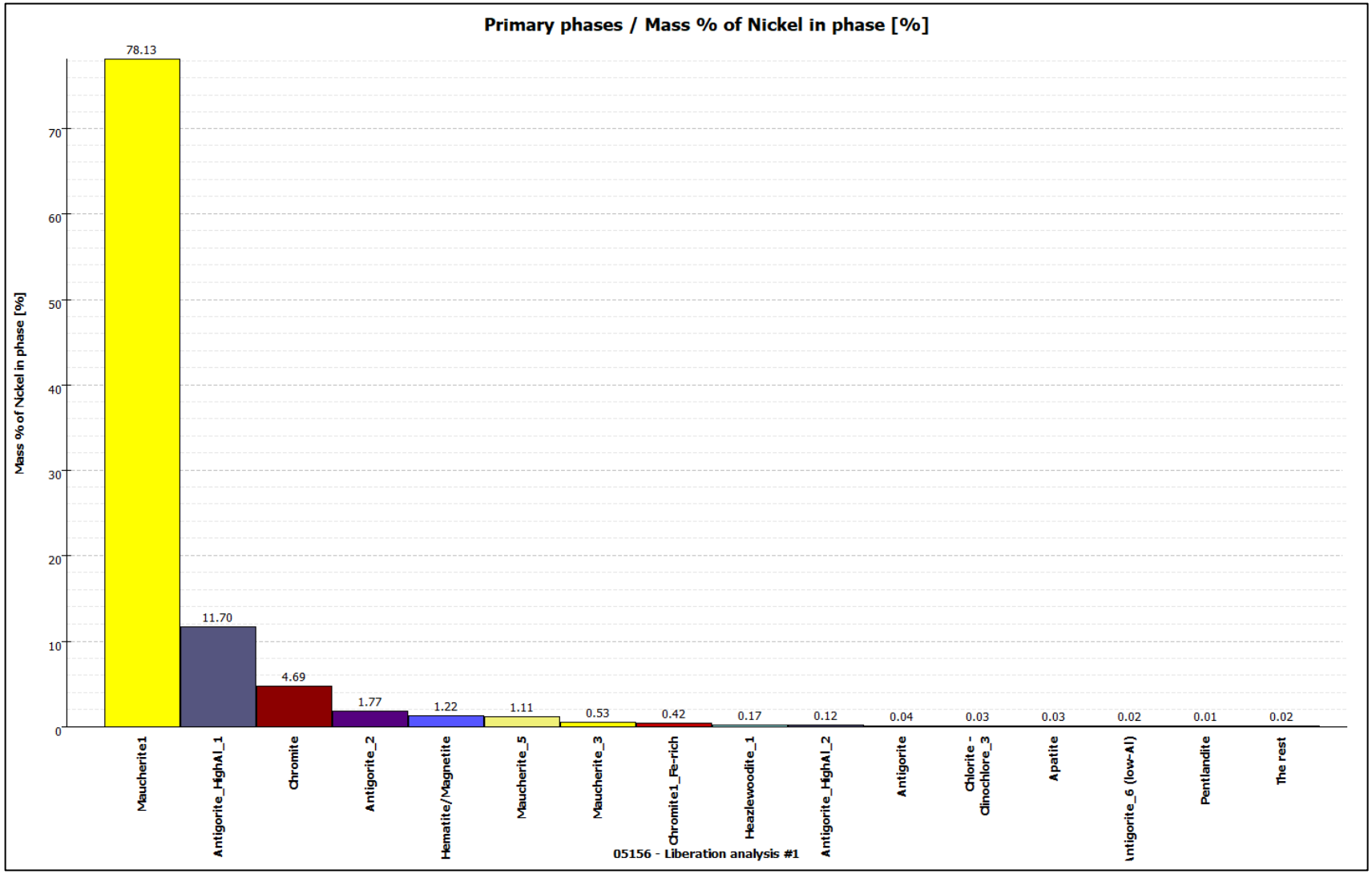
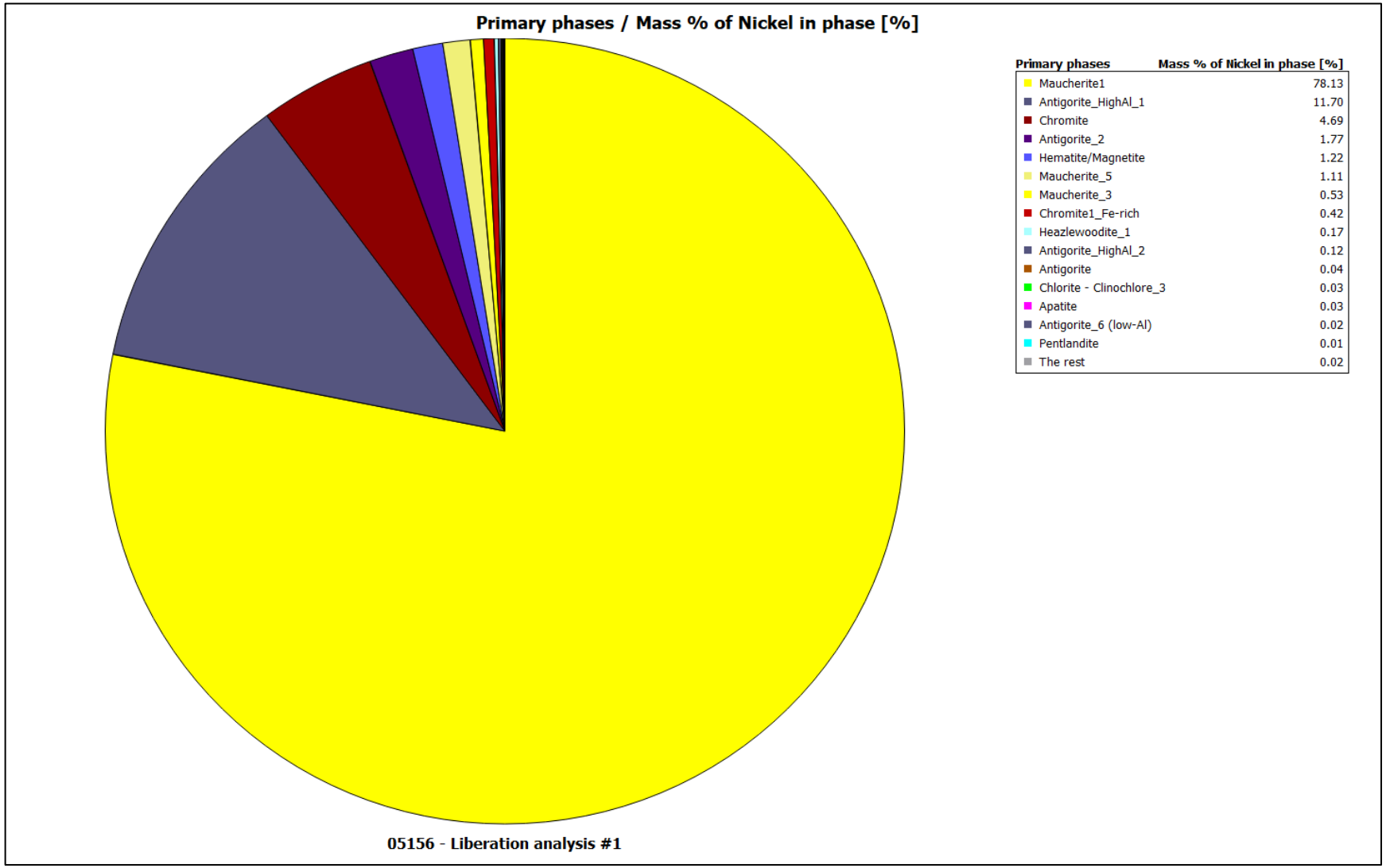
XVIII. Sample IMK – 05156 – 4